Investigating the Sensitivity of Non-Small Cell Lung Cancer to Cisplatin using MicroRNA-184 loaded Chitosan Nanocarriers

Giulia Scagnetti

A thesis submitted in partial fulfilment of the requirements of

Liverpool John Moores University for the degree of Doctor of Philosophy.

July 2022

Declaration

The work presented in this thesis was carried out at the Byrom Street City Campus of Liverpool John Moores unless otherwise stated. The work is the original work of the author.

While registered as a candidate for the degree of Doctor of Philosophy, for which submission is now made, the author has not been registered as a candidate for any other award. This thesis has not been submitted in whole, or in part, for any other degree.

James Parsons Building

Byrom Street City Campus

Liverpool John Moores University

3 Byrom Street

L3 3AF

Liverpool

UK

This work is dedicated to every single person

of the big broad family of “along the river Bagnolo”,

also referred as “joppe Bagnò”.

And mainly to my Dad: I hope that wherever you are, you miss me as much as I miss you.

Acknowledgements

This thesis is the results of a journey. There are plenty of people that deserve to be acknowledged as without them, I would have never arrived at this finish line.

My supervisors Prof. Imran Saleem and Dr. Kehinde Ross had supported me throughout the many challenges encountered during the past years. I would like to express my sincere gratitude towards their mentorship and to the time they managed to dedicate me, despite their research duties. Their support in crucial stages was key to allow me to continue towards the goal.

I would also like to acknowledge Prof. Mark Holland for his help and support during the challenges faced due to the COVID19 pandemic; and Dr. Matt Roberts for always helping with any issue arising in the chemistry laboratories. A special mention goes to Dr. Francesca Giuntini, for being the Italian door to knock to for a research and non-research related talk; and to Dr. Darren Sexton for the conversations not only flow-cytometry related.

In addition, I would like to thank my advisors from University of Liverpool Dr. Lakis Liloglou and Dr. Michael Davies for gifting us the cell lines employed int this study, and the friend and lab mate Talhat Chaudhry for performing with me the confocal microscopy experiments.

I must acknowledge that there were many people who helped me throughout this journey outside the “workplace”.

Firstly, I will not be grateful enough to my family for giving me the opportunity to study and to pursue this pathway. They have always believed in me way more than I have ever done, and they have always been my safe place to go to. Never ending gratitude goes to my mum Patrizia, for her remote, endless and discrete caring. She has been an example of resilience mixed with intelligence, love and kindness. A huge thank you goes to my number one supporter, which is my sister Valentina, that has always expressed me her love without asking for it back.

Even though the PhD years have been a steep mountain to climb, I am grateful because my Dad Ivano prepared me on how to hike since when I was a kid. I would have preferred to have him by my side for all the journey, however unfortunately, I had to hike on my own most of this mountain. I will never forget the joy and positiveness he used to carry around, and I will also never forget how essential he has been to become the person I am today.

Realistically, this thesis would have not been done without Vera, one of the best people I know. She has been sister, friend, flatmate, colleague, mentor, advisor, carer, person to go and laugh about something or to cry about something. She is one of a million and I will never be grateful enough to have her in my life. She means everything to me.

The net of Italian and international friend that we created during the year has become a second family. And it really made the difference to thrive in every circumstance. A huge thank you for every single moment goes to Valeria, David, Michele, Paolo, John, Lalli, Giummi, Talhat, Hique, Thais, Seba, Kan, and anyone else I met during the past years.

I had a broad squad of remote supporters from Italy, that were never too far away than a voice message. Laura, Sere, Saretta, Marghe, Elle, Lucia e Cate: a “thank you” is probably not enough to describe how grateful I am of having such good friends around me. A special mention to Diego and Massi for the IT (and laugh) support.

Abstract

Lung cancer cancer is the number one cause of death worldwide. The difficulty of detecting the malignancy at early stages of its progression is the primary reason for the high mortality related to lung cancer. When surgery is not a feasible option, cisplatin and platinum-based compounds are the first-line therapeutic agents employed to treat patients. However, cisplatin treatment often results in unsuccessful therapies owing to the development of drug resistance. Progress has been made in last decade to improve the chemotherapeutic approach to lung cancer, such as drugs targeting genetic modifications and immunotherapy. However, for majority of the patients cisplatin-based therapy is still the primary choice.

Oligonucleotide therapeutics have increased in the past 20 years as novel compounds to treat several pathologies including cancer. They are based on the mimicry or inhibition of non-coding RNAs, which are known to be involved in the regulation of gene expression. To date, more than 15 drugs have been approved by the FDA for human use, which showcase the great promise held by this compound class. MicroRNAs are short non-coding oligonucleotide which modulate protein expression. Since their discovery, they have been involved in several steps of carcinogenesis, including the development of drug resistance.

One possible approach to tackle lung cancer was to sensitise cells to cisplatin via modulating the expression of miRNA involved in cisplatin resistance. Among the miRNA involved in the development of drug resistance, this work was focused on a miRNA named miR-184, which was demonstrated to be downregulated in non-small cell lung cancer (NSCLC) cells. Our results showed that the transfection of Calu-3 cells with miR-184 mimic sensitised the cells to cisplatin, diminishing its IC50 from 14.35 ± 1.28 µM to 9.42 ± 1.47 µM. Furthermore, our results suggested that cisplatin treatment together with miR-184 mimic transfection increased Calu-3 (epithelial adenocarcinoma) apoptotic and necrotic cell populations, in comparison to cisplatin only treatment. Thus, showing promise in miR-184 as a therapeutic target for lung cancer.

One of the major difficulties related to oligonucleotide therapeutics is their challenging delivery. These include events that prevent oligonucleotide to exert their action, such as nuclease degradation, poor internalisation at the cellular level and lysosomal degradation once uptaken from the cells.

One promising approach to enhance oligonucleotide therapeutics is represented by their complexation within nanoparticles (NPs). This study developed a NPs formulation using

chitosan derivatives employing the Taguchi Design of Experiment to find the optimum formulation (L18 orthogonal array). The formulations were prepared within a microfluidic device, which allows quick preparation and easier scalability of the formulation compared to conventional methods. The manufactured CHT NPs were of a nano-meter size range and the optimum formulation had size of 105.9 ± 11.00 nm for CS HCl, 142.73 ± 6.60 nm for CS GLU, 199.20 ± 8.50 nm for CS GLY and 142.15 ± 5.75 nm for CS ASP. In addition, NPs were able to complex with the miR-184 mimic (EE% > 91.83 ± 0.89). Confocal microscopy revealed that the NPs were successfully internalised by Calu-3 cells, thus confirming that the formulation enhanced the oligonucleotide uptake.

Finally, the current study investigated the expression of four known miR-184 targets (BCL-2, c.myc, TNFAIP-2, AKT-2) to explore the mechanism to enhance cisplatin cytotoxicity. Our findings revealed that miR-184 might enhance cisplatin cytotoxicity via targeting BCL-2 (and therefore inducing apoptosis), and/or c-myc and TNFAIP-2 (and therefore decreasing cell proliferation).

List of Abbreviations

ADC	Adenocarcinoma
AE	Amplification efficacy
AE%	Percentage of amplification efficiency
ALK	Anaplastic lymphoma kinase
ASGR	Asialoglycoprotein receptor
BCL-2	B-cell lymphoma
cDNA	Complementary DNA
CHT	Chitosan
CI	Confidence interval
CPP	Cell-penetrating peptide
CS ASP	Chitosan Aspergillus
CS GLU	Chitosan glutamate
CS GLY	Glycol chitosan
CS HCl	Chitosan hydrochloride
Ct	Cycle treshold
DMEM	Dulbecco's modified eagle's medium
DMF	Dimethylformamide
DMSO	Dimethylsulphoxide
DoE	Design of experiment
DOX	Doxorubicine
EDTA	Ethylenediaminetetraacetic acid
EE%	Encapsulation efficiency
EGFR	Epidermal growth factor receptor
Em	Emission wavelength
Ex	Excitation wavelength
FBS	Foetal bovine serum
FRR	Flow rate ratio
FSC	Forward scatter
GalNac	N-Acetylgalactosamine
GOI	Gene of interest
HA	Hyaluronic acid
IASLC	International Association for the Study of Lung Cancer's
IHC	Immunohistochemistry
JAM-A	Junction adhesion molecule A
LCLC	Large-cell carcinoma
MEM	Minimum eagle media
MIAT	Myocardial infarction-associated transcript
MTT	3-(4,5-Dimethylthiazol-2-yl)-2,5-Diphenyltetrazolium Bromide
-ve	Negative charge
NSCLC	Non-small cell lung cancer
$NH3^+$	Amino group
NPs	Nanoparticles
NTC	Non-targeting control
OSCC	Oral squamous cell carcinoma

+ve	Positive charge
PD-1	Programmed cell death-protein 1
PDL-1	Programmed cell death-protein-1 ligand
PI	Propidium iodide
PAMAM	Poli(amidoamine)
PBS	Phosphate buffer saline
PCR	Polymerase Chain Reaction
PDI	Polydispersity index
PDSM	Polydimethylsiloxane
PEG	Polyethylene glycol
PEI	Polyethylimine
PLGA	Poly lactic-co-glycolic acid
PMMA	Poly(Me methacrylate)
PS	Phosphatidylserine
PU	Polyurethane
PVDF	Polyvinylidene difluoride
Rig-1	Retinoic-acid inducible gene I
RISC	RNA-induced silencing complex
RIPA	Radio immuno precipitation assay
RT-qPCR	Real time quantitative PCR
S/N	Signal to noise
SCLC	Small cell lung cancer
SD	Standard deviation
SDS-PAGE	Sodium dodecyl sulfate-polyacrilamide gel electrophoresis
SCC	Squamous-cell carcinoma
SSC	Side scatter
TLR	Tool-like receptor
TBS	Tris buffered saline
TBST	Tween-TBS
TE	Tris-EDTA
TFR	Total flow rate
Tm	Melting temperature
TNFα	Tumor necrosis factor
TNFAIP2	TNF alpha induced protein 2
TNM	Tumour, node, metastasis
TPP	Tripolyphosphate
UCA 1	Urothelial cancer associated 1
WHO	World Health Organisation

Table of Contents

List of Figures

List of Tables

1 Introduction

1.1 Lung cancer

The World Health Organization (WHO) estimated that among all cancer types, there were 2.2 million new cases of lung cancer and 1.80 million lung cancer-related deaths in 2020 (Ferlay et al., 2021). The online website GLOBOCAN provides graphical visualization of databases for 185 countries and 36 cancer types, and it reports that in 2020 lung cancer accounted for 11.4% of all cancer cases and 18% of cancer-related deaths (Sung et al., 2021). The 1 and 5-year-survival-rate related to lung cancer are 26% and 5% respectively, making lung cancer the number one of cancer deaths worldwide. Moreover, according to GLOBOCAN projections of cancer incidence and mortality for the period 2020-2040, lung cancer has been estimated to increase to 61% for incidence and 65.8% for mortality (Bray et al., 2018; Ferlay et al., 2021).

Lung cancer can be classified into several subtypes, differing from each other mainly by histological features and therapeutic implications. Firstly, lung cancer can be divided into two categories: small-cell-lung cancer (SCLC) and non-small-cell lung cancer (NSCLC) which is the most common amongst patients (Rodriguez-Canales et al., 2016). Following the development of new immunohistochemistry (ICH) techniques for histology evaluation and molecular profiling, in 2015 the WHO revised the 2004 classification of lung cancer particularly in regards of the sub-classification of NSCLC phenotypes. According to the 2015 publication, NSCLC cases were classified into adenocarcinoma (ADC), squamous-cell carcinoma (SCC) and large-cell carcinoma (LCLC). Moreover, the 2015 classification suggested the immunohistochemical evaluation of NSCLC subtypes to evaluate genetic modifications, such as epidermal growth factor receptor (EGFR) mutations and anaplastic lymphoma kinase (ALK) rearrangements which are the most common in patient tumours (Tsao et al., 2016), and therefore, they could be used to implement personalized treatments where applicable (Travis et al., 2015). The main differences among the diverse phenotype of NSCLC are displayed in Table 1.1.

Table 1.1 NSCLC phenotypes and their differences in terms of incidence (%), location where they are identified, histologic characteristics and ICH markers used to identify them.

Name	Incidence (%)	Location	Histologic Features	ICH markers
Adenocarcinoma (ADC)	38.5	periphery of lungs	glandular differentiation; lepidic, acinar, papillary, micropapillary and solid patterns can be present either alone or intermixed in the same tumour.	mucicarmin (to confirm mucin production); annapsin A expression; TTF1 expression.
Squamous Cell Carcinoma (SCC)	20	Central location, spreading to bronchus	shows keratinisation and/or intercellular bridges	p40, p63, cytokeratins 5/6 (squamous cell differentiation markers) expression
Large-Cell Lung Carcinoma (LCLC)	2.9		no keratinisation, no glandular or small cell-differentiation	no mucin production; no TTF-1 or p40
NSCLC-NOS			histological features and HIC phenotypes can't be classified in any of the NSCLC subtypes.	

Following the identification of lung cancer phenotype, the malignancy is classified according to the primary tumour, regional lymph node involvement and presence of metastases, as suggested by the International Association for the Study of Lung Cancer's (IASLC) staging project (Goldstraw et al., 2016). The main criteria for such tumour, node, metastasis (TNM) classification are displayed and broadly described in the cited paper (Goldstraw et al., 2016). Following the assignment of the TNM values to a tumour, this can be further classified into a stage that ranges from I to IV (Figure 1.1). Unfortunately, majority of lung cancer cases are diagnosed when they are at stage III or IV of its development, meaning that most of the patients present metastatic disease at the time of diagnosis and consequently, majority of the times surgical intervention is not a feasible option and treatment of lung cancer requires effective therapies.

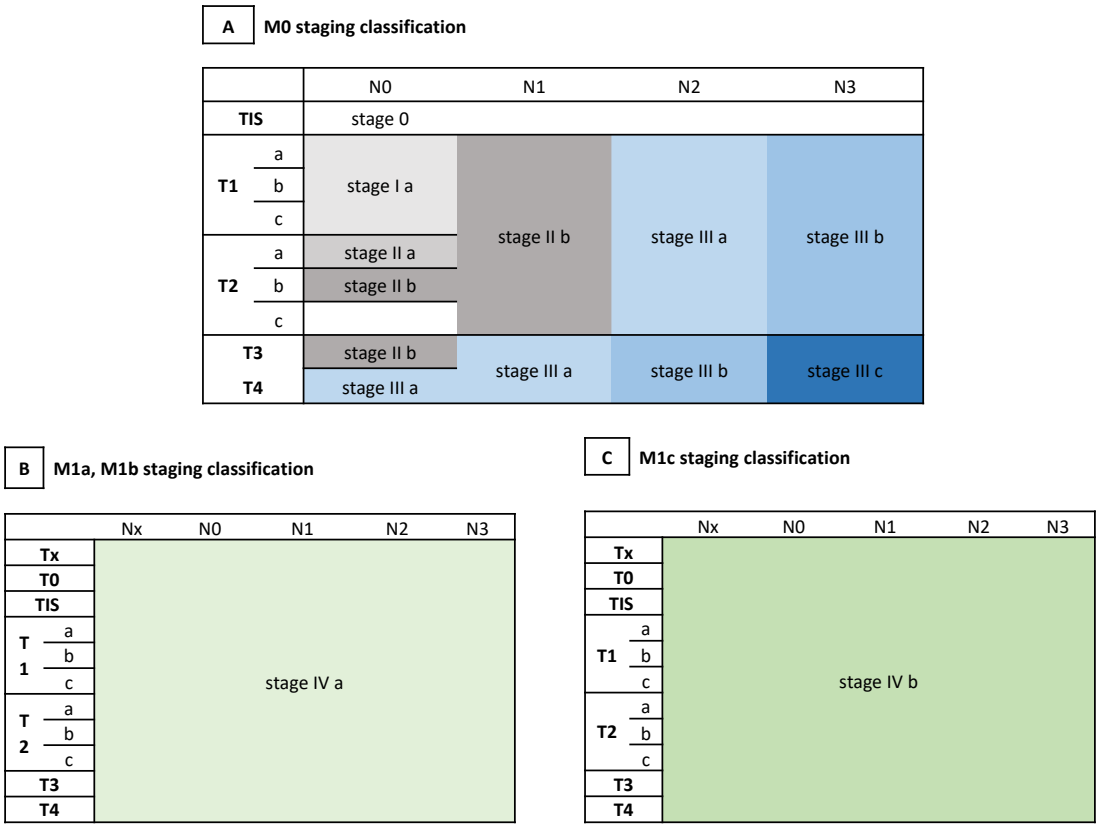

Figure 1.1 Lung cancer staging identification via the TNM (Tumour, Node, Metastasis) classification method. Staging followed when the tumour (A) has no metastasis; (B) has pleural or pericardial nodules (M1a) or one single extra thoracic metastasis (M1b); and (C) lung cancer identification for malignancies with more than one extra thoracic metastasis in multiple organs.

1.1.1 Lung cancer treatment

Traditionally, cytotoxic therapies have been widely used either alone or in combination with radiotherapy or other chemotherapy agents in late stage tumours (Hirsch et al., 2017). The classes of chemotherapeutic agents which diminish tumour growth and improve patient quality of life and survival rates include platinum-based compounds (cisplatin, carboplatin, oxaliplatin), taxanes (paclitaxel, docetaxel, or vinorelbine), antimetabolites (gemcitabine or pemetrexed), or vinca alkaloids (vinblastine).

Over the past decades, lung cancer therapies advanced from cytotoxic agents to a more rational approach based on the histology cancer subtype and on the occurrence of genetic modifications (Herbst et al., 2018). The discovery of immunohistochemical subtypes and genetic modification evaluation in lung cancer diagnosis has led to a more effective and tailored treatment of the disease. Hence, lung cancer subtypes presenting genetic modification (such as EGFR, ALK, ROS1, BRAF V600E, NTRK) are treated with specific and

tailored drugs, showing promising results in terms of clinical outcomes (Arbour & Riely, 2019). Osimertinib, Alectinib, Crizotinib, Debrafenib, Larotrectinib are examples of drugs used in patients bearing such genetic modifications (Duma et al., 2019). A further alternative to traditional chemotherapeutic agents for tumour types without the mentioned genetic modification is immunotherapy (Carbone et al., 2017; Gandhi et al., 2018; Morabito, 2018). One successful immunotherapy approach is based on the PD-1/PDL-1 pathway. Programmed cell death protein-1 (PD-1) is expressed on the surface of T-cells, and its ligand PDL-1 is produced by numerous cells. The binding of PDL-1 with PD-1 inactivates T-cells and it is used to maintain human's body homeostasis. However, malignancies often overexpress PD-L1 as a mechanism of defence against the host's immune system. The PD1/PDL-1 interaction can be blocked by antibodies directed against PD-1 or PDL-1 to restore T-cells function (Kroemer et al., 2013; Naylor et al., 2016; Pardoll, 2012). Therefore, prior to assessing the optimal cytotoxic chemotherapy agent for a patient, a further PDL-1 assessment is carried out to give patients a score depending on tumour expression of PDL-1, which is categorized as low (PD-L1 <1%), intermediate (PD-L1 1-49%), and high (PD-L1 ≥50%). The score will define the monoclonal antibody to be used and whether their combination with cytotoxic chemotherapy agents can be beneficial (**Figure** 1.2). Generally, patients with high PD-L1 expression are offered a single agent between pembrolizumab, atezolizumab, or cemiplimab while patients with intermediate levels of PD-L1 are treated with a chemotherapy agent in combination with pembrolizumab or nivolumab plus ipilimumab. Lastly, patients with PD-L1 <1% usually receive a chemotherapy agent in combination with pembrolizumab or nivolumab or ipilimumab (Duma et al., 2019; M. Miller & Hanna, 2021).

Despite the novel development of therapeutic approaches to treat late-stage lung cancer cases, including personalised therapies based on gene-driven mutations (such as ALK, RET or ROS1 fusion, BRAF or MET mutation, EGFR deletion) or on PDL-1 score of the malignancies, the use of cytotoxic chemotherapeutic agents remains a cornerstone in the treatment of non-small cell lung cancer. This is due to either the limited percentage of people presenting targeted mutation (less than 30%) and to the limited percentage of malignancies that can be treated with immunotherapy, given that only patients having PDL-1 score above 50% witness an improved overall survival in comparison with patients treated with chemotherapy (Sezer et al., 2021). Thus, patients without gene-driven modifications and with PDL-1 score below 50% rely on cytotoxic chemotherapy agents to treat and reduce tumour progression. As a result, the insurgence of drug resistance still represents a major issue to be tackled to improve survival rate of lung cancer patients (Florea & Büsselberg, 2011; Makovec, 2019).

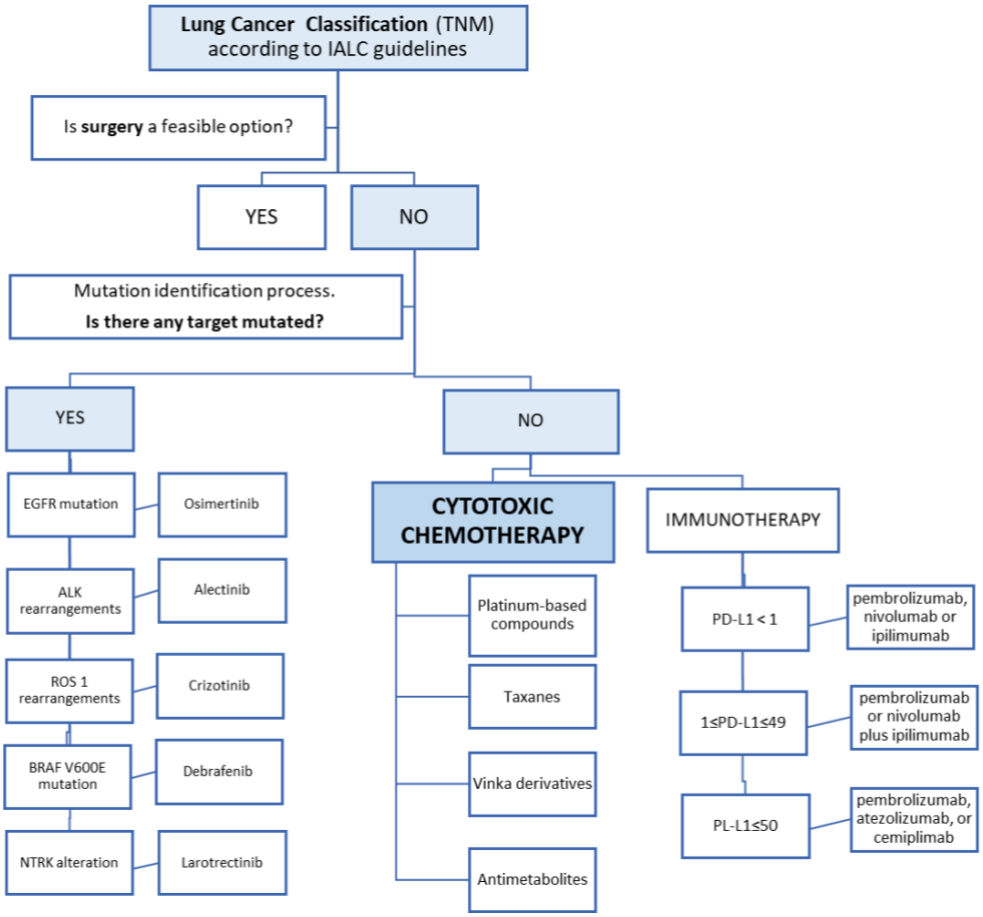

Figure 1.2 Lung cancer therapy identification pathway. Once the malignancy has been identified according to the TNM staging, further diagnostic tests are undertaken to investigate the presence of gene-driven mutations (EGFR, ALK, ROS1, BRAF V600E, NTRK) that can be helpful to provide a specific therapy for the patient. When there are no gene-driven mutations, cytotoxic chemotherapy and/or immunotherapy are the routes to follow for treatment.

1.1.2 Cisplatin Therapy

Among the cytotoxic chemotherapeutic agents approved for cancer treatment, the first-line choice for lung cancer (Lemjabbar-Alaoui et al., 2015) is often platinum-based drugs, of which cisplatin (cis-diamminedichloroplatinum (II)) is the main component. Cisplatin Molecular Weight (mW) is 301, log P is -2.19 and water solubility 2.53 mg/mL.

Cisplatin is administered by intravenous infusion, and once in the bloodstream it is highly bound to plasma proteins because of platinum reactivity towards thiol groups of certain amino acids such as cysteine (Cepeda et al., 2007). Cisplatin molecules which are not bound to plasma proteins rapidly diffuses into tissues. Here, transmembrane proteins have been found to be responsible for cisplatin internalisation into cells, such as efflux ATPases and solute carriers. Once inside the cells, following the exchange of chloride ions with water molecules, cisplatin exerts its cytotoxic activity via binding to the N7 reactive centre on purine residues (mainly guanine residues). Thus, the formation of DNA-cisplatin adducts (**Figure** 1.3) causes DNA damages, and therefore elicits DNA repair mechanism (Dasari & Bernard Tchounwou, 2014). However, cisplatin adducts can drive the activation of several responses which contribute to cell death. Cisplatin-induced oxidative stress, modulation of mitochondria calcium concentration, p53 and AKT activation are examples of transduction pathways that cisplatin promotes with all culminating in apoptosis (Siddik, 2003). Following cisplatin absorption, it distributes mainly in bladder, muscles, testicle, pancreas and spleen. Its excretion occurs via urine, though small amounts of cisplatin are eliminated via bile and faecal excretion (Shen et al., 2012).

A decreased cell division is the main effect of cisplatin and, accordingly, it shows highest activity in rapidly proliferating cells. Thus, cisplatin cytotoxicity is not only observed in cancer cells but also in healthy cells, leading to the occurrence of side effects. Those can include gastrointestinal tract damages (Yamamoto et al., 2013), myelosuppression due to injury of bone marrow (Lucas et al., 2013), which are the most severe side effects of cisplatin-based therapy. However the most usually observed, noticed in 30–40% of patients, is nephrotoxicity (Crona et al., 2017; Miller et al., 2010; Pabla & Dong, 2008). This is manifested as acute kidney injury (AKI), salt or magnesium wasting and loss of urinary concentrating ability (Loren et al., 2021; Xiang et al., 2019).

As a consequence, researchers have synthesised cisplatin derivatives to improve its cytotoxicity and simultaneously diminish side effects related to cisplatin utilisation (**Table** 1.2). Among the cisplatin-based derivatives, carboplatin and oxaliplatin are the most used.

Nevertheless, despite these molecules present an improved therapeutic index, they are not effective towards all the types of cancer. For NSCLC cisplatin still remains the first line drug of choice used, either alone or in combination with other chemotherapeutic agents (Ali et al., 2022).

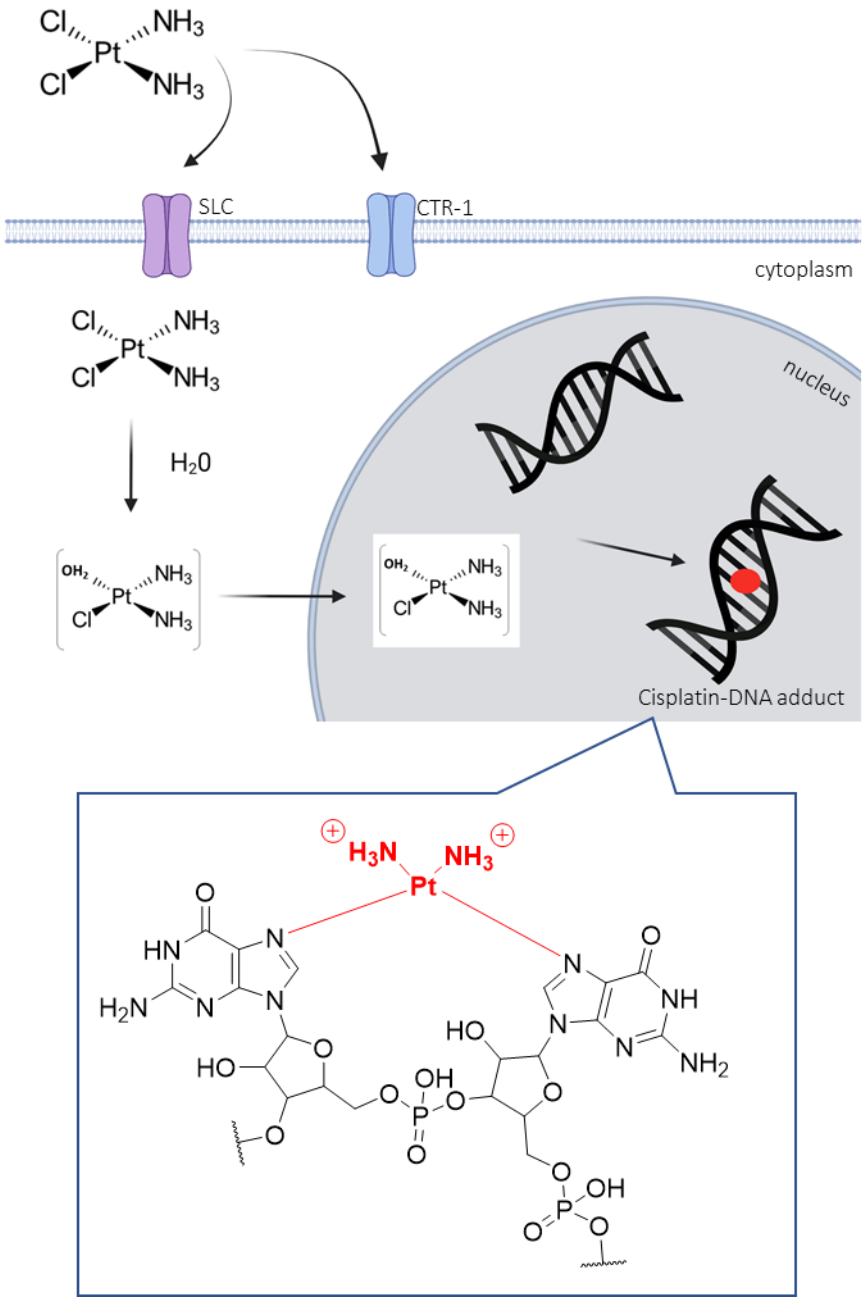

Figure 1.3 Cisplatin mode of action. After cisplatin diffusion into tissues, it is internalised into cells thanks to specific proteins such as solute carrier importers (SLC) and copper transporter proteins (CTR-1). Following uptake, chlorine is displaced from the cisplatin molecule by water molecules. Thus, after the diffusion into the nucleus cisplatin binds to the DNA and forms cisplatin-DNA adducts leading to DNA damage. The formation of DNA adducts is due to the binding between cisplatin and to the Nitrogen (N) of purine bases, mainly guanosine residues.

Table 1.2. Marketed cisplatin derivatives, their advantages compared to cisplatin and clinial trials in which they were tested.

Cisplatin Derivative (marketed name)	Advantage	Clinical Trials number
Oxaliplatin (Eloxatin ™)	Improved water solubility	NCT00004126, NCT00217282
Carboplatin (Paraplatin ®)	Reduced nephrotoxicity and nausea	NCT00735878, NCT00387660
Satraplatin	Reduced drug resistance	NCT00370383
Nedaplatin	Reduced Nephrotoxicity	NCT04524299, NCT02643407

However, continuous, or multiple administrations of cisplatin, do not often result in successful treatment: patients who initially responded to treatment quickly become insensitive to the chemotherapy, resulting in treatment failure. Patients often relapse to the treatment owing to the development of resistance to the cisplatin-based therapy, which on a cellular level means that tumour cells fail to undergo apoptosis at clinically relevant drug concentrations. Several factors have been proposed to explain the mechanisms of cisplatin resistance in NSCLC(Howell et al., 2010), which include:

- a diminished accumulation of drug within the cells, that can be ascribed either to a decrease in drug uptake or to an increase in drug efflux (via the increase in the expression of efflux transmembrane pumps), or to both.
- a decreased interaction of the drug with its target (DNA) as a consequence of drug target alteration.
- drug inactivation due to the increased concentrations of intercellular thiols, to which cisplatin will bind.
- reduced activation of apoptotic pathways as a result of increased processing of drug-induced DNA damages.

The high frequency of cisplatin resistance occurrence has led to severe limitations in cisplatin clinical use. One promising route to reduce such cisplatin resistance is by exploiting non-coding RNA targeting therapeutics, especially microRNAs.

1.2 Non-coding RNA

In 2003, as a follow-up of the Human Genome Project intended to sequence the human genome, the ENCODE project (Encyclopedia of human genome) was initiated (Feingold et al., 2004). In 2012, results obtained from the ENCODE project revealed that most of the genome is transcribed into RNA, while only approximately 2% of the transcript encodes for proteins (Dunham et al., 2012). The remaining 98% is not inactive – as it was believed to be before the ENCODE project, in fact it was called "junk DNA" - but is composed of non-coding RNAs (ncRNA) that play a crucial role in the regulation of gene expression

According to their function, ncRNAs can be divided into housekeeping ncRNAs -ribosomal RNA (rRNA), transfer RNA (tRNA) and regulatory ncRNAs. Based on the number of bases, regulatory nc-RNA can be further divided into two classes: small ncRNA having approximately 20-200 nucleotides (nt) and long non-coding RNA (lncRNA) >200 nt (**Figure** 1.4). The former group include microRNAs (miRNAs), one of which is the focus for this project.

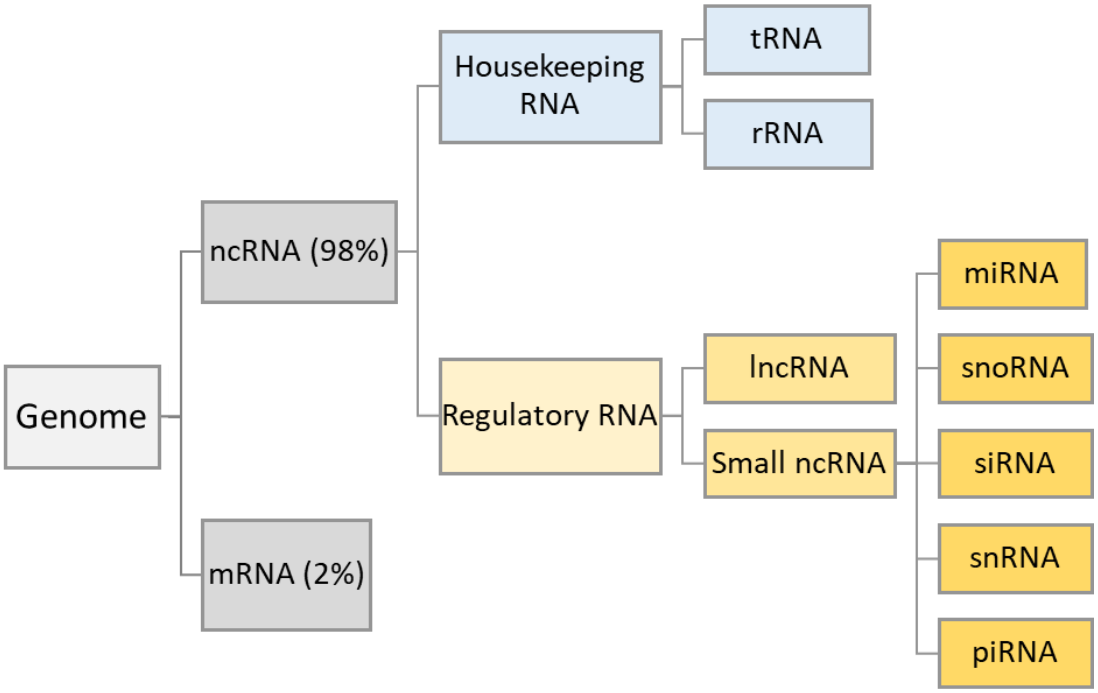

Figure 1.4 Classification of Genomic RNA. Only 2% of the genome is composed of messenger RNA (mRNA) that directly encodes for proteins, while the remaining 98% is composed of regulatory ncRNA. Those can be further classified into housekeeping RNA (tRNA and rRNA) and regulatory RNA (lncRNA, miRNA, snoRNA, siRNA, snRNA, piRNA).

1.2.1 MicroRNAs

MicroRNAs (miRNA) are the most studied class of small ncRNAs. In 1993 Lee et al discovered a non-protein coding gene in *Caenorhabditis elegans*, called lin-4, which produced a single stranded, 22 nt-long ribonucleic acid (RNA) molecule (Lee et al., 1993). The RNA molecule was found to directly supress translation of lin-14 mRNA by partially binding to the 3′ untranslated region (3′ UTR) in an antisense manner leading to a reduction in protein level (Lee et al., 1993; Wightman et al., 1993). Another regulatory ncRNA called let-7 was discovered in *C. elegans* in 2000: same as lin-4, let-7 was involved in the regulation of lin-14 expression (Reinhart et al., 2000). Shortly after let-7 identification, studies by Pasquinelli *et. al* showed its conservation across many species including humans (Pasquinelli et al., 2000). Therefore, in order to distinguish these RNAs from the other classes of regulatory RNAs, they were termed microRNAs (miRNAs) (Lagos-Quintana et al., 2001; Lau et al., 2001)

The biogenesis of miRNAs is a multi-step process that starts in the nucleus with the action of RNA polymerase II (Borchert et al., 2006), which transcribes double-stranded primary-miRNAs (pri-miRNAs) from the human genome (Cai et al., 2004), followed by its transformation in pre-miRNAs by DROSHA-DGCR8 complex (Han et al., 2004). Exportin-5 and RAN-GTPase then transport the newly synthesized pre-miRNA from the nucleus to the cytoplasm (Y. Zeng & Cullen, 2004). Here, the RNase II enzyme Dicer removes the hairpin loop from the pre-miRNA, releasing the 22-ns double stranded miRNA (ds-miRNA) (Chendrimada et al., 2005; MacRae et al., 2007). The dsRNA can then bind Argonaute 2 (Ago2) (Khvorova et al., 2003) which is included in the RNA-induced silencing complex (RISC complex) and therefore forming the miRNA-containing-RNA-induced silencing complex (miRISC) (Chendrimada et al., 2005). During miRISC assembly, one strand (named “guide strand”) is retained within the RISC complex to recognize the target mRNA (Kobayashi & Tomari, 2016) while the other strand (named “passenger strand” or miRNA*) is traditionally known to undergo degradation, although many recent studies demonstrates that it can also regulate gene expression (Finnegan & Pasquinelli, 2013; Havens et al., 2012; S. Yang et al., 2011). The region in miRNA responsible for its function is called ‘seed’ region, usually conserved within nucleotide residues 1-8 at the 5′ end of the miRNA. This region is essential for the binding of the guide strand to the complementary target mRNAs 3′ UTR (Bartel, 2009) via Watson-Crick interactions. Binding of the seed region with the target mRNA 3′ UTR represents the crucial step of miRNA protein expression regulation. As a matter of fact, miRNA-mRNA binding in the presence of AGO2 leads to translational repression through mediating cleavage and/or

degradation of the target mRNAs (Decker & Parker, 2012; Eichhorn et al., 2014; Winter et al.,2009) (**Figure** 1.5).

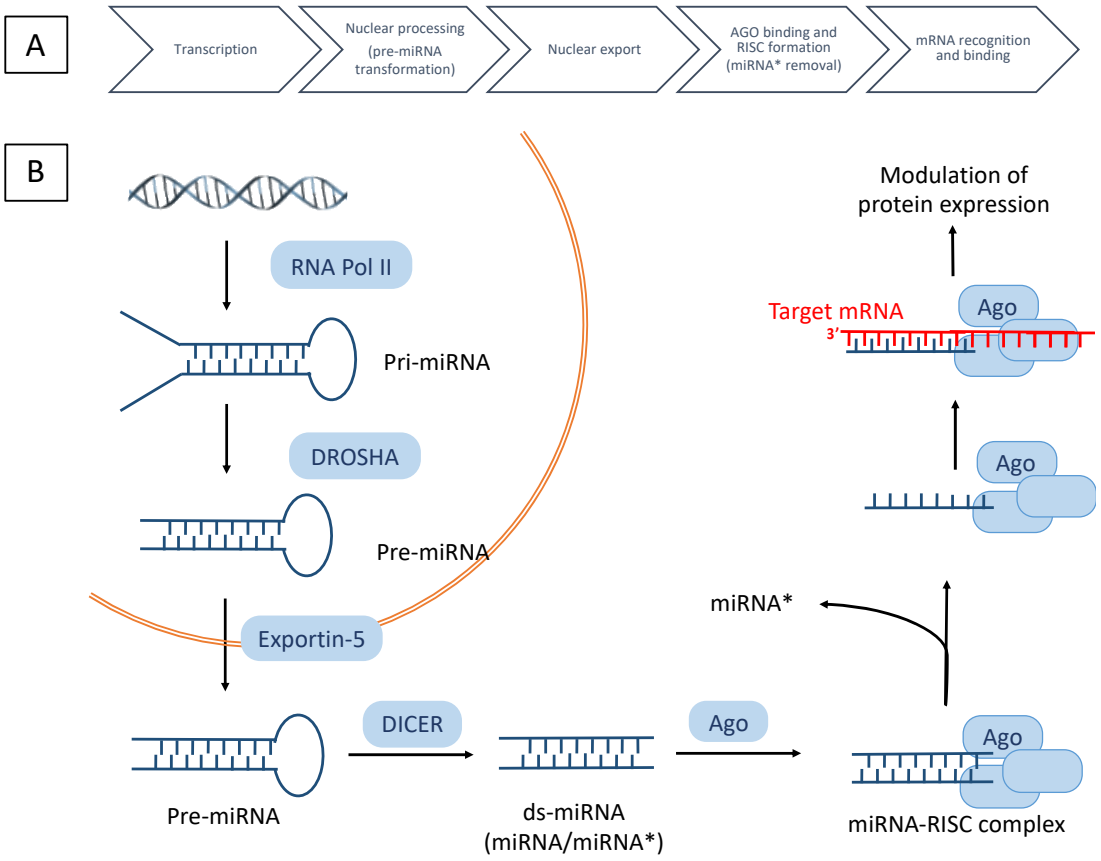

Figure 1.5 miRNA biogenesis and mode of action. (A) schematic summary of the steps of miRNA biogenesis; (B) diagram representing DNA biogenesis starting from its transcription in the nucleus to mRNA binding and protein expression modulation.

1.2.1.1 MicroRNA in lung cancer

The first evidence for miRNA involvement in cancer came from Calin and colleagues (Calin et al., 2002a), while the first study reporting the involvement of miRNAs in lung cancer was carried out by Takamizawa (Takamizawa et al., 2004). The study was conducted on 143 NSCLC samples from patients that had a follow up of at least five years after lung cancer resection. Results revealed that the samples could be divided into two groups: one cluster presenting reduced expression of let-7 and a second cluster presenting higher levels of let-7. The first group also showed a significantly shorter survival compared to the latter group, thus providing the first evidence of correlation between miRNA alteration and poor survival in lung cancer. In addition, *in vitro* study on A549 (NSCLC ADC cell line) with overexpressed let-7 inhibited lung cancer growth confirming the crucial role played by let-7 in lung cancer progression (Takamizawa et al., 2004). A subsequent profiling study in SCLC cells (ACC-LC-172, SK-LC-2) and NSCLC cells (Calu-6, epithelial cell line; PC-10 and ACC-LC-176, SCC cell line) observed the overexpression of a miRNA cluster (miR-17-92 cluster) in SCLC cells and in the majority of the NSCLC phenotype (Hayashita et al., 2005). The overexpression of the miR-17-92 cluster in A549 significantly improved cells growth and therefore, the overexpression of miR-17-92 cluster was related with lung cancer progression.

The "hallmarks of cancer", which defines the biological capabilities acquired during the multistep development of human tumours are: sustaining proliferative signalling, evading growth suppressors, resisting cell death, enabling replicative immortality, inducing angiogenesis, activating invasion and metastasis, reprogramming energy metabolism, evading immune destruction and ability to generate genome instability and mutation (Hanahan & Weinberg, 2011). Results from several studies have reported the role played by miRNA in every stage of lung cancer genesis and development (Ghafouri-Fard et al., 2020). Table 1.3 summarises the most studied miRNA involved in lung cancer related to the hallmarks in which they are involved with linked references.

One of the most intensively studied RNA is miR-21, and its role as tumour promoter (oncogene) was proven in lung cancer. The upregulation of miR-21 was correlated with poor survival within patients, hence suggesting its role as oncogene. This hypothesis was then confirmed by studies revealing PTEN (Xue et al., 2016), PDCD4 (Jiang et al., 2017) and HIF1-α (Pezzuto & Carico, 2018; Semenza, 2003), which are well known tumour suppressor genes, as direct targets of miR-21 in lung cancer. In addition, miR-21 was found to be involved in chemotherapy resistance, particularly in cisplatin resistance (Dong et al., 2019; L. Xu et al., 2014). For example, the expression of SMAD7, one of the proteins activated following

cisplatin-dependent DNA damage was repressed by miR-21 (Karger et al., 2016). Moreover, miR-21 upregulation was found not only in lung cancer tissue samples, but also in plasma (Liu et al., 2017) and serum samples (W. Zhao et al., 2015) of patients. Thus, suggesting the potential of miR-21 as a tool for lung cancer diagnosis.

Recent studies have suggested that miR-199a-3p acts as a tumour-suppressor in lung cancer, with Calu-3 (epithelial ADC cell line) cells and PC9 (ADC cell line) cells presenting lower levels of miR-199a-3p and showing increased cell proliferation compared to controls. Moreover, *in vivo* studies performed by the same group reported that BALB/C mice transfected with Calu-3 cells and treated with miR-199a-3p mimic resulted in the inhibition of tumour growth compared to control (H. Liu et al., 2021). Furthermore, findings by Guo revealed that miR-374a-5p was responsible for tumour proliferation and migration. The miR-347 was downregulated in NSCLC cells compared to normal cells, and the overexpression of miR-374-5p in A549 cells was responsible for a decrease in cell proliferation and in the ability of cells to migrate (Guo et al., 2021). In addition, a study carried out by Wei revealed that miR-550a-3-5p was significantly upregulated in exosomes isolated from the plasma of lung cancer patients with brain metastasis (Wei et al., 2021). Thus, could be further investigated to reveal the involvement of miR-550a-3p-5p in the development of brain metastasis in lung cancer patients and a potential way to prevent their formation.

Table 1.3 miRNA involved in lung cancer and their role linked to the "cancer hallmark", as defined by Hanahan et. Al (Hanahan & Weinberg, 2011).

cancer hallmark	miRNA involved	up/down-regulated	description	References
sustaining proliferative signaling	miR-96	downregulated	It targets and downregulates Anaplastic lymphoma kinase (ALK) expression, which is involved in the initiation of Ras and PI3K apoptotic pathways	(Vishwamitra et al., 2012)
	miR-760	downregulated	It suppresses non-small cell lung cancer proliferation and metastasis by targeting (and inhibiting the expression of) ROS1, involved in the ROS1/Ras/Raf/MEK/ERK pathway	(W. Wang & He, 2020)
evading growth suppressor	miR-15a /miR-16a	downregulated	miR-15a and miR-16 targets are G1 cyclines: when downregulates (in the presence of overexpressed miR-15 and miR-16) would promote cell cycle arrest	(Bandi et al., 2009)
	miR-641	downregulated	Its upregulation would decrease MDM2 and therefore increase of p53 pathway enhancing apoptosis	(Kong et al., 2018)
resisting cell death	miR-184	downregulated	BCL-2 upregulation is responsible for apoptosis inhibiton and cisplatin resistance occurrence	(Tung et al., 2016a)
	miR-130-b	upregulated	MicroRNA-130b promotes lung cancer progression via PPARγ/VEGF-A/BCL-2-mediated suppression of apoptosis	(Tian et al., 2016)
enabling replicative immortality	miR-29	downregulated	Its overexpression leads to restore of DNA methyltransferase patterns, resulting in control of expression of methylation-silenced tumour suppressor genes therefore tumour-suppressive effect.	(Ling et al., 2013)

cancer hallmark	miRNA involved	up/down-regulated	description	References
inducing angiogenesis	miR-126	downregulated	Its upregulation leads to angiogenesis inhibition via targeting VEGF-A	(Liu et al., 2009)
	miR-494	upregulated	Promotes angiogenesis via targeting and lowering PTEN expression, a VEGF suppressor.	(Wang et al., 2015)
activating invasion/metastasis	miR-200 family	downregulation	involved in the epithelial-to-mesenchymal transition process. miR-200 downregulation enhances lung cancer cells motility and metastasis formation via targeting PDL-1 and CD8+T cell immunosuppression and metastasis formation.	(Chen et al., 2014)
reprogramming energy metabolism	miR-144	downregulated	Leads to upregulation of GLUT-1 and hence glucose uptake	(LIU et al., 2016)
	miR-31-5p	upregulates	It downregulates the inhibitor of HIF-1a, therefore enhancing glycolysis and cell survival	(Zhu et al., 2019)
evading immune destruction	miR-34a	downregulated	suppresses PDL-1 expression	(Cortez et al., 2015)
	miR-197	downregulated	suppresses PDL-1 expression	(Fujita et al., 2015)
generate genome instability	miR-128-3p	upregulated	It targets (and therefore downregulates) SPTAN1, protein responsible for causing acceleration of chromosomal instability and cell cycle arrest	(Zhang et al., 2017)
	miR-21	upregulated	Downregulates tumour suppressor PTEN stimulating growth and invasion.	(Zhang et al., 2010)

1.2.1.2 MicroRNA-184

MiR-184 was observed to play a crucial role in neuroblastoma, (Y. Chen & Stallings, 2007), squamous cell carcinoma of the tongue (Wong et al., 2008), hepatocellular carcinoma (Wu et al., 2014), glioma (Malzkorn et al., 2010), nasopharyngeal carcinoma (Zhen et al., 2013), colorectal cancer (Wu et al., 2017) and clear-cell carcinoma (Huang et al., 2016). Several studies linked miR-184 with the progression of lung cancer, and with occurrence of cisplatin resistance. The relevant published studies highlighting the role of miR-184 in lung cancer and in cisplatin resistance are summarised in Table 1.4.

A seminal study by Liu on NSCLC cell lines A549 and SPCA-1 revealed a decrease in cell proliferation following miR-184 mimic treatment, while transfection of miR-184 inhibitor determined an increase on cell growth instead. In addition, c-myc, an upstream regulator of cell-cycle, was evaluated as direct target of miR-184. Transfection of miR-184 mimic resulted in decreased expression of c-myc while transfection of miR-184 inhibitor resulted in upregulation of c-myc. In conclusion, the study firstly observed the downregulation of miR-184 in lung cancer tissues, identified c-myc as its direct target and responsible for tumour proliferation *in vitro* (Liu et al., 2014).

Similarly, Lin investigated miR-184 expression in 124 samples from NSCLC patients revealed miR-184 downregulation compared to normal tissues. The transfection of A549 and TL-1 cells with miR-184 precursor significantly decreased cell proliferation, while the opposite was observed when cells were transfected with miR-184 inhibitor. Moreover, similarly to Liu, the study observed that c-myc was direct target of miR-184 (Lin et al., 2015).

In addition, Pan analysed miRNA array data from the GEO database and investigated the interaction network of several miRNAs, including miR-184, in smoker and non-smoker groups of NSCLC patients. The analysis revealed that among other miRNAs, miR-184 was showing the largest difference in expression in the two groups. They observed that down regulation of miR-184 expression was linked to increased expression of Akt2 protein and subsequent activation of PI3K-Akt2 pathway leading to increased cell survival (Pan et al., 2019).

Moreover, miR-184 was also found to be a potential biomarker for lung cancer diagnosis and to predict response to treatment with gefitinib, an EGFR inhibitor. To this extent Ding investigated miR-184 levels in serum of NSCLC patient before and after gefitinib treatment and compared it to control patients, observing a significant decrease in miR-184 expression in patients compared to control group. Furthermore, they compared miR-184 expression to the outcome of gefitinib treatment. Their outcomes revealed the presence of increased miR-184

levels in samples of patients responding to the treatment, while a further decrease of miR-184 was witnessed in non-responsive patients, compared to serum levels before treatment (Ding et al., 2020). Likewise, the study by Li proved the potential of miR-184 as a biomarker for Osimertinib resistance. Analysing miR-184 levels in exosomes of Osimertinib-resistant (H1975-OR) and Osimertinib-sensitive (H1975) cells, and in sample of NSCLC patients before and after the appearance of osimertinib resistance, their finding reported an increase in miR-184 levels in exosomes of both Osimertinib-resistant cells and samples of patients after developing drug resistance (X. Li et al., 2021).

Thus, the above studies underlined a strong correlation between miR-184 downregulation and cell proliferation and metastasis formation, emphasising the potential of miR-184 as a target for the development of a novel therapeutic approach for lung cancer treatment. Moreover, an additional side of the involvement of miR-184 in lung cancer is represented by the potential investigation of miR-184 levels in serum as molecular biomarkers for lung cancer diagnosis and for prediction of treatment outcomes (Ding et al., 2020; X. Li et al., 2021) (Table 1.4).

Table 1.4. Summary of studies investigating the role of miR-184 in lung cancer.

Reference	miR-184 levels	Target identification	Outcome of the study
(Zhen Liu et al., 2014)	downregulated	c-myc	miR-184 downregulation increased cell proliferation
(Lin et al., 2015)	downregulated	c-myc	miR-184 mimic treatment inhibits cell proliferation and invasion capability of NSCLC cells
(Tung et al., 2016a)	downregulated	BCL-2	miR-184 downregulation Confers cisplatin resistance
(Pan et al., 2019)	downregulated	Akt2	miR-184 downregulation was responsible of increasing the expression of Akt2, therefore increasing cell survival
(Longqiu et al., 2020)	downregulated	Splicing factor 1 (SF-1)	downregulation of miR-184 enhances cell proliferation and promotes cisplatin resistance
(Ding et al., 2020)	downregulated		Serum miR-184 levels can potentially be used as molecular markers to diagnose NSCLC
(X. Li et al., 2021)	upregulated in exosomes		The expression levels of miR-184 derived from exosomes in the peripheral blood of NSCLC patients could be used as biomarkers to indicate osimertinib resistance.

1.2.1.3 MicroRNA-184 and cisplatin resistance in lung cancer

Mounting studies demonstrated the role of miR-184 in the occurrence of resistance to chemotherapeutic agents in cancer. The connection between miR-184 and the occurrence of drug resistance in lung cancer was observed for gefitinib (Ding et al., 2020) and osimertinib (X. Li et al., 2021; Vadla et al., 2022), and discussed in section 1.2.1.2. Moreover, two independent studies demonstrated the direct involvement of miR-184 with cisplatin resistance in NSCLC cells (Longqiu et al., 2020; Tung et al., 2016).

Tung demonstrated that cisplatin resistance in TL-1 cells was dependent on miR-184 expression and conferred by E6 oncoprotein. Firstly, the study showed that miR-184 was downregulated in TL-1 cells compared to control cells (being TL-10 cells) while E6 expression was considerably higher in TL-1 cells. Secondly, the study investigated the influence of miR-184 on cisplatin sensitivity. The IC50 of cisplatin was calculated for cisplatin alone and following miR-184 upregulation or downregulation, that was obtained either via miR-184 mimic/inhibitor transfection, or via E6 oncoprotein silencing/overexpression. Their findings revealed a significant decrease in cisplatin IC50 following miR-184 upregulation. Thus, highlighting that miR-184 downregulation might confer cisplatin resistance in lung cancer cells. Moreover, the study demonstrated that miR-184 may confer cisplatin resistance via targeting BCL-2: low levels of miR-184 were concomitant to high expression of BCL-2, which role is to inhibit intrinsic apoptosis pathway activation (Youle & Strasser, 2008). Thus, the high expression of BCL-2 would promote cell proliferation and determine the increase in the IC50 value of cisplatin. The *in-vitro* findings were backed-up by investigation of miR-184 and BCL-2 levels in NSCLC samples from 139 patient, of which 59 showed high E6, low miR-184 and high BCL-2 expression. The same 59 patient showed unfavourable response to cisplatin treatment compared to the others employed in the study (Tung et al., 2016).

A study carried out by Longqiu also associated miR-184 downregulation with the occurrence of cisplatin resistance (Longqiu et al., 2020). The correlation between the long non-coding RNA myocardial infarction-associated transcript (MIAT), miR-184 and cisplatin resistance was assessed in tissues from NSCLC patients. In lung cancer tissues, MIAT resulted to be overexpressed compared to lung tissues. Subsequently, the activity of MIAT as miR-184 sponge was predicted by bioinformatics databased (Starbase v2.0, miRcode, TargetScan) and investigated by analysing miR-184 expression in H1299-CDDP cells, a cisplatin resistant lung cancer cell line. Following silencing of MIAT, a significant increase in miR-184 was observed. Moreover, MTT assays conducted in H1299-CDDP cisplatin-resistant cells after MIAT silencing revealed a decrease in cell proliferation thus confirming MIAT to act as miR-184 sponge. The downregulation of miR-184 (via MIAT sponging) and its involvement in regulating cisplatin sensitivity was also assessed *in vivo*. Mice were inoculated with either H1299-CDDP or with MIAT-silenced H1299-CDDP cells, and treated with controls (no cisplatin, PBS) or cisplatin. In H1299-CDDP inoculated mice, tumour weight and size diminished after cisplatin treatment compared to control, while in MIAT-silenced H1299-CDDP treated mice, cisplatin treatment resulted in a further decrease of tumour growth. Altogether, these findings showed a

significant role played miR-184 in enhancing cisplatin sensitivity of NSCLC (Longqiu et al., 2020).

Therefore, the evidence provided by the studies reported above suggest a central role played by miR-184 in the determination of cisplatin resistance in NSCLC, ascribing the occurrence of cisplatin resistance to the low expression of miR-184 and to a consequent increased expression of anti-apoptotic genes such as BCL-2.

1.2.2 MicroRNA therapeutics

Given the central role played by miRNA in the development of several pathologies, targeting miRNAs has emerged as a promising tool for the treatment of various diseases including several types of cancer (Slaby et al., 2017), infective pathologies, cardiovascular and respiratory diseases (Poller et al., 2018). The development of miRNA-based therapeutics is based on the logic of restoring miRNA expression to non-pathogenic levels, via either replacing downregulated miRNA or depleting upregulated miRNAs. The most studied and promising approach to target miRNAs is achieved by oligonucleotide-based therapeutics, as they can interact with their targets via Watson-Crick base paring. Synthetic oligonucleotides mainly employed include antisense oligonucleotides (ASO), double-stranded RNAs (dsRNAs), small interfering RNA (siRNA), short hairpin RNA (shRNA), miRNA mimics, miRNA sponges, and others (Khvorova & Watts, 2017).

Strategies used to target miRNA employing oligonucleotide-based therapeutics can be classified as miRNA mimicry and miRNA inhibition. The former consists in the delivery of miRNA mimics, synthetic oligonucleotides having a sequence that is identical to the target miRNA and therefore it is useful to replenish downregulated miRNA. On the other hand, miRNA inhibition encompasses the use of synthetic oligonucleotides which can inhibit or block the function of over-expressed miRNAs such as (a) ASOs, having a sequence that is complementary to one of the target miRNAs they are able to bind with miRNA and prevent them from exerting their action, and (b) miRNA sponges, molecules that can sequester miRNA within their structure and hence avoid miRNAs binding to their targets (Rupaimoole & Slack, 2017).

At present at least 15 RNA-based therapeutics which have been approved by the FDA or the EMEA (**Table** 1.5) and majority of them are based on miRNA inhibition.

Table 1.5 List of oligonucleotide therapeutics as of Jun 2022 (according to the website https://www.fda.gov/drugs/new-drugs-fda-cders-new-molecular-entities-and-new-therapeutic-biological-products/novel-drug-approvals-2022). The table also reports modification in the structure, company marketing them, indication, administration and approval year of FDA-approved oligonucleotide based therapeutics.

oligonucleotide type	Name	Modification	Company	indication	Administration	approval year
ASO	Kynamro (Mipomersen)	2'-MOE	Ionis Pharmaceuticals	Hypercholesterolemia	subcutaneous	2013
ASO	Tagsedi (Inotirsen)	2'-MOE; GalNac-conjugated	Ionis Pharmaceuticals	TTR-mediated amyloidosis	subcutaneous	2018
ASO	Waylivra (Volanorsen)	2'-MOE	Ionis Pharmaceuticals /Akcea	Familiar chylomicroenemia syndrome	subcutaneous	2019
ASO	Vyondys 53 (Golodirsen)	2'-MOE, PMO	Sarepta Therapeutics	Duchenne muscular dystrohy	subcutaneous	2019
ASO	Amondys 45 (Casimirsen)	PMO	Sarepta Therapeutics	Duchenne muscular dystrohy	subcutaneous	2021
siRNA	Givlaari (Givosiran)	2-F'/2'-MOE; GalNac-conjugated	Alnylam Pharmaceuticals	Acute hepatic porphyriasis	subcutaneous	2019
siRNA	Oxlumo (Lumasiran)	2-F'/2'-MOE; GalNac-conjugated	Alnylam Pharmaceuticals	Primary hyperoxaluria type 1	subcutaneous	2020
siRNA	Leqvio (inclisiran)	2-F'/2'-MOE; GalNac-conjugated	Alnylam Pharmaceuticals/Novartis	Hypercholesterolemia	subcutaneous	2021

oligonucleotide type	Name	Modification	Company	indication	Administration	approval year
siRNA	AMVUTTRA (vutisiran)		Alnylam Pharmaceuticals/Novartis	hereditary TTR-mediated amyloidosis	subcutaneous	2022
ASO	Vitravene (fomivirsen)	PT	Ionis Pharmaceuticals	Cytomegalovirus infection	intravitreal	1998 (withdrawn 2002)
ASO	Exondys 51 (Eteplirsen)	2'-MOE, PMO	Sarepta Therapeutics	Duchenne muscular dystrohy	intrathecal	2016
ASO	Spinraza (Nusinirsen)	2'-MOE	Ionis Pharmaceuticals	Spinal muscular atrophy	intrathecal	2016
RNA	Comirnaty (Tozinameran)		BioNTech/Pfizer	COVID-19	intramuscular	2020
RNA	MRNA-1273		Moderna/NIAD?BARDA	COVID-19	intramuscular	2020
siRNA	Onpattro (Patisiran)	2-F'/2'-MOE	Alnylam Pharmaceuticals	TTR-mediated amyloidosis	intravenous	2018
ASO	Viltolarsen (Viltepso)	2'-MOE, PMO	NS pharma	Duchenne muscular dystrohy	intravenous	2020

1.2.2.1 Oligonucleotide therapeutics for lung cancer

To date, the marketed oligonucleotide therapeutics are not intended to be used for lung cancer. However, some promising candidates based on miRNA mimicry reached the clinical stage of drug development for lung cancer treatment, providing encouraging outcomes.

The miRNA therapeutic named MR34, a lipid nanoparticles formulation of miR-34a, reached clinical trial stage for treatment of several malignancies including lung cancer. Although the study was withdrawn due to adverse effects in majority of the patients involved in the study, the encapsulation of miR-34 in the lipid formulation was key to promote miR-34 therapeutic effect (Beg et al., 2017; Hong et al., 2020). MiR-34 was demonstrated to be downregulated in several type of malignancies such as lung, liver, skin, prostate and breast cancer (Bader, 2012), and its low expression was correlated with survival enhancement via targeting mRNA of proteins involved in apoptosis (such as p53, c-MET (Hong et al., 2020) and BCL-2) and tumour immune evasion (such as PD-L1(Cortez et al., 2015)). Following promising results obtained *in vitro* and *in vivo*, demonstrating miR-34 replacement ability to reduce cell proliferation, migration and invasion, clinical phase I study on MRX34 in patients with refractory advanced solid tumours (liver cancer, NSCLC, lymphoma, melanoma, multiple myeloma, or renal cell carcinoma) started in 2013 (NCT01829971). However, the study terminated in 2016 due to the occurrence of five serious immune-related adverse event (Hong et al., 2020). In 2016 a Phase I clinical study to investigate the benefits of MRX34 in melanoma was initiated, though it was withdrawn few months later due to the emerging results obtained from the previous Phase I clinical study (NCT02862145).

Moreover, another miRNA mimic therapeutic reaching clinical study stage was miR-16 mimic formulated within bacterial-derived nanocells systems (NCT02369198). Outcomes from the Phase I clinical study in patients with NSCLC and malignant pleural mesothelioma reported partial response in one patient (out of the 27 involved in the study) that lasted for a period of 32 weeks. However, even though results were encouraging, the study presented limitations such as the impossibility to confirm miR-16 knockdown due to the lack of after-treatment tissue biopsy that led to the termination of the investigation of safety and tolerability of the drug (van Zandwijk et al., 2017).

In addition, G3139 (NCT00005032), AZD4785 (NCT03101839), OGX-011 (NVT00471432), AEG35156 (NCT005558922), EDM1201081 (NCT01040832), ELI-002 (NTC04853017), AZD8701 (NCT04504669) are example of ASO currently under clinical investigation for lung cancer treatment.

1.2.3 Challenges in oligonucleotides delivery

One of the major limitations of oligonucleotide therapeutics translation from bench to bedside relates to oligonucleotide delivery. Systemically delivered oligonucleotide face challenges soon after injection. In particular, the first obstacle oligonucleotides face is nuclease degradation that can drastically reduce their bioavailability (Jason et al., 2004). Moreover, the presence of exogenous nucleic acids in the blood stream triggers the innate immune response due to the interaction with pattern recognition receptors, including membrane-bound Toll-like receptors (TLRs) or cytosolic retinoic-acid inducible gene I (RIG-I) family receptors (Dorner et al., 2009). In addition, oligonucleotides are subject to rapid renal clearance (Juliano, 2016). One additional factor to be considered is the poor specificity of oligonucleotides to target tissues leading to the occurrence of adverse side effects (Geary et al., 2015).

Plasma proteins play a crucial role in oligonucleotides bioavailability, as binding prevents them from being rapidly excreted by glomerular filtration: hence in the development of novel oligonucleotide therapeutics plasma protein binding is a key factor to consider avoiding rapid excretion and failure of therapeutic action

In addition, regardless of the administration route chosen, oligonucleotide must reach the target tissues intact. Here they would exert the desired activity providing they are internalised (usually via endocytosis) in the cell of interest, reach the right intercellular compartment (nucleus or cytoplasm), avoid lysosomal degradation and avoid exocytosis mechanisms. Therefore, numerous improvements have been applied to oligonucleotides to provide better therapeutic outcomes and increase the possibility of translation of oligonucleotide-based therapeutics into clinic. Possible solutions to obtain successful oligonucleotide delivery include chemical modifications, beneficial to prolong their shelf life and to preserve the nucleic acid molecules from protein binding, nuclease and lysosomal degradation; conjugation of oligonucleotide with specific molecules such as lipids or other nucleic acids that can drive the oligonucleotide to tissue of interest, such as the N-acetylgalactiosamine (GalNac) (Niar et al 2014) and complexation within nanoparticles (lipid-base NPs, polymeric-based NPs or novel biomimetic vectors) to improve targeted delivery, avoid degradation and promote cellular uptake.

1.2.3.1 Oligonucleotide modification

Early unmodified oligonucleotide-based therapeutics retained several issues that can be summarised into poor serum stability due to nuclease sensitivity, low uptake, low binding affinity towards their target, low tolerability due to unspecific targeting and immune-response triggering (Dhuri et al., 2020; Khvorova & Watts, 2017a; Rinaldi & Wood, 2018). Hence, with the purpose of developing more easily translatable oligonucleotide therapeutics, several modifications have been developed.

Phosphorothioate derivatives (PS-ASO or first generation ASO) were firstly generated by replacing the non-bridging oxygen in the phosphate group with a sulphur atom. PS-ASO modification resulted in improved ASO trafficking, improved cellular uptake and decreased sensitivity to nucleases (Eckstein, 2014). However, despite the advantages brought about by PS modifications, PS-ASO resulted in significantly lower binding affinity and in addition, they were still subject to nuclease degradation. The first oligonucleotide-based therapeutic employed and approved by FDA in 1998 was Fomivirsen, a PS-modified ASO used for cytomegalovurs (CMV) retinitis infections. The drug was withdrawn from the market due to low demand (Hutcherson & Lanz, 2002), however the high dosage needed to reach significant outcomes, revealed the need of additional modification to the oligonucleotide structure to further improve their pharmacokinetics and pharmacodynamics properties (**Table** 1.6).

Further modification imparted to ASOs (second generation oligonucleotides) involved the exploitation of the 2' position in the ribose molecule. The replacement of the -OH group (on RNA molecules) with a methyl group (resulting in 2'-OMe ASO) was used a starting point to produce ASO derivatives with improved target affinity and reduced nuclease sensitivity (Choung et al., 2006; Cummins et al., 1995). Following several variants of 2'-alkylated oligonucleotides, medicinal chemists agreed on the 2'-O-methoxyethyl (2'-MOE) modification being the best modification to provide the desired outcomes (Martin, 1995). Kynamro, a 2'-MOE ASO to treat hypercholesterolemia was the first oligonucleotide-based drug approved by FDA carrying such modification (McGowan et al., 2012). A large majority of the oligonucleotide-based drugs approved in the following year carry the 2-MOE modification, revealing its crucial role in advancing oligonucleotide therapeutics. In addition, the 2' position on the ribose molecule was further exploited to produce 2'-fluoro (2'-F) ASO derivatives with further improved binding affinity. In 2018 FDA approved Patisiran, a siRNA carrying a 2-F modification which is employed for the treatment of hereditary transthyretin-mediated amyloidosis (**Table** 1.5)

Third-generation ASOs were produced via modifications applied in the furanose ring of the ribose molecule, such as locked nucleic acid (LNA) molecules, peptide nucleic acids (PNA) (Nielsen et al., 1991) and phosphoroamidate morpholino oligomers (PMOs) (Nan & Zhang, 2018). The main advantage of third generation oligonucleotides is the reduction of ASO conformation flexibility that brings about a considerable improvement in ASO binding affinity to their target. As of March 2022, the latest oligonucleotide-based drug approved was Casimirsen, a PMO-ASO utilised for Duchenne muscular dystrophy revealing the promise of oligonucleotide modification in providing more effective therapeutics (Table 1.5).

The modification imparted to oligonucleotide therapeutics have been firstly developed and applied to ASO, however they have been extended to the other types of oligonucleotides therapeutics such as siRNA. At present, oligonucleotides therapeutics are designed with combinations of the mentioned modification (such as Golodirsen (Heo, 2020), Eteplirsen (Syed, 2016), and Vitolarsen (Dhillon, 2020)). The aim of combining more than one modification is to further improve their delivery, binding affinity, target recognition and to lower adverse effect occurrence.

Table 1.6 List of the most common chemical modification imparted to oligonucleotides. Modifications are divided according to the place on the oligonucleotide where they are imparted (sugar or backbone). The table also provides modifications description, and the advantages and disadvantages they brought about in the oligonucleotide therapeutic.

	Type	Description	Advantages	Disadvantages	Used for
BACKBONE MODIFICATIONS	phosphorotioate (PS)	non-bridging oxygen atom is replaced with suphur group	improve stability against nucleases; higher binding to plasma proteins (that can carry the oligonucleotide to the target site) hence improved pharmacokinetic properties; increased hydrophobicity	Lower binding affinity to mRNA targets	ASO
	phosphoester	neutral phopsphoester oligonucleotides are incorporated within siRNA hence they become prodrug called "short interfering ribonucleic neutral molecules"	massive RNAi response (due to the cleavage of phosphoester group once the molecule is internalized)		siRNA
SUGAR MODIFICATIONS	peptide nucleic acids (PNA)	sugar backbone is replaced with synthetic poly ethileneimine scaffold with nucleobase acetic acid connected to every second backbone nitrogen atom via amine bond	improve stability against nucleases and proteases; stronger affinity to RNA targets		siRNA ASOs
	2'-OMe	2'OH group of the ribose is replaced with 2'-methoxy group	higher affinity to RNA; higher stability against nucleases	still sensitive towards serum nucleases	
	2'-F	2'OH group of the ribose is replaced with 2'-fluoro	higher binding affinity		
	2'-MOE	2'OH group of the ribose is replaced with 2'-methoxyethoxy group	higher affinity to RNA; higher serum stability (however phosphorotioate still necessary for good stability in serum); higher miRNA inhibition activity		
	Locked Nucleic Acid (LNA)	2'OH group of the ribose is replaced with 2',4'-o-methylene bridge	highest RNA affinity (reached by reducing the conformational flexibility of nucleotides)	anti miRNA activity only slightly higher.	
combination of chemical modifications		more than one of the abovementioned modifications co-exist in the same oligonucleotide molecule	benefit of the combined modification together in one molecule		

1.3 Nanoparticles

The pioneers of the use of nanoparticles (NPs) for therapeutic application were Metchnikov and Ehrlich with their works on phagocytosis (Cooper, 2008) which led them to the Nobel Prize for immunology in 1908, it was only from the late 1970s that NPs studies developed, reaching more than 30,000 publications in 2021. Nanoparticles that are intended to be used for therapeutic applications, including diagnosis and treatment of various disease, are referred as "nanomedicine". The European Science Foundation's Forward Look Nanomedicine in 2005 defines nanomedicine as follows: "*Nanomedicine uses nano-sized tools for the diagnosis, prevention and treatment of disease and to gain increased understanding of the complex underlying patho-physiology of disease. The ultimate goal is to improve quality of life*" (Andersson, 2005).

The advantages brought about by the use of NPs as vehicles to deliver active ingredients are broad (De Jong & Borm, 2008; Fattal & Fay, 2021). Firstly, NPs can be produced starting from different material such as lipids (Lokugamage et al., 2021), natural and synthetic polymers (Risnayanti et al., 2018), metals (Hou et al., 2020), biologic material (Parodi et al., 2012) and using different methods (Calvo et al., 1997; Lee et al., 2011; Torbensen et al., 2021; Vauthier & Bouchemal, 2009). Thus, researchers have a broad range of possibilities to choose from to manufacture the best nanoparticle platform to suit their need. Secondly, the encapsulation of drugs within NPs allows the increase of drug solubility and stability in fluids, whilst decreasing its cytotoxicity and hence the occurrence of adverse effects. In addition, they can provide controlled release of the cargo (depending on the degradation rate of the polymer chosen) and targeted delivery. The latter is possible thanks to the presence in majority of the polymer used of reactive groups, that can be functionalised in order to prepare target-specific carriers (Yetisgin et al., 2020).

Although NPs are versatile, having characteristics that can be customized in relation to their application, and have shown many advantages in advancing treatment of several diseases (demonstrated by a large number of NPs-based therapeutics approved by EMA and FDA since 2005), the translation from laboratory to clinic still represents a major challenge. Traditional methods of NPs preparation can have significant batch-to-batch variations, leading to poor reproducibility of results and consequent difficulty in industrial production and market access (Hung et al., 2007; Stavis et al., 2018; Yin et al., 2014).

1.3.1 Nanomedicine for miRNA delivery

An effective delivery system for oligonucleotides is expected to protect oligonucleotides from the adsorption of serum proteins and degradation of nucleases, enhance tissue penetration, improve cell targeting and cell entry, as well as enhance intracellular bioavailability at the desired biological target. After entering the cells, the ideal NP system should ensure that the oligonucleotides can escape from the endosomes and enter the cytoplasm (Järver et al., 2012; Y. Sun et al., 2017).

As discussed in above sections (1.2.3, 1.2.3.1) the delivery of oligonucleotides represents the principal limitation to the development of oligonucleotide therapeutics. NPs is an additional delivery platform to further improve oligonucleotide pharmacokinetic properties and enhance their translation into clinic. NPs can adsorb or encapsulate miRNAs within various polymers, protecting them from enzymatic degradation and they are able to cross biological barriers – mainly via endocytosis - and enhance cellular uptake (Lee et al., 2019).

As discussed in section 1.2.2.1, even though there are no miRNA therapeutics approved to be used in humans, the two miRNA therapeutics that reached clinical studies (MRX34 and miR-16) were both NPs formulated oligonucleotides. Thus, this may highlight the potential in the use of NPs to overcome the major challenge in the translation of miRNA therapeutics from bench to bedside.

1.3.2 Nanotechnology for cancer targeting

Several strategies have been utilised by researchers to target cancer via nanotechnology. Active and passive targeting are the two main strategies employed to address cancer detection and treatment.

Passive targeting is based on the difference in composition of the tumour microenvironment in comparison with normal tissues. In particular, tumour tissues are characterised by larger pore-size than epithelial tissues. The manufacture of NPs with size up to 400 nm can be used to encapsulate drugs that are retained in the tumour tissue for a longer time than in healthy tissues This difference can be addressed by NPs that are able to penetrate into tumour tissues only and not into adjacent cells. (Ravar et al., 2016; Szczepanowicz et al., 2016). In addition, the enhanced permeability and retention effect (EPR) witnessed in tumours can be exploited. The EPR effect is based on the increased vascularisation of tumour tissues and diminished volume of fluids returned to the lymphatic system. Abraxane ® is a formulation of albumin NPs loaded with paclitaxel which was discovered to have a beneficial effect in reducing pancreatic cancer via targeting. Its effect was attributed to albumin binding to a receptor in

the surface of vascular endothelial cells, therefore exploiting the EPR effect on tumour cells (Hama et al., 2021).

On the other hand, the active targeting approach consists of NPs that are functionalised on their surface with molecules that can bind to specific molecules in tumour cells. Therefore, the effect of the drug loaded into the NPs is limited to the tumour cells only. One example is the preparation of NPs that are functionalised with Hyaluronic Acid (HA), which can bind to CD44, a cell membrane glycoprotein that regulates interaction, adhesion and migration of cells. CD44 is often upregulated in tumour cells, therefore NPs functionalised with HA were proved to provide a sustained release of Taxol into breast cancer cells, compared to free drug delivery (X. yan Yang et al., 2013).

1.3.3 Polymeric NPs for lung cancer treatment

Polymers are widely used for NPs preparation due to their innate properties, such as the versatility of structural conformations, biodegradability, and ease of synthesis, which have served to be beneficial for the design of polymeric NPs. In particular, cationic polymers have emerged as promising candidates for non-viral gene delivery systems, given they can be easily conjugated with genetic material via electrostatic attraction at physiological pH: the negative charges of nucleic acids will bind with the positive charges of polymeric chains (Lee et al., 2019). Such polymers include poly(l-lysine) (Kadlecova et al., 2013), poly(l-ornithine), linear and branched polyethyleneimine (PEI) (Von Harpe et al., 2000), diethylaminoethyl-dextran, poly(amidoamine) dendrimers (PAMAM), and poly (dimethylaminoethyl methacrylate). Moreover, natural polymers, such as chitosan, dextran, gelatin, pullulan, and their derivatives have also been explored (Rai et al., 2019).

Several factors can influence the ability of cationic polymers to carry nucleic acids, including their structure, molecular weight, and surface charge. Therefore, their flexible properties together with their facile synthesis, allow researchers to have a broad range of materials available to develop the best delivery system for the specific purpose.

One of the first research studies demonstrating miRNA delivery via NPs for lung cancer investigated the encapsulation of miR-145 mimic within NPs manufactured by modifying short branch polyethylenimine (PEI) with polyurethanes (PU): the negative charges of the oligonucleotide allowed the facile complexation with the positive charges of the polymer used. *In vitro* studies using patient-derived cells, revealed the promising effect of miR-145-

loaded PU-PEI NPs alone or in combination with cisplatin or radiotherapy to decrease cell proliferation and inhibit invasion. This was associated with elevation of miR-145 expression and downregulation miR-145 targets. *In vivo* studies in mice models previously inoculated with lung cancer cells and treated with miR-145 loaded PU-PEI NPs via intratumor injection, confirmed the results obtained *in vitro* and prolonged the survival of untreated tumour-bearing mice (Chiou et al., 2012) (Table 1.7).

Two separate studies modified PEI with hyaluronic acid (HA) and used it to prepare NPs carrying miR-34a (Trivedi et al., 2017) or miR-125b (Parayath et al., 2021). Both the studies highlighted the advantage of using HA, even though it was negatively charge and thus would potentially interfere with miRNA complexation. However, it was advantageous to modify PEI, with the facile chemical reaction between PEI positive charges and HA negative groups reduce PEI positive charges, that often resulted in cell membrane disruption and consequently severe cytotoxicity (Table 1.7).

More recent studies on polymeric NPs for miRNA cargo for lung cancer treatment were carried out by Maghsoudnia and Xing. The former indicated the successful inhibition of cell growth due to the delivery of let-7-loaded dendrimers into cells mitochondria (Maghsoudnia et al., 2020). The study firstly revealed the successful complexation of let-7 within poly(amidoamine) (PAMAM)-TPP dendrimers and within PAMAM-TPP hyaluronic acid (HA) modified dendrimers. Uptake studies by fluorescence microscopy revealed that both the dendrimers were uptaken via A549 cells and consequently, cytotoxicity study on A549 cells via Annexin-V/FITC flow cytometry assay reported an increase in apoptotic cells after treatment with let-7-PAMAM-TPP dendrimers. Additionally, mRNA expression study in A549 cells was investigated to identify potential targets of let-7: the study reported a decrease in KRAS expression and an increase in p-21 expression compared to controls, thus suggesting them to be potential targets of let-7 in A549 cells (Maghsoudnia et al., 2020) (Table 1.7).

The study by Xing demonstrated modification of PEI with N-isopropylacrylamide and the obtained polymer (PEN) was used to prepare NPs that could successfully complex miR-29a mimic and protect it against nuclease degradations. Fluorescence microscopy revealed an uptake of the PEN NPs comparable to Lipofectamine transfection (a commercially available transfecting reagent) of miR-29a into A549 cells. Cytotoxicity studies conducted by the group revealed an increase in the apoptotic rate in cells treated with PEN NPs loaded with miR-29a compared to controls (Xing et al., 2020) (Table 1.7).

The mentioned studies provide examples of how NPs can be beneficial in advancing the delivery of oligonucleotides to address lung cancer. Moreover, Table 1.7 provides a broader summary of pre-clinical studies on miRNA therapeutics delivered via polymeric NPs for lung cancer.

Table 1.7 Summary of nanomedicine studies focused on lung cancer treatment via the delivery of miRNAs complexed within polymeric NPs.

Reference	miR-involved	Polymer used	*in vitro/ in vivo*	delivery route (when *in vivo*)	outcome
(Chiou et al., 2012)	miR-145	PU-PEI	tissue samples/ *in vivo*	intratumoral	Reduced tumour growth and metastasis, sensitized tumours to chemoradiotherapies
(Trivedi et al., 2017)	miR-34a	HA-PEI and HA-PEG NPs	*in vitro* (A549)		induction of cell apoptosis
(Parayath et al., 2021)	miR-125b	hybrid PEI-Hyaluronic Acid NPs	*in vivo*	intraperitoneal	miR-125b is successfully delivered
(Maghsoudnia et al., 2020)	let-7	PAMAM dendrimers	*in vitro* (A549)		
(Xing et al., 2020)	miR-29a	N-Isopropylacrylamide-modified-PEI NPs	in vitro (A549)	intraperitoneal	anti-proliferative effect, inhibition of migration/invasion

1.3.4 Chitosan for miRNA delivery

Chitosan (CHT) is a polysaccharide composed of repeated glucosamine and N-acetyl-glucosamine units. It is obtained by alkaline deacetylation of chitin, which can be extracted from crustacean shells (Younes et al., 2015) or from fungi cell walls (Ghormade et al., 2017). Its properties include good biocompatibility, favourable biodegradability, low cytotoxicity, antibacterial and mucoadhesive properties (Abd El-Rehim et al., 2012; Kumirska et al., 2011; Matica et al., 2019; Muxika et al., 2017). Thus, unsurprisingly CHT has been employed by several researchers as starting material to produce NPs intended for oligonucleotide delivery (**Table** 1.8).

Due to the presence of protonated amino (NH_3^+) groups on its structure (**Figure** 1.6), CHT is positively charged at pH values used for pharmaceutical applications. This characteristic renders CHT suitable to complex with negatively charged molecules, such as oligonucleotides.

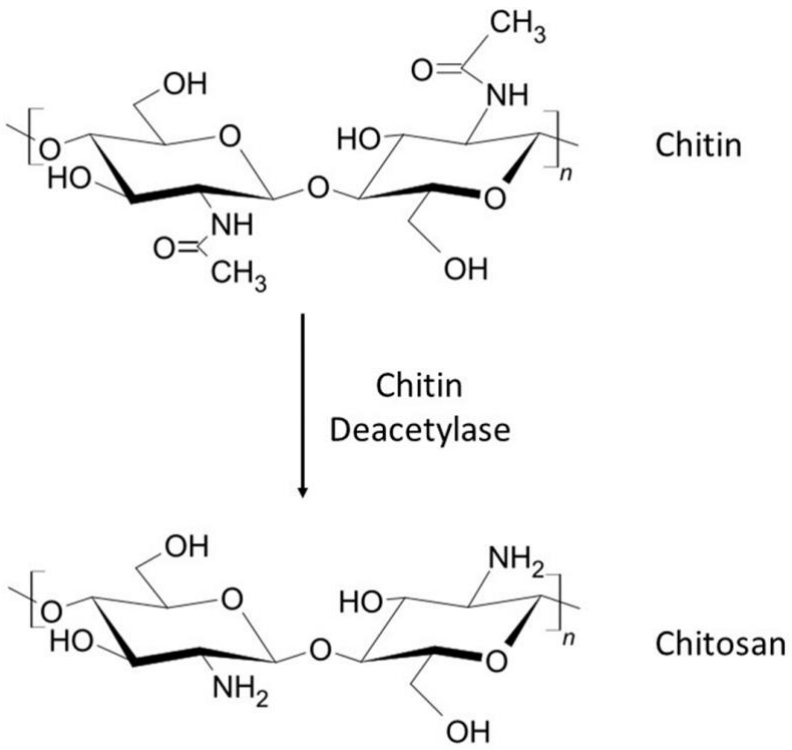

Figure 1.6 Chitin and chitosan structure. Chitosan derives from the deacetylation of chitin, which is extracted from natural sources as fungi cell walls or crustaceans.

The delivery of miRNA involved in the pathogenesis of cancer malignancies via CHT NPs has been investigated by several studies. Kaban investigated the delivery of miR-141 or miR-200c in breast cancer cell lines MCF-7, MDA-MB-231, and MDA-MB-435 (Kaban et al., 2016, 2017, 2019). Following assessment of the downregulation of the two oligonucleotides in cancer cell lines compared to normal breast cell line, the studies demonstrated the uptake of the CHT NPs loaded with miR-200 or miR-141 via confocal microscopy. Complete uptake of the CHT NPs was observed following 24 h of the treatment. Moreover, uptake of the NPs was confirmed by the upregulation of miR-141 or miR-200c levels via qPCR analysis. In addition, the blank NPs were not toxic, thus highlighting the safety use of CHT in formulation of NPs for therapeutic applications. On the other hand, a reduced cell viability was reported for loaded CHT NPs treated cells, as a further confirmation of the delivery of intact miRNA mimic into cancer cells. The study also assessed the efficacy of the miRNA-loaded CHT NPs on the expression of target genes VEGF and E-cadherin, which are proteins involved in the development of tumour metastasis. Even though results showed a slight decrease in the expression of VEGF and E-cadherin, the study reinforced the successful delivery of the NPs, while suggesting the effect of miR-200c and miR-141 on decreasing angiogenesis and the process of metastasis formation (Kaban et al., 2016, 2017, 2019).

Similarly, Santos Carballal performed a study involving the delivery of the hybridised miR-145-3p and miR-145-5p in MCF-7 breast cancer cell lines via CHT NPs (Santos-Carballal et al., 2015). Following successful complexation of the miRNA duplex within CHT NPs, the study confirmed NPs internalisation within the cells after 24 h. Moreover, the study compared the transfection efficiency of the loaded NPs to commercial transfection reagents and found comparable levels of target gene reduction (Santos-Carballal et al., 2015).

The efficacy of CHT as delivery system for miRNAs was also assessed in prostate cancer (Gaur et al., 2015a), ovarian cancer (Suardi et al., 2020; Ysrafil et al., 2020) and gastrointestinal stromal cancer (Tu et al., 2017). Findings from all the mentioned studies confirm the advantages of the use of CHT as carrier for miRNA mimics, such as successful internalisation, low cytotoxicity, effective mRNA downregulation. However, the use of CHT NPs carrying miRNAs to lung cancer cells has not been thoroughly exploited.

The safety and efficient gene silencing of CHT nanocarriers have been certified not only *in vitro*, but also *in vivo*, in mice injected with triple negative breast cancer cells (Deng et al., 2014b) and prostate cancer cells (Gaur et al., 2015), in mice macrophage cells (Nguyen et al., 2019) or in mice models with multiple sclerosis (Shamaeizadeh et al., 2022). The study by

Deng involved the treatment of tumour-bearing mice with miR-34 and DOX-loaded HA-CHT NPs delivered via tail-vein injection and resulted in a significant decrease in tumour size compared to control. Thus, confirming the efficient delivery of the oligonucleotide by CHT NPs (Deng et al., 2014). Likewise, Gaur delivered miR-34a-loaded CHT NPs or controls to prostate cancer-bearing mice via tail-vein injection. Mice were treated with miR-34a-loaded NPs or with controls (naked miR-34): results revealed that the delivery of miR-34a via CHT NPs considerably decreased tumour growth and increased apoptosis in comparison to naked oligonucleotide delivery, thus underline the beneficial effect of CHT NPs in preventing oligonucleotide degradation. Given the correlation between miR-34a downregulation and tumour progression in prostate cancer, the drop in tumour size reported by the study was interpreted as successful delivery of the oligonucleotide to the target (Gaur et al., 2015).

At present, there are only few studies in literature reporting successful use of miRNA-loaded CHT NPs for lung cancer treatment, which are discussed in section 1.3.4.2 (G. Huang et al., 2021; Nafee et al., 2007; Taetz et al., 2009; H. Z. Zhu et al., 2020).

1.3.4.1 Chitosan derivatives in miRNA delivery

The major limitation in the utilization of CHT is the poor solubility in water at physiological pH due to NH_3^+ groups protonation. Thus, improving chitosan structure by exploiting the hydroxyl (OH^-) and amino (NH_3^+) groups of chitosan was necessary to impart new properties to the polymer and to broaden its applications (Figure 1.7). The formation of chitosan salts such as chitosan hydrochloride (CS HCl) demonstrated improved chitosan solubility, while still retaining the polymer properties, in the delivery of miRNAs in breast cancer (Deng et al., 2014) and oral squamous cell carcinoma (Li et al., 2022). Deng prepared CHT NPs using CS HCl as polymer and tripolyphosphate (TPP) and hyaluronic acid (HA) as cross linkers and loaded the NPs with miR-34a mimic and DOX. Their finding revealed that utilising CS HCl still provided successful encapsulation of the oligonucleotide within the NPs. Moreover, the incubation of the loaded NPs with RNAase enzyme for 24 h resulted in preventing miRNA mimic degradation compared to naked miR-34a incubated with the enzyme. The study also proved successful NPs internalisation via confocal microscopy and increased miR-34a expression following loaded-NPs treatment. Additionally, the group observed decreased *in vitro* cell viability of MDA-MB-231 triple negative breast cancer cell line after treatment with miR-34a NPs, as well as no change in the percentage of viable cells treated with blank NPs (Deng et al., 2014) (Table 1.8).

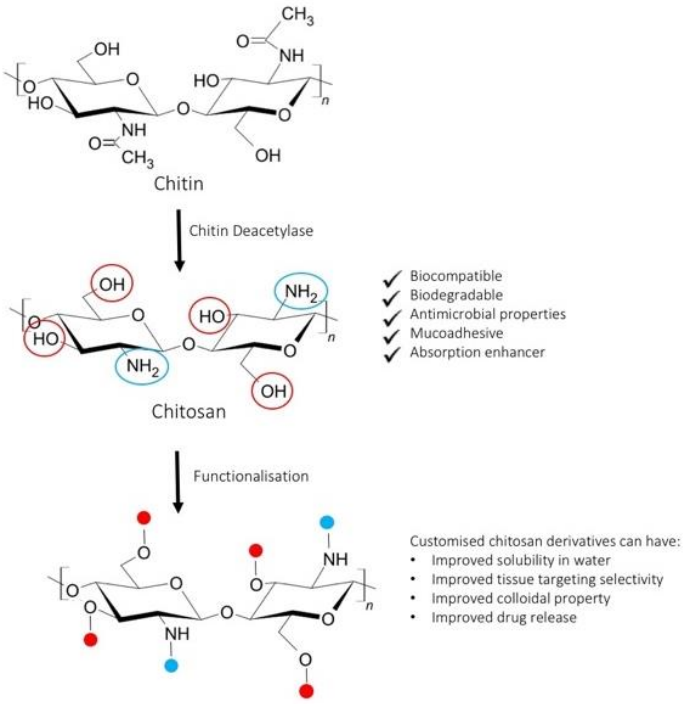

Figure 1.7 Formation of CHT derivatives. Exploiting OH^- and NH_3^+ on CHT molecule allows the formation of chitosan derivatives with improved properties.

Similarly, Li employed CS HCl to produce a biomimetic platform for the delivery of miR-144 and miR-145a, which are downregulated in oral squamous cell carcinoma (OSCC). Following complexation of CS HCl with the miRNA mimics, the NPs were coated with macrophage-derived exosomes. The formed nanoplatform based on CS HCl was able to protect the oligonucleotide from RNAase degradation, as well as to deliver miR-144 and miR-451 into OSCC cell lines. Therefore, altogether the results obtained by the above studies by Deng and Li suggested that the use of water-soluble derivatives brought about the advantages of improved solubility, while retaining chitosan properties of successful complexation with oligonucleotides and favourable uptake by cells.

In addition, *in vivo* assessments of the advantages of using CHT derivatives have been reported. The studies by Ragelle demonstrated that modifying chitosan with a small peptide (Arginine-Glycine-Asparagine), improved targeted delivery of miR-34a and its anti-cancer activity *in vivo*, in SiHa cells transfected mice (Ragelle et al., 2014; Héloïse Ragelle et al., 2016). Moreover, Park developed a chitosan derivatives named galactosylated-chitosan (GC) which was further modified by Ning (Ning et al., 2019; Yu et al., 2015) by grafting onto it the anticancer drug 5-fluorouracil to produce GC-FU. The obtained polymer was employed to

prepare NPs carrying miR-122, and its delivery was found to increase cellular apoptosis into hepatocellular cancer cells and to reduce metastasis formation *in vivo* (Park et al., 2003).

Together, these studies with water-soluble chitosan derivatives maintain the advantages of unmodified polymer together with improving its solubility properties. Therefore, the chemical modification of CHT to produce water-soluble derivatives represents a promising strategy to broaden CHT application in the pharmaceutical field (Table 1.8).

Table 1.8 List of published studies regarding the use of CHT NPs for the delivery of miRNAs.

Reference	Polymer used	miRNA loaded	Application	*In vitro/ex vivo*
(Ysrafil et al., 2020)	CHT medium molecular weight (mW)	miR-155-5p	Ovarian cancer	SKOV3 cells
(Suardi et al., 2020)	CHT medium mW	miR-155-5p	Ovarian cancer	SKOV3 cells
(Kaban et al., 2019)	CHT medium mW	miR-141	breast cancer	cell lines MCF-7, MDA-MB-231, and MDA-MB-435
(Kaban et al., 2016)	CHT medium mW	miR-200c	Breast cancer	cell lines MCF-7, MDA-MB-231, and MDA-MB-435
(Deng et al., 2014a)	CS HCl	miR-34a	Triple negative breast cancer	breast cancer cell lines MCF-7, MDA-MB-231, MDA-MB-435
(Z. Wang et al., 2016)	CS HCl	miR-21	Osteogenesis	human bone marrow mesenchymal stem cell
(K. Li et al., 2022)	CS HCl	miR-144 and miR-451a	Oral squamous cell carcinoma	UM-SCC083A and UPCI-SCC029B cell lines

Reference	Polymer used	miRNA loaded	Application	*In vitro/ex vivo*
(K. Li et al., 2022)	CS HCl	miR-144 and miR-451a	Oral squamous cell carcinoma	UM-SCC083A and UPCI-SCC029B cell lines
(Kaban et al., 2017)	CHT medium mW	miR-141	Breast cancer	breast cancer cell lines
(Tu et al., 2017)	CMC conjugated with tocopherol	miR-218	Gastrointestinal stromal tumour	GIST882 cell line
(Louw et al., 2016)	CHT with different mW	miR-124	Spinal cord injury	Cells isolated microglia cells from neonatal rat
(Gaur et al., 2015a)	Not stated	miR-34a	Prostate cancer	PC3 cells and mice injected with PC3MM2 cells
(Shamaeizadeh et al., 2022)	CHT low mW	miR-219a-5p	multiple sclerosis	Cells and mice models
(Santos-Carballal et al., 2015)	Not stated	miR-145-5p and miR-145-3p	Breast cancer	*In vivo* studies on mice models
(Nguyen et al., 2019)	CHT modified with PEG	miR-33	Cardiovascular diseases	C57BL6 wild-type (mice and peritoneal macrophages cells

1.3.4.2 Chitosan to deliver oligonucleotide in lung cancer

Regarding the utilisation of CHT to deliver oligonucleotides in lung cancer, some studies showed its promising application in enhancing drug delivery and uptake. In 2007, Nafee (Nafee et al., 2007) and Taetz (Taetz et al., 2009) showed the ability of the water soluble CHT derivatives (section 1.3.4.1) to enhance cellular uptake of an ASO (a 2'-O-methyl-modified RNA with a phosphorothioate backbone, directed against human telomerase) when the polymer was used to coat poly lactic-co-glycolic acid (PLGA) NPs. Confocal studies with a fluorescent labelled ASO revealed that the CS HCl coating of PLGA NPs enhanced uptake of the nanostructure in A549 and Calu3 cells. Furthermore, cytotoxicity studies showed a decrease of A549 cell survival when treated with the ASO-complexed chitosan-coated PLGA NPs, confirming the successful internalisation of the drug into the desired cells.

More recently, studies carried out by Zhu and Huang provide examples of the benefits of using chitosan-derivatives NPs for the detection and treatment of lung cancer, respectively (Huang et al., 2021; Zhu et al., 2020). The study by Huang showed the formation of α-linoleic acid-modified chitosan NPs, complexed with phenylboronic acid and loaded with gefitinib and an antimiR-21 oligonucleotide. Uptake studies by flow cytometry and confocal microscopy on lung cancer cell lines exhibited efficient internalization of the nanocarrier by the cells. In addition, the treatment of cells with the nanomedicine considerably increased the expression of PTEN –usually downregulated by miR-21– compared to the treatment with naked antimiR-21, thus suggesting the promising ability of the employed chitosan-derivative in the delivery and uptake of oligonucleotide (Huang et al., 2021).

1.3.4.3 Chitosan nanoparticles preparation: the rise of microfluid approaches

The traditional methods for chitosan NPs preparation is named ionic gelation (Calvo et al., 1997): when chitosan is mixed with a negatively charged molecule, often referred as "cross-linker" (such as sodium trypolyphosphate (TPP), alginate, dextran sulphate or ATP), NPs forms spontaneously due to interactions occurring between the positive charges on chitosan molecules and negative charges available on the cross-linker (Figure 1.8).

This one-step process allows preparation of NPs in a considerably easy way, compared to other methods of NPs preparation such as solvent evaporation (used for PLGA, PEI and their derivatives) or thin-film evaporation (used for liposomes). However, despite its advantages in comparison with other methods of NPs production, ionic gelation still presents high batch-to-batch variability and poor scalability that have limited chitosan NPs (similar to other NPs types) translation into clinics. Therefore, microfluidic technologies that can potentially overcome

limitations related to manufacture that impede NPs translation into clinic have emerged (Chiesa et al., 2018; Roces et al., 2019; Roces, Lou, et al., 2020). In 2006, Withesides defines microfluidic as "The manipulation of fluids in channels with dimensions of tens micrometres". At the time, application of this novel lab-on-a-chip technology was still very new and limited to screen parameters for protein crystallisation (Whitesides, 2006). Since then, microfluidics technology has advanced considerably, and its applications comprehend but are not limited to pharmaceutics and particularly NPs preparation.

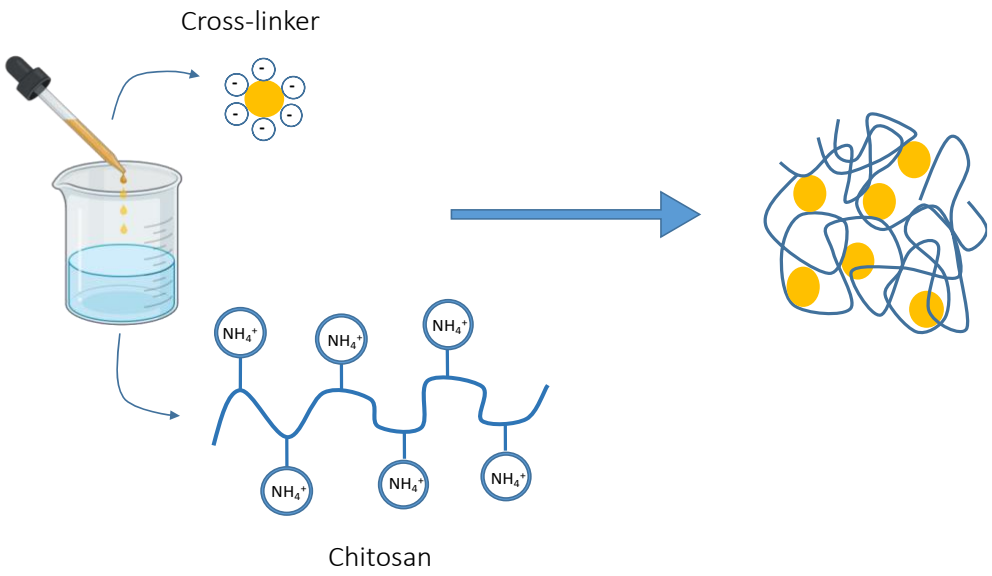

Figure 1.8 Ionic gelation technique of CHT NPs Preparation. Upon addition of a negatively charged molecule (crosslinker) to a chitosan (positively charged) solution, NPs form through the establishment of electrostatic interactions (Calvo et al., 1997).

Microfluidic mixing technology facilitates fluids to combine under controlled conditions. Generic components of microfluidic mixing systems include a chip in which the mixing takes place; an inlet method to allow fluids to enter the chip; methods for moving fluids around the chip thus allowing them to combine; collection vessel and other optional devices (detectors, analytical components) (**Figure** 1.9).

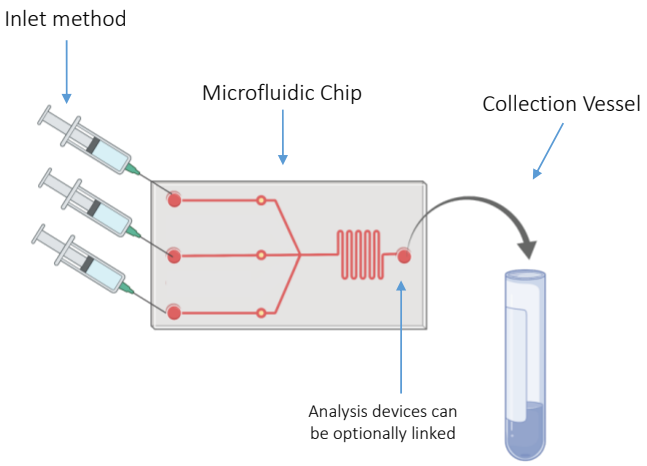

Figure 1.9 Generic components that a microfluidic device must have. An inlet method (usually linked to pumps or devices that can allow fluid to enter the chip), microfluidic chip, and a collection vessel. Analytical components can be linked at the microfluidic device to provide analysis of the output.

Consequently, microfluidic device enables precise control over many parameters such as inlet volumes, droplet generation, mixing ratio (parameter named flow rate ratio-FRR- which is the ratio of solutions used to prepare NPs) and speed (known as total flow rate-TFR-which is the speed fluid flows through the channels) that conventional techniques of mixing do not permit. Hence, it is clear how NPs preparation could benefit from microfluidic mixing technology, not only the control over the mentioned parameters can reduce user variability and batch-to-batch variation, but it also offers a quicker and continuous preparation leading to easier and more accurate scalability of the product.

Fluids in a microfluidic device are combined by laminar flow and mixing occurs via diffusion. A very important parameter to understand is how mixing between fluids occurs (both at the macro- and micro- scale) is Reynold number (Re):

$$Re = \frac{ruD_h}{m} = \frac{uD_h}{n}$$

where r is fluid density, m is fluid dynamic viscosity, n is the kinematic viscosity, u the fluid velocity and D_h is the diameter of the channel. D_h is a defined as:

$$D_h = \frac{4A}{P_{wet}}$$

where A is the cross-sectional area of the channel and P_{wet} is the wetted perimeter of the channel.

In microfluidic systems, Re is usually smaller than 100 hence the flow is laminar. In systems primarily governed by laminar flow, mixing of fluids occurs by passive molecular diffusion that is defined as "process of spreading molecules from a region of higher concentration to one of lower concentration by Brownian motion, which results in a gradual mixing of material". Therefore, mixing of fluids within microfluidic devices is time consuming; thereby two methods to aid diffusion have been developed:

- Active mixing, which use external energy input together with fluid pumping energy to accelerate mixing process;
- Passive mixing, which use only fluid pumping and relies on special channel having patterns designed to maximise contact surface area and aid mixing.

Although active mixing is more efficient than passive mixing, it requires external power sources linked to the device resulting in higher costs and more expensive NPs production. Therefore, passive methods that do not require additional energy have been preferred by researchers.

Among the different passive mixers developed, staggered herringbone mixers (SHB) developed by Stroock in 2002 resulted in being very efficient for NPs preparation (Stroock et al., 2002). In SHB mixers, grooved pattern placed within the channels provides the formation of transverse flows, that confers the mixing in a chaotic flow (**Figure** 1.10). Given its high efficiency, SHB have gained particular attention in NPs formulation to the extent that there is availability on the market of equipment based on this technology optimized for NPs preparation. An example of commercially available microfluidic-device based on SHB mixing is NanoAssemblr by Precision Nanosystem. This device provides the further advantage of the ease of scalability of the formulations thus giving an additional feature to the use of microfluidic technology to advance the translation of nanomedicine (Khadke et al., 2020).

The use of microfluidic mixing technology for the preparation of NPs has become of high interest among researchers. Its employment in the preparation of liposomes has showed great promise for the encapsulation of oligonucleotides (Lou et al., 2020), peptides, proteins (Hussain et al., 2020), lipophilic and hydrophilic small molecules (Roces, Port, et al., 2020). Likewise, it has been exploited for the preparation of NPs employing diverse polymers such as PLGA (Roces, Hussain, et al., 2020; Vu et al., 2019) , PEI (Qiu et al., 2020), polycaprolactone-block-poly(ethylene oxide) (Bains et al., 2017) and chitosan (Chiesa et al., 2019; Escareño et al., 2021).

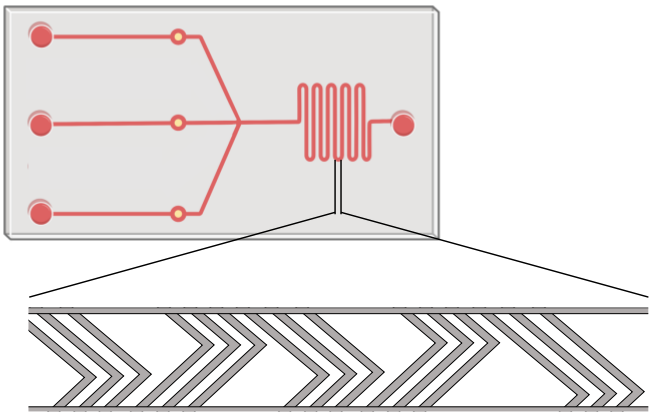

Figure 1.10 Staggered Herringbone (SHB) pattern. In SBH the grooved patterns allow the flow to become chaotic.

The first published study showing microfluidic-manufactured chitosan NPs, is the study carried out by Lan. The study demonstrated for the first time the successful formation of chitosan-silica NPs within a microfluidic device composed of Poly(Me methacrylate) PMMA, one of the most common used material to produce microfluidic cartridges. The study demonstrated the advantage of the ease in controlling NPs size according to the variation in the flow rate of fluids, together with the outcome of having spherical NPs (which was confirmed by electron microscopy). In addition, the study investigated the possibility of incorporating bovine serum albumin (BSA) as a model protein into the NPs. Results showed significantly higher encapsulation efficiency of the NPs compared to chitosan alone, thus highlighting the promising utilisation of microfluidics as a method to prepare chitosan NPs (Lan et al., 2010).

Consequently, Majedi published the successful formation of CHT NPs with microfluidic, applying the ionic gelation of CHT with ATP (Sadat Majedi et al., 2012) and a second study employing a water-soluble modified CHT (Majedi et al., 2012). In both cases, the studies showed the advantages of microfluidics in providing a better control on NPs size, a higher uniformity of the formulation via the control of flow ratio, and reproducibility of the results obtained compared to bulk mixing. Moreover, the NPs prepared with the water-soluble CHT derivatives were also investigated for their ability of encapsulating Paclitaxel (PTX), and therefore their potential application in cancer treatment. Results showed higher encapsulation efficiency of PTX compared to bulk method, as well as smaller size of the PTX-loaded NPs (Majedi et al., 2012).

Similarly, Chen compared microfluidic preparation of CHT NPs to traditional mixing (Chen et al., 2014). In the study, CHT was cross-linked with phosphodiester-guanine

oligodeoxynucleotide (CpG), thus showing the ability of CHT NPs prepared via microfluidic of complexing not only with small molecules (Majedi et al., 2012) and protein (Lan et al., 2010) as shown in previous studies, but also with oligonucleotides. The study confirmed not only Majedi results in terms of reproducibility and size tuneability, but also investigated NPs cytotoxicity and cellular uptake. Interestingly, NPs prepared with microfluidics caused a 3-fold higher cellular uptake compared to NPs prepared with bulk method in a human embryonic kidney (HEK293) cell line. This was ascribed to the reduced polydispersity of the formulation prepared with the microfluidic device, and to the smaller size which ultimately provided a easier uptake.

Furthermore, Shamsi in 2017 investigated the ability of microfluidic prepared NPs to deliver streptokinase in mice (Shamsi et al., 2017; Shamsi & Zahedi, 2017). Results demonstrated that the NPs were able to deliver the enzyme into the plasma intact compared to injection of naked streptokinase or blank NPs, thus confirming the known safety of CHT NPs *in vivo*, with the additional advantages brought about by the microfluidic preparation.

1.4 Thesis Aims and Objectives

The aim of this project was to deepen the understanding of miR-184 involvement in lung cancer proliferation and development, to explore its role in enhancing the sensitivity of NSCLC cells to cisplatin, and to develop CHT NPs encapsulating miR-184 mimic for its delivery to NSCLC cells.

The aim was achieved through the following objectives:

i) Development of CHT NPs via microfluidic mixing technology, investigating the parameters which affect NPs size, PDI and charge. Therefore, encapsulation of miR-184 mimic into the optimised CHT NPs and evaluation of their internalisation by NSCLC cells.

ii) Investigation of the expression of miR-184 in a panel of NSCLC cells having different sensitivity to cisplatin. Consequently, evaluation of the role of miR-184 in promoting cisplatin sensitivity.

iii) Examination of any variation of miR-184 potential target genes to evaluate the mechanism through which miR-184 contributes to confer cisplatin sensitivity.

2 Material & General Methods

2.1 Materials

Lung cancer cell lines were a kind gift from Dr Lakis Liloglou and Dr Michael Davies, both from the University of Liverpool. The cell lines and lung cancer phenotype from which they were initially derived are displayed in **Table** 2.1. The material used for the experiments are listed throughout the following section as they are mentioned.

Table 2.1: Cell lines employed in the study and lung cancer from which they were obtained.

	Cell Type	Derived from
A549	epithelial	ADC
Calu-3	epithelial	ADC
Calu-6	epithelial	ADC
CORL-23	epithelial	LCC
H358	epithelial	/
LUDLU-1	epithelial	SCC
SK-MES	epithelial	SCC
SKLU	epithelial	ADC

2.2 NPs manufacture via microfluidic technology (blank and loaded)

Unmodified CHT derived from Aspergillus (CS ASP, gifted Prof. Saleem collaborators) and three water-soluble chitosan derivatives, chitosan hydrochloride (CS HCl) and chitosan glutamate (CS GLU) from Heppe Medical, and glycol chitosan (CS GLY) from Sigma Aldrich (**Table** 2.2). Given the presence of several positive charges on their backbones, a salt carrying negative charges (sodium tripolyphosphate (TPP), Thermo Fisher, UK) was chosen as a cross-linking molecule.

Table 2.2 Specification of Chitosans employed in this study.

	Molecular Weight (kDa)	Deacetylation Degree (%)	Article number
CS ASP	Not provided	Not provided	n/a
CS HCL	200-800	75-90	54039
CS GLU	200-800	75-90	54041
CS GLY	200-500	80-90	G7753

For the preparation of NPs, a cartridge made of polydimethylsiloxane (PDSM) was placed into the Nanoassemblr® Benchtop instrument, and two 15 mL centrifuge tubes (one to collect the formulation and one to collect waste) were placed in the designated channel holders. The Nanoassemblr® software was set up with the following parameters: Flow Rate Ratio (FRR) ranging from 1:1 to 1:8, Total Flow Rate (TFR) ranging from 0.64 mL/min to 1 mL/min, syringe volume, total volume, initial waste and final waste. To promote consistency and diminish user variability, polymer and cross-linker solution were loaded into 1 mL syringes; chitosan solutions were always placed on the left channel while TPP solution was in the right channel. The total volume of formulation prepared was 1 mL, while initial waste and final waste were kept at 0 μL, given previous study that showed no variation in size and PDI by discarding the initial and final output of the device.

2.2.1 Blank NPs optimisation

The first step of this study aimed at identifying and understanding the parameters that influence NP size and polydispersity index (PDI). CS ASP was dissolved in 1% acetic acid, while water-soluble derivatives and the cross-linker were dissolved in distilled water. The pH of polymer solutions was adjusted to 5 with diluted 1M NaOH and solutions were kept in a 4°C fridge for up to one month.

2.2.1.1 Taguchi Design of Experiment

A Taguchi design of experiment (DoE) L18 orthogonal array was constructed by using Minitab 16 Statistical Software® (Minitab Inc., Pennsylvania, USA). Taguchi DoE is a statistical method that consists in defining the parameters (factors) needed to obtain the best outcome. It is a commonly used method in Research and Development departments given that several software provides built-in Taguchi designs that allow a facile approach to reduce experiments variance (Nazir et al., 2015).

The DoE was composed of four variables or factors (polymer concentration and TPP concentration, TFR and FRR set at three or six levels, as indicated in **Table** 2.3). The software output for the L18 orthogonal array provided a set of 18 formulations (**Table** 2.4). These parameters were used for all the chitosan types employed in the study. Each formulation was performed in triplicate and size and poly-dispersity index PDI were measured as detailed in **section 2.3.1**.

Optimum conditions were indicated by a high signal to noise (S/N) ratio, which corresponds to minimum variance of the outcome, and a better performance with the target output parameters (that were particle size and PDI). Optimisation of the particle size and PDI was performed using the Taguchi's 'smaller-is-better' criterion to achieve a particle size and a PDI as small as possible. Following Taguchi's DoE analysis, the software calculates the combination of parameters that would give NPs with the smaller size and PDI. Hence, the formulation with the indicated parameters was produced and analysed, and it was chosen in further investigations.

2.2.1.2 Flow Rate Ratio Investigation

Following Taguchi DoE, blank NPs were further optimised via investigating the influence of FRR on particle size and PDI. The best formulation for each CHT derivatives was identified from the DoE, and the parameters to produce it were not modified except for FRR. Therefore, NPs were prepared changing FRR values ranging from 1:1 to 1:8 (chitosan concentration:TPP concentration). The best blank formulation was finally identified for all the chitosan derivatives and chosen for further studies.

Table 2.3. Parameters employed to set Taguchi design L18 orthogonal array. The mixed-levels design was already established within the software. Three variables ([CHT], [TPP] and TFR) were set at three levels, while one variable (FRR) was set at 6 levels.

Variables	[CHT] (mg/mL)	[TPP] (mg/mL)	TFR (mL/min)	FRR (CHT:TPP)
Levels	0.25	0.25	0.64	2 : 1
	0.5	0.5	0.8	3 : 1
	1	1	1	4 : 1
				5 : 1
				6 : 1
				7 : 1

Table 2.4: Set of 18 formulations to perform as resulted from Taguchi DoE L18 orthogonal array. The DoE was constructed via Minitab 16 Statistical Software®(Minitab Inc., Pennsylvania, USA), employing a mixed-levels design with 4 variables.

Formulation	FRR (CHT:TPP)	TFR (mL/min)	[CHT] (mg/mL)	[TPP] (mg/mL)	CHT:TPP mass ratio
A	2 : 1	0.64	0.25	0.25	2 : 1
B	2 : 1	0.8	0.5	0.5	2 : 1
C	2 : 1	1	1	1	2 : 1
D	3 : 1	0.64	0.25	0.5	1.5 : 1
E	3 : 1	0.8	0.5	1	1.5 : 1
F	3 : 1	1	1	0.25	12 : 1
G	4 : 1	0.64	0.5	0.25	8 : 1
H	4 : 1	0.8	1	0.5	8 : 1
I	4 : 1	1	0.25	1	1 : 1
J	5 : 1	0.64	1	1	4.88 : 1
K	5 : 1	0.8	0.25	0.25	4.88 : 1
L	5 : 1	1	0.5	0.5	4.88 : 1
M	6 : 1	0.64	0.5	1	3.07 : 1
N	6 : 1	0.8	1	0.25	24.57 : 1
O	6 : 1	1	0.25	0.5	3.07 : 1
P	7 : 1	0.64	1	0.5	13.53 : 1
Q	7 : 1	0.8	0.25	1	1.69 : 1
R	7 : 1	1	0.5	0.25	13.54 : 1

2.2.2 MiRNA encapsulation optimisation

The parameters identified via the blank optimisation studies were used to prepare oligonucleotide-loaded NPs. The oligonucleotides employed in this study, human miR-184 mimic and miR-184 hairpin inhibitor, were purchased from Dharmacon, UK (product number C-300635-03-0050 and IH-300635-05-0050, respectively). A non-targeting control (NTC) (Dharmacon, UK, product number CN-001000-01-50) was also used as a control for cell biology assays. Oligonucleotide sequences are displayed in Table 2.5. The oligonucleotides were reconstituted as per manufacturer suggestions by adding 700 μL of siRNA buffer solution (Dharmacon, UK) to obtain a solution with a concentration of 70 μg/μL (or 70 μM). After mixing the vial by vortexing to allow powder solubilisation, oligonucleotide solutions were divided in aliquots and stored at -20°C.

To reduce nuclease contamination and avoid oligonucleotide degradation, CHT derivatives and TPP were dissolved in nuclease-free water (ThermoFisher, UK). Nuclease-free plasticware was used and when not possible, Diethyl Pirocarbonate (DEPC)-treated glassware was employed.

Different amounts of miRNA mimic (5, 10 or 20 μg) were added to the TPP solution to reach a CHT:miRNA mimic ratio (w/w) of 100:1, 50:1 and 25:1. Hence, NPs were prepared as stated above by using the parameters identified in the blank NPs optimisation studies. The NPs were transferred into a 1.5 mL Eppendorf tube and centrifuged in a BenchTop Eppendorf® centrifuge for 45 min at 12000 x g to allow the separation of non-encapsulated miRNA. The supernatant was collected and used to evaluate oligonucleotide encapsulation efficiency (EE%) of the NPs (section 2.2.2), while the pellet was used for subsequent experiments.

Table 2.5. miR-184 mimic and hairpin inhibitor employed in the study, their molecular weight and sequence.

	sequence	*Molecular Weight (kDa)*
Hsa-miR-184 mimic	UGGACGGAGAACUGAUAAGGGU	14,105.4
Hsa-miR-184 hairpin inhibitor	Not provided	17,120
miR-184 non targeting control (NTC)	UCACAACCUCCUAGAAAGAGUAGA	Not determined

2.3 NPs characterisation

2.3.1 Size and PDI

NPs were characterized in terms of particle size and zeta potential by dynamic light scattering (DLS) using a Malvern nano ZS (Malvern Panlytical, Worcestershire, UK). For size and polydispersity index (PDI) characterisation, NPs suspension without further dilution was transferred into a cuvette and inserted into the instrument. Three measurements at 25°C were conducted and size/PDI values recorded following the parameters summarised in (Table 2.6).

Table 2.6 NPs size, PDI and Z potential parameters employed for Malvern Zetasizer Nano 2S.

	Size & PDI measurement	Z-Potential Measurement
Temperature	25 °C	25 °C
Refractive Index	1.330	1.330
Equilibrium Time	30 s	30 s
Cell type	634-0675 (VWR)	DTS1070
Number of runs	Automatic	Automatic
Number of Measurement	3	3
Sample concentration	undiluted	undiluted

2.3.2 Encapsulation Efficiency

To evaluate the ability of CHT NPs to complex with the oligonucleotide, NPs encapsulation efficiency (EE%) was investigated. The oligonucleotide-loaded NPs were centrifuged at 12000 x g and 10 µL of supernatant were used to quantify oligonucleotide concentration using QuantiFluor® RNA System (Promega, UK). The system contains a fluorescent RNA-binding dye with excitation wavelength (Ex) of 492nm and emission wavelength (Em) of 540 nm, allowing sensitive and quantitative analysis of the RNA content in a sample.

Given the small volumes available for analysis, the assay was conducted in a 96-well plate following the "Protocol for Quantitative RNA in Multiwell Plates" provided by the manufacturer. Firstly, all the kit components were thawed at room temperature and the dye was protected from light. Once thawed, the QuantiFluor® RNA Dye was diluted 1:400 with 1xTris-EDTA (TE) buffer, to prepare enough working solution to analyse standards, samples and controls. Afterwards, the RNA standard from the manufacturer was diluted with 1xTE buffer to prepare 7 standards with concentrations ranging from 50 ng/µL to 0.78 ng/µL. Subsequently, 200 µL of working solutions were dispensed into the wells of a black-walled 96-

well plate, followed by the addition of 10 μL of standard, NPs supernatant or controls. RNA standards, NPs supernatants and controls were dispensed in duplicate.

The plate was wrapped in foil to protect the dye from light, and fluorescence (Ex 492 nm/Em 540 nm) was measured on CLARIOstar plate reader (BMG Labtech, Aylesbury, UK). RNA concentration was calculated as follows: blank sample fluorescence was subtracted (1X TE Buffer) from all the standard and unknown samples, the corrected data from the RNA standards were used to generate a standard curve of fluorescence versus RNA content (ng) in each sample (**Figure** 2.1); RNA concentration of the sample was calculated from the standard curve equation (**Figure** 2.1).

Encapsulation Efficiency (EE%) was then calculated by subtracting the amount of oligonucleotide in the supernatant of the formulation after centrifugation, to the initial amount of oligonucleotide used to prepare the formulation, following the equation:

$$EE(\%) = \frac{total\ oligonucleotide\ loaded\ in\ formulation(ng) - oligonucleotide\ in\ supernatant(ng)}{total\ oligonucleotide\ loaded\ in\ the\ formulation\ (ng)} x100$$

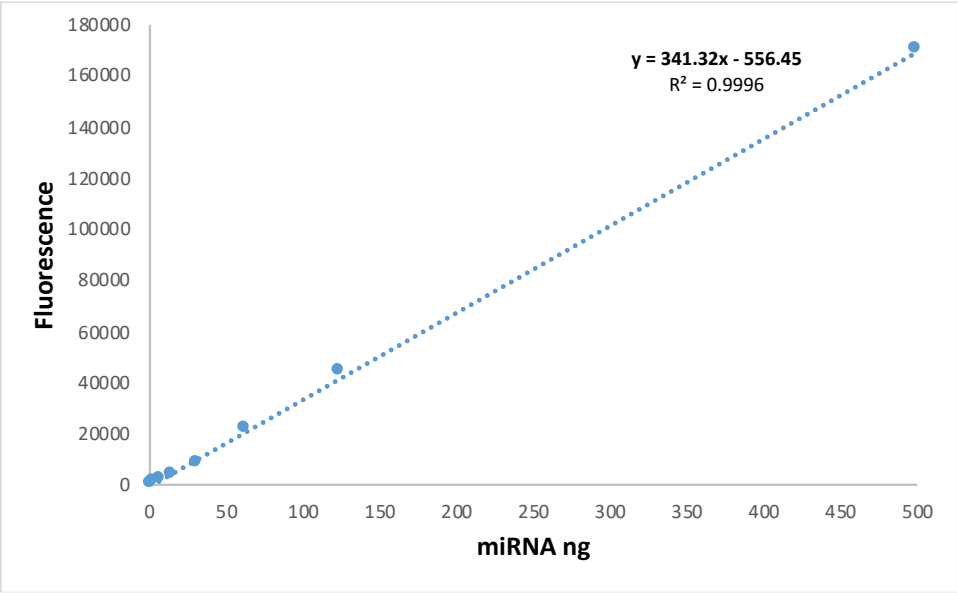

Figure 2.1 Calibration Curve generated to evaluate miRNA EE%.

2.3.3 Gel retardation Assay

To confirm the complexation of the miR-184 mimic with CHT NPs, agarose gel electrophoresis technique was employed. Agarose gel electrophoresis is a laboratory method commonly used to separate nucleic acids in a mixture according to their molecular size. The gelation of agarose polymer leads to the formation of non-covalent bonds between molecules, thus creating a

network of bundles. If an electrical field is applied, nucleic acids will be able to move across the gel: in particular, the negatively charged nucleic acids (due to the phosphate groups of the backbone) will migrate towards the positive anode. Since the mass/charge ratio of different fragment of the same nucleic acid is similar, their separation occurs only based on their size. Therefore, the bigger the molecule, the shorter the distance travelled towards the anode. By measuring the retardation of the oligonucleotide-loaded NPs on an agarose gel, and comparing them with appropriate controls, it was possible to have an indication of the successful complexation of the oligonucleotide with the polymer (Masoodi et al., 2021).

Agarose gel was prepared by suspending agarose in 1 X Tris acetate EDTA buffer to reach a concentration of agarose of 2.5% (w/v) in a conical flask. The suspension was heated in a microwave for up to 2 min to dissolve the agarose. After adding 1 µL of SYBR® Safe DNA stain (Thermo Fisher, UK) to the gel solution, it was poured into a gel tray with a comb to form loading wells and allowed to set. Afterwards, the gel was placed into an electrophoresis chamber and covered with 1xTE buffer. Samples were prepared by adding 7 µL of NPs (prepared as described above) or oligonucleotide solution (used as control) to 1 µL of DNA-loading dye (ThermoFisher Scientific, UK). The gel was run for at 60V for 1 or until the dye reached the bottom of the gel, indicating that the run of the samples towards the gel was completed. The gel was removed from the chamber and gel images were produced using a UV transilluminator image analyser.

2.4 Cell culture and transfection

2.4.1 General cultivation

All the reagents used for the following experimental sections were purchased from Sigma Aldrich, UK unless otherwise stated.

All cell culture and passage techniques were carried out in a laminar flow hood under sterile conditions. Cells were maintained in a cell culture incubator at 37°C in 95% air and 5% CO_2. They were cultivated in Dulbecco's Modified Eagle's Medium (DMEM) with the exception of Calu-3 cells that were grown in Minimum Eagle Media (MEM). Both MEM and DMEM were supplemented with 1% Penicillin/Streptomycin solution and 10% of foetal bovine serum (FBS).

2.4.2 Cell thawing and recovery

Cells gifted by Dr. Liloglou and Dr. Davies were stored in Liquid Nitrogen and thawed upon necessity. They were thawed as follows: cells stored in cryovials were carefully taken out from

the Liquid Nitrogen storage and de-frosting was facilitated by placing them in a 37°C water bath. When almost all the content of the cryovial melted, it was quickly transferred in a 15 mL Falcon tube containing 9 mL of pre-warmed complete media and centrifuged at 1200 x g for 5 min (Eppendorf centrifuge 5804R) at 25˚C, with the aim of removing residual Dymethyl Sulfoxide (DMSO) used to freeze cells (section 2.4.4) that otherwise will cause cell death. Supernatant was removed, cell pellet was resuspended in 5 mL complete media and transferred into a T75 flask containing 10 mL of pre-warmed complete media. The flask was stored in a cell culture incubator to allow cell attachment to the flask wall, recovery and growth.

Once confirmed that cells attached to the flask walls, to guarantee cells recovery media was replaced daily until cells reached the desired confluency.

2.4.3 Cell Passaging

To allow cells to grow and avoid over-confluency, which could lead to variations in experiment outcomes, upon reaching 70-80% confluence, cells were passaged as follows: firstly, media was aspirated from the T75 flask and the monolayer was washed with 5 mL of phosphate-buffer solution (PBS) to remove any residual media and protein that may affect the effectiveness of trypsin; secondly, to allow enzymatic dissociation of cells from the flask walls, after PBS aspiration 5 mL of trypsin-EDTA solution was added to the monolayer. Trypsin is a proteolytic enzyme that can digest proteins: hence it is able to degrade proteins responsible for cell adhesion to the flask wall, therefore allowing their detachment. EDTA is a chelator and given its capability of binding calcium and magnesium its action is beneficial to remove those ions that are present in the extracellular matrix and helps cell-cell adhesion: cell-to-cell adhesion obscures the proteins that trypsin is going to attack, hence the use of both EDTA and trypsin has a synergistic effect aiming to detach cells from the flask wall (Hacking & Khademhosseini, 2013).

Following trypsin-EDTA addition, the flask was incubated at 37°C, 5% CO_2 for 5-10 min (these are the conditions under which trypsin works at its optimum); cell detachment was monitored using a light microscope and when majority of cells had detached, pre-warmed complete media was added to the flask to inactivate trypsin, that otherwise would continue its activity by striping cell surface protein and killing cells. Complete media is used to inactivate trypsin given that the FBS used to supplement it contains α-1 antitrypsin, a protein that inhibits trypsin by covalent binding to it. Hence, the cell suspension was centrifuged at 3000 x g (Eppendorf centrifuge 5804R) for 5 min to ensure separation of detached cells from any

residual trypsin. Following centrifugation, the supernatant was removed, cell pellet was resuspended in 10 mL of complete media and the suspension was seeded in new complete media-containing flasks, prior its splitting in 1:3 or 1:5 ratio to allow cells growth. Media was changed every 2-3 days according to cell-growth speed.

2.4.4 Cell Storage

For cryostorage, cells that reached 70-80% confluence were detached from the flask as previously described (section 2.4.3). Once lifted and centrifuged, the cell pellet was resuspended in 1 mL of freezing media, composed of 70% media (MEM or DMEM according to cell type), 20% FBS and 10% DMSO. The latter is used to promote cell recovery when cells are thawed, given it prevents the formation of ice crystals which otherwise lyses the cells during thawing. Cell suspension in freezing media was quickly but carefully transferred in cryovials, and those were placed into an isopropanol containing vessel named Mr. Frosty (Thermofisher Scientific, UK) and stored at -80°C before transfer to liquid nitrogen the following day for long-term storage. Using a Mr. Frosty filled with isopropanol allows the optimal freezing rate, which is approximately -1°C/min: in this way cells will reach the freezing point very slowly avoiding harsh and quick temperature variations.

2.4.5 Cell Plating

For cell plating, cells that reached 70-80% confluence were detached from the flask as previously described. Once lifted and centrifuged, cell pellet was resuspended in 5 mL of media and 10 µL of the cell suspension were then loaded into the chamber of a haemocytometer. Cells were then counted with the aid of the haemocytometer grid: in particular, the number of cells in the 4 corners of the device were counted and the average was calculated. To calculate the cell concentration (number of cells/mL) of the suspension, the equation used was the following:

$$cells\ concentration\ = \frac{cells\ counted}{4} 10^4\ cells\ per\ mL$$

According to the experiment that was carried out, different plates were required (96-, 24- and 6- well plates). Given that the surface areas of wells differ depending on the plate used, to ensure a similar cell density across all the experiments different amounts of cells were seeded in the different plates employed. Table 2.7 summarise the type of plate used and the concentration of cells seeded for every experiment. Hence, after cells suspension was diluted

according to the number of cells required, cells were seeded into the wells and plates were incubated for 24 h prior to treatment.

Table 2.7. Summary of the types of well-plates used (96-, 24- or 6- well plates), the experiments in which each of them were used (application), their surface area (cm^2), number of cells seeded per well and volume of cell suspension.

Type of plate	Well surface area (cm^2)	Application	Cell suspension per well (mL)	cells per well
96-well plate	0.32	Alamar Blue assay	0.2	$1*10^4$
24-well plate	1.9	Flow cytometry, Western Blot	0.5	$6*10^4$
6-well-plate	9.6	Baseline experiment, oligonucleotide delivery experiments, Confocal microscopy	2	$3*10^5$

2.4.6 Cell Transfection

2.4.6.1 Cell Transfection via INTERFERin®

INTERFERin® reagent (PolyPlus, France) was used for transient transfection of the cell lines, to allow delivery of the oligonucleotides (miR-184 mimic, miR-184 inhibitor and NTC control) into the cells. INTERFERin® contains cationic molecules that allows an efficient and quick transfection process of miRNAs and siRNAs (*INTERFERin - SiRNA / MiRNA Transfection Reagent*).

24 h after cells plating, oligonucleotides transient transfection was performed according to the manufacturer instruction. Oligonucleotides were diluted in media without serum in a 1.5 mL Eppendorf and vortexed for 10 s to allow mixing. To prepare transfection mix, the required amount of INTERFERin® reagent was added into the Eppendorf containing the oligonucleotide dilution, vortexed for 10 s and incubated at room temperature for 10 min to promote the formation of transfection complexes between oligonucleotides and INTERFERin®. During complexation formation, growth media covering the monolayer of cells in wells was removed and replaced with the required amount of complete media. Hence, the required volume of transfection mix was added into each well and the plate was incubated at 37°C for up to 48 h to allow oligonucleotides to exert their action. The final concentration of oligonucleotide in the wells ranged from 1 nM to 50 nM, according to the type of plate used the manufacturer protocol recommends a specific amount (µL) of INTERFERin® to prepare transfection mix and of growth media to add the wells.

The amounts of reagents used according to each application are summarised in **Table** 2.8.

Table 2.8 volume of INTERFERin®, growth media and complexation mix used for Alamar BLue assay, Flow cytometry assay, and oligonucleotide delivery experiments.

Application	Well-plate used	Number of cells per well	complexation mix (µL)	INTERFERin® per well (µL)	growth media added (µL)
Alamar Blue	96	$1*10^4$	50	0.75	150
Flow Cytometry, Western Blot	24	$6*10^4$	100	2	400
oligonucleotide delivery	6	$3*10^5$	200	5	1800

2.4.6.2 Cell Transfections via Nanoparticles

Optimized formulations were employed to investigate whether NPs would allow the successful delivery of miR-184 mimic. Blank and loaded NPs were prepared as described in sections 2.2.1 and 2.2.2. Following centrifugation, supernatant was removed, NPs pellet was resuspended in 1 mL of media without serum (final oligonucleotide concentration was 700 nM or 10 ng/mL) and the obtained suspension was further diluted with growth media according to the final concentration on wells desired. Growth media was removed from cells seeded the previous day and NPs dilutions added to each plate. The amount of NPs dilution, according to the application and to the final concentration desired are summarised in Table 2.9.

Table 2.9 Summary of the preparation of NPs dilution for cell treatment according to the application (Alamar Blue assay, Flow cytometry, oligonucleotide delivery experiment).

Application	Well-plate used	Number of cells per well	oligonucleotide concentration (nM)	Final solution (mL)	NPs solution (µL)	growth media (µL)
Alamar Blue	96	$1*10^4$	5	0.2	1.43	198.57
			20	0.2	5.71	194.28
Flow Cytometry	24	$6*10^4$	5	0.5	3.57	496.43
			20	0.5	14.28	485.72
oligonucleotide delivery	6-	$3*10^5$	5	2	14.28	1985.72
			20	2	57.14	1942.86

2.4.7 Cisplatin Treatment

Cisplatin (50 mg) was purchased from Sigma Aldrich, UK and dissolved in 5 mL of dimethylformamide (DMF) to give a stock solution of 33.3 mM. The solution was aliquoted and stored at -4°C. The stock solution was further diluted to obtain a starting solution of 2 mM to facilitate the preparation of cisplatin dilutions, that were prepared in growth media with concentration ranging from 1 to 1000 mM as reported in Table 2.10.

Therefore, 24 h after cells seeding growth media was removed and 200 µL of each dilution (for Alamar Blue assays) or 500 µL (for flow cytometry assay) was added to 96- or 14- well plates respectively, the plates were incubated for 24 or 48 h according to the experiment.

Table 2.10 Cisplatin dilutions

[cisplatin] in well	[cisplatin] starting solution	Final Volume	Volume of cisplatin solution needed	Volume of growth media
mM	mM	(µL)	(µL)	(µL)
1000	2	1000	2	998
500	2	1000	4	996
250	2	1000	8	992
125	2	1000	16	984
100	2	1000	20	980
75	2	1000	26.67	973.33
50	2	1000	40	960
25	2	1000	80	920
10	2	1000	200	800
5	2	1000	400	600
1	2	1000	2000	1000

2.4.8 Combination of Cisplatin and oligonucleotide treatment

For proliferation assays in which combinations of oligonucleotide and cisplatin were tested, oligonucleotides were delivered either via INTERFERin® or via NPs. In both cases, cisplatin dilution and oligonucleotide solutions were prepared doubling their concentration to ensure that the final concentration of cisplatin and oligonucleotide in wells were the same as the experiments where the two drugs (cisplatin and the oligonucleotides) were tested separately. Figure 2.2 shows the procedure followed to treat the plates. After preparing drugs solutions, plates in which cells were seeded 24 h before, were taken out from the incubator and growth media was removed. Consequently, the required amount of growth media, transfection mix or NPs dilution, and cisplatin dilution were added to each well according to Table 2.11.

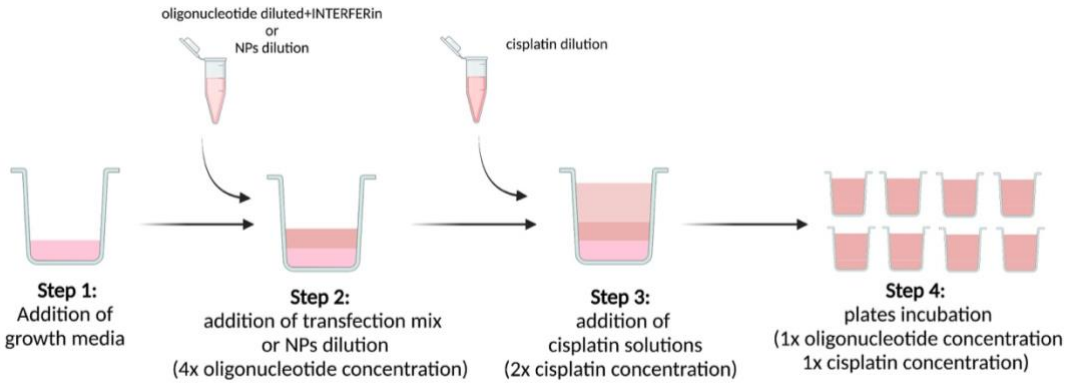

Figure 2.2 Steps performed to carry out cytotoxicity experiments of combination of oligonucleotide and cisplatin. To have the desired concentration of cisplatin and oligonucleotide solution (or NPs solution), firstly media was added to the well, followed by the addition of 2x transfection mix or 2x NPs solution. Afterwards, 2x cisplatin solution was added to the well: in this way the final concentration of oligonucleotide or NPs and cisplatin in each well was 1x, hence the desired one.

Table 2.11 Volume of growth media, transfection mix or NPs dilution, and cisplatin dilution added to each well according to the experiment that was carried out.

Application	growth media (µL)	Transfection mix or NPs dilution (µL)	Cisplatin dilution (µL)	Final volume on well (µL)
Alamar Blue	50	50	100	200
Flow Cytometry	100	100	200	400

2.5 Proliferation

2.5.1 Alamar Blue Assay and IC50 determination

Alamar Blue is a cell viability assay based on the reduction of resazurin into its oxidised form, resorufin: resazurin can be used as a dye to monitor the number of viable cells in a sample. As shown in **Figure** 2.3, Resazurin is a blue water-soluble molecule that gives a low fluorescent signal (Ex 530 nm, Em 590 nm). Molecules produced by the mitochondrial respiratory chain, such as $NADH/H^+$ and $NADPH/ H^+$, can reduce resazurin into its reduced form resorufin, which is pink and gives a high fluorescent signal (Ex 530, Em 590). Thus, given that only living (and metabolically active) cells produce molecules that can reduce resazurin to resorufin, high fluorescence in a sample indicates the presence of viable cells. Moreover, the fluorescent signal is proportional to the number of living cells in the sample. For this reason, Alamar Blue assay was employed to assess cytotoxicity of cisplatin, oligonucleotides and combination of cisplatin and oligonucleotides. 10% DMSO was employed as positive control to show cell death, while cells treated with media only (and therefore viable) were used as negative control.

Growth media was removed from the cells 24 or 48 h after treatment. Cell layers were washed twice with 0.2 mL pre-warmed PBS to remove any residual media or protein that could interfere with the assay. Afterwards, 0.1 mL of 1 mg/mL resazurin solution in PBS was added to each well. Plates were wrapped in foil and incubated at 37°C for 3 h. To assess cell viability, fluorescence was measured at excitation of 530 nm and emission of 590 nm on a CLARIOstar plate reader (BMG Labtech, Aylesbury, UK).

Fluorescence values obtained from plate readings were analysed using GraphPad Prism 8.0 Software. Firstly, data were normalised using 10% DMSO as positive control (0% viability) and untreated cells as negative control (100% viability). Consequently, following the "log[inhibitor] vs normalised response" model, dose-response curves were generated and IC50 was calculated. R^2 value higher than 0.9 was considered as an indicator that data were a good fit for the model.

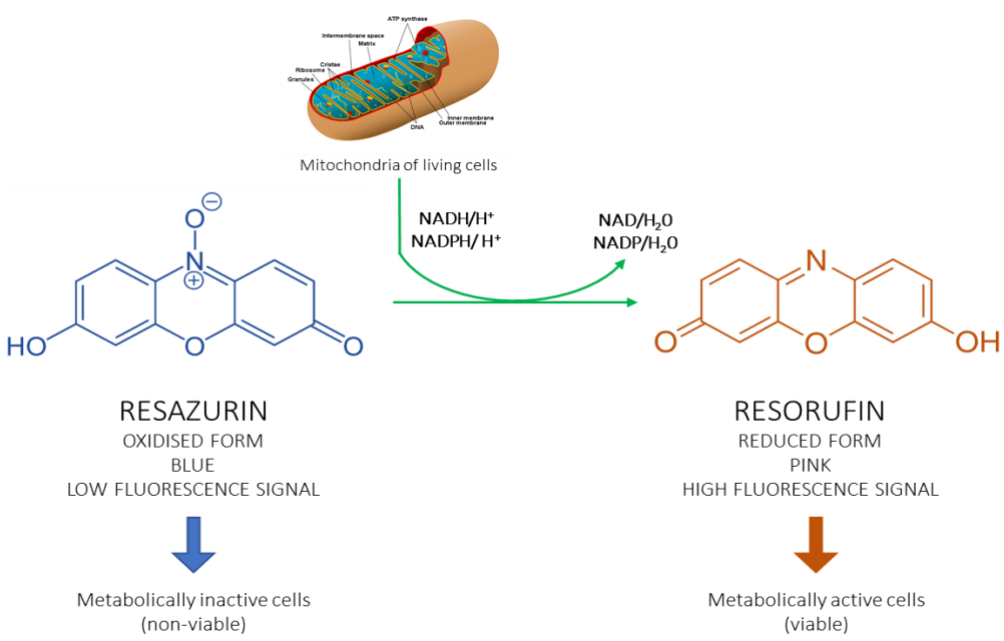

Figure 2.3 mechanisms of resazurin reduction in resorufin by molecules (NADPH and NADH) produced by mitochondria of living (metabolically active) cells. The reduction of resazurin into resorufin (that gives an intense pink fluorescent signal) can be used as an indicator of the presence of metabolically active cells in the sample. Moreover, the amount of resorufin produces is proportional to the fluorescence registered by the instrument therefore for this reason Alamar Blue assay is employed to determine the percentage of viable cells in a sample.

2.5.2 Flow cytometry

Flow cytometry is a widely used laboratory technique, that has application in several fields including immunology, molecular biology, cancer biology and infectious disease monitoring. It is a laser-based technology which enables the monitoring of whole cell populations or single cell morphology and composition. Flow cytometry is based on the detection of fluorescence by an array of detectors (Jaroszeski & Radcliff, 1999).

Traditional flow cytometry instruments consist of three elements: fluidics (sheath fluids that deliver the sample to the interrogation point where it is analysed), optics (excitation laser and collection optics, including filters of specific wavelengths) and electronics (components allowing the conversion of signals from detectors into digital signals) (Büscher, 2019). The sample to analyse is directed to the interrogation point via the sheath fluid (usually buffered saline) that arrange the cells into a single file. Once reached the laser intercept, the sample interrupts the laser light and scatter it into two dynamics named forward scatter (FSC) and side scatter (SSC). The FSC detector is located opposite to the laser beam, therefore as the cell moves through the laser beam it creates a "shadow" on the detector behind (Givan, 2001) (**Figure** 2.4). This can then be used to determine the size of the cell, the bigger the cell the

bigger the shadow created. On the other hand, the SSC detector sits perpendicularly to the laser beam (**Figure** 2.4): as the light hits the cell, internal cellular components cause light scatter. Thus, SCC is used as an indication of cell complexity, given that the more the light is scattered, the more granulated (and complex) the cell is. These two components are then compiled in a plot named scatter plot, where populations of similarly sized cells will group together, as with cells of a similar complexity (**Figure** 2.5). From this plot the nature of the cellular population can be determined: healthy cells will group together in a particular region of the graph whereas cells undergoing apoptosis tend to shrink in size yet become more complex moving them into another region of the plot (**Figure** 2.5).

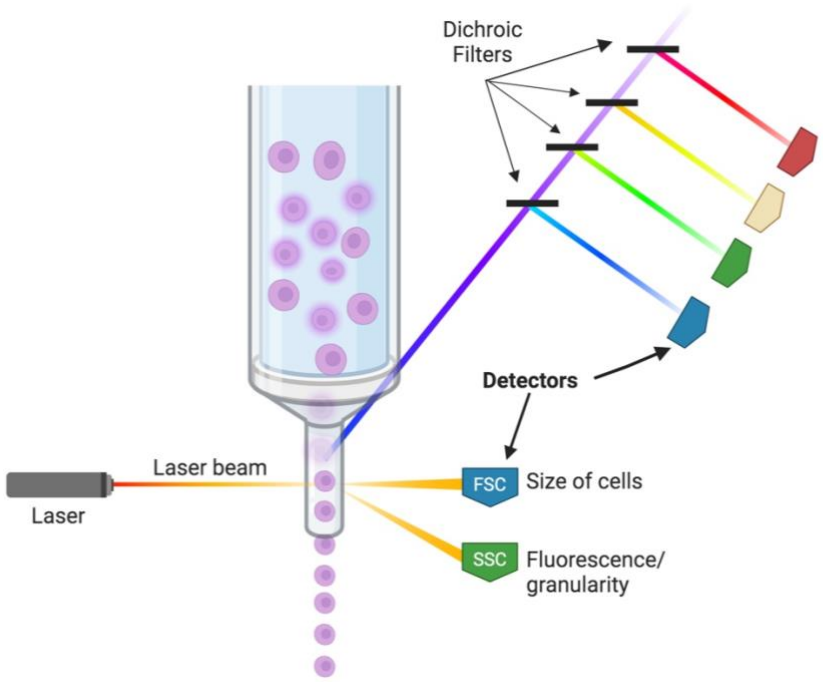

Figure 2.4 Basic components of a flow cytometry device.

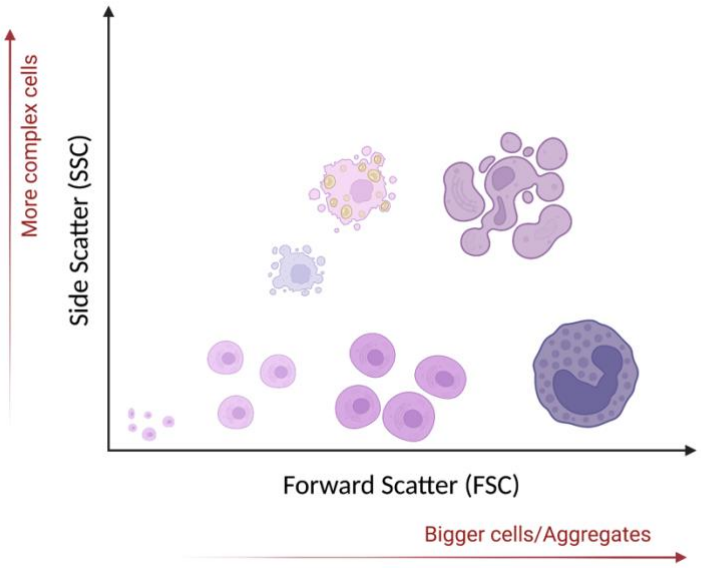

Figure 2.5 Example of cells sorting on a scatter plot. The scatter graph plots the forward scatter (FSC) towards the side scatter (FSC). Therefore, the bigger the cells, the further on the right side of the x axis they will appear. On the other hand, the more granulated the cells, the higher on the y-axis they will be.

In addition to the FFS and SSC data gathered, the flow cytometer also measures cellular fluorescence. This can be useful to measure any change in cell fluorescence due to treatments or to the addition of specific probes to samples. As shown in **Figure** 2.4, the flow cytometer can be equipped with filters that will register only a single or a range of specific wavelengths. The machine utilised in this study was a BD accuri C6 (BD, New Jersey, USA) with four channels for fluorescence intensity, FL-1, FL-2, FL-3, and FL-4 (**Figure** 2.4).

To perform the flow cytometry study, cells were plated in a 24-well plate (**section 2.4.5**) and treated according to the experiment that was carried out (**section 2.4.6**). 48 h after treatment, cells were trypsinised using 250 µL of trypsin in each well. After cell detachment from the well, 750 µL of complete media were added in each well and cell lysate was collected in Eppendorf tubes. Tubes were centrifuged and the supernatant was discarded. The cell pellet was then washed with PBS via gently pipetting the liquid up and down to allow resuspension, followed by centrifugation. Supernatant was discarded and the wash step was repeated one more time to ensure media component were removed from the sample.

2.5.2.1 Flow cytometry setting and gating strategy

Prior to each experimental procedure untreated cells either stained or un-stained were analysed to create a background profile for the cells, whereby the SSC and FSC population will be gated (**Figure** 2.6), and the background fluorescence measured (**Figure 2.7**). The gating defined was then kept throughout the experiments.

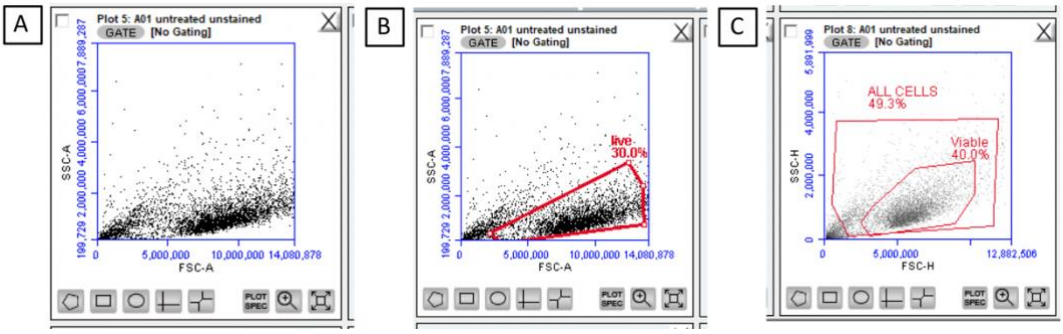

Figure 2.6 Flow cytometry gating strategy. Scatter plot A, B and C show how cells were generally gated for flow cytometry experiments. (A) represents an example of an ungated scatter plot for untreated Calu-3 cells; (B) shows how live cells were identified; (C) reports the final gating, in which events registered towards the origin of the plot (debris) are excluded from the total number of events.

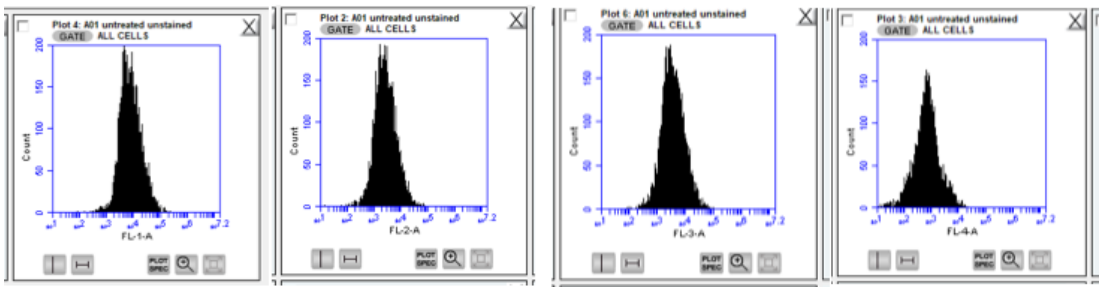

Figure 2.7 Background fluorescence of untreated Calu-3 cells as registered by the four filters built in the device (FL-1, FL-2, FL-3, FL-4).

2.5.2.2 Annexin-FITC/PI analysis

One application of the flow cytometry technique is to monitor cell death via AnnexinV-FITC/PI staining. AnnexinV is a calcium-binding protein that binds the lipid phosphatidylserine (PS), while propidium iodide (PI) is a cell-impermeable dye that binds the DNA. The treatment of cells with AnnexinV-FITC and PI allows the evaluation of the percentage of apoptotic and necrotic cells in a sample. This is possible because the membrane of cells is composed of lipids, such as phosphatidylserine (PS), that are differently distributed in the inner and outer leaflet

of the membrane. Viable cells normally distribute PS in the inner leaflet, whilst apoptotic cells present PS on the outer surface. Thus, cells undergoing apoptosis can bind AnnexinV, which can be fluorescently labelled to allow the detection of a signal. On the other hand, necrotic cells present damaged membrane and cannot bind to AnnexinV. However, necrotic cells can be detected via treatment with PI: the dye is not able to pass the cell membrane and therefore will bind to the DNA of necrotic cells (Van Engeland et al., 1998).

The signal of AnnexinV-FITC was detected by FL-1 (or FL-2) filter, while the PI signal is registered by the FL-3 filter (**Figure** 2.8). Thus, the two fluorescence values (FL-1 and FL-3) for each events (cells) passing through the laser beam are detected and plotted in a dot plot (**Figure** 2.9) to allow the quantification of viable (AnnexinV negative, PI negative), early apoptotic (AnnexinV positive, PI negative), late apoptotic (AnnexinV positive PI positive) and necrotic cells (AnnexinV negative, PI positive) (Crowley et al., 2016; Kumar et al., 2015; Wallberg et al., 2016).

Therefore, following cells trypsinisation and resuspension, AnnexinV-FITC/PI staining was performed as follow. AnnexinV-FITC/PI were purchased Invitrogen, UK (Catalogue Number BMS500FI-300). Firstly, AnnexinV-FITC solution (200 µL) was added to the pellet and resuspended via pipetting. The suspension was incubated in the dark for 10 min at room temperature. Subsequently, the suspension was centrifuged, the supernatant discarded, and the pellet was resuspended in 200 µL of PI solution. Prior to analysis of every sample, the suspension was mixed by vortexing to ensure sample homogeneity. The comparison between the background fluorescence of unstained (**Figure 2.7**) and stained cells (**Figure** 2.8), and between the dot plots of stained and unstained cells (**Figure** 2.10) allowed the determination of successful staining. Data were exported from BD Accuri software as percentages of viable, early apoptotic, late apoptotic, and necrotic cells in each sample analysed.

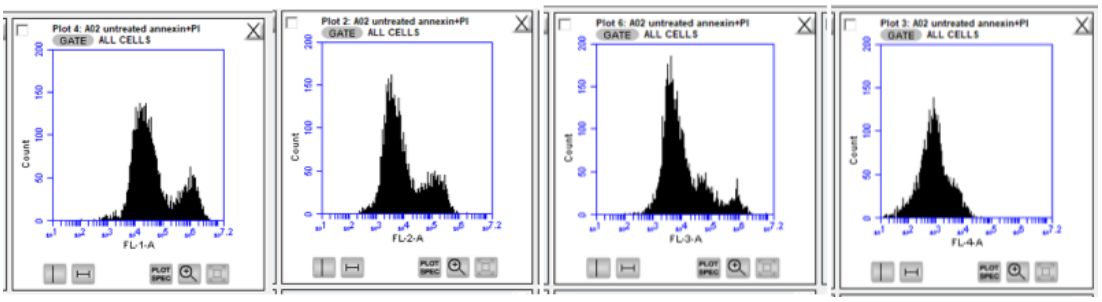

Figure 2.8 Fluorescence of untreated Calu-3 cells following staining with AnnexinV-FITC and PI as registered by the four filters built in the device (FL-1, FL-2, FL-3, FL-4). The AnnexinV-FITC fluorescence is detected by FL-1 or FL-2, while the fluorescence of PI is registered by FL-3. As it can be seen in the 3 fluorescence graphs of FL-1, FL-2 and FL-3, there is an additional peak compared to untreated unstained Calu-3 cells (Figure 2.7), while there is no difference in the signal detected by FL-4.

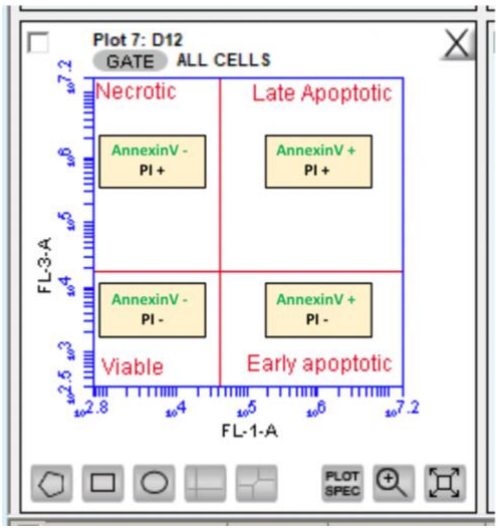

Figure 2.9 Dot plot obtained by plotting FL-1 fluorescence towards FL-3 fluorescence. Events recorded for each sample in this dot plot allowed the quantification of viable, early apoptotic, late apoptotic and necrotic cells.

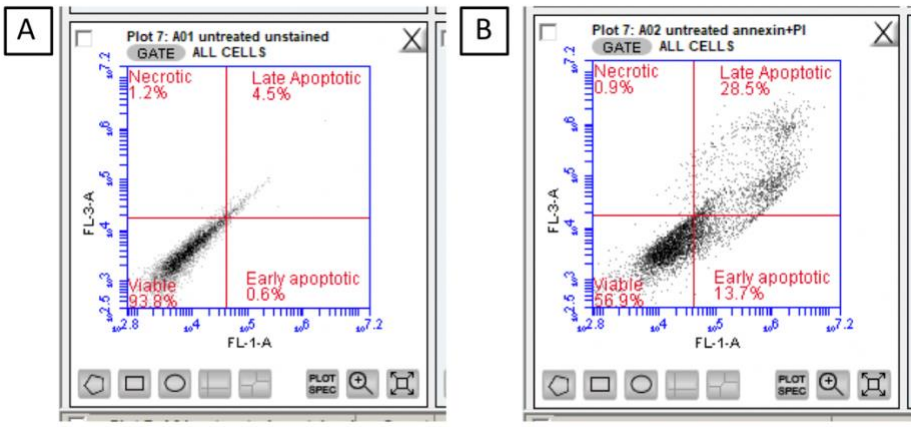

Figure 2.10 Dot plots generated by plotting FL-1 fluorescence towards FL-2 fluorescence for (A) unstained Calu-3 and (B) stained Calu-3 with AnnexinV-FITC/PI.

2.6 RNA Extraction and Polymerase Chain Reaction

Gene expression was analysed as follows: RNA isolation and quantification, complementary DNA (cDNA) generation to allow the conversion of RNA fragments into double stranded hybrid RNA-DNA molecules and finally real time quantitative PCR (RT-qPCR).

Nucleic acid quantification can be either absolute, using DNA standards at known concentration, or relative, that will determine the expression of the gene of interest compared to the expression of a reference gene (or house-keeping gene), that should not have significant variation in expression across different experimental conditions (Benes & Castoldi, 2010; Bustin et al., 2005).

2.6.1 RNA isolation and quantification

The three most commonly employed techniques for RNA extraction from tissue samples are: organic extraction, silica-membrane based spin column technology, and paramagnetic particle technology (Chacon-Cortes & Griffiths, 2014; Tan & Yiap, 2009). The first one is largely employed in research laboratories, and often the organic extraction of RNA from lysates is obtained using chloroform and phenol-guanidine isothiocyanate solutions. Still, the extract obtained are often contaminated by solvents, proteins, DNA and other cellular materials. For this reason, silica-based extraction is frequently used this approach does not require the use of toxic solvents, is relatively simple and provides yield of total intact RNA with low levels of contamination. However, silica-based extraction does not provide DNA separation from the extract. Thus, can cause interference with cDNA generation and RT-qPCR steps. In this study, total RNA was extracted from cells using ReliaPrep™ miRNA Cell and Tissue Miniprep System (Promega). The kit is based on the use of a silica-based column designed to extract total RNA, including miRNA, from samples. Furthermore, it incorporates a DNase treatment step to reduce genomic DNA contamination.

For RNA extraction, plates were placed on ice and growth media removed and cell layers washed with ice-cold PBS. Subsequently, the monolayer was treated with a lysis solution containing lysis buffer (provided with the kit) and 1-thioglycerol. The lysis solution was gently pipetted up and down to facilitate cell detachment and lysis. Lysates were place in 1 mL microcentrifuge tubes and used for RNA extraction immediately or stored at -20°C for future use.

Following lysis (or after lysates thawed at room temperature, if stored at -20°C), samples were vortexed for 10 s to promote and ensure cell lysis. RNA Dilution Buffer (RDB;130 µL) was added

to the lysates, vortexed for 10 s to mix and centrifuged at 12000 x g for 2 min. The clear supernatant was carefully transferred into a clean tube, avoiding transfer of any pelleted material that could interfere with the extraction process. Isopropanol (400 µL) was added to the supernatant, and the solution transferred into a ReliaPrep™ minicolumn placed in a collection tube. The mini-column was centrifuged at 12000 x g for 30 s, the flow-through discarded and the column washed twice with 500 µL RNA Washing solution (RWA): centrifugation was performed at 12000 x g for 30 s for the first wash and for 2 min for the second wash. Nuclease-free water (40 µL) was added to the column and a further centrifugation of 1 min was performed to elute nucleic acids from the column. To eliminate genomic DNA from the eluate, 5 µL of DNase I and 5 µL of DNase buffer were added to the eluate and the mixture incubated at room temperature for 5 min. The reaction was stopped by addition of 150 µL of lysis solution and 300 µL of 95% ethanol were added to tubes and vortexed for 10 s. The content of the tubes were transferred to a new ReliaPrep™ minicolumn (placed on top of a collection tube), centrifuged at 12000 x g for 30 s, and washed twice with RWA as before. Finally, 20 µL of nuclease-free water was added to the column, and the eluate collected by centrifugation at 12000 x g for 1 min.

Total RNA concentration in the extract was quantified using a Nanodrop™ 2000 ultraviolet-visible (UV-Vis) spectrophotometer (Thermo Fisher, UK), with optical densities (OD) of 260 nm and 280 nm averaged from triplicate readings. The absorbance ratio between 260/280 nm was used to determine the quality of the isolated RNA, with ratios of 1.9-2.1 denoting RNA of good quality. Isolated RNA was stored at -80°C until further work.

2.6.2 cDNA synthesis

To analyse gene expression via real-time quantitative PCR (RT-qPCR) the single stranded RNA material was converted into complementary DNA (cDNA) using miScript II RT reagents (Qiagen, Manchester, UK). This kit includes poly(A)polymerase to catalyse the polyadenylation of all the RNAs species in the sample. The addition of an oligo dT primer that specifically binds to polyadenylated tails of fragments and that binds to the reverse transcriptase, guarantees that all the species in the samples are transcribed.

Template RNA was thawed on ice whilst 10x miScript nucleics mix (containing deoxy oligonucleotides necessary for the cDNA transcription, oligo d-T primer necessary for the reverse transcriptase to start its activity, and ATP used by the poly (A)polymerase enzyme), RNase-free water and 5x miScript HiFlex Buffer were thawed at room temperature. Among the two buffers provided in the kit, HiFlex Buffer and HiSpec buffer, the former was chosen as it contains an adjuvant that promotes the reverse transcription of both miRNA and mRNA. Following manufacturer's instructions, a master mix was prepared as shown in Table 2.12, with 300 ng total RNA. A second master mix was prepared without reverse transcriptase to investigate the presence of any interfering genomic material in the cDNA preparation process. Samples were centrifuged briefly and incubated at 37°C for 60 min in a heating block. Finally, samples were heated to 95°C for 5 min to terminate the reaction. The cDNA obtained was either stored at -20°C for future applications or diluted adding 200 µL of Nuclease-free water to the reaction tube.

Table 2.12 cDNA master mix composition.

Master mix. Component	what it contains	Volume/reaction (µL)
5x miScript HiFlex Buffer	Adjuvants to convert miRNA and mRNA into cDNA	4
10x miScript Nucleics Mix	ATP, d-NTP, oligo d-T primer	2
miScript Reverse Transcriptase Mix	Reverse Transcriptase, poly(A)polymerase	2
RNase-free water		Up to 12
Template RNA		Variable
Total Volume		**20**

2.6.3 RT-qPCR

In this study, RT-qPCR was performed using reagents and consumables from Qiagen, Manchester, UK, unless otherwise stated. At all stages of experimental setup, filtered RNase-free pipette tips and RNase-free environment was used. Bench surfaces were sprayed with RNAseZap (ThermoFisher Scientific, UK) prior to start experiments.

Polymerase chain reaction (PCR) is a process that allows DNA amplification and it is commonly used in research laboratories to detect genes expression. To perform PCR it is necessary: a double stranded DNA as a starting point, a thermostable DNA-polymerase – enzyme that can synthesise a complementary sequence of basis for any DNA strand providing it is double stranded, and a primer that is necessary for the enzyme to start its activity. Using primers specific for a gene result in amplification and subsequent detection of only the gene of interest.

The activity of the enzyme is controlled by changes in temperature, usually: at 95°C the enzyme is not active, but the high temperature allows DNA denaturation from dsDNA to single stranded (denaturation phase); at 60°C the enzyme is still not active, but the primer can bind its complementary gene (annealing phase); at 72°C the enzyme is at its optimum working conditions (extension phase). These variations in temperature are repeated cyclically to create millions of copies of the gene of interest: after the first cycle there are only two copies of the gene of interest (the initial copy and the copy created during the first cycle), however after the second cycle the sample will contain 4 copies of the gene. Therefore, the DNA will be copied following an exponential trend.

To monitor the amount of DNA that has been copied the PCR product can be run on an agarose-stained gel (the brighter the signal, the more the DNA was copied). However, Real Time PCR (RT-PCR) allows the monitoring of PCR efficiency via a device which detects the fluorescence generated by adding a fluorescent probe or dye to the sample. One of the most common used dye to generate fluoresce in PCR applications is SYBR GREEN, that gives a bright fluorescent signal (E_x 492, E_m 540) when bound to ds-DNA fragments. Therefore, the higher the fluorescent signal is, the higher is the number of copies in the sample. A software linked to the PCR machine will provide a sigmoidal curve based on the detected SYBR GREEN signal (**Figure** 2.11) (Arya et al., 2005; Navarro et al., 2015).

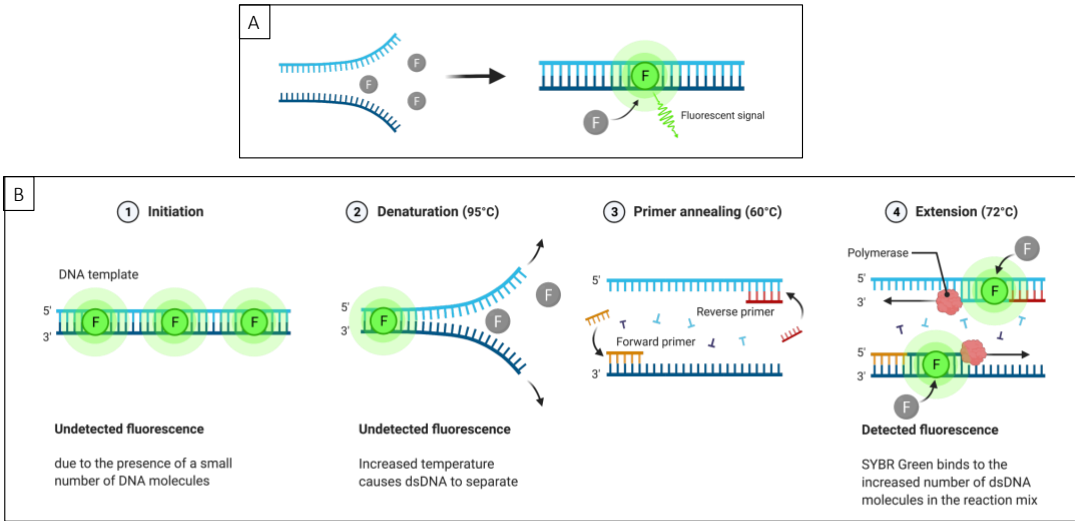

Figure 2.11 Diagram of SYBR mechanism of action. (A)SYBR Green mechanism of action: binding of SYBR Green with dsDNA produce a fluorescent signal that can be detected; (B) RT-PCR monitoring of dsDNA copies formation via SYBR Green.

QuantiTect Primer Assays (hsa-miR184, hsa-SNORDD48, hsa-SNORDD68, has-SNORDD72, GAPDH, BCL2, c-myc, TNFAIP-2, AKT-2) were employed in this study (**Table** 2.13). Prior to perform RT-qPCR, the primers were centrifuged and reconstituted in 1.1 mL of TE buffer. All primer products will be referred to as Primer mix. For miRNA expression quantification, has-SNORDD48, hsa-SNORDD68 and hsa-SNORDD72 were screened to identify the best reference gene for the experimental conditions use, while GAPDH was used as housekeeping gene for mRNA expression. The use of different reference genes depending on the nucleic acid expression investigated was in line with qPCR principles that a suitable reference gene should have a similar size of the target gene quantified (Vandesompele et al., 2002).

PrecisionPLUS SYBR Green Master Mix (Primer Design), 10x miScript Universal Primer, RNase-free water and Primer mix were thawed at room temperature, while template cDNA was thawed on ice. Reaction master mixes were scaled up according to the number of samples to test, based on the amounts shown in **Table** 2.14.

Table 2.13 List of QuantiTect Primer Assays employed in this study and their catalogue number.

Primer assay	Catalogue number	GeneGlobe ID
hsa-miR-184	249900	/
hsa-SNORDD 48	249900	/
hsa-SNORDD 68	249900	/
hsa-SNORDD 72	249900	/
GAPDH	249900	QT00273322
BCL-2	249900	QT00044646
c-myc	249900	QT00035406
TNFAIP-2	249900	QT00098343
AKT-2	249900	QT00085001

Table 2.14 PCR Reaction mix components and volumes used.

Component of Reaction Mix	What it contains	Volume (µL)
PrecisionPLUS SYBR Green Master Mix	SYBR green, DNA Polymerase, deoxy nucleotides	10
Universal Primer	Reverse Primer	2
Primer	Forward Primer	2
RNase-free water		4
Total Volume		18

Subsequently, 18 µL of reaction mix was aliquoted into 0.1 mL PCR strip tubes followed by addition of 2 µL of template cDNA. A "no template control" was added to each run to identify any contaminating DNA in the reaction reagents by substituting template cDNA with 2 µL of RNase-free ddH20. Strip tubes were placed into a 72-well rotor-disk which was placed inside of a Rotor-Gene Q real time cycler, supported by Rotor-Gene Q version 2.1.0.9 software (Qiagen, UK). RT-qPCR was set-up as follows: 95°C for 2 min followed by 40 cycles of 95°C for 10 s (denaturation), 60°C for 60 s (annealing) and 70°C for 30 s (extension). A post PCR run melt curve was performed to confirm the specificity of the primers: tubes were subject to an increase in temperature of 1°C per second, starting at 60°C and terminating at 95°C. The increase in temperature denatures double-stranded DNA causing SYBR green to dissociate, thus the melt curve analysis allows quantification of the resultant loss of fluorescence. The

presence of more than one curve represents low specificity of the target used, and therefore poor-quality results. The melting temperature (Tm) varies depending on the base composition of each target DNA, giving an indication of target specific binding and allowing any anomalies to be removed in further analysis (Ririe et al., 1997).

Data for each run were exported and analysed for relative quantification of the genes of interest. Firstly, analysis of the melt curve was performed to evaluate target specificity. Secondly, the percentage of amplification efficiency (AE%) for each sample was evaluate: this parameter will give an indication of how much the sample have been amplified during the PCR cycles. Data were considered of relevant quality when having AE% values higher than 80% and differing one from each other of ±10%.

Two important values were determined prior to data analysis: threshold, a value determined and adjusted above the background noise, and cycle threshold (C_t), that is the cycle number at which the amplification curve crosses the threshold line (**Figure** 2.12).

Results were analysed following the comparative Ct method ΔΔCt method (Livak & Schmittgen, 2001). Data were normalised to a housekeeping gene, whose expression remained relatively stable between samples and experiment, and quantified and depicted relative to the experimental control group: $\Delta\Delta Ct = \Delta Ct_{treated} - \Delta Ct_{untreated}$. $\Delta Ct_{treated}$ is the mean Ct of the gene of interest (GOI) minus the mean Ct of the housekeeping control ($Ct_{GOI} - Ct_{Control}$) from duplicate analysis of the experimental treatment groups. Whilst $\Delta Ct_{untreated}$ is the mean Ct of the GOI minus the mean Ct of the normalisation control ($Ct_{GOI} - Ct_{Control}$) from duplicate analysis of the experimental control group.

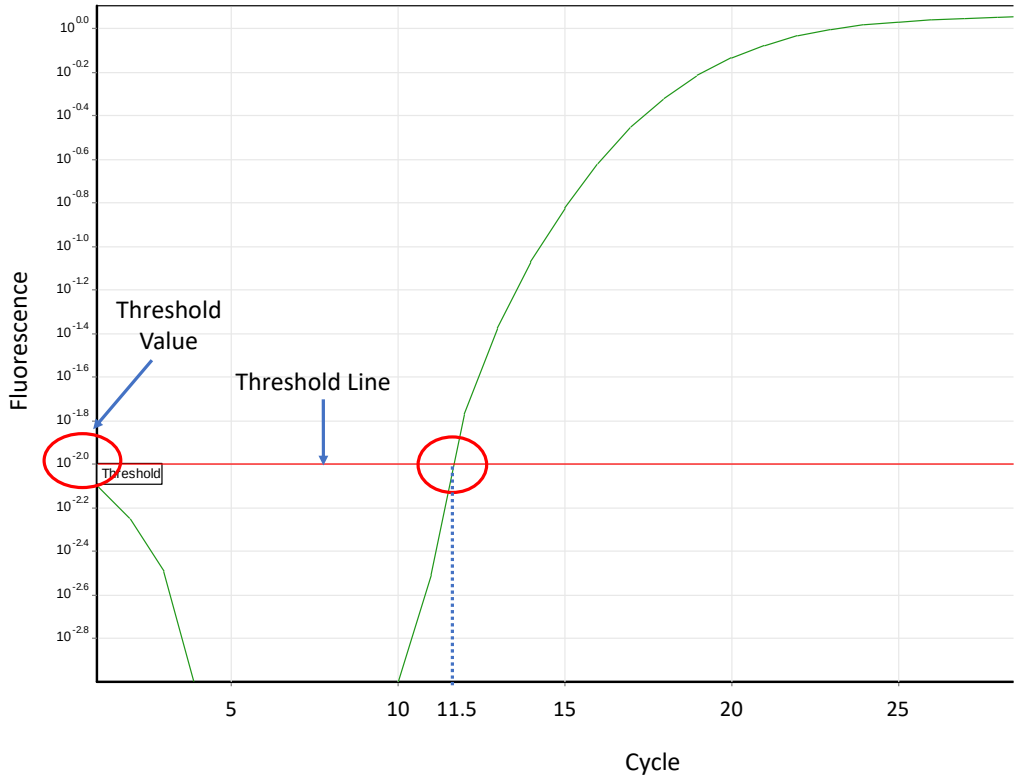

Figure 2.12 RT-PCR curve (linear curve) and Ct identification. Once the PCR run completed, a threshold was set to remove any background noise (threshold line). The Cycle number in which the sample curve meets the threshold line is the Ct value for the specific sample.

2.7 Western Blot

Sodium dodecyl sulfate-polyacrilamide gel electrophoresis (SDS-PAGE) followed by Western Blotting is a common technique used to detect the presence of a protein in a sample (Taylor & Posch, 2014) and was used to evaluate the impact of the oligonucleotide treatments of target gene expression, specifically BCL-2. All the steps were performed using reagents, consumables and equipment purchased from Bio-Rad, Watford, UK unless otherwise stated.

2.7.1 Protein Isolation and Quantification

Cells were detached from plates by trypsinisation as described above. The cell suspension was transferred into 2 mL microcentrifuge and centrifuged for 5 min at 3000 x g (Eppendorf centrifuge 5804R). The supernatant was discarded and the tubes containing cell pellet were place on ice to ensure sample stability. Pellets were suspended in 120 μL of lysis buffer composed of Radio Immuno Precipitation Assay buffer (RIPA) and Protease inhibitor 10:1. RIPA buffer was composed of 150 mM sodium chloride, 1.0% Triton X-100, 0.5% sodium

deoxycholate, 0.1% sodium dodecyl sulphate (SDS), 50 mM Tris, components that cause cell membrane degradation and lysis. Protease inhibitor is added to RIPA buffer to ensure that cell proteases would not degrade proteins.

Pierce BCA protein assay kit (Thermofisher scientific, UK) was used to quantify the amount of protein in the samples, following the manufacturer's instructions. The assay is based on the colorimetric detection of protein via bicinchonic acid (BCA): firstly, in alkaline environment proteins can reduce Cu^{2+} in Cu^{1+}; secondly, BCA chelates Cu^{1+} forming a purple-coloured complex that absorbs light at a wavelength of 562 nm. To perform the assay, a range of bovine serum albumin (BSA) standards were prepared from 0-2000 µg/mL. Working reagent was prepared by mixing BCA reagent A (containing alkaline BCA solution) and reagent B (containing Cu^{2+}) in 50:1 ratio. Then 10 µL of BSA standards and unknown samples were pipetted in duplicate into a 96-well plate followed by the addition of 200 µL of working reagent. After incubation at 37°C for 30 min, the plate was cooled to room temperature and absorbance was measured at 562-590 nm on a CLARIOstar plate reader (BMG Labtech, Aylesbury, UK). Protein concentration in the unknown samples was calculated as follows: data from the BSA standards were used to generate a standard curve of absorbance versus BSA concentration, hence protein concentration of the sample was calculated from the standard curve.

2.7.2 SDS-PAGE

To facilitate protein separation by size the sample can be treated with a negatively charged molecule (sodium dodecyl sulphate (SDS)) that creates a negative halo around the protein. Therefore, protein net-charge becomes negative, and the charge/size ratio is similar for all the proteins in the sample allowing their separation by size.

Running buffer was prepared, containing 25 mM Tris base, 190 mM glycine, 0.1% SDS pH ~8.3. Laemmli buffer (65.8 mM Tris-HCl, pH 6.8, 2.1% SDS, 26.3% (w/v) glycerol, 0.01% bromophenol blue) was purchased from BioRad (4x) and was mixed with 100mM DDT. For electrophoresis, 20 µg of sample lysate was diluted 1:4 in 4X Laemmli buffer containing 100 mM DTT and heated at 95°C for 5 min to reduce and denature the sample, respectively. Following this, the sample was loaded into wells of 12% polyacrylamide mini-PROTEAN TGX precast gel within an electrophoresis chamber filled with running buffer. Precision plus protein Kaleidoscope molecular weight marker was loaded into another well. The gel was run at 150 V for 45 min or until the migration front reached the bottom of the gel.

2.7.3 Western blotting

Protein transfer on to a membrane was performed using the semi-dry method (Litovchick, 2018). This was achieved by applying voltage a system composed of filter paper, the polyacrylamide gel in which protein have been separated and a membrane (nitrocellulose or polyvinylidene difluoride (PVDF)). **Figure** 2.13 shows how the components were stacked to ensure protein transfer: when electricity is applied, the negatively charged protein (due to the presence of SDS) will migrate towards the positive anode. Transfer buffer (48 mM Tris base, 39 mM glycine, 0.04% SDS, 20% methanol) and 10X Tris buffered saline (TBS) (200 mM Tris base, 1500 mM sodium chloride, pH ~7.6) were prepared.

A polyvinylidene difluoride (PVDF) membrane was used, hence it was activated for 2 min in methanol. The activated membrane, filter paper and the gel were equilibrated in ice cold transfer buffer for 5 min prior to transfer. The gel and membrane were sandwiched between blotting paper (**Figure** 2.13) and soaked in transfer buffer before rolling to remove air bubbles. Protein was transferred onto the membrane using Trans-blot turbo transfer apparatus run at 25 V constant and up to 1.0A for 30 min.

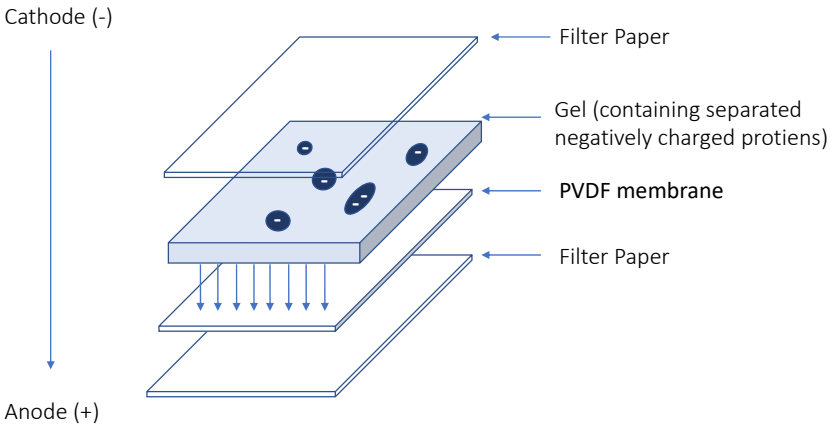

Figure 2.13 Mechanism of protein transfer from polyacrylamide Gel to PVDF membrane. Gel and membrane are stacked in a sandwich in the order displayed in the image. The application of electricity to the system allows the migration of negatively charged protein to the positive anode and hence to be entrapped by the membrane.

Finally, to detect the protein of interest antibody probing was performed. to the primary antibody binds to the protein of interest, while a secondary antibody will bind to the primary antibody. The secondary antibody is usually labelled with a reporter, an enzyme that is able to catalyse the formation of a fluorescent product that can be detected. Therefore, the

detection of the product will indicate the presence of the protein of interest in the sample (Figure 2.14).

Following protein transfer, TBS+Tween80 (TBST) (1:10 dilution of 10X TBS with addition of 0.1% (v/v) Tween20) and blocking buffer (5% (w/v) fat-free milk in TBST) were prepared.

The membrane was submerged in 10 mL of blocking buffer, covered and agitated on an orbital shaker for 1 h at room temperature. Next, the membrane was washed in 10 mL TBST and incubated with primary antibody, diluted in blocking buffer overnight at 4°C, whilst being kept on a Stuart roller shaker (Cole-Parmer, Straffordshire, UK). The following day, the membrane was washed in TBST for 5 x 5 min to remove any remaining primary antibody, before incubation in horse radish peroxidase (HRP)-conjugated secondary antibody (Table 2.15) diluted with TBST agitated on an orbital shaker at room temperature for 1 h. Subsequently, the secondary antibody was removed and to prevent any interference of residual secondary antibody during the visualisation process, the membrane was washed for 5 x 5 min in TBST. Following washing, HRP substrate was prepared by mixing components of the Clarity western ECL substrate kit in a 1:1 ratio (2 mL: 2 mL). This was then added to the protein side of the membrane and incubated for 5 min at room temperature (Figure 2.14). The membrane was then removed from the substrate solution and placed in a ChemiDoc XRS+ digital imager where it was visualised and quantified.

2.8 Confocal microscopy

Briefly, Calu-3 cells were plated on a cover slip placed on a 6-well plate (section 2.4.5) and treated (section 2.4.6) as explained above. Following 48 h of incubation, media was removed from wells and cell layers were washed with PBS twice. Subsequently, 2 mL of 4% paraformaldehyde was added to each well to allow cells fixing onto the coverslip and left at room temperature for 10 min. Following fixation, the coverslip was washed twice with PBS. Cells were mounted with 4',6-diamidino-2-phenylindole (DAPI) containing fluoromount G mounting medium. Images were collected using a Zeiss LSM 710 Confocal microscope using oil immersion objective 63x. Images of the DAPI stained nucleus were captured using excitation wavelength 405 nm (blue laser), emission wavelengths 410 – 496 nm and laser power 0.8%. Images of the TAMRA labelled oligonucleotide were captured using an excitation wavelength of 542 nm (red laser), emission wavelength 542 – 568 nm and laser power 20%.

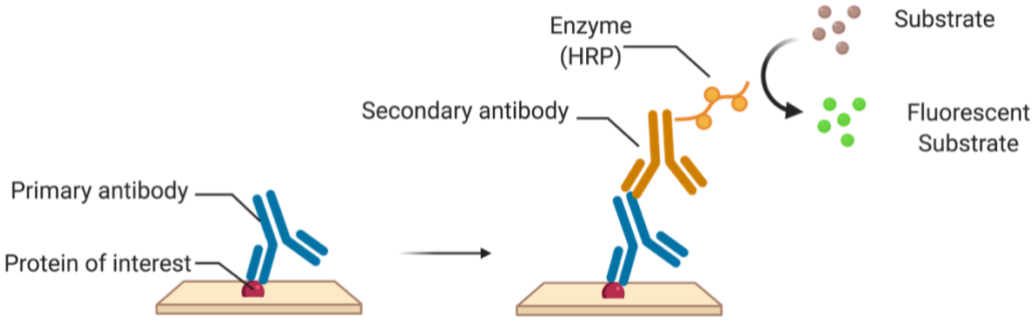

Figure 2.14 Protein of interest detection after protein transfer. A primary antibody specific for the primary of interest binds to the protein. Afterwards, a secondary antibody (complementary to the primary antibody) bins to the primary antibody. The signal is detected given the conjugation of the secondary antibody with an enzyme (commonly horse radish peroxidase (HRP) that catalyse the transformation of a substrate in a fluorescent product.

Table 2.15 List of primary and secondary antibody used for western blot experiments.

Antibody used	Antibody type	Catalogue Number
BCL-2 primary	Rabbit monoclonal	Ab182858
Secondary antibody	Donkey anti-rabbit	Invitrogen, SA1-200
β-actine	Mouse monoclonal	Sigma, A1978
Secondary antibody	Goat anti-mouse	Sigma, A-3682

2.9 Statistical Analysis

All values were expressed as mean ± standard deviation of three independent experiments (*n=3*) unless otherwise specified. Data was subjected to normality testing and once confirmed appropriate parametric analyses, t-test or One-way analysis of variance (ANOVA) (groups ≥3) with Dunnet's or Tukey's post-hoc test was used to compare data sets. A *P* value of <0.05 indicates statistically significance throughout the studies. The *P* values are expressed as **P*<0.05, ***P*<0.01, ****P*<0.001, *****P*<0.0001.

Taguchi DOE statistical analysis was performed using IBM SPSS statistic software. Multiple regression analysis, Analysis of Variance (ANOVA) and F-Test have been used to build prediction models for nanoparticles size and PDI. One-way ANOVA with Tukey post hoc test was employed to compare formulations obtained from study.

For cell biology studies, statistical analysis was performed using GraphPad Prism 8.04 statistical software using ANOVAs. Dunnett's or Tukey's post-test were employed according to the experiment carried out. Particularly, Dunnet's post-test was used when comparing the mean of a samples to the mean of a control treatment, while Tukey's post-test was employed to compare the mean of a sample with the mean of every other sample of the experiment.

3 Optimisation of Chitosan Nanoparticles formulation for microRNA Delivery

3.1 Introduction

Chitosan (CHT) is a natural polymer that can be extracted from several natural sources such as crustaceans and fungi. It has interesting properties such as biocompatibility, biodegradability, mucoadhesive and antimicrobial properties (section 1.3.4). Given its properties, chitosan applications span through food, cosmetic, agriculture and pharmaceutical applications (Aider, 2010; Bellich et al., 2016; Dash et al., 2011; Ta et al., 2021).

The use of CHT and CHT derivatives (section 1.3.4 and Figure 1.7) for pharmaceutical applications has been exploited by many researchers for the delivery of small molecules (Al-Kassas et al., 2016; Coutinho et al., 2020; Tzeyung et al., 2019), proteins (Hoseinpur et al., 2022; Radwan et al., 2022) and oligonucleotides (Miele et al., 2021; M. Nguyen et al., 2019; Ragelle et al., 2014).

The scalability of laboratory-manufactured NPs to industry products faces numerous challenges, including poor reproducibility of results, difficulty of producing big batches with retention of similar properties at laboratory scale. From a laboratory point of view, NPs prepared with microfluidic showed better properties in terms of control over size, reproducibility and polydispersity index compared to bulk methods (Chiesa et al., 2019). Published studies revealed the promising use of microfluidic mixing technology to prepare CHT NPs for various applications (Majedi et al., 2013; Pessoa et al., 2017; Sadat Majedi et al., 2012; Shamsi et al., 2017; D. Yang et al., 2021). However, the optimisation of NPs made of water-soluble CHT derivatives via microfluidic intended for oligonucleotide delivery has still not been fully investigated, except for the study of Chen (Chen et al., 2014).

Recently, miR-184 involvement in the development and spread of several types of malignancies was investigated (Chen & Stallings, 2007; Huang et al., 2016b; Malzkorn et al., 2010; Wu et al., 2014). Researchers underlined its downregulation in lung cancer cell lines and patient-derived tissues compared to non-cancerous tissue. The low levels of miR-184 in cancer cells might drive cancer progression as well as influence the cells sensitivity towards cisplatin (Longqiu et al., 2020; Tung et al., 2016). For these reasons, miR-184 replacement

therapy seems a promising strategy to tackle lung cancer and therefore, a miR-184 mimic was selected as model oligonucleotide to investigate NP-mediated oligonucleotide delivery.

The overexpression of oligonucleotide *in vitro* can be reached via the use of transfection reagents, such as plasmids, lipid molecules or commercially available kits. They are non-viral vectors that can be used to introduce naked nucleic acids into eukaryotic cells, therefore the effect of the oligonucleotide on the cells can be investigated (Wang et al., 2018). Commonly, these reagents are lipid molecules that create pores within the cell membranes to allow oligonucleotides entrance inside the cell, where they would then be able to exert their action. Among them, INTERFERin® is a reagent marketed by PolyPlus that is composed of cationic molecules that can shuttle the negatively charged oligonucleotides inside the cytoplasm. It has been used for the successful transfection of siRNA (Chapard et al., 2014), miRNA mimics (Qi et al., 2016) and single- or double-stranded DNA (Seifert et al., 2015) into mammal cells. In this study, transfection of Calu-3 cells via INTERFERin® was investigated and compared to miR-184 delivery via NPs.

3.2 Aims

The aim of this study was to optimise and compare the CS HCl, CS GLU and CS GLY NPs for the delivery of miR-184 mimic into Calu-3 cells. This was achieved through the following objectives:

- Optimising the formulation of the CS NPs using microfluidic mixing technology;
- Investigating the capability of CS NPs to complex with miR-184 mimic;
- Examination of miR-184 expression in a panel of NSCLC cells;
- Optimising the transfection of miR-184 mimic via INTERFERin®;
- Confirm the successful uptake of miR-184 mimic-loaded CS NPs in Calu-3 cells.

3.3 Methods

3.3.1 Chitosan nanoparticles optimisation via microfluidic

Chitosan NPs were prepared with chitosan derived from aspergillus (CS ASP) and three water soluble derivatives, CS HCl, CS GLY and CS GLU using Nanoassemblr® Benchtop, as described in section 2.2. The optimisation was performed in two steps: firstly, a Taguchi DoE was performed (the parameters used are explained in 2.2.1.1) and secondly a flow ratio investigation was carried out as described in section 2.2.1.2. NPs were characterised measuring their size and PDI using a Malvern nano ZS (Malvern PANalytical, Worcestershire, UK) as reported in section 2.3.1. Optimisation was conducted to reach NPs size below 300 nM and PDI value smaller than 0.35.

3.3.2 miR-184 mimic encapsulation and gel retardation assay

miR-184-loaded NPs were prepared and characterised (size, PDI, Zeta Potential, EE%) as described in section 2.2.2 and 2.3.2, respectively. To investigate the successful complexation of the oligonucleotide within the NPs, a gel retardation assay was performed as described in 2.3.3.

3.3.3 Housekeeping Gene Screening and miR-184 Baseline Investigation

As outlined in section 2.4, lung cancer cell lines were plated, and 48 h afterwards harvested. Total RNA was extracted, cDNA was generated, and RT-qPCR was performed. Results were analysed by comparing Ct values of each reference for all the cell lines (section 2.6).

After the identification of a normalisation gene, miR-184 expression in all the cell lines (listed in section 2.1) was investigated. However, qPCR results were not analysed as stated in section 2.6.3 given the lack of a control group (such as untreated cells) to which miR-184 expression could be related. Hence, results were analysed by comparing ΔCt values, where ΔCt is defined as:

$$\Delta\mathrm{Ct} = \mathrm{Ct}\ (\mathrm{miR} - 184) - (\mathrm{Ct\ normalisation\ gene})$$

3.3.4 MicroRNA-184 Mimic and Inhibitor Transfection via INTERFERin®

The miR-184 mimic (product number C-300635-03-0050) and inhibitor (IH-300635-05-0050) used in this study and the non-targeting control (NTC) (product number CN-001000-01-50) were purchased from Horizon. Calu-3 and Calu-6 cells were plated and treated as previously described (section 2.4) to have a final miR-184 mimic concentration in wells of 5, 20 and 700 nM and of mIR-184 inhibitor of 5 and 20 nM. 48 h after treatment, cells were harvested and total RNA was extracted, cDNA was generated and RT-qPCR was performed (section 2.6.1, 2.6.2 and 2.6.3).

3.3.5 miR-184 mimic Delivery via CS HCl NPs

MiR-184-loaded CS HCl NPs, NTC-loaded CS HCl NPs and Blank NPs were prepared as described (section 2.2.2). Therefore, Calu-3 cells were treated with the CS HCl NPs and 48 h after treatment were harvested, total RNA was extracted, cDNA was generated and RT-qPCR was performed (section 2.6.1, 2.6.2 and 2.6.3). Results were normalized to untreated NPs.

3.3.5.1 Confocal Imaging

To visually confirm NPs internalisation, a fluorescently labelled oligonucleotide (5'TAMRA-miR-184 mimic, purchased by Dharmacon, UK) was employed to prepare CS HCl NPs using the optimum parameters obtained from the encapsulation study. Calu-3 cells were plated on glass cover slips in 6-well plates and treated with the 5'-TAMRA-184-NPs. Images of the DAPI stained nucleus were captured as stated in section 2.8.

3.3.6 Statistical Analysis

Statistical analysis for Taguchi DoE was performed with MiniTab Statistical software. For the other experiments, GraphPad Prism 8.0 statistical software was used. In both cases, one-way ANOVA with Dunnett's or Tukey's comparison tests were applied (section 2.9) in accordance with the experiment carried out and stated throughout the results. All values are expressed as mean ± standard deviation (SD) of a variable number of independent experiments, which is stated throughout. The *P* values are expressed as **P*<0.05, ***P*<0.01, ****P*<0.001, *****P*<0.0001.

3.4 Results

3.4.1 Blank Chitosan Nanoparticle Optimisation

3.4.1.1 Taguchi Design of Experiment (DoE)

To optimise the parameters (FRR, TFR, [polymer], [TPP]) for the formulation of blank CHT NPs, a Taguchi DoE was employed. The output of Minitab indicated a set of 18 experiments that was performed for each CHT derivatives employed in the study.

Minitab Statistical Software was employed to analyse the set of 18 formulations and to determine the influence on NPs size and PDI of the investigated parameters. FRR resulted to be the parameter conveying the highest influence on NPs size and PDI for all the CS derivatives. On the other hand, TFR resulted to be the parameter having the least impact on NPs size and PDI for all the CS derivatives, except for CS ASP, where CHT concentration resulted to have the least influence instead. The remaining parameters, being CHT and TPP concentration, resulted to impact on NPs size and PDI without a specific pattern (CHT concentration had a higher impact on NPs size and PDI for CS HCl and CS GLU, whilst TPP concentration seemed to be more relevant to determine CS GLY and CS ASP size and PDI). Table 3.1 provides a summary of the ranking values of each parameter for all the CS derivatives investigated.

As reported in Table 3.2, the NPs size ranged from 89.15±26.29 nm to 4290.66±1292.92 nm for CS HCl, 165.3±3.75 nm to 1538.5±5 nm for CS GLU, 2288.33±1658.51 to 191.50±24.77 for CS GLY and from 1606.25.50±1514.27 to 213.65±19.58 for CS ASP. Table 3.2 also reported PDI values for all the formulations performed, which range from 0.29±0.04 to 0.62±0.23 for CS HCl, 0.14±0.06 to 0.56±0.01 for CS GLU, 0.91±0.16 to 0.11±0.14 for CS GLY and 0.65±0.0.14 to 0.24±0.04 for CS ASP.

Table 3.1 Summary of ranking values of each parameter for the 4 types of chitosan employed in the study.

	CS GLU	CS GLY	CS HCl	CS ASP
FRR	1	1	1	1
TFR	4	4	4	3
[CHT]	3	2	3	4
[TPP]	2	3	2	2

The Taguchi DoE analysis with the 'smaller-is-better' criterion was employed to determine the values of each parameter that would provide the best outcome, which for the purpose of our study corresponded to the smaller size and smaller PDI. Parameters scoring the higher S/N ratio corresponded to the optimum condition to employ to prepare the formulations (Figure 3.1).

CS HCl: the best formulation was manufactured employing the following parameters: CS HCL concentration 0.5 mg/mL, TPP concentration 0.25 mg/mL, TFR 0.64 mL/min and FRR 4:1 (Table 3.3, Figure 3.1 A) which are the parameters used to prepare formulation G (Table 3.2). The optimum formulation was prepared and showed a size of 105.96 ± 11.00 nm and a PDI of 0.29 ± 0.04 and it was employed to carry out further studies (Table 3.3).

CS GLU: the parameters to produce the smaller size and PDI was: CS GLU concentration 0.5 mg/mL, TPP concentration 0.25 mg/mL, TFR 1 mL/min and FRR 5:1 (Table 3.3, Figure 3.1 B). The optimum calculated formulation was manufactured and showed a size of 142.73 ± 6.60 nm and a PDI of 0.34 ± 0.08 and it was employed to carry out further studies (Table 3.3).

CS GLY: the best formulation with a size of 199.20 ± 8.50 nm and a PDI of 0.22 ± 0.01, which was employed for further study (Table 3.3) was employed with CS GLY concentration of 0.25 mg/mL, TPP concentration of 0.5 mg/mL, TFR of 0.64 mL/min and FRR 5:1 (Table 3.3, Figure 3.1 C).

CS ASP: the best formulation was manufactured employing the following parameters: CS ASP concentration 0.5 mg/mL, TPP concentration 0.5 mg/mL, TFR 0.64 mL/min and FRR 5:1 (Table 3.3, Figure 3.1 D). The resulting formulation showed a size of 142.15 ± 5.75 nm and a PDI of 0.52 ± 0.05, which was employed for further study (Table 3.3).

Table 3.2 Size (nm) and PDI values of CS NPs prepared with parameters indicated by Taguchi DoE. (n=3, mean ± SD).

	CS HCl		CS GLU		CS GLY		CS ASP	
	Size (nm)	PDI	Size (nm)	PDI	Size (nm)	PDI	Size (nm)	PDI
A	4023.66 ± 212.36	0.34 ± 0.16	803.45 ± 12.35	0.31 ± 0.07	1133.70 ± 496.50	0.65 ± 0.41	267.60 ± 94.04	0.45 ± 0.02
B	4290.66 ± 1292.92	0.42 ± 0.28	1538.50 ± 5.00	0.56 ± 0.01	1438.00 ± 252.14	0.91 ± 0.16	389.40 ± 54.16	0.57 ± 0.21
C	3006 ± 466.66	0.62 ± 0.23	2429.00 ± 594.35	0.33 ± 0.07	2288.33 ± 1658.51	0.45 ± 0.47	3864 ± 4560.83	0.31 ± 0.03
D	3818 ± 532.25	0.45 ± 0.44	1046.50 ± 154.70	0.40 ± 0.09	284.07 ± 93.93	0.11 ± 0.14	1216.75 ± 809.28	0.24 ± 0.04
E	3752.66 ± 1260.42	0.52 ± 0.16	1907.00 ± 33.00	0.24 ± 0.06	1663.00 ± 254.57	0.97 ± 0.05	1551.55 ± 1709.01	0.40 ± 0.02
F	130.46 ± 14.84	0.36 ± 0.07	288.15 ± 18.94	0.25 ± 0.06	749.57 ± 71.05	0.59 ± 0.12	264.60 ± 17.53	0.66 ± 0.15
H	158.6 ± 7.83	0.36 ± 0.05	519.50 ± 24.95	0.26 ± 0.00	790.87 ± 137.12	0.73 ± 0.12	213.65 ± 19.58	0.47 ± 0.02
I	4022.33 ± 715.06	0.48 ± 0.08	2451.50 ± 13.50	0.27 ± 0.02	1523.33 ± 668.33	0.95 ± 0.09	1606.25 ± 1514.26	0.66 ± 0.18
J	251.1 ± 82.31	0.48 ± 0.015	485.25 ± 14.70	0.26 ± 0.05	406.37 ± 32.36	0.22 ± 0.11	229.90 ± 53.03	0.51 ± 0.11
K	102.50 ± 39.17	0.38 ± 0.1	165.30 ± 3.75	0.16 ± 0.07	441.77 ± 151.49	0.37 ± 0.14	221.45 ± 55.50	0.54 ± 0.06
L	109.51 ± 18.26	0.34 ± 0.06	254.80 ± 6.45	0.14 ± 0.06	410.87 ± 55.55	0.30 ± 0.19	135.45 ± 13.08	0.48 ± 0.23
M	220.46 ± 37.51	0.47 ± 0.04	340.30 ± 14.44	0.28 ± 0.07	257.47 ± 42.37	0.15 ± 0.02	203.55 ± 20.85	0.47 ± 0.13

	CS HCl		CS GLU		CS GLY		CS ASP	
	Size (nm)	PDI	Size (nm)	PDI	Size (nm)	PDI	Size (nm)	PDI
N	148.16 ± 29.15	0.38 ± 0.06	294.65 ± 94.97	0.25 ± 0.03	1217.40 ± 215.73	0.74 ± 0.23	399.95 ± 188.01	0.50 ± 0.36
O	89.15 ± 26.29	0.37 ± 0.05	199.40 ± 0.55	0.23 ± 0.02	312.02 ± 129.76	0.22 ± 0.07	328 ± 145.66	0.57 ± 0.09
P	198.83 ± 58.01	0.38 ± 0.04	664.85 ± 4.50	0.23 ± 0.02	1204.33 ± 89.76	0.85 ± 0.05	216.10 ± 30.40	0.56 ± 0.01
Q	2360.33 ± 417.90	0.36 ± 0.16	959.85 ± 319.64	0.35 ± 0.08	191.50 ± 24.77	0.18 ± 0.04	466.65 ± 2.75	0.56 ± 0.12
R	126.39 ± 59.55	0.38 ± 0.03	316.80 ± 14.10	0.34 ± 0.01	1280.87 ± 634.89	0.83 ± 0.16	169.75 ± 28.49	169.75 ± 0.09

Table 3.3 Parameters employed for each CHT to prepare the best formulation according to NPs size and PDI using MiniTab statistical software. (n=3, mean ± SD).

	FRR	TFR	[CHT] mg/mL	[TPP] mg/mL	SIZE (nm)	PDI
CS CHl	4:1	0.64	0.5	0.25	105.9 ± 11.00	0.29 ± 0.04
CS GLU	5:1	1	0.5	0.25	142.73 ± 6.60	0.34 ± 0.08
CS GLY	5:1	0.64	0.25	0.5	199.20 ± 8.50	0.22 ± 0.01
CS ASP	5:1	0.64	0.5	0.5	142.15 ± 5.75	0.52 ± 0.05

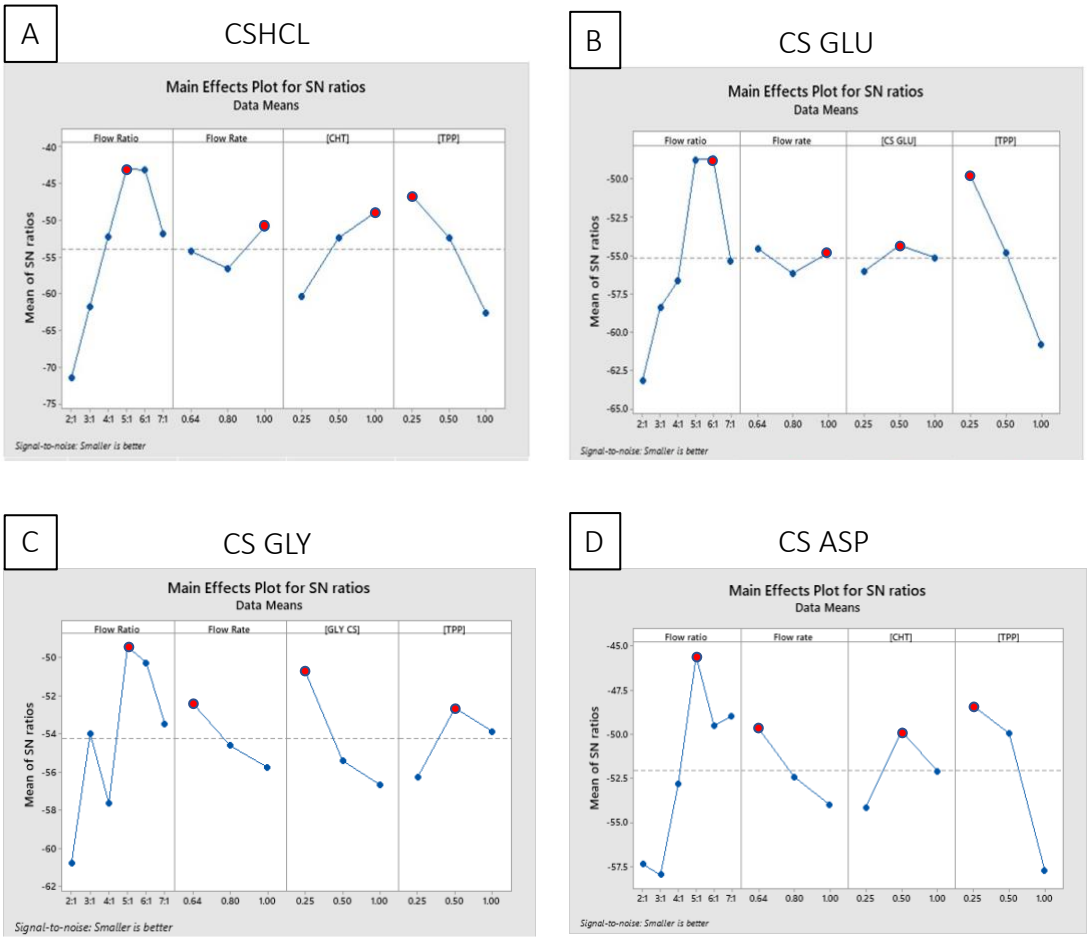

Figure 3.1 Mean signal-to-noise (S/N) graphs (A- CS HCl; B-CS GLU; C-CS GLY, D-CS ASP) for particle size response and parameter ranking for the Taguchi Design of experiment. The red dots highlight the best level for each factor (n=3, mean ± SD).

3.4.1.2 Design of Experiment Analysis

Multiple linear regression analysis was performed for particle size and PDI for each CHT derivatives, and the outcome indicated which parameter influenced with significance NPs size and PDI, respectively (**Table** 3.4). The models calculated for CS GLY and CS ASP to predict NPs size indicated that none of the variable employed in the study could predict NPs size with statistical significance. On the other hand, models computed to predict CS HCl particle size indicated that all the investigated parameters affected NPs size with statistical significance. Only FRR and TPP concentration affected NPs size with statistical significance for GS GLU. Regarding the calculated models to predict PDI values, only FRR and TPP concentrations for CS HCl resulted to predict PDI values with statistical significance. The multiple linear regressions for CS GLU, CS GLY and CS ASP to predict PDI revealed that none of the parameter investigated could predict PDI with significance.

To predict CS HCl NPs size, it is possible to solve the equation resulted from the regression analysis, using specific coefficients for each independent factor (displayed in **Table** 3.4) as follow:

Particle size= 4453.58 – 654.55(A) – 617.255(B) – 2228.75(C) + 1945.29(D),

where (A) is FRR value, (B) is TFR value, (C) and (D) are CS HCL and TPP concentrations.

Similarly, it is possible to predict CS GLU NPs size solving the following equation, using the specific coefficients for each independent factor (displayed in **Table** 3.4):

Particle size= 25.994 – 200.398(A) + 903.003(B) - 88.946(C) + 1307.525(D),

where (A) is FRR value, (B) is TFR value, (C) and (D) are CS GLU and TPP concentrations.

Moreover, the multiple linear regression analysis provided an R^2 value for each analysis. The R^2 indicated the percentage of the variability of the dependent variable (output, being NPs size or PDI) that is explained by the independent factors of the model. As it is displayed in **Table** 3.5, the R^2 value for the models describing CS HCl NPs size and CS GLU NPs size resulted to be the highest: the model that predicts CS HCl NPs size describes the 63% of the outcome, while the model for CS GLU NPs size describes the 58.3%. The remaining models scored considerably lower values compared to the one describing CS HCl and CS GLU size, particularly CS ASP size (11.3%), CS ASP PDI (8.7%), CS GLU PDI (8.4%), CS GLY size (8.3%), CS GLY PDI (5.4%) and CS HCl PDI (1.94%).

Table 3.4 Outcomes from the multiple linear regression of NPs size and PDI data for CS HCl, CS GLU, CS GLY, CS ASP (*, p<0.05).

		Particle size			PDI		
	Predictor (Symbol)	Coefficients	T	p	Coefficients	T	p
CS HCL	Constant	4453.58	4.28	<0.001*	0.29	2.32	0.02
	Flow Rate Ratio	-654.55	-7.03	<0.001*	-0.17	-1.47	0.014*
	Total Flow Rate	-617.25	-0.57	<0.001*	0.04	0.33	0.74
	CS HCL	-2228.75	-4.43	<0.001*	0.04	0.71	0.48
	TPP	1954.29	3.81	<0.001*	0.19	3	0.004*
CS GLU	Constant	25.994	0.055	0.957	0.431	4.49	0.000*
	Flow Rate Ratio	-200.398	-4.703	0.000*	-0.015	-1.69	0.096
	Total Flow Rate	903.003	1.827	0.074	-0.082	-0.82	0.415
	CS HCL	-88.946	-0.381	0.705	-0.041	-0.86	0.39
	TPP	1307.525	5.602	0.000*	0.021	0.43	0.664
CS GLY	Constant	676.501	0.714	0.479	0.427	1.39	0.168
	Flow Rate Ratio	-106.398	-1.253	0.216	-0.018	-0.67	0.502
	Total Flow Rate	967.942	0.983	0.330	0.244	0.76	0.446
	CS HCL	119.192	0.256	0.799	0.188	1.25	0.216
	TPP	-212.741	-0.457	0.649	-0.201	-1.34	0.185
CS ASP	Constant	2687.205	2.213	0.034	0.536	4.06	0.00
	Flow Rate Ratio	183.653	1.068	0.294	0.03	1.58	0.12
	Total Flow Rate	-3631.559	-1.972	0.06	-0.185	0.92	0.36
	CS HCL	1363.457	1.109	0.27	0.133	0.99	0.32
	TPP	-1019.166	0.992	0.329	-0.138	-1.23	0.22

Table 3.5 summary of R^2 values describing the model fit for all the chitosan employed in the study. The models that describe the output with the highest percentage are CS HCl NPs size (63%) and CS GCLU NPs size (58.3%).

		CS HCL	CS GLU	CS GLY	CS ASP
SIZE	R^2	0.630	0.583	0.083	0.113
	Model Fit (%)	63%	58.3%	8.3%	11.3%
PDI	R^2	0.194	0.084	0.054	0.087
	Model Fit (%)	1.94%	8.4%	5.4%	8.7%

Therefore, to test whether the overall regression model was a good fit for the data, an ANOVA analysis was performed, and the F value was calculated for each model. **Table** 3.6 reports ANOVA tables for the two models for each chitosan employed and revealed that for CS HCL and for CS GLU the independent variables ([TPP], [CS HCl], TFR, FRR) statistically significantly predict NPs size. Specifically for CS HCl NP size, F (4, 49) = 20.87, p = 0.001, and for CS GLU NPs size, F(4, 49) = 15.39, p = 0.000, hence the regression models are a good fit of the data. However, ANOVA analysis and F test performed on the remaining models, revealed that the calculated model for CS GLY NPs size, CS ASP NPs size, CS HCl PDI. CS GLU PDI, CS GLY PDY ad CS ASP PDI cannot predict particle size and PDI with statistical significance. These results are in line with the calculated R^2 value for the same models, which resulted to be considerably lower compared to the one obtained for the models describing CS HCl NPs size and CS GLU NPs size (**Table** 3.6).

Table 3.6 One-way ANOVA table to evaluate the model fit for CS HCl (A), CS GLU (B), CS GLY (C), CS ASP (D) NPs size and PDI.

		Source	Degree of freedom	Sum of squares	Mean square	F	P
CS HCL	NP SIZE	Regression	4	113870048.9	1363769.836	20.874	<0.001*
		Residual error	49	66824721.97			
		Total	53	180694770.8			
	NP PDI	Regression	4	0.244	0.06	2.953	0.029
		Residual error	49	1.10	0.02		
		Total	53	1025			
CS GLU	NP SIZE	Regression	4	41719.423	10429.856	15.398	0.000*
		Residual error	49	33189.882	677.345		
		Total	53	74909.305			
	NP PDI	Regression	4	1.146	0.286	77.715	0.000*
		Residual error	49	0.181	0.004		
		Total	53	1.326			
CS GLY	NP SIZE	Regression	4	3192481.448	798120.362	0.703	0.594
		Residual error	49	55631049.120	1135327.533		
		Total	53	58823530.570			
	NP PDI	Regression	4	0.521	0.130	1.105	0.365
		Residual error	49	5.776	0.118		
		Total	53	6.297			
CS ASP	NP SIZE	Regression	4	6321252.79	1580313.20	0.99	0.43
		Residual error	49	49496585.72	1596664.05		
		Total	53	55817838.51			
	NP PDI	Regression	4	0.055	0.014	0.737	0.57
		Residual error	49	0.582	0.019		
		Total	53	0.637			

3.4.1.3 Investigation of FRR on NPs Size

According to Taguchi DoE analysis with the 'smaller-is-better' criterion, FRR was the parameter that influenced NPs size with the highest ranking for all the CHT derivatives. Therefore, FRR investigation was performed to lessen the S/N ratio and understand the variation in NPs size and PDI. Formulations were prepared with FRR values ranging from FRR 1:1 to 8:1, while CHT concentration, TPP concentration and TFR were fixed according to best formulation obtained as outcomes from the Taguchi DoE (**Table** 3.3).

For the four CHT derivatives, formulation prepared with FRR values of 1:1 resulted in NP size exceeding the nanometer scale (**Figure** 3.2). From FRR values of 2:1 to 7:1, particle size decreased as the flow ratio decreased. Statistical analysis revealed that NPs prepared with FRR of 1:1 were statistically different compared to all the other formulations. On the other hand, NPs prepared with FRR ranging from 2: 1 to 7:1 were not statistically significant among them, but different from 1:1 (**Figure** 3.2). For these reasons the optimum formulation identified for each CHT derivative was the one obtained as Taguchi DoE outcome (**Table** 3.3).

Given the best formulation outcomes from Taguchi DOE and the statistical analysis of the DoE output (multiple linear regression, one-way ANOVA, F-test), out of the four CHT derivative tested CS HCl and CS GLU gave the smaller size, the best reproducibility of results and the model with the highest significance and R^2 value. For this reason, the optimum formulation of CS HCl and CS GLU generated with the Taguchi DoE were selected for further studies.

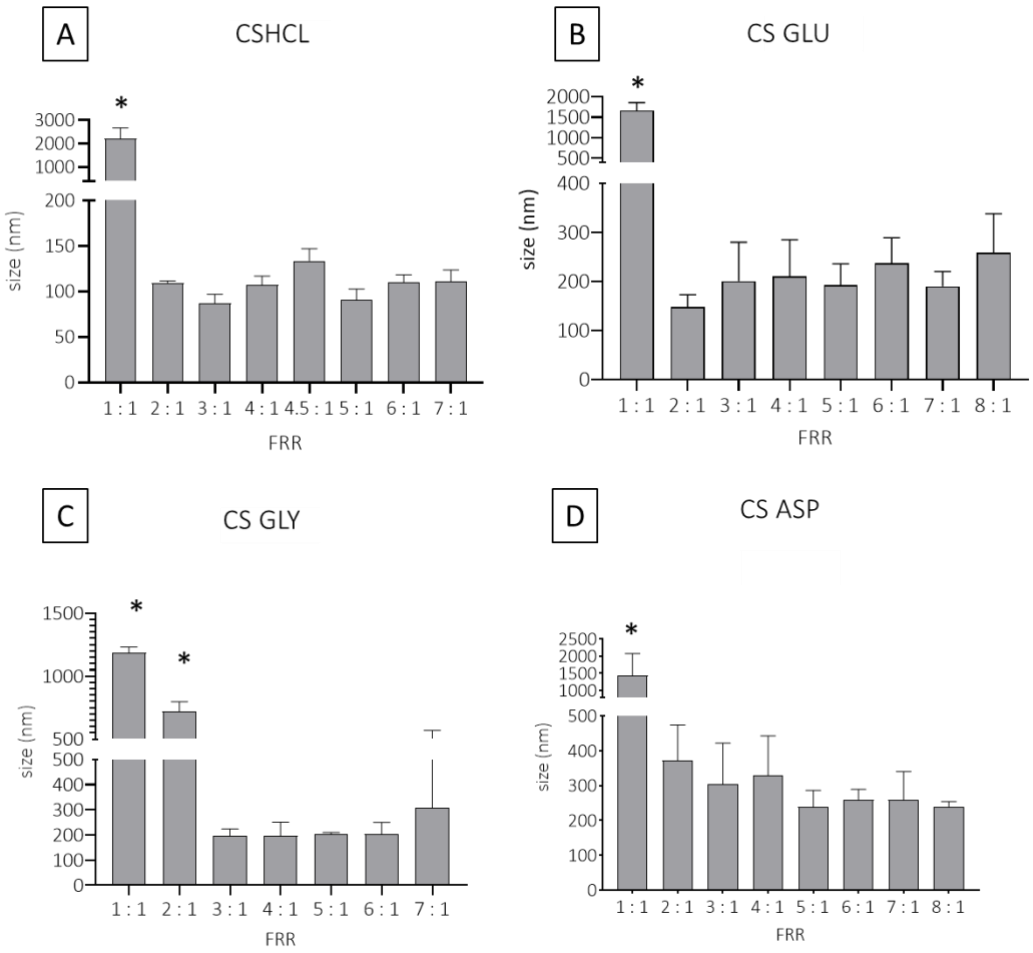

Figure 3.2 FRR investigation for CS HCl (A), CS GLU (B), CS GLY (C) and CS ASP (D). NPs were prepared with FRR values ranging from 1:1 to 8:1. For all the CHT derivatives employed, 1:1 FRR was responsible of micrometer-sized NPs. Additionally, decreasing values of FRR from 2:1 to 8:1, was linked to a decrease in NPs size for all the CS derivatives. One-way ANOVA with Tukey's post test revealed that NPs prepared with FRR values of 3:1 to 8:1 were not statistically different from each other. However, they were different to NPs prepared with 1:1 FRR value (and 2:1 FRR for CS GLU) (n=3, mean ± SD; *, $p<0.05$).

3.4.2 miR-184 mimic Encapsulation

The study revealed that the EE% of miR-184 mimic within the CS HCl and CS GLU NPs was ≥92 % (**Figure** 3.3 **A** and **D**). For both CS GLU and CS HCl the EE% increased as the CHT:miR-184 w/w ratio decreased. The rise was significant for CS HCl 25:1 and for CS GLU 50:1 and 25:1. Accordingly, for both CS GLU and CS HCl an increase in size was reported when CHT:miR-184 w/w ratio decreased , which resulted to be different from Blank NPs for CS HCl NPs prepared with 50:1 and 25:1 ratios, and for CS GLU 25:1 NPs. The PDI of the miR-184-loaded NPs increased as the ratio CHT:miR-184 mimic decreased for CS HCl, and the formulation prepared with 25:1 ratio had a PDI significantly different from blank NPs. On the other hand, no variations were reported for the PDI of CS GLU miR-184-loaded formulations (**Figure** 3.3 **B** and **E**). The overall trend for NPs Zeta Potential for both the CHT employed was that the decrease of miR-184:CHT ratio caused a decrease in the Zeta Potential, that was significant for CS HCl 50:1 and 25:1, and for CS GLU 25:1 (**Figure** 3.3 **C** and **F**).

Moreover, **Figure** 3.4 displays a comparison of NPs prepared with the two CHT derivatives. Results showed no difference in size, PDI, zeta potential and ability to load miR-184 mimic.

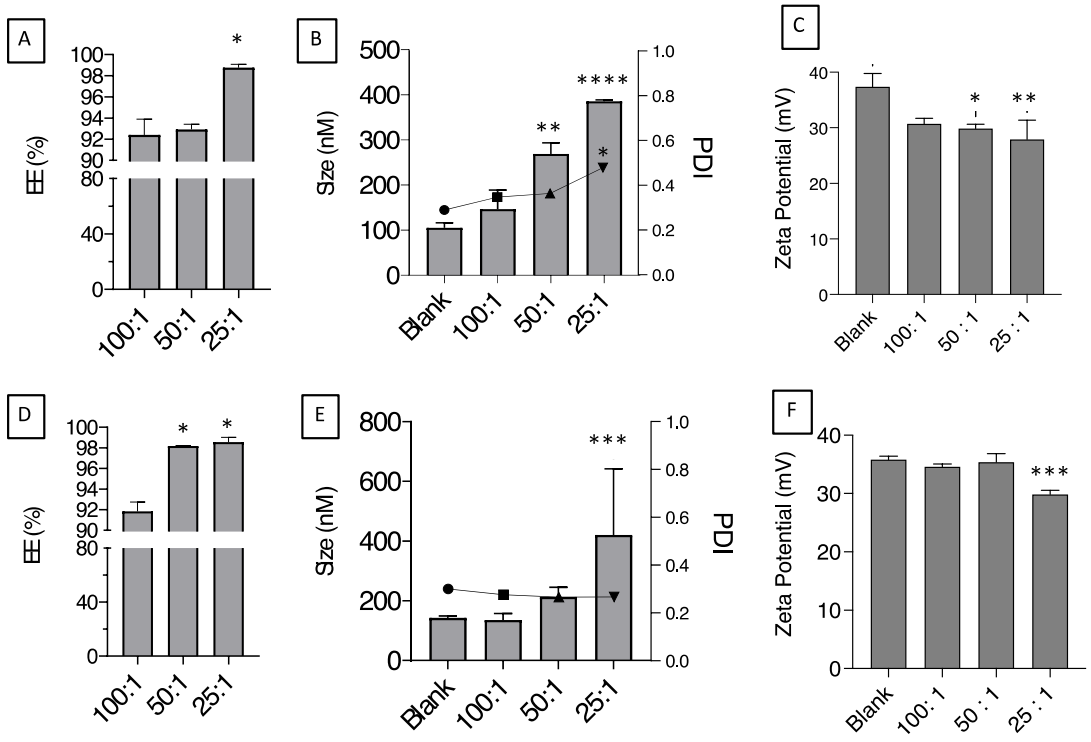

Figure 3.3 CS HCl (A, B and C) and CS GLU (D, E and F) miR-184 Encapsulation efficiency (EE %), size (nM), PDI and Zeta Potential (mV). The optimum Blank formulation was employed to investigate the ability of CS HCl and CS GLU of complexing with mIR-184 mimic. Formulations were prepared with increasing amounts of oligonucleotide to reach CHT: miR-184 ratio of 100:1, 50:1 or 25:1. Decreasing the ratio CHT:miR-184, caused an increase of EE% (A, D), NPs size and PDI (B, E), while NPs zeta potential (C,F) decreased. For the EE %, one-way ANOVA with Tukey's post test was performed, while for size, PDI and Zeta potential, one-way ANOVA with Dunnet's post-test was performed (n=3, mean ± SD; * p<0.05; ** p<0.01; *** p<0.001; **** p<0.0001).

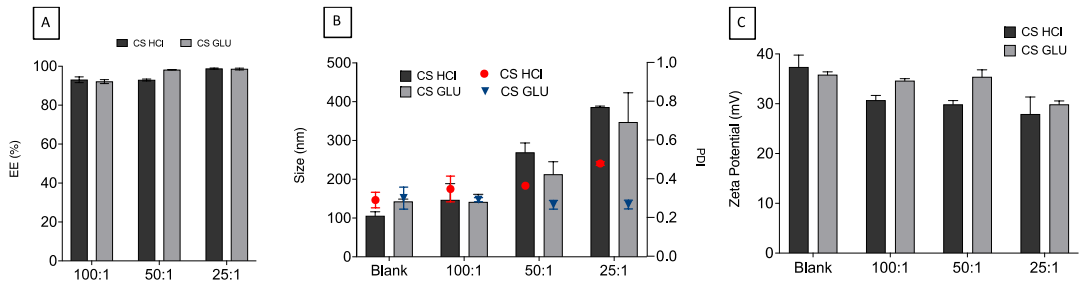

Figure 3.4 Comparison between CS HCl and CS GLU encapsulation efficiency (EE%) (A), size (nM) (B), PDI (B) and Zeta Potential (mV) (C). Paired t-test conducted on CS HCl and CS GLU for miR-184 EE%, size, PDI and Zeta Potential at 100:1, 50:1, 25:1 polymer:miR-184 mimic ratio revealed no statistical significance between the properties of NPs prepared with the two CHT derivatives (n=3, mean ± SD).

3.4.3 Gel Retardation Assay

Results obtained from the gel retardation study are shown in **Figure** 3.5. miR-184 at decreasing concentration were loaded in wells 1-5 and used as controls, while miR-184 NPs were loaded in wells 6-11. Following gel electrophoresis, free miR-184 mimic (line 1-5) migrated towards the positive electrode and as expected, decreased luminescence was observed as the concentration of miR-184 mimic decreases. For lanes 6-8 (miR-184-loaded CS HCL NPs) and 9-11 (miR-184-loaded CS GLU NPs) there was a visible luminescence in the well that cannot be seen in control wells, meaning that miR-184 was not able to move towards the positive electrode and was retained within the wells: this can be attributed to the successful complexation of miR-184 mimic within the NPs at all the CHT:miR-184 w/w ratio investigated.

For both CS HCL and CS GLU, results showed a brighter signal on wells for formulations prepared with CHT:miR-184 w/w ratio of 50:1 (lanes 7 and 10, highlighted in green in **Figure** 3.5 **C**) and 25:1 (lanes 8 and 11, highlighted in blue in **Figure** 3.5 **D**), compared to CHT:miR-184 ratio of 100:1 (lanes 6 and 9, highlighted in red in **Figure** 3.5 **A**) due to the higher amount of miR-184 mimic employed to prepare the formulations. Additionally, for both CS HCL (lane 8) and CS GLU NPs (lane 11) prepared with CHT:miR-184 mimic ratio of 25:1 and for CS HCL NPs prepared with CHT:miR-184 ratio w/w 50:1 (lane 7) there was a slightly visible signal towards the positive electrode, indicating that some of the miR-184 mimic did not complex within the polymer. However, this signal is much darker than the relative controls that are line 3 (control for lane 8 and 11 **Figure** 3.5 **D**) and lane 4 (control for line 7 **Figure** 3.5 **C**) suggesting that majority of the miR-184 mimic employed to manufacture the NPs is complexed within the nanocarrier.

Results from the gel retardation assay suggest that there were no observable differences in the ability of CS HCl or CS GLU to retain the miR-184 mimic. Thus, together with previous results (**section 3.4.2, Figure** 3.4) and with the lack of time and resources, only CS HCl was selected for further studies.

A

Well number	Sample loaded	[miR-184] ng/μL	μL loaded	miR-184 on well (ng)
1	miR-184	1000	7	7000
2	miR-184	100	7	700
3	miR-184	20	7	140
4	miR-184	10	7	70
5	miR-184	5	7	35
6 and 9	CHT:miR-184 100:1	5	7	35
7 and 10	CHT:miR-184 50:1	10	7	70
8 and 11	CHT:miR-184 25:1	20	7	140

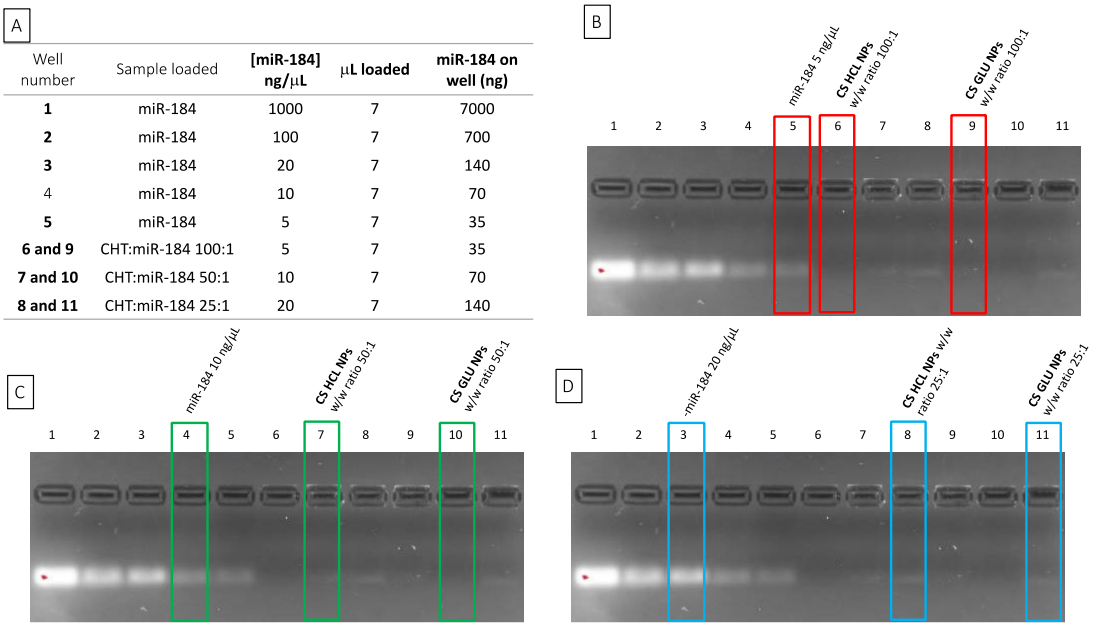

Figure 3.5 Gel retardation assay outcomes for CS HCl and CS GLU. Gel retardation assay was performed to investigate the complexation of the oligonucleotide within the polymer. CS HCl NPs were loaded in wells 6-8, CS GLU NPs in wells 9-11, while miR-184 mimic dilutions were loaded into wells 1-5 and used as control. (A) summary of sample loaded into wells 1-11 and the miR-184 concentration reached on the wells. (B) Red bar highlight lanes 5 (control), 6 and 9: samples loaded into those wells had 5ng of miR-184 mimic; (C) green bar highlight lanes 4 (control), 7 and 10, having 10ng of miR-184 in the well; (D) Blue bar highlight lanes 3 (control), 8 and 9, which had 20ng of miR-184 mimic loaded into the wells.

3.4.4 Housekeeping gene screening and identification

Four housekeeping genes were screened, hsa-SNORDD48, hsa-SNORDD68 and hsa-SNORDD72, to identify a reference gene with stable expression across the cell lines. Among the four reference genes screened, SNORDD 48 resulted to be the most stable across the cell lines and did not show any statistical significance in all the cell lines and for this reason SNORDD 48 was chosen as reference gene for further studies (**Figure** 3.6 **A**). Results obtained for SNORDD-72 expression in A549 and SK-MES were statistically different compared to the other cell lines (**Figure** 3.6 **B**). Similarly, SNORDD 68 expression in CORL-23 was significantly different (**Figure** 3.6 **C**).

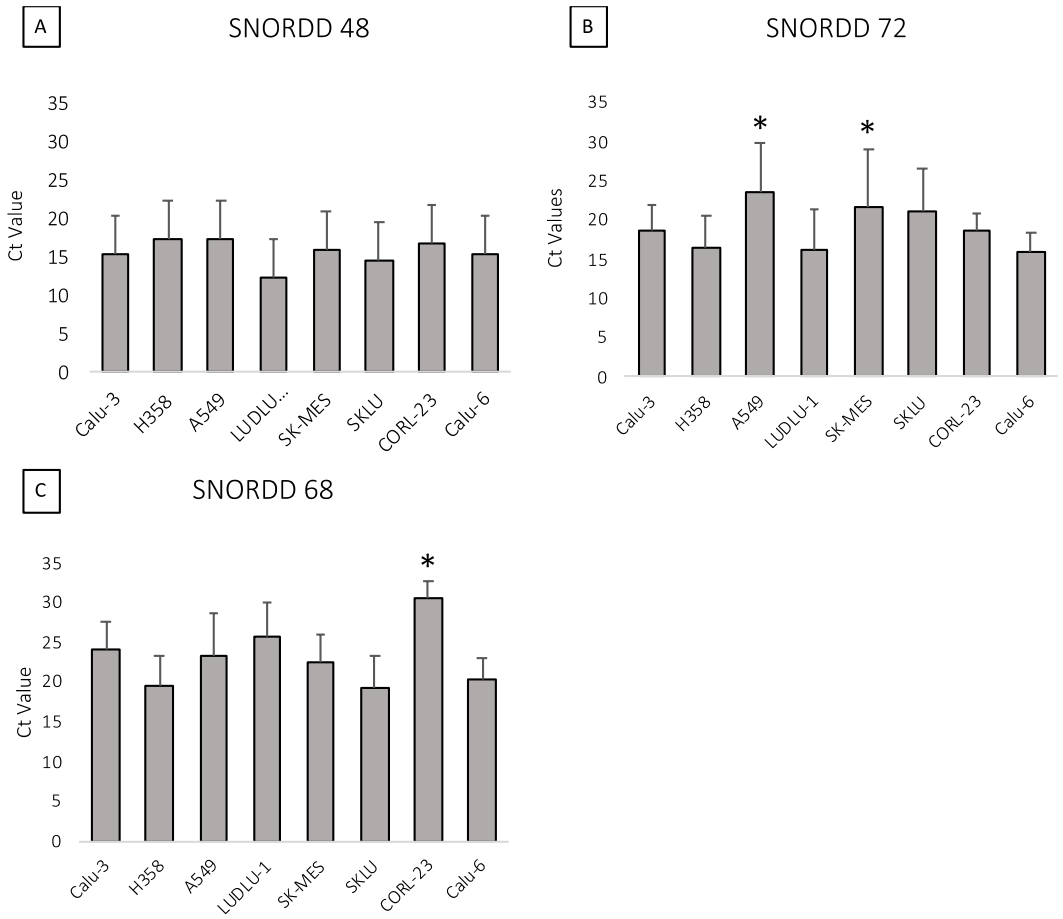

Figure 3.6 Normalisation genes screened across the panel of NSCLC cell lines. SNORDD 48 (A), SNORDD 72 (B), and SNORDD 68 (C). Baseline levels of the three genes were assessed in all the cell lines via RT-qPCR. Ct values were compared via one-way ANOVA statistical analysis, with Tukey's post-test. Results revealed no statistical significance among the Ct values registered for all the cell lines employed. On the other hand, A549 and SK-MES for SNORDD 72 and CORL-23 for SNORDD 68 were statistically significance compared to the other cell lines (n=3, mean ± SD; * $p<0.05$).

3.4.5 miR-184 Baseline Investigation

Once SNORDD48 was identified as reference gene, miR-184 expression relative to SNORDD48 was investigated in the panel of NSCLC cell lines available. As outlined in 2.1, the cell lines were gifted from Dr. Michael Davies and Dr. Lakis Liloglou. Previous studies from their research group showed a different sensitivity of the cells towards cisplatin, particularly Calu-3, H358, A549 and LUDLU-1 were found to be the less sensitive to cisplatin (**Figure** 3.7 **B**) (Alnefaie, 2020). Results are displayed by subtracting Ct value relative to SNORD48 to Ct value relative to miR-184 for each cell line. Statistical analysis revealed that none of the cell line of the panel had a statistically different miR-184 expression compared to the others (**Figure** 3.7 **A**).

A

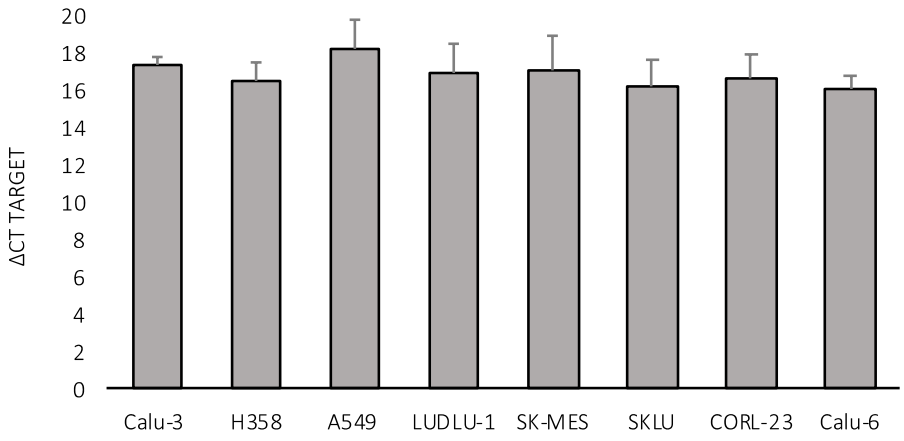

B

IC50 (μM)	7.01	6.9	4.92	4.152	3.079	2.56	1.61	1.1

Figure 3.7 miR-184 expression investigation across NSCLC cell lines available, and their IC50 according to previous studies. Baseline levels of miR-184 in the cells lines was evaluated via RT-qPCR. Results are displayed as ΔCt target, meaning that miR-184 expression in each cell line was subtracted to SNORDD48 expression in the same cell line. (A) Following One-way ANOVA with Tukey's post test, no statistically significant variation in miR-184 expression was observed (n=3 ± SD). (B) IC50 values of the cell lines as reported in previous studies by Alnefaie from University of Liverpool, who kindly gifted the cell lines for this study (Alnefaie, 2020).

3.4.6 MicroRNA-184 mimic and inhibitor Transfection to NSCLC Cells via INTERFERin®

To assess whether INTERFERin® was a suitable transfection reagent for elevation of miR-184 expression in Calu-3 cells, three concentrations of miR-184 mimic (5, 20 an 700 nM) and two concentration of miR-184 inhibitor (5 nM and 20 nM) were tested and miR-184 expression assessed by RT-qPCR. These concentrations were chosen given that, as per manufacturer instruction, the best transfection efficiency may vary from 1 nM to 50 nM depending on the cell line used (*INTERFERin - SiRNA / MiRNA Transfection Reagent*, accessed 18 June 19.) .

Cells transfected with miR-184 mimic showed an increase in miR-184 expression that was proportional to the amount of miR-184 used for the treatment. Cells treated with 5 nM miR-184 mimic recorded an increase in miR-184 relative expression of 3000-fold, while for 20 nM NPs the expression increased of 4000-fold (**Figure** 3.8). Statistical analysis of results showed that miR-184 relative expression in samples treated with the miR-184 mimic was statistically significant compared to untreated cells and cells transfected with a non-targeting control (NTC) oligonucleotide **Figure** 3.8.

Cells transfected with miR-184 inhibitor showed only a modest decrease in miR-184 expression. However, the decrease was not statistically significant compared to untreated cells (**Figure** 3.9).

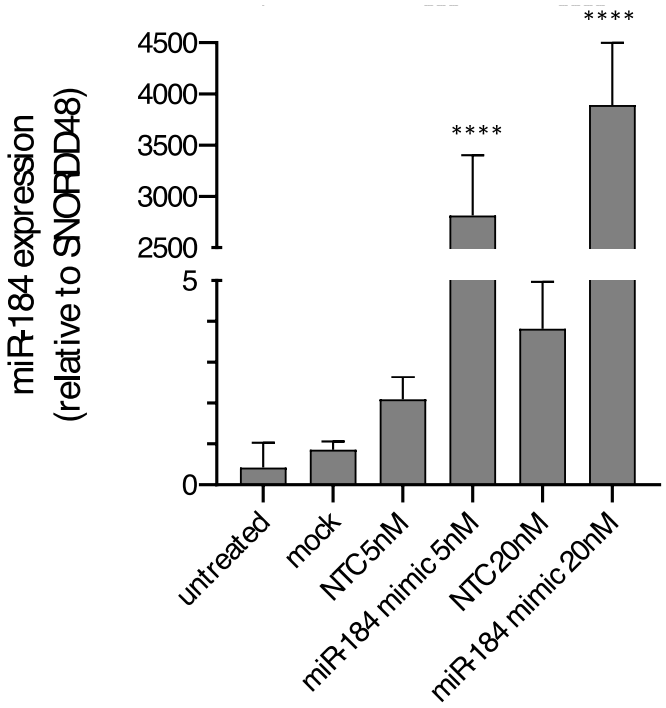

Figure 3.8 miR-184 expression of Calu-3 cells transfected with 5 nM or 20 nM miR-184 mimic and controls (non-targeting control (NTC), mock (INTERFERin® only), and untreated cells to which results were normalised. Performing the one-way ANOVA statistical analysis with the Tukey's post-hoc analysis revealed that both 5 nM and 20 nM miR-184 mimic led to significant increases of miR-184 expression compared to untreated cells or NTC transfected cells (n=3, mean ± SD; **** $p < 0.001$).

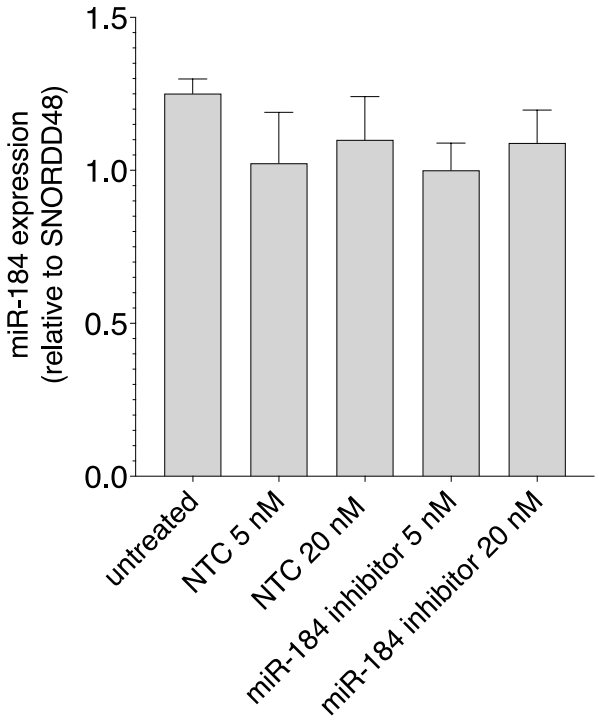

Figure 3.9 miR-184 expression of Calu-3 following transfection with miR-184 inhibitor. Cells transfected with 5 nM or 20 nM miR-184 inhibitor or non-targeting control (NTC). Untreated cells were used to normalise cells. Performing the one-way ANOVA statistical analysis with the Tukey's post-hoc analysis revealed no statistical significance among the treatments. (n=3, mean ± SD).

3.4.7 miRNA-184 Mimic delivery via CS HCl NPs

Three dilutions of miR-184-loaded NPs were tested, having a final concentration of miR-184 of 700 nM (undiluted NPs as prepared from NanoAssemblr), 20 nM and 5 nM. Similarly, three NTC-loaded NPs (having a final concentration of NTC of 700 nM, 20 nM or 5 nM) dilutions were prepared and used as controls. Blank NPs dilution will be referred to as 700, 20, 5 as they were prepared by diluting Blank NPs with the same dilution factor used to prepare 700 nM, 20 nM or 5nM miR-184-loaded or NTC-loaded NPs. For all the concentration tested, miR-184 relative expression increased compared to untreated cells or cells treated with mock treatments (Blank NPs).

Cells treated with miR-184-loaded NPs showed an increase in miR-184 expression that was proportional to the amount of miR-184 used for the treatment. Cells treated with 700 nM NPs recorded an increase in miR-184 relative expression of 300-fold, while for 20 nM NPs and 5 nM NPs the expression increased of 40 and 7 folds respectively (**Figure** 3.10).

Statistical analysis of results showed that miR-184 relative expression in samples treated with the three dilutions of mi184 mimic-loaded NPs was statistically significant compared to untreated cells and to the related Blank NPs or NTC-loaded NPs treatment.

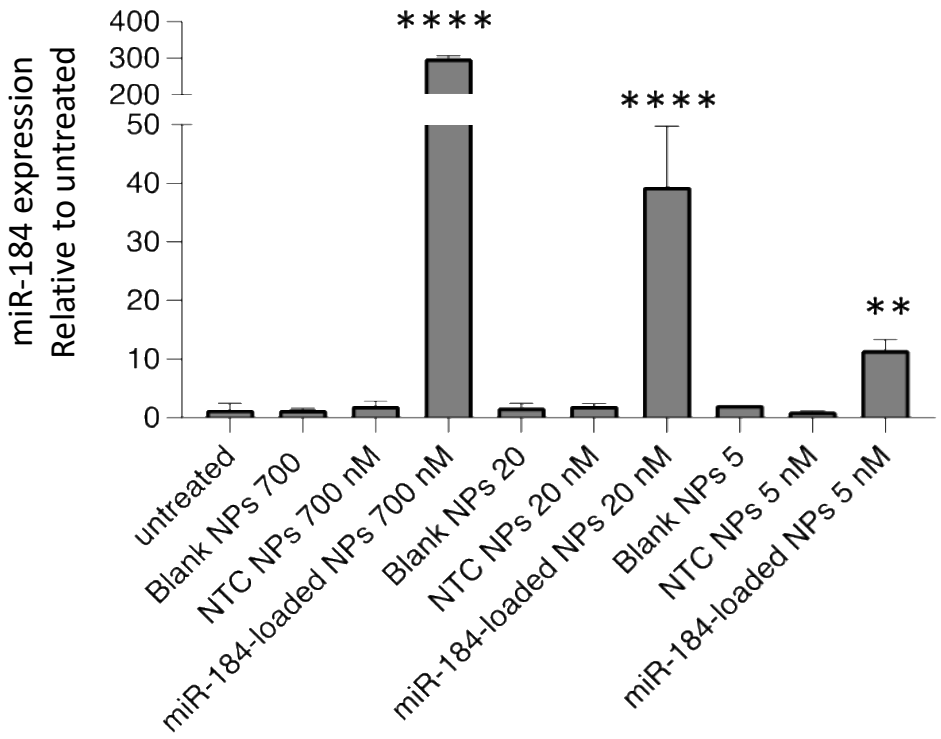

Figure 3.10 miR-184 loaded NPs, NTC-loaded NPs and blank treatment of Calu3 cells. One Way ANOVA with Dunnet's post test was employed. Each loaded formulation was compared with Blank NPs, NTC-NPs and untreated treatment. Results revealed that cells treated with miR-184 loaded NPs increased miR-184 relative expression significantly of 300-fold and 40-fold when 700 nM and 20 nM miR-184 mimic is delivered, respectively (n=3, mean ± SD, ** $p<0.01$; **** $p<0.0001$).

3.4.8 Confocal Imaging

Visual confirmation of NPs internalisation by confocal light microscopy is shown in **Figure** 3.11. Nuclei of Calu-3 cells were stained by DAPI (blue channel) whereas the 5'-TAMRA-miR-184 mimic is shown in red channel. The two channels were merged in overlay images: (A) negative control: Calu3 cells treated with blank NPs; (B) positive control: Calu3 cells treated with 5'-TAMRA-miR-184 mimic transfected via Interferin®; (C) and (D) Calu3 cells treated with 5'-TAMRA-miR-184 mimic-loaded CS HCl NPs. Images suggest that the 5'-TAMRA-miR-184 loaded NPs were internalised into the cell cytoplasm. Red fluorescence carried by the 5'-TAMRA-miR-184 mimic loaded into the CS HCl NPs could be observed in the space surrounding the nuclei (blue light) indicating internalisation and successful cytoplasmic delivery, as indicated by the arrows in **Figure** 3.11 **C** and **D**. Moreover, the red fluorescence observed in (B) is comparable to the red fluorescence that can be seen in (C) and (D), thus suggesting that not only CS HCl can favour the uptake of miR-184 mimic, but the transfection efficiency is similar to that obtained by traditional commercial products.

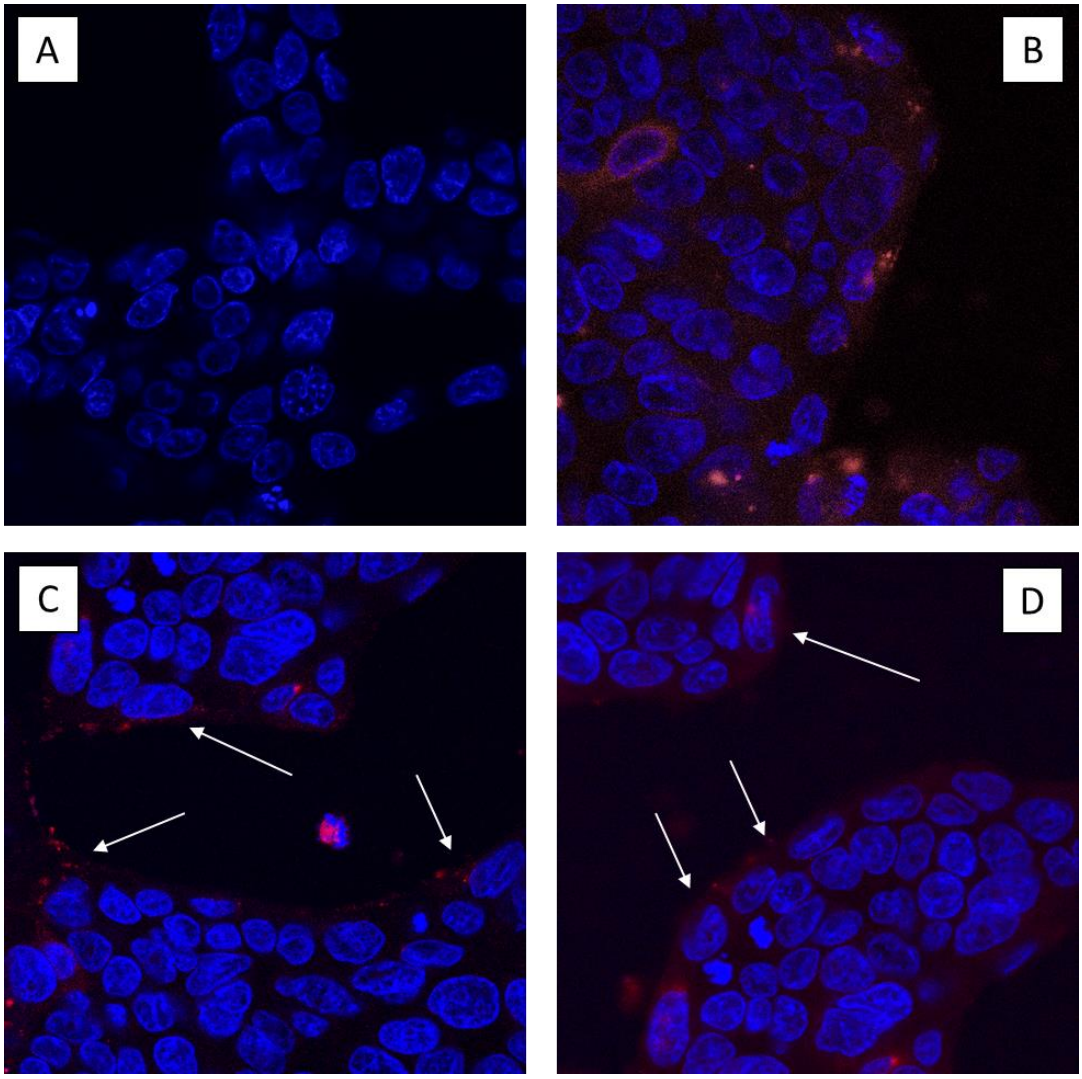

Figure 3.11 Confocal microscopy study of miR-184 mimic-loaded CS HCl NPs uptake by Calu3 cells. Nuclei were stained with DAPI (blue), while for visualisation of miR-184 mimic, a fluorescently labelled oligonucleotide (5'-TAMRA-miR-184 mimic, red) was employed. (A) Calu3 cells treated with blank NPs: only the nuclei are visible. There is no background red fluorescence from the cells or the NPs; (B) Calu3 cells transfected with 5'-TAMRA-miR-184 mimic via INTERFERin®: the red fluorescence brought about by the 5'-TAMRA dye is localised outside the nuclei (blue) suggesting miR-184 internalisation; (C) and (D): two different fields of view of Calu3 cells treated with 5'-TAMRA-miR-184 mimic-loaded CS HCl NPs: the red fluorescence is localised around the blue nuclei similarly to (B), thus confirming that NPs are successfully uptaken by Calu3 cells.

3.5 Discussion

3.5.1 Chitosan Nanoparticles Blank Optimisation

To manufacture a chitosan-based carrier useful for the delivery of oligonucleotide molecules, four chitosan derivatives were chosen, one non-animal extract (CS ASP) and three water soluble derivatives (CS GLU, CS HCL and CS GLY). All of them were positively charged at the working pH used, hence NPs formation was reached through electrostatic interaction with the negatively charged cross-linker (TPP) (Calvo et al., 1997). Given the novelty of using microfluidic technology for the preparation of CHT NPs it was essential to investigate which parameters had the highest influence in NPs size and PDI. For this reason, an L18 orthogonal array mixed-design Taguchi DoE was constructed, performed, and analysed by Minitab 16 Statistical Software®.

Results for the four CHT employed revealed that among the parameters investigated, FRR had the higher impact on size and PDI (**Figure** 3.1). FRR is defined as the ratio of polymer: cross-linker that the microfluidic device would use to prepare a certain formulation. Thus, the FRR being the parameter with the higher influence on NPs size can be explained via the change in positive (+ve) to negative (-ve) charge ratio in solution. The +ve charges are carried by the polymer given the amino groups (NH_3^+) in its backbone, while the -ve charges are conveyed by the cross-linker (TPP). Therefore, FRR variations would bring about a variation in polymer:cross-linker ratio, and subsequently to a change in +ve: -ve ratio, that ultimately was responsible for the NPs formation via electrostatic interaction by ionic gelation (Pant & Negi, 2018). Hence, FRR influenced NPs size as it reflects the amount of +ve and -ve charges in solution, thus enhancing or discouraging aggregates formation (Amin & Boateng, 2019; Chai et al., 2021). Interestingly, CHT concentration and TPP concentration ranked as second and third for the influence they have on NPs size (**Table** 3.1). As explained for FRR, a variation in the number of CHT and TPP molecule in solution results in a variation of the amount of +ve and -ve in solution. Therefore, the use of different concentrations of CHT and TPP to produce NPs would also result in a difference in the amount of +ve and -ve charges in solution. Thus, meaning that NPs size and PDI would change accordingly to the variations of CHT and TPP concentrations.

For all the chitosan derivatives TFR resulted to have the least influence on NPs size. TFR is defined as the sum of volumetric flow that passes through the microfluidic channels per unit of time (in this case min). Hence, it is deducible that at the TFR values tested the volume of solutions that flows into the channel had little or no influence on NPs size and PDI. Similarly,

the studies carried out by Chai on lignin/CHT NPs and Conner on lipid NPs reported no significant impact on size after variations of TFR values. In their study, initial concentrations of polymer and cross-linker used are the one defining considerable variations in NPs size (Chai et al., 2021; Conner et al., 2020). Those findings are relatable to the results of this study, given that the highest influence on NPs size was brought about by the presence of +ve and -ve, rather than to the velocity at which the NPs were produced.

Given that FRR had the highest influence on NPs size, a further FRR investigation was performed. The optimum formulation for each chitosan was chosen as a starting point while FRR was varied ranging from 1:1 to 8:1. Results from all the four CHT types revealed that NPs size decreased as FRR increased (from 1:1 to 8:1). This can be attributed to the ratio of +ve: -ve charges in solution. Increasing FRR value means lower number of -ve charges available in solution to create interactions with the positively charged polymer (Calvo et al., 1997; Koukaras et al., 2012), thus the final product resulted in smaller aggregates. In addition, a common behaviour among all the CHT types was observed: NPs produced with FRR of 1:1 showed a size in the micro-meter scale. In accordance with the study of Majedi and Nasti, on hydrophobically modified CHT NPs and CHT/Hyaluronic Acid, the micro-meter size of NPs produced with 1:1 FRR value was a consequence of the pH of the final formulation obtained. As the solution pH controls the balance between electrostatic repulsion and hydrophobic attraction forces, an increase in pH that occurs when CHT and the basic cross-linker solution are mixed at certain FRR values, will result in the polymer becoming less soluble in its solvent (water for CS GLU, CS HCL and CS GLY; acetic acid for CS ASP) and thus driving the polymer to partially self-assemble and precipitate. In this study, it is reasonable that the final pH of the formulation prepared with FRR of 1:1 resulted to be higher than the other formulations, leading to the formation of micrometre-sized aggregates. On the other hand, as FRR increases (from 2:1 to 8:1) the volume of cross-linker in solution diminishes and consequently the variation in pH of the final solution did not cause variation in the polymer solubility (Majedi et al., 2014; Nasti et al., 2009). Therefore, NPs prepared with FRR lower than 1:1 did not result in micrometer size.

The regression analysis performed on Taguchi DoE showed that the models created by the software could not predict NPs size for CS GLY, and PDI for all the derivatives. Moreover, the R^2 calculated was higher for the model calculated for CS HCL (64%) and for CS GLU (58%), whilst it was lower for CS GLY (9.3%) and for CS ASP (11.3%). Besides, results showed that CS HCL and CS GLU could provide smaller particles compared to CS ASP and to CS GLY, as it can

be seen via DoE and via FRR investigation results. For this reason, only the CS HCL and CS GLU were kept for subsequent studies.

Taguchi DoE results were additionally computed to investigate the influence of the selected parameters on NPs PDI. Similar to NPs size, FRR was the parameters affecting PDI with the highest ranking followed by either CHT concentration or TPP concentration, and to TFR. However, regression analysis of the models revealed a very low R^2 for the four chitosan derivatives (**Table** 3.5), meaning that only a small percentage of the output can be predicted by the calculated model. However, the PDI results obtained from the DoE and the subsequent FRR investigation revealed that PDI values were similar to PDI values obtained by several other studies producing NPs via microfluidic technology. The very low PDI values are usually ascribed to the laminar flows imparted by SHB-shaped channels (Belliveau et al., 2012).

3.5.2 miR-184 mimic encapsulation

To investigate whether the optimised CHT NPs prepared via microfluidic mixing technology are suitable carriers for miRNA mimics, encapsulation study was performed on CS HCL and on CS GLU NPs. The miR-184 loaded NPs were prepared using the best optimum formulation obtained from the blank NPs optimisation (**Table** 3.3)

Increasing amounts of miR-184 mimic (to reach CHT: miR-184 mimic w/w ratio of 1:25, 1:50 or 1:100) were added to the cross-linker solution during the formulation preparation. Characterisation of the obtained formulations revealed that encapsulation efficiency (EE%) was higher than 90% for all the CHT:miR-184 w/w ratio tested, with both CS HCl and CS GLU. The high encapsulation efficiency of miRNA within chitosan NPs has already been noticed by others (Denizli et al., 2017; Gaur et al., 2015; McKiernan et al., 2013). Similarly, to our results, in the study from Wu the EE% was close to 100% when a higher amount of mimic was loaded into the formulation. The high EE% reached at certain w/w ratios of CHT:miR-184 reflects an increase in the -ve /+ve ratio in solution, that is beneficial for the formation of more electrostatic interaction between the negatively charged oligonucleotide and the polymer (Wu et al., 2016). In the study carried out by Nguyen, a lower EE% efficiency (approximately 60%) resulted from the complexation of miRNA mimic within PEGylated-chitosan: the modification of CHT on the amine residue resulted in a decrease in the +ve charges available to the mimic to interact with the polymer. This resulted in a lower -ve /+ve charges ratio and a lower EE% compared to NPs in which CHT derivatives with higher +ve charges were employed (Nguyen et al., 2019).

The size of miR-184-loaded NPs increased significantly compared to blank NPs. In particular, for NPs prepared with CHT: miR-184 ratio of 25:1 w/w NPs size resulted almost doubled compared to blank. The additional -ve charges brought in the formulation by the oligonucleotide phosphate groups contribute to the formation of additional electrostatic interaction that will result not only in higher drug encapsulation, but also in the formation of bigger complexes (De La Fuente et al., 2008; Deng et al., 2014).

3.5.3 Gel retardation assay

To confirm complexation of miR-184 mimic with the polymer, a retardation assay on agarose gel was performed. Retention of the miR-184 loaded NPs within the well demonstrated complexation of the oligonucleotide (**Figure** 3.5**)**. Several studies reported that low -ve /+ve charge ratio brings about weak electrostatic interaction formation and subsequent partial complexation of the oligonucleotide with the polymer. Consequently, gel retardation assay for those studies showed a darker signal on the well and a bright signal at the bottom of the gel, given that the mobility of the oligonucleotide is not retarded by its complexation (de Souza et al., 2018; Kaban et al., 2017; Lu et al., 2019; Guangsheng Wu et al., 2016).

In our study, partial uncomplexed miR-184 was observed in CS HCL and CS GLU NPs prepared with a w/w ratio of 25:1, given that some naked miR-184 mimic appeared to have migrated to the bottom of the gel. The 25:1 formulation that showed this behaviour had the higher amount of mimic loaded and therefore a lower chitosan content. This has been observed in previous studies (Rojanarata et al., 2008; Sharma et al., 2013; P. Sun et al., 2016), in which a lower content of chitosan resulted in less strong electrostatic interaction with the oligonucleotide and consequently partial uncomplexed miR-184 could be seen at the bottom of the gel. On the contrary, complete complexation of miR-184 with CS HCl and CS GLU was observed for 100:1 and 50:1 formulation, given that the bright signal of the dye was observed only on the loading well.

The miR-184 mimic loaded NPs prepared with the two CHT derivatives showed similar properties in terms of, size, PDI, Zeta potential, miR-184 mimic loading (**section 3.5.2**) and miR-184 mimic complexation. However, the study published by Techaarpornkul investigating the difference in RNA silencing of siRNA loaded CHT NPs prepared with CS HCl and CS GLU, observed an increased cytotoxicity of CS GLU compared to CS HCl in HeLa cells (Techaarpornkul et al., 2010). In addition, interestingly the study carried out by Kozté compared the ability of CS HCl and CS GLU in enhancing intestinal permeability. Their results

suggested that CS HCl was a better permeation enhancer compared to CS GLU. Thus, revealing that CS HCl might facilitate cellular uptake in a better way than CS GLU (Kotzé et al., 1999). Therefore, for these reasons and for the lack of time and resources, only CS HCl was selected for further experiments.

3.5.4 Housekeeping gene screening and miR-184 expression investigation

Prior to performing studies involving the investigation of miR-184 expression both endogenous (baseline levels investigation) or after supplementation (miR-184 mimic transfection) it was necessary to find a normalisation gene that was stable across the cell lines and that could be used to analyse miRNA RT-qPCR data. As explained in section 2.6.3, the general recommendation for relative gene expression analysis requires normalisation of the target gene with a reference gene belonging to the same class of RNA, (Vandesompele et al., 2002). Thus, for miRNA expression normalisation endogenous control should belong to the class of small non-coding RNAs such as miRNA, small nuclear RNA (snRNA), small nucleolar RNA (SNORDD). SNORDD RNAs are commonly used as normalisers for miRNA relative quantification via RT-qPCR, as their expression resulted to be stable in several cell lines and experimental conditions (Bignotti et al., 2016). Hence, 3 SNORDD RNAs previously used in published studies were identified and their expression across the panel of cell lines was investigated (Bignotti et al., 2016; Sperveslage et al., 2014).

Even though the normalisation genes screened revealed to be stable across the panel of cell lines, SNORDD 48 was chosen as the best normaliser for the panel of cell lines available. This was due to statistical analysis of results revealing no statistical significance in its expression across all the cell lines. Little significant variations were reported for SNORDD72 and SNORDD68, therefore they were not selected for this study. However, they are potential promising candidates for miRNA expression studies in those cell lines (Figure 3.6).

Earlier studies suggested that downregulation of miR-184 expression was linked to cisplatin resistance in NCSLC cell lines (Longqiu et al., 2020; Tung et al., 2016). Therefore, miR-184 expression was examined in the panel of NSCLC cell lines gifted from Dr. Lakis Liloglou and Dr. Michael Davies. Previous studies on the same cell lines revealed a different sensitivity towards cisplatin: the study by Alnefaie on those cell lines observed Calu-3 to be the most resistant and Calu-6 the most sensitive towards cisplatin (IC50 values from this study are shown in Figure 3.7) (Alnefaie, 2020). Therefore, given published studies linking cisplatin resistance to miR-184 downregulation in NSCLC, a difference in miR-184 expression across the cell lines was

investigated. However, no significant difference in miR-184 expression was observed among the panel of cell lines examined. These findings were in contrast to the study carried out by Tung and Longqiu. However, the former study was conducted by analysing miR-184 expression in tissue samples from NSCLC patients, which can be significantly different to cultured cell lines. In addition, Tung confirmed their observation from patients in TL-1 cells, which is not a NSCLC-derived cell line. On the other hand, the study by Longqiu was carried out using H1299 cells, which was not employed in this study. Even though H1299 cell line is an epithelial cell line derived from NSCLC, results obtained from different cell lines cannot be directly compared due to the vast differences that intercurred among different phenotypes of cells lines derived from the same malignancy (Longqiu et al., 2020; Tung et al., 2016).

3.5.5 Transfection of miR-184 mimic and inhibitor via INTERFERin(R)

INTERFERin® is a cationic transfection reagent marketed by Polyplus for the delivery of miRNA and siRNA into adherent and suspension cells, and the successful delivery of siRNA into Calu-3 cells via INTERFERin® had already been reported in literature by Chen (Chen et al., 2019). However, the manufacturer did not provide information of successful transfection of miRNA mimics in Calu-3 cells, nor was it mentioned in the literature regarding previous research involving miRNA mimic transfection of Calu-3 cells (*Cell Transfection Database, accessed 21 April 2019*). For this reason, the ability of INTERFERin® to transfect miR-184 was investigated via treating the cells with two different concentrations of miR-184 mimic (5 nM and 20 nM), and relative controls being NTC-transfected cells (5 nM and 20 nM), mock treated cells (with INTERFERin® only) and untreated cells.

Following analysis of the q-PCR results, the outcome of the experiment revealed that the treatment of Calu-3 cells with miR-184 mimic and INTERFERin® brought about an increase in relative miR-184 expression of 3000 and 4000-fold for 5 nM and 20 nM treatment, respectively, compared to untreated cells. Moreover, the increase in miR-184 expression was significantly higher than mock-treated cells and NTC-transfected cells, thus suggesting that the increase of miR-184 expression was due to the ability of the transfecting reagent to promote the internalisation of the oligonucleotide in Calu-3 cells.

Additionally, confocal microscopy image confirmed the successful transfection of the 5'-TAMRA miR-184 by Calu-3 cells via INTERFERin® (**Figure** 3.11 **B**).

Given the successful results in the delivery of miR-184 mimic via INTERFERin®, the delivery of miR-184 inhibitor via the same reagent was investigated and the expression of miR-184 was measured via q-PCR. Results revealed that the treatment with miR-184 inhibitor brought about a slight decrease in miR-184 expression for both the working concentration employed (5 nM and 20 nM). However, the decrease was not statistically significant compared to untreated cells. The analysis of the three independent experiments performed revealed that there was a slight decrease in miR-184 expression for all the replicates. Therefore, this might suggest that the amount of miR-184 inhibitor used was too low to detect a change in miR-184 expression via the DDCt method.

The DDCt method considers the expression of a gene of interest (GOI) (miR-184 in this study) in comparison to the expression of a reference gene (SNORDD 48 in this study). The expression of both genes is recorded for untreated cells and for treated cells (in this case, miR-184 inhibitor transfected cells) (Livak & Schmittgen, 2001). Even though the cell culture condition employed to carry out the independent experiments were the same, the function, behaviour, and biology of the cells in culture cannot be totally controlled. Therefore, the inter-day variations in cell behaviour can also lead to small variations in genes expression (Osorio et al., 2019; Snijder & Pelkmans, 2011). In the case of the present study, the small variations that might have occurred in SNORDD48 and miR-184 expression in untreated cells and in treated cells brought about by the cell culture condition used revealed no statistical difference in diminishing miR-184 expression.

In conclusion, despite majority of the studies published in literature employ Lipofectamine™ to transfect Calu-3 cells with miRNA mimic (Bartoszewska et al., 2017; Shanshan Chen et al., 2015; Lihua Liu et al., 2019; Ye et al., 2017; L. Zhang & Yu, 2018; X. Zhang et al., 2012) this study demonstrate that INTERFERin® is a valid alternative to obtain miRNA mimic transfection of Calu-3 cells. On the other hand, further studies are needed to confirm the ability of INTERFERin® to deliver miR-184 inhibitor in Calu-3 cells, and to assess the efficiency of miR-184 inhibitor to reduce miR-184 expression in Calu-3 cells.

3.5.6 miR-184 Delivery via Chitosan Nanoparticles

The ability of the NPs to deliver a miR-184 mimic to NSCLC was investigated. Thus, the miR-184-loaded NPs could be used to deliver miR-184 mimic into cells to enhance their cisplatin sensitivity (chapter 4 and chapter 5).Calu-3 cells were chosen, as they were reported to have a higher IC50 (and consequently a lower sensitivity to cisplatin) compared to the other cell

line of the panel (Alnefaie, 2020). Application of the miR-184-loaded NPs to Calu-3 cells for 48 h elevated miR-184 levels by up to 300-fold when the undiluted formulation was employed to treat cells (700 nM NPs) (**Figure** 3.10). Thus, confirms the ability of CHT NPs to promote the uptake of an oligonucleotide that will not be able to cross cell membrane when delivered naked. Xiao obtained similar results, showing that complexation of siRNA within CHT NPs could silence the expression of the target genes in comparison to treatment of cells with non-complexed CHT-siRNA solution (Xiao et al., 2017). Moreover, the delivery of miR-34a via CHT NPs was also assessed *in vivo* (Gaur et al., 2015). Mice were injected with SKMM1 cells (multiple myeloma cell line), and once the tumour reached a decided dimension, mice were treated with miR-34a-loaded CHT NPs. Results revealed that tumour size of mice treated with the miR-34a-loaded NPs decrease significantly compared to untreated mice. Therefore, the NPs were successfully uptaken by the tumour cells and could deliver the oligonucleotide inside the cells. In our study, miR-184 loaded NPs increased significantly miR-184 expression compared to blank NPs and to NTC-loaded NPs for all the concentration of NPs tested. Therefore, given the significant increase in miR-184 expression in cells treated with 700 nM, 20 nM and 5 nM, miR-184 loaded NPs, CS HCl NPs are suitable candidates to deliver oligonucleotide to NSCLC cells (Gaur et al., 2015).

As a visual confirmation of the ability of the NPs to deliver miR-184 and to facilitate its uptake in Calu3 cells, images of cells treated with 5'-TAMRA-miR-184 mimic-loaded NPs were captured. Images showed that the 5'-TAMRA-184-loaded NPs (red fluorescence) are localised in the area surrounding the nuclei (blue fluorescence), thus confirming NPs uptake into the cells. Moreover, the red fluorescence shown by cells treated with 5'-TAMRA-184-loaded NPs (**Figure** 3.11 **C** and **D**) is similar to the one shown by the positive control (**Figure** 3.11 **B**), being cells treated with 5'-TAMRA-184 and transfected with INTERFERin®. Therefore, underlining the ability of CS HCL NPs of not only enhancing miR-184 delivery into the cells, but also to reach a percentage of transfection which is comparable to that obtained with commercial oligonucleotides transfection methods.

3.6 Conclusion

The present study aimed at optimising the formulation of CHT NPs with microfluidic mixing technology, investigating their complexation with miR-184 mimic and confirming the successful uptake of miR-184 mimic *in vitro*. Results revealed that microfluidic mixing technology is a promising approach to manufacture CHT NPs and that CS HCl and CS GLU are promising candidates to load miR-184 mimic. Further assessments conducted with confocal microscopy suggested that miR-184-loaded CS HCl NPs were successfully delivered into Calu-3 cells. In addition, the delivery of miR-184 was optimised also via the use of a commercially available reagent, named INTERFERin®, in Calu-3 cells. Finally, the study focused on investigating the expression of miR-184 in a panel of NSCLC cells, that previous studies reported to have different sensitivity towards cisplatin. However, findings from this study observed no statistical differences in miR-184 expression among them.

4 Effect of miR-184 on Cisplatin Sensitivity to NSCLC cells

4.1 Introduction

Cisplatin resistance represents the primary drawback that limits the success of chemotherapeutic treatment of cancer malignancies, including testicular cancer (de Vries et al., 2020), gastric cancer (M. Li et al., 2019), head and neck squamous cell carcinoma (Griso et al., 2022), ovarian cancer (J. Zhao et al., 2021), osteosarcoma (Y. Liu et al., 2020) and lung cancer (H. Wu et al., 2020; L. Xiao et al., 2017).

Since the first study by Calin linking miRNA deregulation to cancer progression (Calin et al., 2002b), many miRNAs have been linked to several cancer processes, including the occurrence of drug resistance (Baldassari et al., 2018; Chaudhary et al., 2017; Mao et al., 2019; A. Zeng et al., 2018). The involvement of miR-184 in cisplatin resistance has been demonstrated in oral squamous cell carcinoma (Fang et al., 2017) and lung cancer (Longqiu et al., 2020; Tung et al., 2016b). Longqiu and Tung suggested that downregulation of miR-184 was linked to unfavourable response to cisplatin and lung cancer progression. Their studies demonstrated that replenishment of miR-184 caused an increase in cytotoxicity, as well as a decrease in migration and invasion of NSCLC cells, compared to cells not overexpressing miR-184. Furthermore, the treatment of cisplatin together with miR-184 mimic enhanced sensitivity of lung cancer cells towards cisplatin leading to more favourable outcome of the treatment (Longqiu et al., 2020; Tung et al., 2016a).

The translation from *in vitro* miR-184 overexpression to *in vivo* (and *ex-vivo*) oligonucleotide delivery remains challenging given the limitation related to oligonucleotides administration, such as poor bioavailability, short half-life, poor uptake and low target-specificity (Roberts et al., 2020) (section 1.2.3). Despite the advances in oligonucleotide therapeutics brought about by the development of chemically-modified or conjugated molecules, encapsulation of oligonucleotides within polymeric NPs represents a promising tool to advance oligonucleotide therapeutic further (Dogra et al., 2022; F. Li et al., 2018; L. Li et al., 2022; Malik et al., 2020). Chitosan is a promising cationic polymer candidate for the successful delivery of miRNA (Gaur et al., 2015a; Kaban et al., 2019; Ning et al., 2019). Chitosan hydrochloride (CS HCl) is a chitosan salt form that was introduced in 2008 in the European Pharmacopeia 6.0, making this derivative attractive for pharmaceutical applications (Wei Chen et al., 2012), (Q. X. Wu et al., 2016) (Y. Wang et al., 2018). Our promising findings displayed and discussed in Chapter 3 outlined the successful uptake of miR-184 mimic in Calu-3 cells following its loading into CS HCl NPs.

4.2 Aim

In this chapter, the roles of miR-184 in cisplatin sensitivity of NSCLC cells was investigated. This was achieved by the following objectives:

- Assessment of cisplatin sensitivity in Calu-3 and Calu-6 cells.
- Investigation of cisplatin sensitivity in Calu-3 cells following transfection of miR-184 mimic or miR-184 inhibitor.
- Investigation of the effect on cisplatin sensitivity of miR-184 mimic-loaded CS HCl NPs.
- Evaluation of the effect of miR-184 mimic and miR-184 inhibitor on cisplatin induced apoptosis.

4.3 Methods

4.3.1 Determination of the Effect of Cisplatin on Cell Viability of NSCLC cells

Alamar Blue assays were performed to assess cytotoxicity of the treatments as outlined in section 2.5.1. Cells were treated with cisplatin concentration ranging from 1 µM to 250 µM for 24 or 48 h. After normalisation of the fluorescence values, dose-response curves of cisplatin concentration (log[M]) versus cell viability (%) were generated with GraphPad Prism version 8.0 based on the non-linear regression analysis "log[inhibitor] vs normalised response" model. Additionally, the analysis generated the IC50 value, 95 (%) of likelihood and R^2 of the calculated curve. The IC50 of cisplatin on Calu-3 cells in the presence of miR-184 mimic and inhibitor was investigated by transfecting the cells with the oligonucleotides via INTERFERin® (5 nM for miR-184 mimic and 5 nM or 20 nM for miR-184 inhibitor) or by addition of miR-184-loaded CS HCl NPs (5 nM or 20 nM).

Four mock treatments were included: (i) control treatment with the solvent used to dissolve cisplatin, dimethylformamide (DMF); (ii) control treatment miR-184 mimic only at concentrations ranging from 0 nM (INTERFERin®) to 50 nM to evaluate its effect on cell viability of miR-184 mimic; (iii) and (iv) cells treatment with CS HCl Blank NPs or NTC-loaded CS HCl NPs (5nM and 20nM) in addition to cisplatin (concentration ranging from 1 µM to 250 µM).

4.3.2 Apoptosis study

AnnexinV-FITC/PI staining was performed as explained in section 2.5.2.2.Following 48 h of treatment with cisplatin and transfection with miR-184 mimic or inhibitor, cells were trypsinised and resuspended in PBS. AnnexinV-FITC (200 µL) stain was added to the cell suspension and incubated for 10 min before addition of the PI (200 µL) staining. Cell suspensions were then centrifuged (Eppendorf Centrifuge 5810-R) for 5 min at 400 x g and analysed via flow cytometry on an BD Accuri C6 with four channels for fluorescence intensity (FL-1, FL-2, FL-3, and FL-4). Data collection and gating strategy were performed as described in chapter 2.

4.3.3 Statistical Analysis

Statistical analysis was performed using GraphPad Prism 8.0 statistical software. One-way ANOVA with Dunnett's or Tukey's comparison tests were applied (section 2.9) in accordance with the experiment carried out and stated throughout the results. All values are expressed as mean ± standard deviation (SD), and the number of independent experiments is stated throughout. The *P* values are expressed as **P*<0.05, ***P*<0.01, ****P*<0.001, *****P*<0.0001.

4.4 Results

4.4.1 Determination of the Effect of Cisplatin on NSCLC cells viability

4.4.1.1 Cisplatin and mock Dimethyl-Formamide Treatment

Given that cisplatin was dissolved in DMF, the toxicity of DMF at the working concentration after 48 h treatment was investigated. The DMF concentration (%) ranged from 0 to 3% as reported in **Table** 4.1. Results from Alamar Blue cytotoxicity assay revealed that cell viability was significantly decreased in cells treated with 1.5% and 3% DMF (**Figure** 4.1). This corresponds to cisplatin concentrations of 500 µM and 1000 µM, respectively. All the remaining concentrations of DMF had no statistically significant effects on cell viability (**Figure** 4.1). Given these results, cisplatin concentration of 500 µM and 1000 µM (Table 4.1, highlighted in red) were not used in further studies, and the highest concentration used was 250 µM.

Table 4.1 Cisplatin concentration values (nM, µM, M, log [M]) employed in this study and corresponding DMF concentrations (%).

DMF concentration	Cisplatin concentration			
%	nM	µM	M	Log[M]
0	1000	1	0.000001	-6
0.01	5000	5	0.000005	-5.30
0.03	10000	10	0.00001	-5
0.08	25000	25	0.000025	-4.60
0.15	50000	50	0.00005	-4.30
0.23	75000	75	0.000075	-4.12
0.30	100000	100	0.0001	-4
0.38	125000	125	0.000125	-3.90
0.75	250000	250	0.00025	-3.60
1.50	500000	500	0.0005	-3.30
3	1000000	1000	0.001	-3

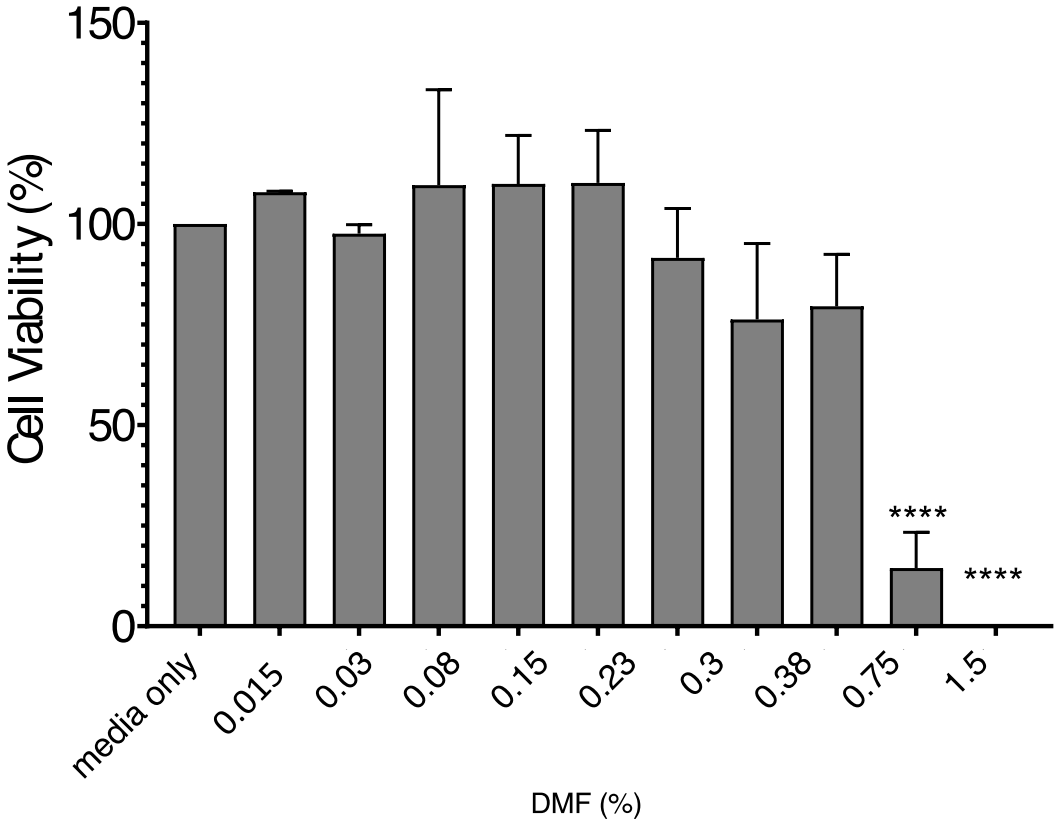

Figure 4.1 Effects of dimethylformamide (DMF) on Calu-3 cells viability. Cells were treated with the indicated doses of DMF in complete media for 48 h and viability monitored using the Alamar Blue assay. For concentrations of DMF up to 0.75% there was no statistically significant effect on cell viability compared to media-treated control cells (one-way ANOVA with Dunnet's post-test was performed) (n=3, mean ± SD, ****p<0.001).

Cisplatin IC50 value for Calu-3 was 154.73 ± 63.65 µM after 24 h treatment. For the 48 h treatment, the IC50 was approximately 10-fold lower, at 14.35 ± 1.28 µM. On the other hand, the IC50 values for Calu-6 was 175.49 ± 1.28 µM after 24 h treatment and similarly, it decreased nearly 10 times for the 48 h treatment, resulting in a value of 17.28 ± 3 (**Table** 4.2). Thus, the dose-response curves for 48 h treatment for both the cell lines shifted to the left if compared to the 24 h treatment curves (**Figure** 4.2). The R^2 values obtained for the curves were 0.92 and 0.94 for Calu-3 at 24 h and 48 h respectively, and 0.94 and 0.92 for Calu6 at 24 h and 48 h respectively, therefore the data fitted the model selected and computed dose-response curves were considered acceptable (**Table** 4.2).

Table 4.2 Summary of LogIC50, IC50 values, 95 % confidence interval (95 % CI) and R squared for Calu-3 and Calu-6 cisplatin treatments. Non-linear regression analysis was performed with GraphPad Prism. The outcomes (LogIC50 values, 95 % confidence interval (% % CI), and R squared values) are reported in the table, together with the IC50 ± SD values obtained by averaging the IC50 values for each replicate. (n=5, mean ± SD).

	LogIC50	95% CI	R squared	IC50 ± SD (µM)
Cisplatin Calu-6 24 h	-4.15	-4.34 to -3.96	0.94	175.49 ± 40.28
Cisplatin Calu-6 48 h	-4.79	-4.97 to -4.65	0.92	17.28 ± 3.74
Cisplatin Calu-3 24 h	-3.93	-4.06 to -3.79	0.92	154.73 ± 63.65
Cisplatin Calu-3 48 h	-4.75	-4.88 to -4.64	0.94	14.35 ± 1.28

In addition, cisplatin IC50 values for Calu-3 and Calu-6 at 24 h and 48 h were statistically different (**Figure** 4.3). However, the IC50 values for cisplatin on Calu-3 compared to Calu-6 were not statistically significant at either time point. This suggests that Calu-3 and Calu-6 have a similar sensitivity to cisplatin, even though a previous study reported Calu-3 cells were less sensitive to cisplatin (IC50 7.01 µM) compared to Calu-6 (IC50 1.10 µM) (Alnefaie, 2020). Therefore, only Calu-3 cells line were used for further investigations of cisplatin sensitivity.

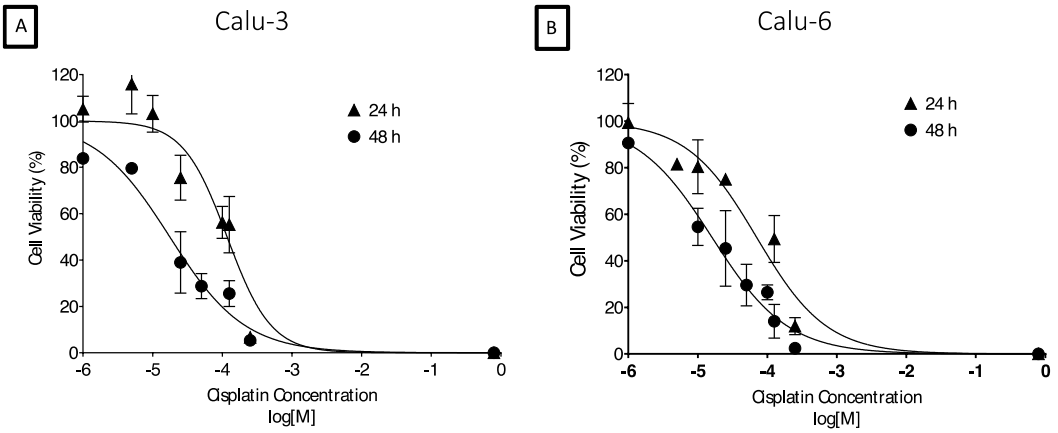

Figure 4.2 Dose-response curves for cisplatin in Calu-3 and Calu-6 cells. Calu-3 (A) and Calu-6 (B) cells were exposed to cisplatin for 24 h or 48 h. Following the incubation period, Alamar Blue assay was performed, and the dose-response curves were generated. For both the cell lines, the 48 h treatment increased cisplatin toxicity compared to the 24 h. (n=3, mean ± SD).

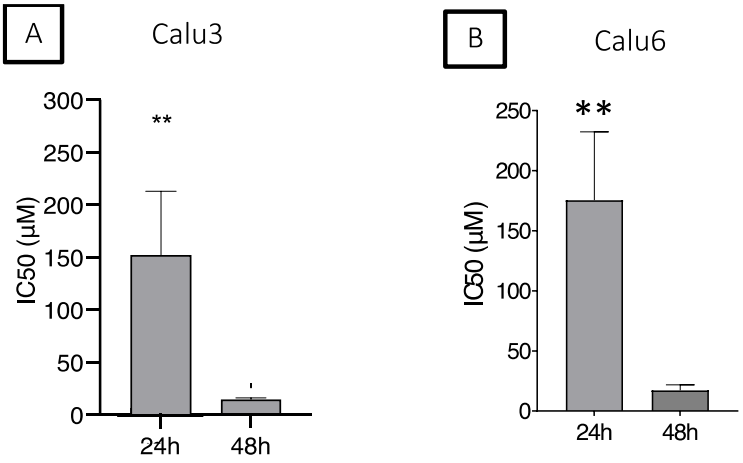

Figure 4.3 Cisplatin IC50 values for Calu-3 and Calu-6. Calu-3 (A) and Calu-6 (B) cells were exposed to cisplatin for 24 h or 48 h. Following the incubation period, Alamar Blue assay was performed, and the IC50 was calculated. T-test revealed that cisplatin IC50 for the 24 h treatments are significantly higher than IC50 following 48 h exposure to the drug (n=3, mean ± SD; ** p<0.01).

4.4.1.2 Effect of miR-184 mimic on NSCLC cells viability

To determine the effect of miR-184 on the viability of Calu-3 cells, initial experiments were performed using INTERFERin® transfection of miR-184 mimic. As displayed in **Figure** 4.4, cell viability slightly increased as the miR-184 concentration increased. However, this was only significant at 20 nM miR-184 mimic (**Figure** 4.4)

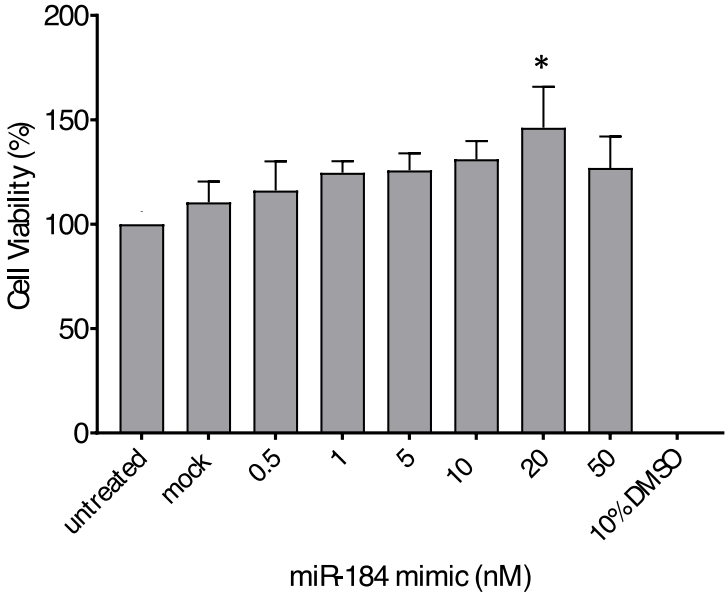

Figure 4.4 Calu-3 treatment with miR-184 mimic. The treatment of Calu-3 with miR-184 mimic (concentration ranging from 0 (INTERFERin ® only or mock) to 50 nM). One-way ANOVA analysis of the results with Dunnet post-test revealed that only the 20 nM was statistically different from the control (untreated cells) (n=3, mean ± SD; *p < 0.05).

4.4.1.3 Effect of miR-184 mimic on cisplatin sensitivity of NSCLC cells

Calu-3 cells were treated with a combination of miR-184 mimic (5 nM) and cisplatin (250 µM to 1 µM) to investigate whether miR-184 mimic could enhance cisplatin sensitivity in Calu-3 cells. As shown in **Figure** 4.5, the dose-response curve (in green) referring to the combination of miR-184 mimic 5 nM and cisplatin shifted to the left compared to cisplatin curve and to the curve of NTC control in combination with cisplatin. The IC50 for cisplatin was 9.42±1.47 µM when in combination with miR-184 mimic, which was lower than the IC50 of cisplatin alone (14.35 ± 1.28 µM) or NTC (13.91 ± 1.64 µM). The R^2 values for the computed models were 0.94 for cisplatin and miR-184 and 0.92 for cisplatin and NTC, therefore both were considered acceptable for the purpose of this study (**Table** 4.3). One-way ANOVA statistical analysis with Dunnet's post-test revealed that the IC50 of cisplatin alone is significantly different from the IC50 of cisplatin in combination with miR-184 mimic. Thus, suggesting that the delivery of miR-184 mimic enhances the sensitivity of Calu-3 cells towards cisplatin. Therefore, miR-184 mimic lowered the dose of cisplatin that is needed to reduce cell viability.

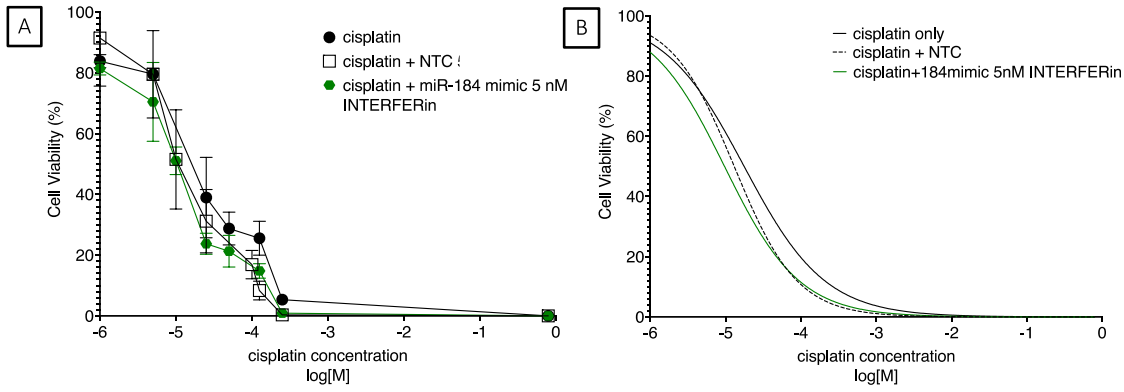

Figure 4.5 Dose-response curves of cisplatin, cisplatin in combination with non-targeting control (NTC) and cisplatin with miR-184 mimic. (A) shows raw data and (B) shows the curve fit as calculated by GraphPad Prism using the raw data gathered. The curve generated with the combination of cisplatin and miR-184 mimic (green) shifted to the left compared to the other curves, suggesting a decrease in cisplatin IC50 brought about by the miR-184 treatment (n=5, mean ± SD for cisplatin only; n=4, mean ± SD for cisplatin and miR-184 mimic; n=2 mean ± SD for cisplatin and NTC).

Table 4.3 Summary of LogIC50, IC50 values, 95 % confidence interval (95 % CI) and R squared for cisplatin and miR-184 mimic treatments. Non-linear regression analysis was performed with GraphPad Prism. The outcomes (LogIC50 values, 95 % confidence interval (% % CI), and R squared values) are reported in the table, together with the IC50 ± SD values obtained by averaging the IC50 values for each replicate. (n=5, mean ± SD for cisplatin only treatment, n=4, mean ± SD for cisplatin and miR-184 mimic via INTERFERin®, n=2, mean ± SD for cisplatin and NTC).

	LogIC50	95% CI	R squared	IC50 ± SD (μM)
Cisplatin only	-4.75	-4.88 to -4.64	0.94	14.35 ± 1.28
Cisplatin + miR-184 mimic 5 nM	-5.01	-5.13 to -4.90	0.94	9.42 ± 1.47
Cisplatin + NTC	-4.85	-5.08 to -4.79	0.92	13.91 ± 1.64

4.4.1.4 Effect of miR-184 inhibitor on cisplatin sensitivity of NSCLC cells

Calu-3 cells were treated with a combination of miR-184 inhibitor (5 nM or 20 nM) and cisplatin (250 µM to 1 µM) to investigate the effect of miR-184 inhibition on cisplatin sensitivity in Calu-3 cells. **Figure** 4.6 **(A and B)** shows the dose-response curve (in lilac) obtained with the combination of miR-184 mimic inhibitor 5 nM and cisplatin. The curve shifted to the right compared to the cisplatin only curve and to the NTC in combination with cisplatin curve. Moreover, **Figure** 4.6 **(C and D)** shows dose-response curve obtained for the 20 nM miR-184 inhibitor treatment (in purple). Similar to the 5 nM inhibitor curve, the 20 nM miR-184 inhibitor curve shifted to the right compared to cisplatin only and to NTC in combination with cisplatin curve. Thus, results indicated that the treatment with miR-184 inhibitor decreased Calu-3 sensitivity towards cisplatin.

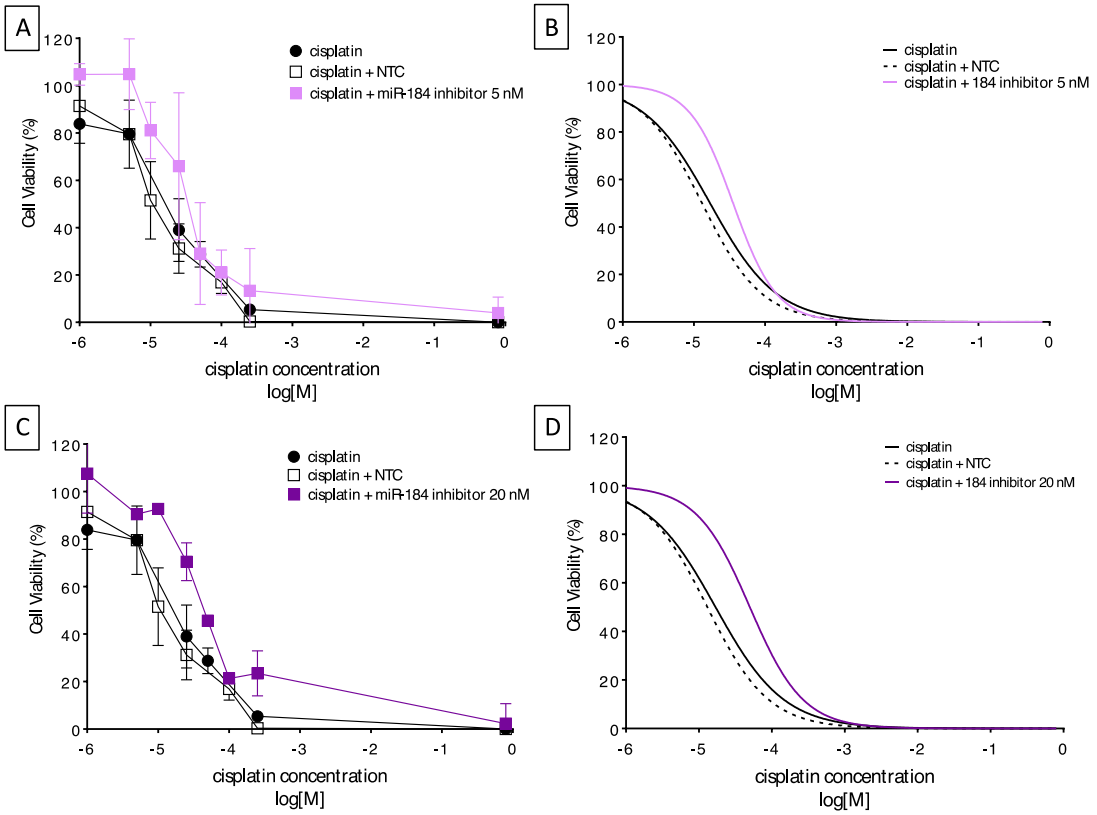

Figure 4.6 Dose-response curves of cisplatin, cisplatin in combination with non-targeting control (NTC) and cisplatin with miR-184 inhibitor 5 nM (A and B) or 20 nM (C and D). (A and C) shows raw data and (B and D) shows the curve fit as calculated by GraphPad Prism using the raw data gathered. The curve generated with the combination of cisplatin and miR-184 inhibitor 5 nM (lilac) or 20 nM (purple) shifted to the right compared to the other curves, suggesting a decrease in cisplatin IC50 brought about by the miR-184 inhibitor treatment (n=5, mean ± SD for cisplatin only; n=3, mean ±SD for cisplatin and miR-184 inhibitor; n=2, mean ±S D for cisplatin and NTC).

The IC50 of cisplatin when associated with miR-184 inhibitor was 34.77 ± 3.99 µM for the 5 nM treatment, and 55.01 ± 4.42 µM when 20 nM of inhibitor was transfected compared to 14.35 ± 1.28 and 13.91 ± 1.64 for cisplatin alone and cisplatin plus NTC, respectively. The R^2 values for the computed models were 0.90 and 0.94 for the 5 nM and 20 nM miR-184 inhibitor, respectively (**Table** 4.4)and therefore both the calculated models were considered acceptable for the purpose of this study. Statistical analysis of the results showed that IC50 values of cisplatin in association with 5 nM or 20 nM miR-184 inhibitor was statistically significant compared to cisplatin only treatment or cisplatin in association with NTC (**Figure** 4.7**).**

Therefore, while the treatment with miR-184 mimic led to a shift to the left of the cisplatin curve, suggesting an increase in cisplatin sensitivity (**section 4.4.1.3**), the treatment with miR-184 inhibitor determined the opposite effect. The cisplatin curved shifted to the right, suggesting that miR-184 inhibitor increased the dose of cisplatin that is needed to reduce cell viability (**Figure** 4.8).

Table 4.4 Summary of LogIC50, IC50 values, 95 % confidence interval (95 % CI) and R squared for miR-184 mimic, inhibitor and cisplatin treatments. Non-linear regression analysis was performed with GraphPad Prism. The outcomes (LogIC50 values, 95 % confidence interval (% % CI), and R squared values) are reported in the table, together with the IC50 ± SD values obtained by averaging the IC50 values for each replicate. (n=5, mean ± SD for cisplatin only treatments, n=4, mean ± SD for cisplatin and miR-184 mimic; n=3, mean ± SD for cisplatin and miR-184 inhibitor; n=2, mean ± SD for cisplatin and NTC).

	LogIC50	95% CI	R squared	IC50 ± SD (µM)
Cisplatin only	-4.75	-4.88 to -4.64	0.94	14.35 ± 1.28
Cisplatin + miR-184 mimic 5 nM	-5.01	-5.13 to -4.90	0.94	9.42 ± 1.47
Cisplatin + miR184 Inhibitor 5 nM	-4.45	-4.60 to -4.30	0.90	34.78 ± 3.99
Cisplatin + miR184 Inhibitor 20 nM	-4.30	-4.44 to -4.15	0.94	55.01 ± 4.42
Cisplatin + NTC	-4.85	-5.08 to -4.79	0.92	13.91 ± 1.64

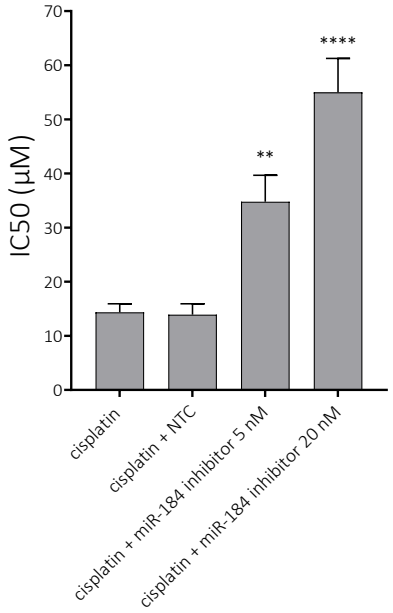

Figure 4.7 Transfection of miR-184 inhibitor decreases Calu-3 cells sensitivity to cisplatin. Calu-3 cells were treated with cisplatin in combination with miR-184 inhibitor, or NTC. One-way ANOVA statistical analysis with Dunnet post-test revealed that the IC50 of cisplatin with miR-184 inhibitor was significantly different from the IC50 of cisplatin alone. Thus, suggesting that the delivery of miR-184 inhibitor decreased the sensitivity of Calu-3 cells towards cisplatin (n=5, mean ± SD for cisplatin only; n=3, mean ± SD for cisplatin and miR-184 inhibitor; n=2, mean ± SD for cisplatin and NTC; ** p<0.01, **** p<0.0001**).**

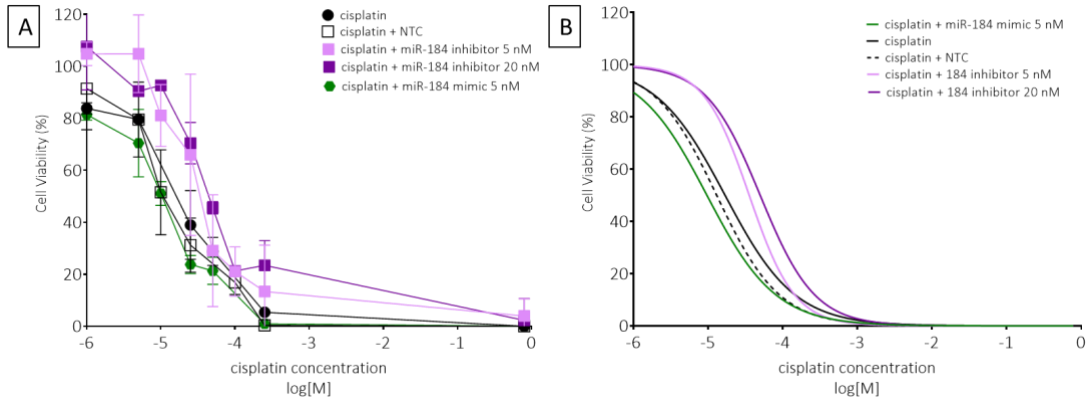

Figure 4.8 Dose-response curves for cisplatin, cisplatin in combination with miR-184 mimic 5 nM, miR-184 inhibitor 5 nM, or miR-184 inhibitor 20 nM. (A) shows raw data and (B) shows the curve fit as calculated by GraphPad Prism using the raw data gathered. The curve generated with the combination of cisplatin and miR-184 mimic shifted to the left compared to cisplatin only curve (black), while the curve generated with miR-184 inhibitor (lilac and purple) shifted to the right compared to the other curves (n=5, mean ± SD for cisplatin only; n=4, mean ± SD for cisplatin and miR-184 mimic n=3, mean ± SD for cisplatin and miR-184 inhibitor; n=2, mean ± SD for cisplatin and NTC).

4.4.2 Effect of miR-184 loaded CS HCl NPs on cisplatin sensitivity

Further investigation involving cisplatin and miR-184 mimic was carried out using CS HCl NPs loaded with miR-184 mimic. Surprisingly, as displayed in **Figure** 4.9, the dose-response curves generated for miR-184-loaded, NTC-loaded or blank CS HCl NPs shifted to the right compared to cisplatin dose-response curve. Thus, suggesting that the delivery of 5 nM miR-184 mimic via CS HCl NPs reduced the sensitivity of Calu-3 cells to cisplatin. Accordingly, the IC50 value raised from 14.35 ± 1.28 µM of cisplatin alone to 40.52 ± 3.52 µM for the combination of miR-184-loaded CS HCl NPs and cisplatin (**Table** 4.5). Interestingly, blank CS HCl NPs and NTC-loaded CS HCl NPs also reduced the sensitivity of Calu-3 towards cisplatin, and their IC50 value were 23.59 ± 1.36 µM and 30.23 ± 7.37 µM, respectively (**Table** 4.5 and **Figure** 4.9).

Furthermore, increasing the amount of miR-184 to 20 nM also elevated the IC50 of cisplatin (63.21 ± 17.27 µM), as well as the IC50 of mock treatments, being 25.49 ± 0.46 µM for cisplatin associated with NTC-loaded NPs and 36.60 ± 8.44 µM for cisplatin in addition to Blank CS HCl NPs (**Figure** 4.10).

In addition, results showed that the increase in cisplatin IC50 was proportional to the increase in the concentration of miR-184 mimic-loaded CS HCl NPs used for the treatment, as it increased from 40.52 ± 3.52 µM for the 5 nM treatment to 63.21 ± 17.27 µM for the 20 nM treatment (**Table** 4.5 and **Figure** 4.10). This can be also visualized by the shift in the relative dose-response curves (**Figure** 4.11), as the curve relative to the 20 nM treatment is more shifted to the right compared to the 5 nM treatment.

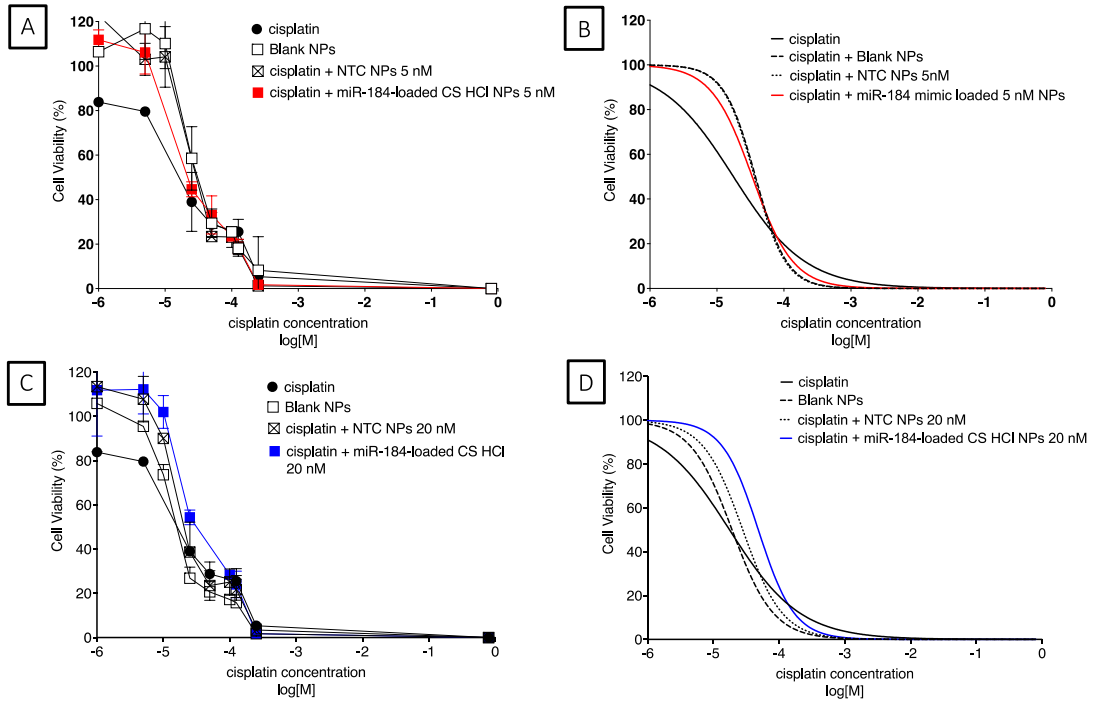

Figure 4.9 Dose-response curves for cisplatin only and cisplatin in association with miR-184-loaded CS HCl NPs and relative controls. (A) and (C) show raw data while (B) and (D) show curves fit as calculated by GraphPad Prism using the raw data gathered. The curve generated with the combination of cisplatin and miR-184 mimic-loaded CS HCl NPs caused a shift to the right of cisplatin dose-response curve, therefore a decrease in cisplatin sensitivity of Calu-3 cells. However, the same behaviour was registered by treatment with blank NPs and NTC-loaded CS HCl NPs (n=5, mean ± SD for cisplatin only, n=4 mean ± SD for cisplatin and miR-184 mimic-loaded CS HCl NPs, n=2 mean ± SD for cisplatin and NTC or Blank NPs).

Table 4.5 Summary of LogIC50, IC50 values, 95% confidence interval (95% CI) and R squared for miR-184 mimic- or NTC-loaded CS HCl NPs, Blank NPs and cisplatin treatments. Non-linear regression analysis was performed with GraphPad Prism. The outcomes (LogIC50 values, 95 % confidence interval (95% CI), and R squared values) are reported in the table, together with the IC50 ± SD values obtained by averaging the IC50 values for each replicate. (n=5, mean ± SD for cisplatin only treatment; n=4 mean ± SD for cisplatin and miR-184 mimic-loaded CS HCl NPs, n=2 mean ± SD for cisplatin and NTC-loaded or Blank NPs).

	LogIC50	95% CI	R squared	IC50 ± SD (µM)
Cisplatin only	-4.75	-4.88 to -4.64	0.94	14.35 ± 1.28
Cisplatin + miR-184 5 nM NPs	-4.47	-4.54 to -4.39	0.95	40.52 ± 3.52
Cisplatin + miR-184 20 nM NPs	-4.32	-4.47 to -4.17	0.93	63.21 ± 17.27
Cisplatin +NTC 5 nM NPs	-4.39	-4.76 to -4.02	0.94	30.23 ± 7.37
Cisplatin + NTC 20 nM NPs	-4.25	-4.57 to -3.92	0.90	25.49 ± 0.46
Cisplatin + 5 nM Blank NPs	-4.72	-4.83 to -4.61	0.93	23.59 ± 1.36
Cisplatin + 20 nM Blank NPs	-4.42	-4.53 to -4.31	0.91	36.60 ± 8.44

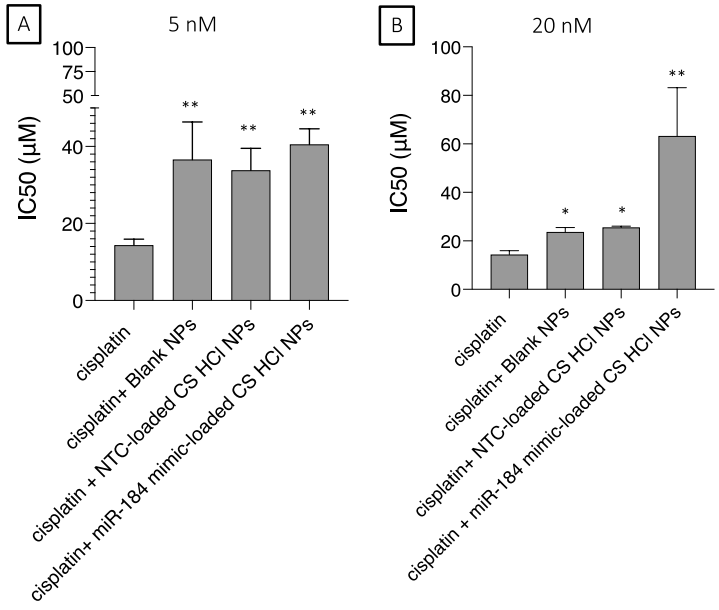

Figure 4.10 Treatment with miR-184 mimic-loaded CS HCl NPs suggested an increase in cell viability. Calu-3 cells were treated with cisplatin in combination with 5 nM (A) or 20 nM (B) of miR-184 mimic-loaded CS HCl NPs, NTC-loaded NPs or Blank NPs. One-way ANOVA statistical analysis with Dunnet's post-test revealed that the IC50 of cisplatin in association with NTC-loaded, Blank and miR-184 loaded NPs is significantly higher compared to the IC50 of cisplatin alone. (n=5, mean ± SD for cisplatin only, n=4, mean ± SD for cisplatin and miR-184 mimic-loaded CS HCl NPs, n=2, mean ± SD for cisplatin and NTC or Blank; **p*<0.05, ***p*<0.01)

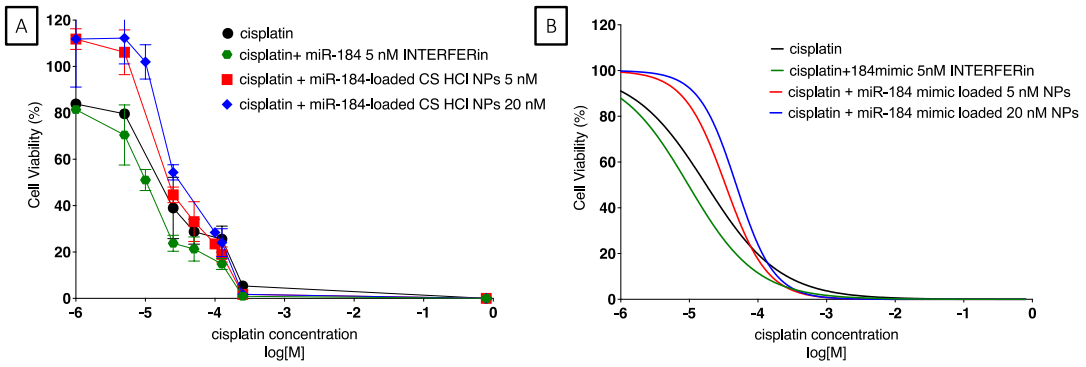

Figure 4.11 Comparison of dose-response curves for cisplatin, cisplatin and miR-184 mimic delivered via INTERFERin®, and cisplatin and miR-184 loaded CS HCl NPs: (A) shows raw data and (B) shows the curve fit as calculated by GraphPad Prism using the raw data gathered. The curve generated for cisplatin in association with miR-184 mimic transfected with INTERFERin® (green) shifted to the left compared to cisplatin dose-response curve (black), suggesting the ability of miR-184 to sensitise Calu-3 to cisplatin. The delivery of miR-184 mimic via CS HCl NPs (red and blue) was responsible of a shift to the right of cisplatin curve, suggesting instead a decrease in Calu-3 sensitivity to cisplatin. Additionally, the shift in the curve for miR-184-loaded CS HCl NPs is directly correlated to the amount of NPs employed to treat the cell: the 20 nM curve (blue) is further to the right compared to the 5 nM curve (red) (n=5, mean ± SD for cisplatin only, n=4, mean ± SD for cisplatin and miR-184 mimic via INTERFERin® or loaded CS HCl NPs).

These observations together suggested that CS HCl was responsible for the increase in the IC50 values of cisplatin. Therefore, cells were treated with CS HCl concentration ranging from 0.75 µg/mL to 187.5o µg/mL and cell viability assessed via Alamar Blue assay. The corresponding amount of miR-184 mimic delivered with each CS HCl concentration is shown in **Table** 4.6, where it can be seen for experiments employing 5nM miR-184 mimic the concentration of CS HCl resulted in approximately 2.70 µg/mL, while for miR-184 20 nM treatments CS HCl concentration was 10.75 µg/mL, (relevant values highlighted in red in **Table** 4.6). As shown in **Figure** 4.12, almost all the concentrations increased Calu-3 cell viability and the increase was statistically significant in the concentration range from 18.75 µg/mL to 187.5 µg/mL (**Figure** 4.12).

Given that the concentration of CS HCl employed in this study were 2.70 µg/mL and 10.75 µg/mL (highlighted in red, **Table** 4.6), these observations suggest the interference of the polymer with the assay, leading to the increase in cisplatin IC50 not only when miR-184 mimic is applied to the cells via CS HCl NPs, but also when blank or NTC-loaded CS HCl NPs treatments are performed (**Figure** 4.9).

Table 4.6 Correlation of CS HCl concentration and miR-184 mimic delivered when complexed within NPs.

[CS HCl]		[miR-184 mimic]
mg/mL	µg/mL	nM
0.375	375	700
0.187	187.50	350
0.093	93.75	175
0.075	75	140
0.0375	37.55	70
0.01875	18.75	35
0.01	10.75	20
0.0075	7.50	14
0.00375	3.75	7
0.0026	2.70	5
0.00075	0.75	1.4

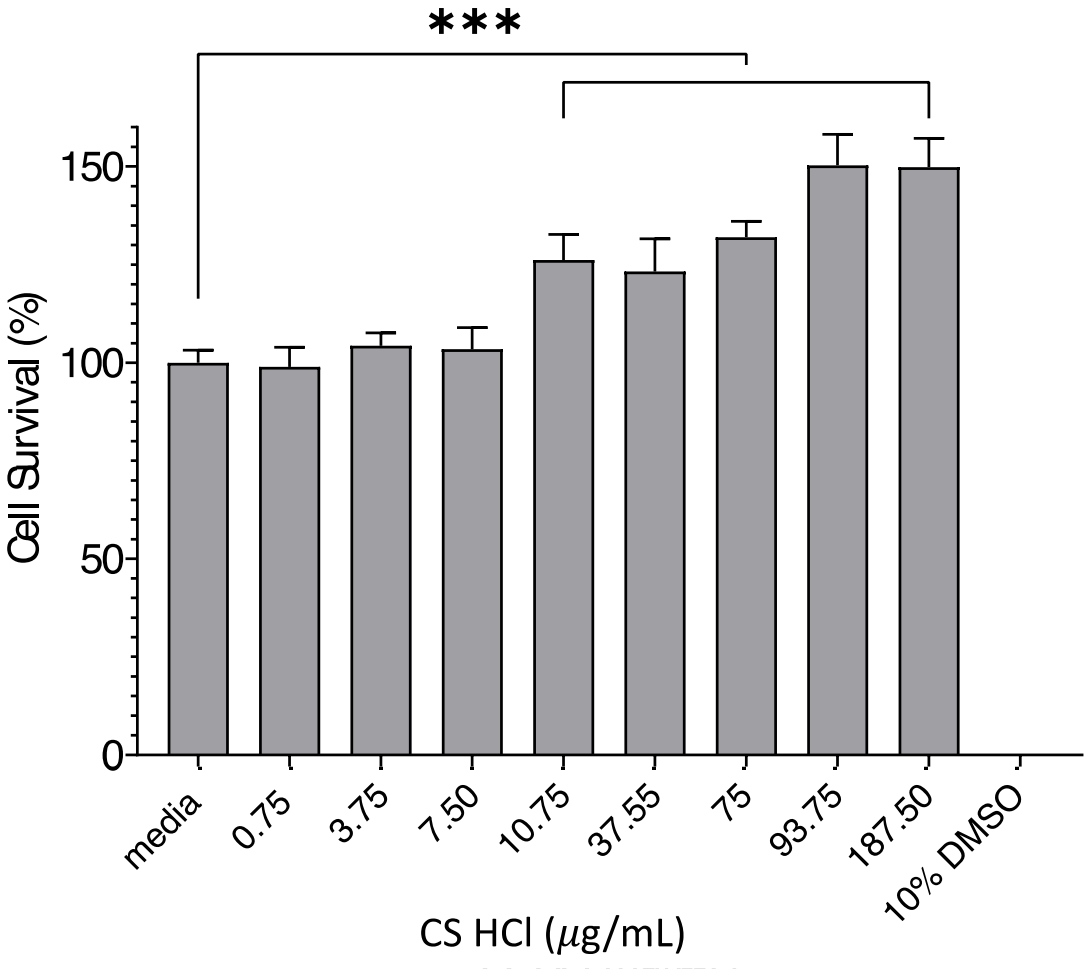

Figure 4.12 cell viability of Calu-3 following treatment with increasing concentrations of CS HCl. The dose-response curve generated for cisplatin in association with CS HCl NPs suggested interference of chitosan with the Alamar Blue reading. The treatment of Calu-3 with increasing concentration of CS HCl suggested that the polymer increased significantly Calu-3 viability for concentrations of chitosan higher than 1.87 μg/mL. The linear increase in cell viability related to the amount of chitosan used for the treatments, suggested the occurrence of interference between chitosan and the Alamar Blue assay employed to assess IC50 of the treatments (n=3, mean ± SD, *** p<0.001).

4.4.3 Effect of miR-184 mimic on cisplatin-induced apoptosis

The effect of miR-184 mimic in enhancing cisplatin-induced cytotoxicity in Calu-3 was investigated further using flow cytometry. Flow cytometry analysis via AnnexinV-FITC and Propidium Iodide (PI) staining was employed to evaluate the influence of miR-184 in cell viability, apoptosis and necrosis. Four populations were visualised for each sample, which were viable cells (AnnexinV-FITC negative, PI negative), early apoptotic cells (AnnexinV-FITC positive, PI negative), late apoptotic cells (AnnexinV-FITC positive, PI positive) and necrotic cells (AnnexinV-FITC negative, PI positive).

As expected, the treatment of cisplatin only (black bars throughout figures) decreased the percentage of viable cells (**Figure** 4.13) at all the concentration tested, compared to untreated.

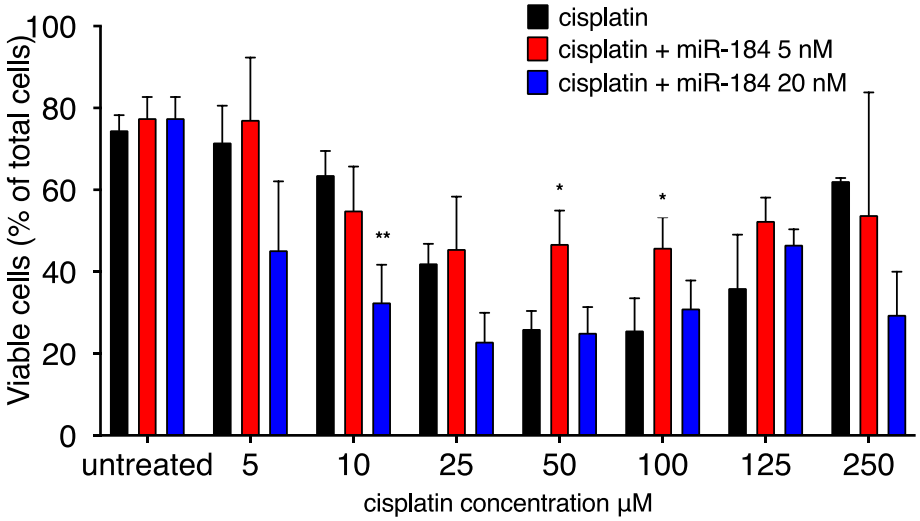

Figure 4.13 Percentage of viable cells following Calu-3 treatment with cisplatin only or in association with miR-184 mimic. Calu-3 cells were transfected with 5 or 20 nM miR-184 mimic and subsequently treated with cisplatin (0 to 250 µM). The statistical analysis performed was a one-way ANOVA with Dunnet's post-test, comparing in each group for cisplatin only treatments with 5 nM or 20 nM miR-184 mimic in association with the same concentration of cisplatin (n=4, mean ± SD; **p*,0.05; ***p*<0.01;).

The decrease in cell viability was proportional to the concentration of cisplatin used to treat the cells, as it decreases linearly from 5 µM to 100 µM. Even though the treatment with 125 µM and 250 µM cisplatin slightly increased the percentage of viable cells compared to treatments at lower concentrations, the behaviour can be attributable to the difficulty of the fluidic system to detect events when cells are exposed to cytotoxic agents at high dosage, as shown in **Figure** 4.14.

The general trend for the population of viable cells, which is shown in **Figure** 4.13, depicts a general decrease of viable cells following the transfection of miR-184 mimic. In particular, the treatment with 20 nM miR-184 mimic (blue bars) caused a decrease in cell viability in most of the samples (5, 10, 25, 50 and 250 µM) compared to cisplatin only treatment. The decrease resulted to be statistically significant for 10 µM cisplatin treatment. Unexpectedly, an overall increase in cell viability caused by the 5 nM miR-184 mimic treatment was registered. These findings might suggest that miR-184 mimic concentrations higher than 5 nM are necessary to observe a variation in the percentage of viable cells via the method used.

Data for early apoptotic cells is displayed in **Figure** 4.15**.** Even though results from the single treatment do not show a consistent trend, it can be seen that the transfection of miR-184 5 nM or 20 nM generally increased the population of early apoptotic cells. It was observed that cisplatin 50 and 100 μM associated with 5 nM or 20 nM miR-184 mimic increased the percentage of early apoptotic cells proportionally to the amount of miR-184 mimic used for the treatment. Thus, suggesting an increased effect of miR-184 depending on the concentration at which it is transfected.

Similarly, as displayed in **Figure** 4.16, the percentage of late apoptotic cells broadly increased following miR-184 transfection. Increasing the concentration of miR-184 mimic transfected from 5 nM to 20 nM caused a rise in the population of late apoptotic cells for almost all the cisplatin concentration tested: cells treatment with 20 nM miR-184 mimic associated with 5, 25, 50, 75 and 100 μM cisplatin recorded a higher number of cells undergoing late apoptosis compared to cisplatin only treatments.

Regarding necrotic cells, the overall trend suggests a rise of the number of necrotic cells caused by miR-184 mimic transfection. The addition to cisplatin of either 5 nM or 20 nM miR-184 mimic was responsible for an increase in the percentage of AnnexinV-FITC negative/PI positive cells, with only the exceptions of 5 nM mimic and 10 μM cisplatin treatment (**Figure** 4.17).

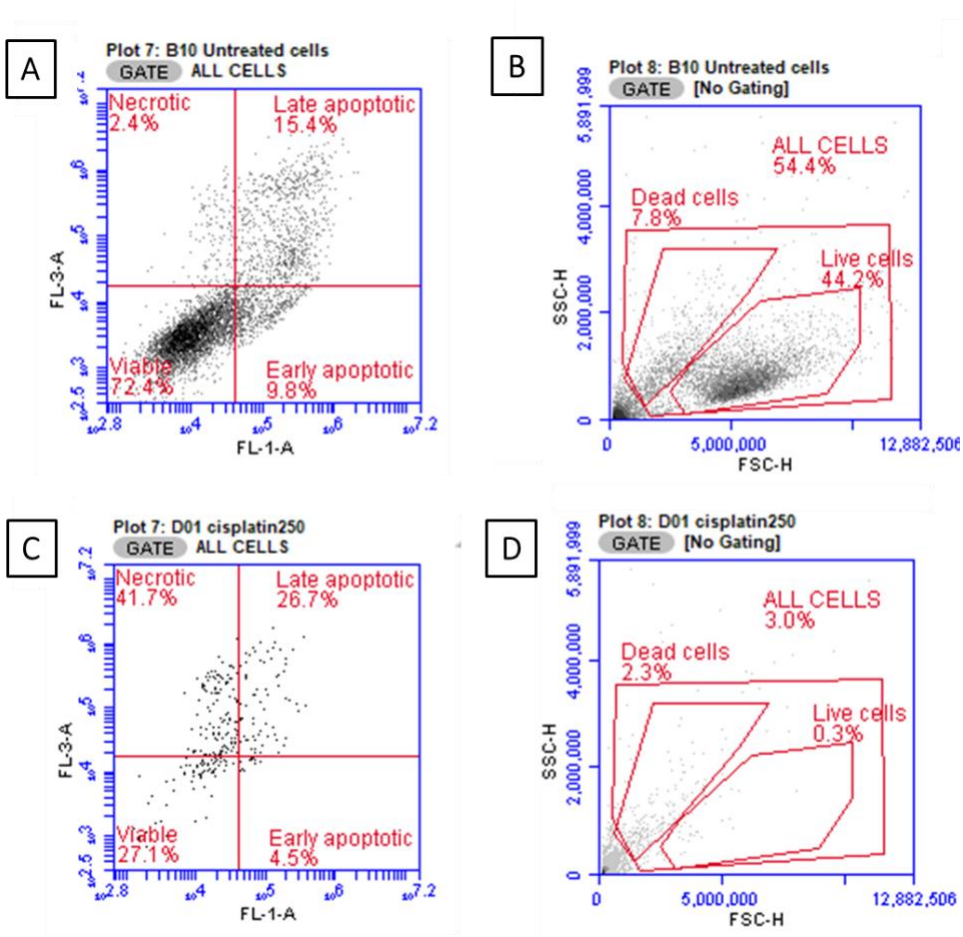

Figure 4.14 Flow cytometry raw data of untreated Calu-3 (A and B) and cisplatin 250 µM-treated cells (C and D). The graph displayed are intended to be explicative and they are representative of the independent experiments carried out (n=4). Results suggest that the lower number of dead cells registered for the cisplatin treatment is due to the lower number of events registered for cisplatin treatments. This is caused by the strong cytotoxicity action of the drug towards the cells.

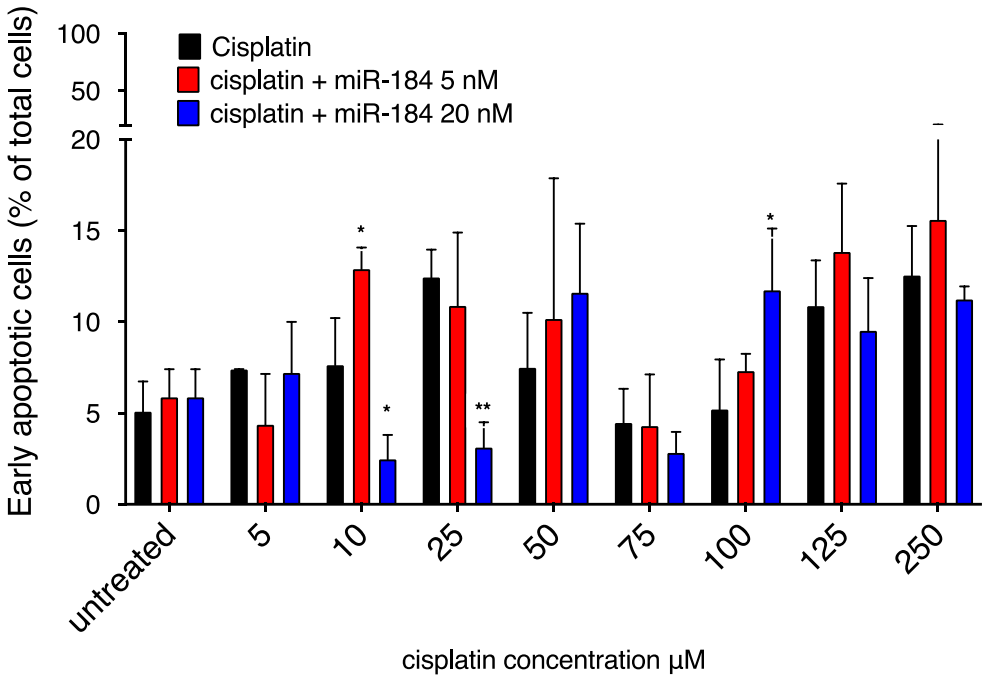

Figure 4.15 Percentage of early apoptotic cells following Calu-3 treatment with cisplatin only or in association with miR-184 mimic. Calu-3 cells were transfected with 5 or 20 nM miR-184 mimic and subsequently treated with cisplatin (0 to 250 µM). The statistical analysis performed was a one-way ANOVA with Dunnet's post-test, comparing in each group for cisplatin only treatments with 5 nM or 20 nM miR-184 mimic in association with the same concentration of cisplatin (n=4, mean ± SD; ** p<0.01; * p,0.05).

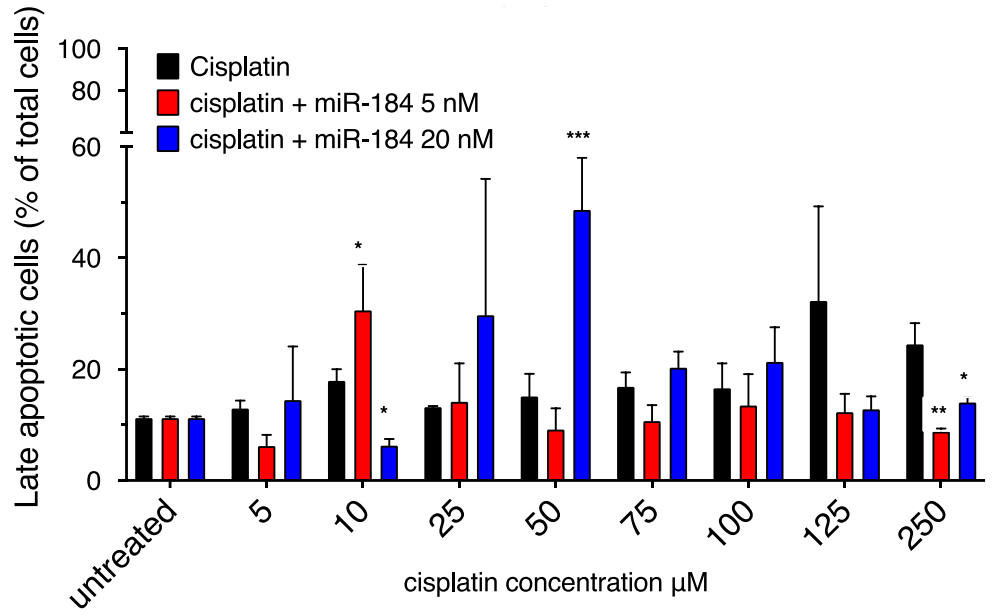

Figure 4.16 Percentage of late apoptotic cells following Calu-3 treatment with cisplatin only or in association with miR-184 mimic. Calu-3 cells were transfected with 5 or 20 nM miR-184 mimic and subsequently treated with cisplatin (0 to 250 µM). The statistical analysis performed was a one-way ANOVA with Dunnet's post-test, comparing in each group for cisplatin only treatments with 5 nM or 20 nM miR-184 mimic in association with the same concentration of cisplatin (n=4, mean ± SD, *** p<0.001; ** p<0.01; * p,0.05).

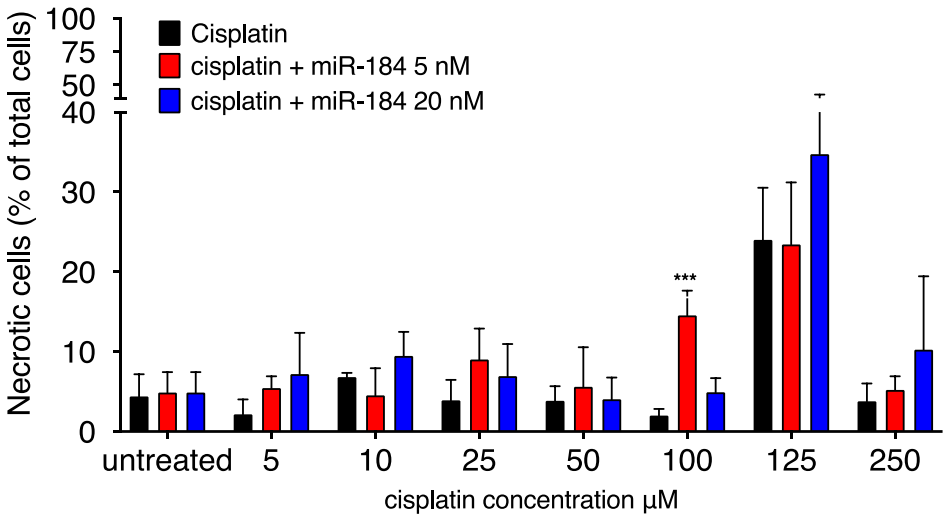

Figure 4.17 Percentage of necrotic cells following Calu-3 treatment with cisplatin only or in association with miR-184 mimic. Calu-3 cells were transfected with 5 or 20 nM miR-184 mimic and subsequently treated with cisplatin (0 to 250 µM). The statistical analysis performed was a one-way ANOVA with Dunnet's post-test, comparing in each group for cisplatin only treatments with 5 nM or 20 nM miR-184 mimic in association with the same concentration of cisplatin (n=4, mean ± SD, *** p<0.001).

4.4.4 Effect of miR-184 inhibitor on cisplatin-induced apoptosis

Flow cytometry was also employed to investigate the effect of miR-184 inhibition on cisplatin-induced cytotoxicity.

As shown in **Figure** 4.18, the transfection of miR-184 inhibitor and the subsequent treatment with cisplatin showed a rise in the percentage of viable cells for all the concentration tested (5 µM to 250 µM), with the exception of cisplatin 250 µM treatment. The increase was significant for miR-184 inhibitor 5 nM and 20 nM treatment for almost all concentrations tested.

As can be seen in **Figure** 4.19 and **Figure** 4.20**,** the treatment of cells with miR-184 inhibitor caused a decrease in the percentage of early apoptotic and late apoptotic cells, respectively. The drop in the number of apoptotic cells was significant for almost all the concentration tested.

Given that miR-184 inhibitor increased Calu-3 cell viability (**Figure** 4.18), decreased the percentage of apoptotic cells (**Figure** 4.19, **Figure** 4.20) and therefore indicated a reduction in Calu-3 cells sensitivity towards cisplatin, a decrease in the percentage of necrotic cells

following miR-184 inhibition was expected. Contrarily, **Figure** 4.21 shows that the transfection of miR-184 inhibitor in association with the cisplatin treatment did not cause a decrease in the number of necrotic cells, compared with the cisplatin only treatment (black bars throughout the graphs). As explained above (**Figure** 4.14 and section **4.4.3**) the increased percentage of necrotic cells following miR-184 inhibitor transfection could be attributed to the general increase in cell viability, and hence in the number of events recorded for the samples in which miR-184 expression was inhibited. As an example, **Figure** 4.22 shows scatter plots for cisplatin only treatment (A) and for cisplatin in association with miR-184 inhibitor (B). As it can be seen from the diagrams, the number of events recorded for the cisplatin only treatment is much lower compared to the combination of cisplatin and miR-184 inhibitor. Thus, meaning that the overall number of cells detected is higher in the mR-184 inhibitor treatment. Therefore, the increase in the number of necrotic cells due to the miR-184 treatment can be ascribed to the overall increased number of cells registered after miR-184 inhibitor transfection.

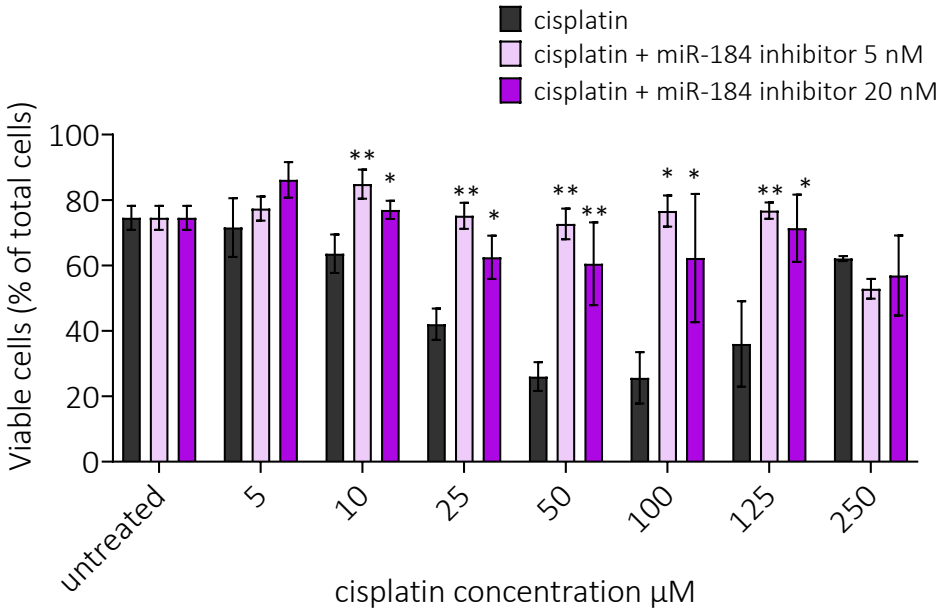

Figure 4.18 Percentage of viable cells following Calu-3 treatment with cisplatin only or in association with miR-184 inhibitor. Calu-3 cells were transfected with 5 or 20 nM miR-184 inhibitor and subsequently treated with cisplatin (0 to 250 µM). The statistical analysis performed was a one-way ANOVA with Dunnet's post-test, comparing in each group for cisplatin only treatments with 5 nM or 20 nM miR-184 inhibitor in association with the same concentration of cisplatin (n=3, mean ± SD; * p<0.05, ** p<0.01).

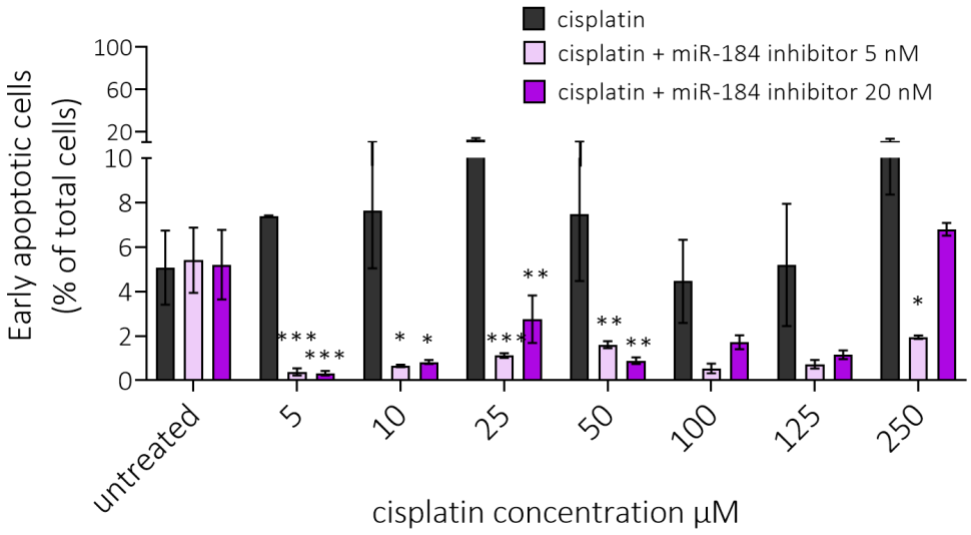

Figure 4.19 Percentage of early apoptotic cells following Calu-3 treatment with cisplatin only or in association with miR-184 inhibitor. Calu-3 cells were transfected with 5 or 20 nM miR-184 inhibitor and subsequently treated with cisplatin (0 to 250 µM). The statistical analysis performed was a one-way ANOVA with Dunnet's post-test, comparing in each group for cisplatin only treatments with 5 nM or 20 nM miR-184 inhibitor in association with the same concentration of cisplatin (n=3, mean ± SD; *** p<0.001; ** p<0.01; * p<0.05).

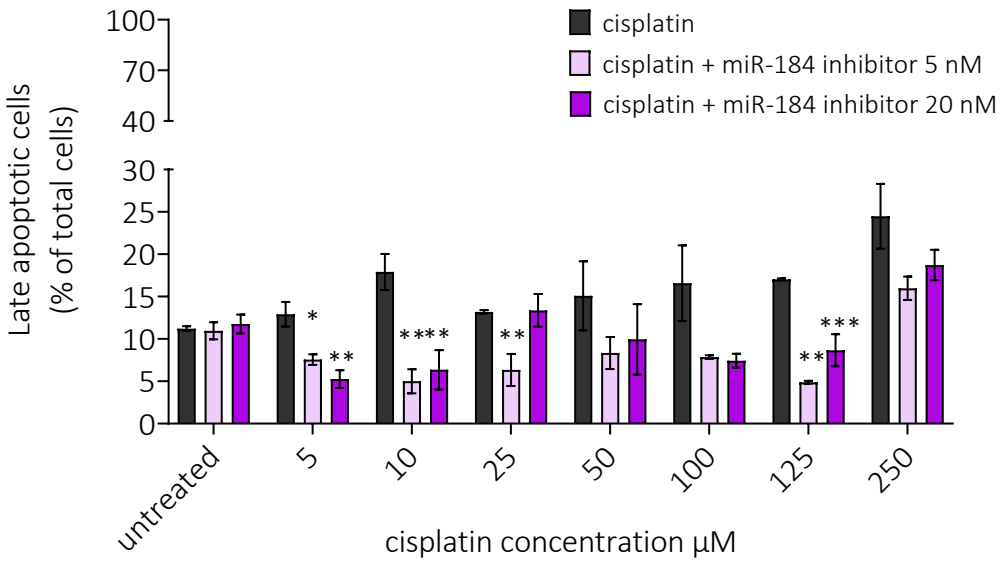

Figure 4.20 Percentage of late apoptotic cells following Calu-3 treatment with cisplatin only or in association with miR-184 inhibitor. Calu-3 cells were transfected with 5 or 20 nM miR-184 inhibitor and subsequently treated with cisplatin (0 to 250 µM). The statistical analysis performed was a one-way ANOVA with Dunnet's post-test, comparing in each group for cisplatin only treatments with 5 nM or 20 nM miR-184 inhibitor in association with the same concentration of cisplatin (n=3, mean ± SD, *** p<0.001; ** p<0.01; * p<0.05).

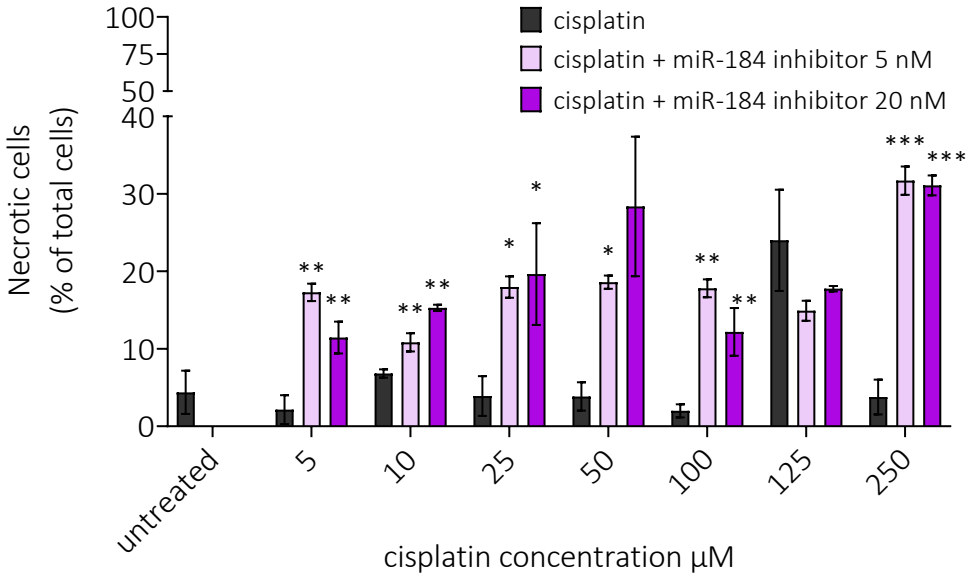

Figure 4.21 Percentage of necrotic cells following Calu-3 treatment with cisplatin only or in association with miR-184 inhibitor. Calu-3 cells were transfected with 5 or 20 nM miR-184 inhibitor and subsequently treated with cisplatin (0 to 250 µM). The statistical analysis performed was a one-way ANOVA with Dunnet's post-test, comparing in each group for cisplatin only treatments with 5 nM or 20 nM miR-184 inhibitor in association with the same concentration of cisplatin (n=3, mean ± SD, *** p<0.001; ** p<0.01; * p<0.05).

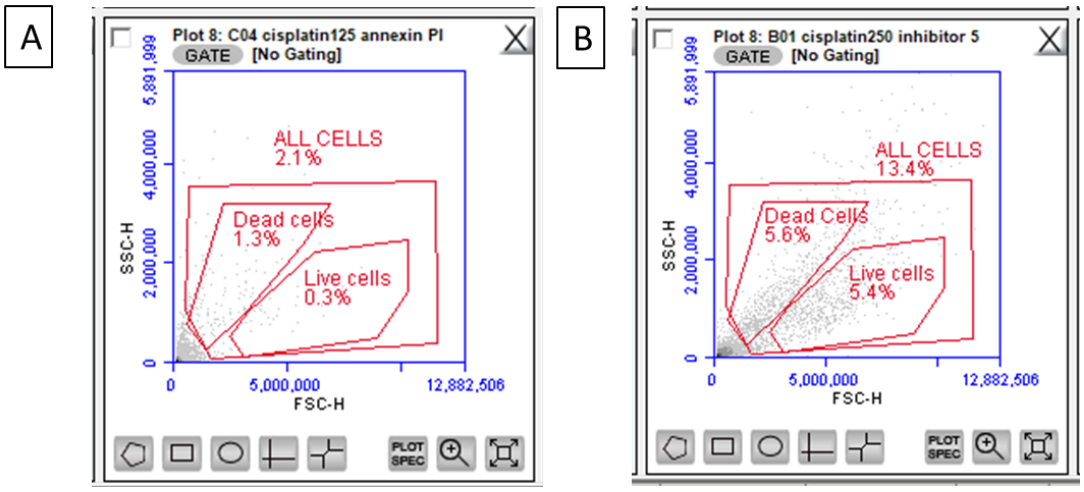

Figure 4.22 Flow cytometry raw data of Calu-3 cells treated with cisplatin only (250 µM) and cisplatin in association with miR-184 inhibitor (5 nM). The graph displayed are intended to be explicative and they are representative of the independent experiments carried out (n=3). Results suggest that the higher number of dead cells registered for the cisplatin treatment is due to the higher number of events registered for cisplatin and miR-184 inhibitor treatments. This would be due to the increased in cell proliferation caused by miR-184 inhibition.

4.5 Discussion

4.5.1 Cisplatin Sensitivity of Calu-3 and Calu-6 cells

The aim of this study was to outline the role of miR-184 in cisplatin sensitivity of NSCLC cells.

Prior studies revealed that Calu-3 cells were less sensitive to cisplatin compared to Calu-6 (Alnefaie, 2020). For this reason, the two cell lines were initially selected to compare their sensitivity to cisplatin. However, our previous studies revealed that their expression of miR-184 was similar (sections 3.4.5 and 3.5.4) and therefore as observed by previous studies, so their sensitivity to cisplatin should be (Longqiu et al., 2020; Tung et al., 2016). Thus, prior to assessing miR-184 mimic ability to enhance cisplatin sensitivity, given that cell lines can considerably evolve and change their genetic, epigenetic and phenotypic characteristics when they are handled in different laboratories following different protocols (Mi et al., 2019), cisplatin IC50 of Calu-3 and Calu-6 was investigated.

Unsurprisingly, IC50 values were different than that identified by the previous study conducted on the same cell line: Alnefaie studies reported cisplatin IC50 to be 7.1 µM for Calu-3 and 1.1 µM for Calu-6 (Alnefaie, 2020). In this study, cisplatin IC50 calculated after 24 h of cell exposure to cisplatin was 154.73 ± 63.65 µM for Calu-3 and 175.49 ± 1.28 µM for Calu-6, while values of 14.35 ± 1.28 and of 17.28 ± 3.74 µM resulted following 48 h exposure (Table 4.2). Therefore, the sensitivity towards cisplatin of the two cell lines was very similar.

It needs to be mentioned that prior to assessing cisplatin IC50, a mock treatment was performed to investigate the cytotoxicity linked to the solvent in which cisplatin was dissolved. Cisplatin was dissolved in DMF given that it was not soluble in NaCl as suggested by manufacturer instructions (*Cis-Diammineplatinum(II) Dichloride Product Number P4394, accessed 21 Apr 19*) and its solubilisation in DMSO was previously reported in literature to confer cisplatin a lack in its activity (Hall et al., 2014). The Alamar Blue assay revealed that when employing cisplatin concentration higher than 250 µM, the cytotoxicity witnessed would have not been linked to cisplatin, but to DMF. Therefore, any working concentration of cisplatin higher than 250 µM was not employed in this study.

4.5.2 Shift of cisplatin dose-response curve following miR-184 mimic and inhibitor transfection

The downregulation of miR-184 in lung cancer has been reported and linked to unfavourable response to cisplatin in lung cancer (Longqiu et al., 2020; Tung et al., 2016). Therefore, the

variation of cisplatin sensitivity in Calu-3 following miR-184 expression modulation was investigated.

The treatment of Calu-3 cells with miR-184 mimic delivered via a commercial transfection reagent, INTERFERin® led to a significant decrease in cisplatin IC50. Results are similar to published studies showing an increase in cell viability associated with miR-184 knockdown in lung cancer cell lines (Lin et al., 2015; Longqiu et al., 2020; Tung et al., 2016b; Zhou et al., 2015).

The correlation between variation in cisplatin IC50 and miR-184 expression was already assessed in lung cancer in TL-1 cells (Tung et al., 2016) and in the cisplatin-resistant H1299 cells (Longqiu et al., 2020). Similar to our findings, in both the cited studies the over-expression of miR-184 was responsible for the decrease in the IC50 value of cisplatin. The study carried out by Tung correlated the enhanced sensitivity to cisplatin to a decrease in the expression of the anti-apoptotic gene BCL-2 (Tung et al., 2016), which was also observed in our study and discussed in Chapter 5.

Interestingly, a decrease in BCL-2 expression was also indicated by Longqiu together with the increase of Bax, a pro-apoptotic gene belonging to the BCL-2 family of proteins (Youle & Strasser, 2008). In addition, as a further evidence of miR-184 promoting apoptosis activation, Longqiu demonstrated the upregulation of cleaved Caspase-3 following miR-184 overexpression: Caspase-3 is known as an executioner caspase in apoptosis because of its role in coordinating the destruction of cellular structures such as DNA fragmentation or degradation of cytoskeletal proteins (McIlwain et al., 2013). Therefore, these findings suggest that the decrease in cisplatin IC50 caused by miR-184 overexpression was due to an increase in the activation of apoptotic pathways, which was also confirmed by our studies (section 4.5.4).

The role played by overexpression of miR-184 in enhancing cisplatin sensitivity was also confirmed by Fang in oral squamous cell carcinoma (OSCC). The upregulation of miR-184 in OSCC cells increased cisplatin cytotoxicity, therefore diminishing cisplatin IC50 (Fang et al., 2017). Interestingly, similarly to the outcomes of Tung and Longqiu, Fang reported that miR-184 overexpression promoted cisplatin cytotoxicity via upregulating caspase-3 and Bax, and suppressing BCL2 expression. Therefore, results from literature confirmed our findings about miR-184 overexpression enhancing cisplatin cytotoxicity.

In addition, our results were supported by the variation in IC50 of cisplatin following transfection of miR-184 inhibitor. This revealed the opposite trend compared to miR-184 mimic treatment: transfection of miR-184 inhibitor led to an increase in the IC50 value of cisplatin (Table 4.4), thus further confirming the involvement of miR-184 in promoting cisplatin cytotoxicity in Calu-3 cells. Moreover, even though the knockdown of miR-184 following miR-184 inhibitor transfection was not detectable through q-PCR as discussed in Chapter 3 (section 3.5.5), miR-184 inhibitor reduced cisplatin sensitivity. In addition, the variation was proportional to the concentration of miR-184 inhibitor used, given that the IC50 of cisplatin increased as the amount of miR-184 inhibitor used for the treatment increased. Therefore, results can additionally be used as a further proof of miR-184 inhibition caused by miR-184 inhibitor treatment.

Taken together, IC50 values obtained following cisplatin treatment and transfection of miR-184 mimic or inhibitor, underline the involvement of miR-184 in modulating cisplatin sensitivity in Calu-3 cells via enhancing apoptosis pathways activation. Thereby, our findings suggest that miR-184 mimic sensitises NSCLC cells to cisplatin.

4.5.3 Shift of cisplatin dose-response curve following miR-184 loaded CS HCl NPs treatment

Given the promising decrease in cisplatin IC50 in Calu-3 cells as a consequence of the transfection of miR-184 mimic (section 4.4.1.2), the effect on cisplatin IC50 following miR-184 delivery via CS HCl NPs was investigated. A significant increase in cisplatin IC50 for cells treated with CS HCl NPs was observed, which increased proportionally to the concentration of miR-184 delivered. This suggested that miR-184 mimic-loaded CS HCl NPs enhanced cisplatin resistance in Calu-3 cells, in contrast with our findings revealing instead that the transfection of miR-184 mimic sensitised cells to cisplatin (section 4.4.1.2).

One explanation for these observations is the possibility of chitosan to interfere with the experimental procedure employed to assess cytotoxicity. The Alamar Blue assay employed to generate dose-response curves is based on the reduction of resazurin (blue, low fluorescent) into its oxidised form, resorufin (pink, highly fluorescent at Ex 530, Em 590). The oxidation reaction happens due to molecules produced by the mitochondrial respiratory chain ($NADH/H^+$ and $NADPH/ H^+$) which can be produced only by metabolically active (and therefore viable) cells (section 2.5.1). However, the reactivity of chitosan and other polymers can be responsible for the occurrence of unintended effects when interacting with biological

materials (Grainger & Castner, 2008). CS HCl has an elevated number of functional group available to react with other molecules such as the protonated amine group (NH_3^+) the chloride ion (Cl^-) and the hydroxide group (OH^-). The NH_3^+, as a hydrogen rich group, can be responsible of reducing resazurin into resorufin and therefore providing a high fluorescent signal. Therefore, the signal detected would be due to the reduction of resazurin induced by chitosan and not by the increase in the amount of viable (or metabolically active) cells in the sample. The reduction of resazurin by tertiary amines was also reported by Bueno (Bueno et al., 2002). Their study proved that tertiary amines catalyse the N–O bond cleavage of the N-oxide ring on the resazurin molecule, giving resorufin. Further, the interference of resazurin with silver NPs, (Mello et al., 2020), carbon nanotubes (Breznan et al., 2015) and cyclodextrins (Csepregi et al., 2018) has already been reported in literature.

The possible interference of blank CS HCl NPs and NTC-loaded CS HCl NPs with the Alamar Blue assay was investigated. Cell treatment with cisplatin in association with Blank CS HCl NPs or NTC-loaded CS HCl NPs caused an increase in cisplatin IC50 comparable to the one witnessed for miR-184-loaded NPs and cisplatin treatment, thus suggesting a potential interaction between the polymer and the assay employed to assess the IC50. In addition, as a further confirmation that the polymer interfered with the assay was carried out employing cells treated with CS HCl at increasing concentrations. Results further confirmed the interference of the polymer with the Alamar Blue, as the fluorescence registered for the CS HCl treated samples was higher than the one registered for untreated cells (**Figure** 4.12).

An investigation of CHT NPs interference was carried out by Jesus in a case study employing CHT NPs prepared with CHT having different degree of deacetylation and employed to assess their immunogenicity (Jesus et al., 2020). In contrast with our findings, their result suggested no interference of the NPs with cell viability of RW 24.6 cells. However, it needs to be mentioned that the method used to assess cell cytotoxicity was different than the one employed in this study and based on absorbance and not on fluorescence.

In conclusion, it is possible that the increase in cisplatin IC50 observed following CS HCl NPs treatments was due to the interference of the polymer with the assay employed to measure cytotoxicity.

4.5.4 Effect of miR-184 mimic and inhibitor on cisplatin-induced apoptosis

To further understand the mechanism through which miR-184 promoted cisplatin cytotoxicity, AnnexinV-FITC/PI staining via Flow cytometry was performed. Our study reported an overall increase in the percentage of early and late apoptotic cells following miR-184 mimic transfection.

Published studies demonstrating that the overexpression of miR-184 mimic sensitises NSCLC cells to cisplatin were carried out by Tung and Longqiu. Their finding suggested that the upregulation of miR-184 enhanced the sensitivity of NSCLC cells (TL-1 for the former and H1299 for the latter) towards cisplatin. The enhanced sensitivity was attributed by both the studies to an increase in the apoptotic rate of cells presenting higher levels of miR-184 (Longqiu et al., 2020; Tung et al., 2016).

The general outcomes from this work are similar to the published studies (Longqiu et al., 2020; Tung et al., 2016), even though the increase was not significant for some of the concentration tested. As discussed above (section 4.5.2), Tung et Longqiu both explained the enhanced cytotoxicity of cisplatin with the increase in the expression of the pro-apoptotic gene BCL-2. In addition Longqiu linked the upregulation of miR-184 with the increased expression of the pro-apoptotic genes Bax and Caspase-3 (Longqiu et al., 2020; Tung et al., 2016b). Similarly, our results discussed in Chapter 5 confirmed the upregulation of BCL-2 protein expression in Calu-3 (chapter 5), thus underlining the involvement of miR-184 in activating apoptotic pathways.

In addition, the increased percentage of apoptotic cells following miR-184 overexpression was observed by Fang in OSCC cells. Similarly to Tung and Longqiu, the behaviour was defended via the increase in Bax and Caspase-3, and the decrease in BCL-2 expression. Therefore, the findings of the current study can be considered aligned to the observation found in literature regarding the link between overexpression of miR-184 and the increase in cisplatin cytotoxicity in NSCLC cells via interaction with apoptosis pathways.

Further, our study observed a variation in the percentage of viable and necrotic cells following miR-184 upregulation. Regarding the population of viable cells, the overall trend for 20 nM miR-184 treatments suggested a decrease in cell viability, while no variation was reported for the 5 nM miR-184 treatment. This might suggest that a higher concentration of miR-184 mimic is needed to reach an outcome detectable with the Flow cytometry AnnexinV-PI/FITC staining. On the other hand, for all concentrations of cisplatin tested the percentage of necrotic cells increased when Calu-3 cells were transfected with miR-184 mimic. Even though the studies

by Tung, Longqiu and Fang reported that miR-184 enhanced cisplatin cytotoxicity primarily through apoptosis (Fang et al., 2017; Longqiu et al., 2020; Tung et al., 2016), our findings suggest an additional increase in the number of necrotic cells following combined cisplatin and miR-184 treatment. This aligns with observations that at certain concentrations of cisplatin, necrosis becomes the principal mechanism through which cisplatin causes cell death via reducing the activation of effector caspases such as Caspase -3 and Capase-9 (Ferrer et al., 2003; Sancho-Martínez et al., 2011; Shibuya et al., 2003). Moreover, Xu demonstrated that necroptosis was directly associated with cisplatin cytotoxicity in renal tubular cells (Yanfang Xu et al., 2015, 2017) and Liu reported an increase in apoptosis and necroptosis following berberine and cisplatin treatment in ovarian cancer cells (Li Liu et al., 2019; Yanfang Xu et al., 2015).

The outcomes from the miR-184 mimic treatment, suggesting miR-184 mimic enhanced cisplatin sensitivity via apoptosis pathways, were also reinforced by results obtained following miR-184 inhibitor transfection. Indeed, overall results obtained from miR-184 inhibitor treatment were opposite to the one obtained following miR-184 mimic transfection.

The transfection of Calu-3 cells with miR-184 inhibitor increased the percentage of viable cells compared to cisplatin only treatment. Therefore, these results are corroborating our thesis regarding miR-184 role in promoting apoptosis. Moreover, the increase in the percentage of viable cells following miR-184 inhibitor treatment is in line with IC50 results discussed above (section 4.5.2), thus together they underline that the knockdown of miR-184 decreased cisplatin sensitivity.

Similar findings were observed by other researchers (Lin et al., 2015; Zhen Liu et al., 2014; Zhou et al., 2015). The study carried out by Lin correlated the increased cytotoxicity of A549 cells presenting low mIR-184 levels with the increased expression of c-myc. Similarly, Liu linked the decrease in cell proliferation caused by miR-184 over-expression to c-myc downregulation. In addition, their findings were also confirmed *in vivo*, showing that tumorigenesis was remarkably reduced in mice injected with A549 and overexpressing miR-184. Given c-myc involvement in carcinogenesis and in particular in NSCLC as highlighted by the above studies, the expression of c-myc was object of this thesis and is discussed in chapter 5.

Moreover, Figure 4.19 and Figure 4.20 show that the inhibition of miR-184 decreased significantly the percentage of early and late apoptotic cells compared to cisplatin only

treatment. The study carried out by Fang in OSCC revealed a similar outcome. The study showed that cells in which miR-184 was downregulated registered a 20% lower percentage of apoptotic cells compared to cells overexpressing miR-184. The modulation of apoptosis was attributed by Fang to Bax, BCL-2, Caspase-3 and SF1 modulation as explained above (Fang et al., 2017).

In addition, researchers agree that the main mechanisms of action of cisplatin consists in causing DNA damages, creating DNA-cisplatin adducts that trigger the activation of cascade of events culminating in the activation of intrinsic apoptotic pathways (section 1.1.2). Therefore, the decrease in the percentage of apoptotic cells following miR-184 inhibitor treatment, suggest the partial loss of function of cisplatin. Given that the decrease in cisplatin activity was subsequent to miR-184 inhibitor treatment, it can be deducted that the knockdown of miR-184 desensitise Calu-3 cells to cisplatin.

In conclusion, following the analysis of Calu-3 behaviour following exposure to cisplatin and miR-184 mimic or inhibitor, our results suggest that miR-184 sensitise Calu-3 cells to cisplatin via promoting the activation of apoptosis and necrotic pathways. However, future works would be needed to further confirm these initial outcomes (section 6.2.4).

4.6 Conclusion

In conclusion, after showing that Calu-3 and Calu-6 cells did not have a different sensibility towards cisplatin, the effect of miR-184 modulation in Calu-3 cells was investigated. The sensitivity of cells towards cisplatin was assessed in the presence of miR-184 mimic or inhibitor, and the resulted IC50 values revealed a decrease in cell proliferation and therefore in cisplatin IC50 following miR-184 mimic transfection. On the other hand, the transfection with miR-184 inhibitor led to an increase in cell proliferation and to a decrease in cisplatin IC50. Given the ability of miR-184 mimic to increase Calu-3 cells sensitivity towards cisplatin, the possibility of delivering miR-184 into Calu-3 cells via CS HCl NPs was investigated. However, an increase in cisplatin IC50 was observed following delivery of the oligonucleotide via CS HCl NPs. This might have been due to interference of chitosan with the Alamar Blue assay given the increase in IC50 noticed after delivery of Blank NPs and NTC-NPs.

In addition, the effect of miR-184 on apoptosis and necrosis was investigated via AnnexinV-FITC/PI staining. Results from the modulation of miR-184 expression (via miR.184 mimic or

inhibitor) suggested that miR-184 enhances cisplatin sensitivity in Calu-3 cells via necrosis and apoptosis.

Altogether, the results from this study suggest that transfection of miR-184 mimic in Calu-3 cells promotes cisplatin-induced cytotoxicity. However, further assessment are needed to confirm that miR-184 mimic-loaded CS HCl NPs can confer a similar enhancement cisplatin cytotoxicity.

5 Effect of MicroRNA-184 on the modulation of MicroRNA-184 targets in Calu-3 cells

5.1 Introduction

MicroRNAs are non-coding RNAs that play an essential role in gene expression. Given their regulatory activity, miRNAs are critical for animal and human development and are involved in a variety of biological processes. Furthermore, aberrant expression of miRNAs is associated with many human diseases (Paul et al., 2018). The crucial step of miRNA protein expression regulation is the binding between the so-called miRNA "seed" region with the target mRNA 3′ UTR region via Watson-Crick base pairing (Bartel, 2009) (section 1.2.1). Consequently, miRNA-mRNA binding is able to mediate the degradation of the target mRNAs (Decker & Parker, 2012; Eichhorn et al., 2014; Winter et al., 2009) (section 1.2.1). In addition, miRNAs can bind to multiple mRNA targets and therefore control multiple intracellular pathways or multiple steps within the same pathway (Rinck et al., 2013; Seok et al., 2016).

Previous studies (Chapter 4) suggested that miR-184 sensitises Calu-3 cells to cisplatin, promoting cell death. This was also observed in other NSCLC cell lines (Longqiu et al., 2020; Tung et al., 2016b). However, the mechanism through which miR-184 exerts such action is still not fully understood. Several genes involved in apoptosis, such as BCL-2 and BAX have been shown to be targets of miR-184 in breast cancer and nasopharyngeal carcinoma (Jinjun Wang, 2021; Zhen et al., 2013a) and lung cancer (Longqiu et al., 2020; Tung et al., 2016b). In addition, miR-184 was discovered to target genes involved in cell metabolism, inflammation and cell cycle control in cancer malignancies, which are summarised in Table 5.1. Those include: i) c-myc (Lin et al., 2015; Liu et al., 2014), that control several aspects of cellular growth and metabolism, via targeting genes involved in numerous cellular functions; ii) TNFAIP2, which is the primary protein induced by tumour necrosis factor alpha (TNFα), that plays multiple roles in cell proliferation, migration, angiogenesis and inflammation (Cheng et al., 2015; Zhensheng Liu et al., 2011; Yu Xu et al., 2013); iii) AKT-2, that is involved in carcinogenesis via modulating the phosphatidylinositol 3-kinase (PI3K) pathway, a pro-survival pathway in cancer (Foley, Bray, Tivnan, Bryan, Murphy, Buckley, Ryan, O'meara, et al., 2010).

Given our observations from Chapter 4 suggesting miR-184 role in enhancing cisplatin resistance, in this chapter the expression of the above miR-184 targets was investigated. The modulation of mRNA and protein expression in the presence of miR-184 mimic or inhibitor

would provide a further understanding of the role played by miR-184 within molecular pathways in Calu-3 cells.

Table 5.1 Summary of the genes investigates in this study as potential miR-184 targets in Calu-3.

	PROTEIN ROLE	MIR-184 TARGET IN CANCER TYPES	EXPRESSION IN CANCER
BCL-2	Inhibit Apoptosis	• breast cancer (Wang, 2021), • oral squamous cell carcinoma (Fang et al., 2017),, • pancreatic ductal adenocarcinoma (Li et al., 2020), colon cancer (Wang et al., 2018) • NSCLC	Upregulated
C-MYC	Controls cellular growth and metabolism	• clear-renal cell carcinoma (J. Huang et al., 2016b), • pancreatic ductal adenocarcinoma (S. Li et al., 2020), • nasopharyngeal carcinoma (Zhen et al., 2013) prostate cancer (Xia et al., 2015) • NSCLC (Lin et al., 2015; Liu et al., 2014).	Upregulated
TNFAIP2	Involved in cell proliferation, migration, angiogenesis	• squamous cell carcinoma of head and neck (Zhensheng Liu et al., 2011), • gastric cancer (Yu Xu et al., 2013) • glioma (Cheng et al., 2015)	Upregulated
AKT-2	Enhances cell survival in cancer	• neuroblastoma (Foley, Bray, Tivnan, Bryan, Murphy, Buckley, Ryan, O'meara, et al., 2010)	Upregulated

5.2 Aim and Objectives

The aim of the current study was to better understand the cell proliferation pathways in which miR-184 is involved, and therefore to investigate the expression of potential miR-184 targets following the modulation of miR-184 expression. The aim was reached through the following objectives:

- Evaluation of BCL-2 mRNA and protein expression
- Assessment of c-myc-2 mRNA expression
- Evaluation of TNFAIP-2 mRNA expression
- Investigation of AKT-2 mRNA expression

5.3 Methods

5.3.1 mRNA Expression Evaluation

Cells were treated with miR-184 mimic-loaded CS HCl NPs or transfected with miR-184 inhibitor via INTERFERin®. Total RNA was extracted, and RT-qPCR performed employing 40 PCR cycles for each experiment (section 2.6). The expression of miR-184 targets relevant to lung cancer were examined, namely BCL-2, c-Myc, TNFAIP2, and AKT-2. Results were normalised using GAPDH as reference gene and blank CS HCl NPs (for miR-184 mimic-loaded CS HCl NPs treatment) or untreated cells (for miR-184 inhibitor transfection) as control treatments.

5.3.2 BCL-2 Protein Expression Evaluation via Western Blot

Cells lysate was processed as outlined in section 2.4.6. Briefly, cells were seeded in a 6-well plate, treated with 20 nM of miR-184-loaded CS HCl NPs, NTC-loaded NPs, blank CS HCl NPs or transfected with 20 nM miR-184 mimic or inhibitor via INTERFERin®. Cells were lysed in RIPA buffer and protein quantified via BCA assay as described in section 2.6.1, SDS-PAGE was performed on a 12% polyacrylamide mini-PROTEAN TGX precast gel (BioRad, Watford, UK) (section 2.7.2) to evaluate for BCL-2 expression by western blotting with rabbit primary monoclonal antibody (AbCam, Ab18285) (section 2.7.3).

5.3.3 Statistical Analysis

Statistical analysis was performed using GraphPad Prism 8.0 statistical software (section 2.9). One-way ANOVA with Dunnett's was used for analysis of all the RT-qPCR data or Tukey's comparison tests were applied in accordance with the experiment carried out and stated throughout the results. All values are expressed as mean ± standard deviation (SD) of a variable number of independent experiments, which is stated throughout. The *P* values are expressed as **P*<0.05, ***P*<0.01, ****P*<0.001, *****P*<0.0001.

5.4 Results

5.4.1 Investigation of BCL-2 expression

The miR-184-loaded CS HCl NPs decreased the expression of BCL-2 mRNA in Calu-3 cells for both 5 nM and at 20 nM treatment: the expression of BCL-2 mRNA was lower in miR-184 mimic-loaded CS HCl NPs samples compared to blank NPs treatments. Specifically, the expression of BCL-2 was 3-fold lower in the 5 nM miR-184-mimic loaded NPs treatment after 48 h, while it was 1-fold lower following treatment with 20 nM NPs (Figure 5.1). On the other hand, the expression of BCL-2 mRNA increased following miR-184 inhibition treatments (Figure 5.2). The rise observed was 0.5-fold for the 5 nM treatment and 2-fold for the 20 nM one compared to untreated cells. Statistical analysis revealed that the increase registered for the 20 nM treatment was significant compared to untreated and NTC-treated samples (Figure 5.2).

The effect of miR-184 mimics and inhibitor on BCL-2 expression at the protein level was also examined. No difference in BCL-2 expression between blank NPs or non-targeting control (NTC)-loaded NPs and miR-184-loaded CS HCl NPs-treated cells was visible. However, the transfection of Calu-3 with miR-184 with INTERFERin® resulted in a small but statistically significant decrease in BCL-2 expression of approximately 10% compared to NTC (Figure 5.3). The expression of BCL-2 protein following miR-184 inhibitor transfection was also examined (Figure 5.3). The quantification of BCL-2 following miR-184 inhibition treatment did not show any statistical variation in BCL-2 expression compared to NTC control treatment.

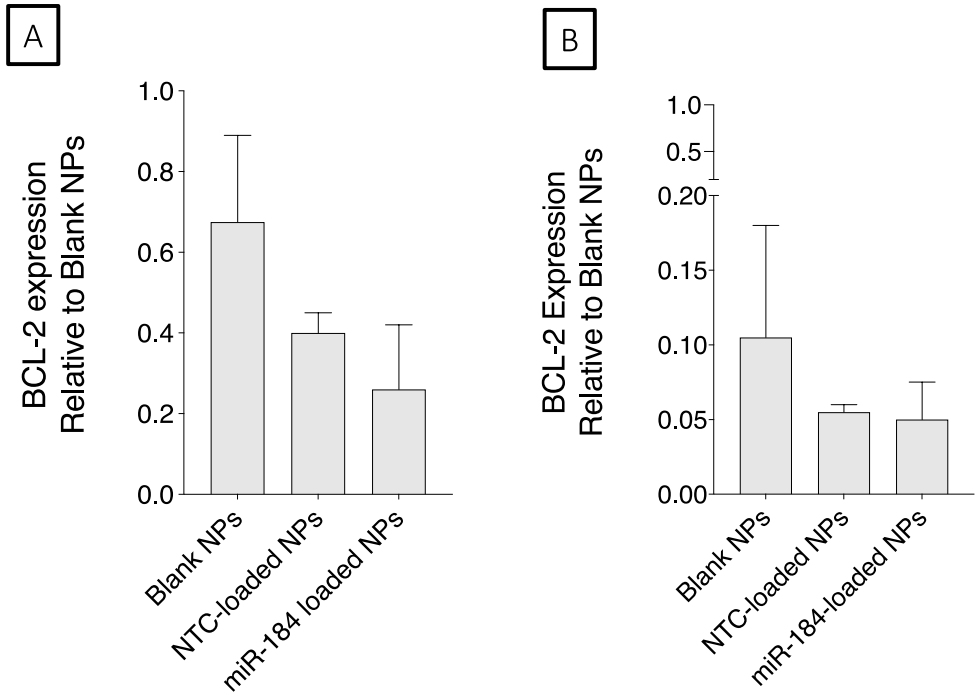

Figure 5.1 BCL-2 expression investigation in Calu-3 cells following treatment with miR-184-loaded CS HCl NPs. Results were normalised to GAPDH and blank NPs used as comparator. One-way ANOVA with Dunnet's post-test was performed. (A) Calu-3 treatment with 5 nM miR-184-loaded CS HCl NPs led to a decrease of BCL-2 mRNA expression. (B) Similatly, the treatment with 20 nM miR-184-loaded CS HCl NPs decreased BCL-2 mRNA expression (n=3, mean ± SD).

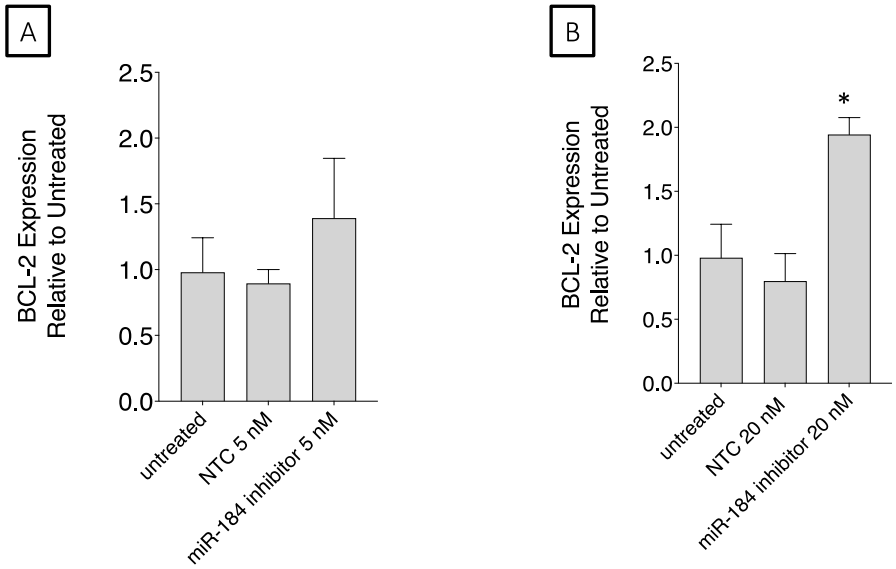

Figure 5.2 BCL-2 expression investigation in Calu-3 cells following treatment with miR-184-inhibitor. Results were normalised to GAPDH and untreated cells used as comparator. One-way ANOVA with Dunnet's post-test was performed. (A) Calu-3 treatment with 5 nM miR-184 inhibitor led to a slight increase in BCL-2 mRNA expression. (B) The treatment with 20 nM miR-184inhibitor led to a significant increase in BCL-2 mRNA expression (n=3, mean ±SD; * p<0.05).

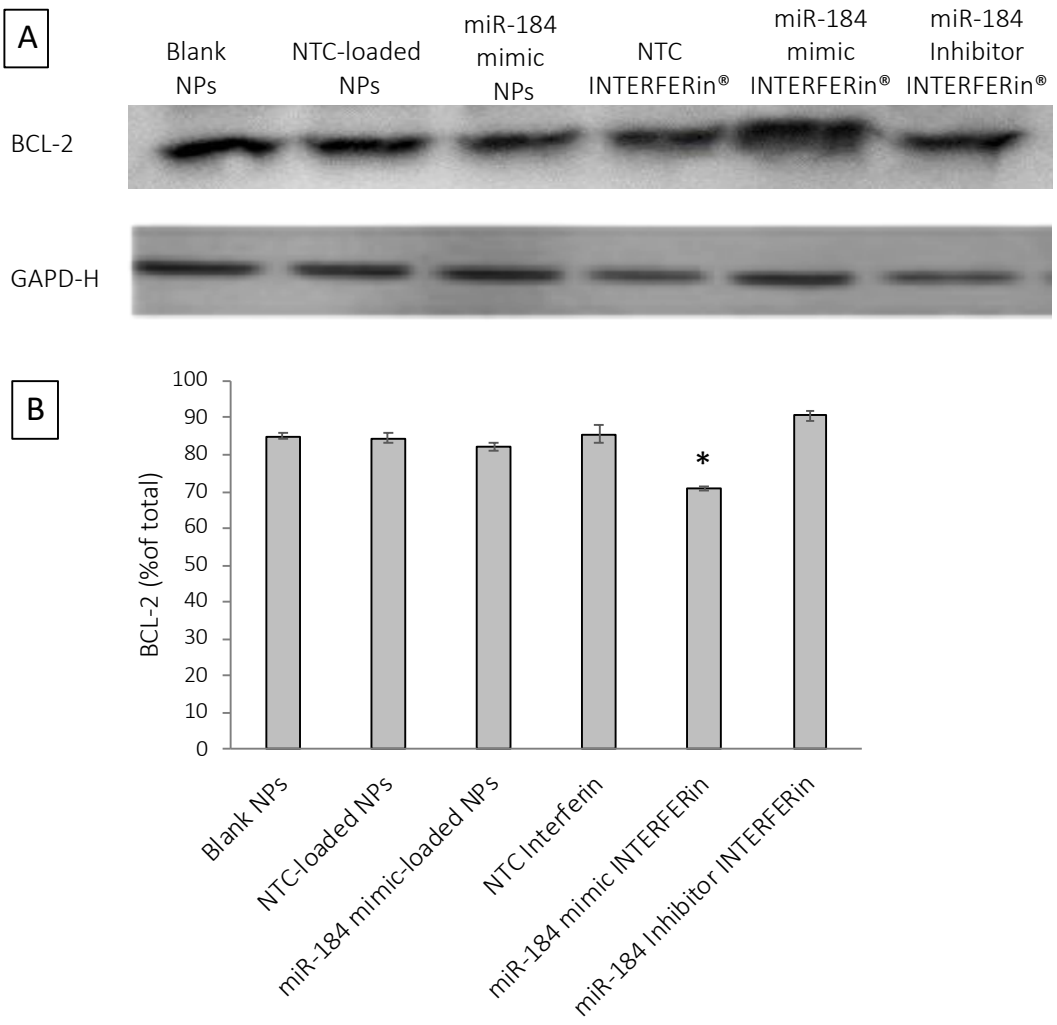

Figure 5.3 investigation of BCL-2 protein expression in Calu-3 following exposure to miR-184 mimic-loaded CS HCl or transfected with miR-184 inhibitor. (A) Calu-3 cells were treated with blank, NTC-loaded or 20 nM miR-184 loaded NPs, or transfected with 20 nM miR-184 mimic, inhibitor or NTC-control via INTERFERin®. Following protein isolation and separation, membrane blocking and separation, Western Blot was performed. (B) Data were normalised to GAPDH and density proportion were calculated from the density of the samples. Delivery of miR-184 mimic via INTERFERin® significantly decreased the expression of BCL-2 protein level in Calu-3 cells (n=2, mean ± SD; * p<0.05).

5.4.2 Investigation of c-myc expression

The investigation of c-myc expression following miR-184-loaded CS HCl NPs or miR-184 inhibitor transfection was carried out. The treatment with 5 nM miR-184-loaded CS HCl NPs treatment increased c-myc expression of almost 2-fold. However, the 20 nM treatment had no effect on the expression of the same target (**Figure** 5.4).

The transfection of miR-184 inhibitor increased in c-myc mRNA expression for both the concentration tested. The rise of mRNA expression was proportional to the concentration of inhibitor used. This was represented in the 3-fold increase for the 5 nM treatment to the 4-fold registered for the 20 nM transfection (**Figure** 5.5).

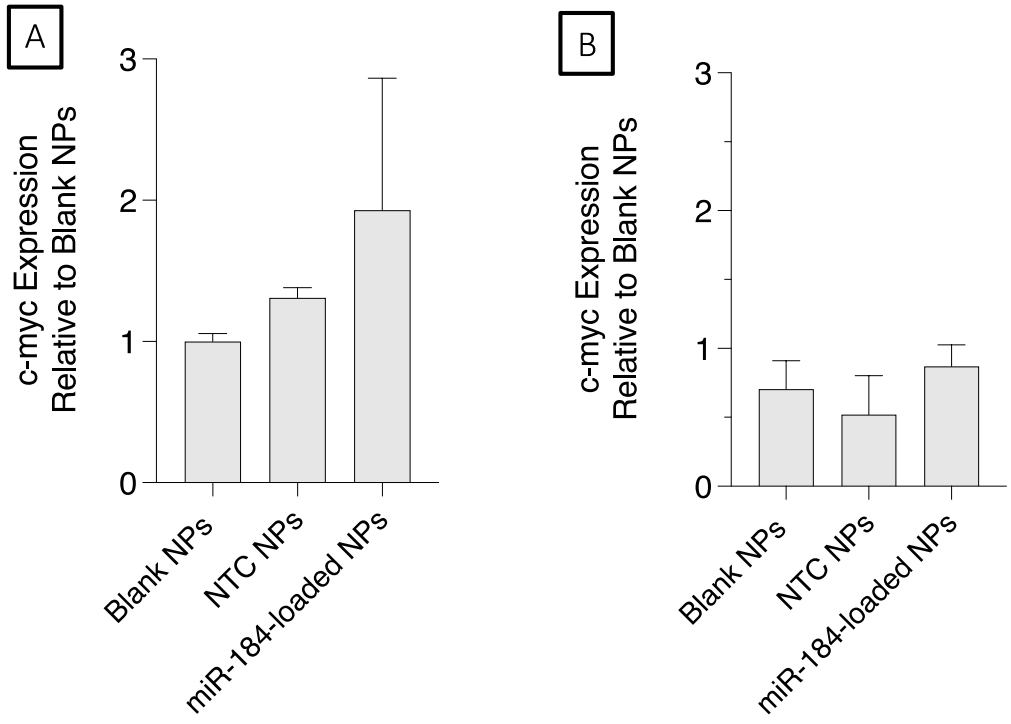

Figure 5.4 Investigation of c-myc expression in Calu-3 following miR-184 mimic-loaded CS HCl NPs. Results were normalised to GAPDH and Blank NPs cells used as comparator. One-way ANOVA with Dunnet's post-test was performed. (A) An increase in c-myc expression was observed for Calu-3 treatment with 5 nM miR-184-loaded CS HCl NPs. (B) The treatment with 20 nM miR-184-loaded CS HCl NPs had no effect on c-myc expression NPs (n=3, mean ± SD).

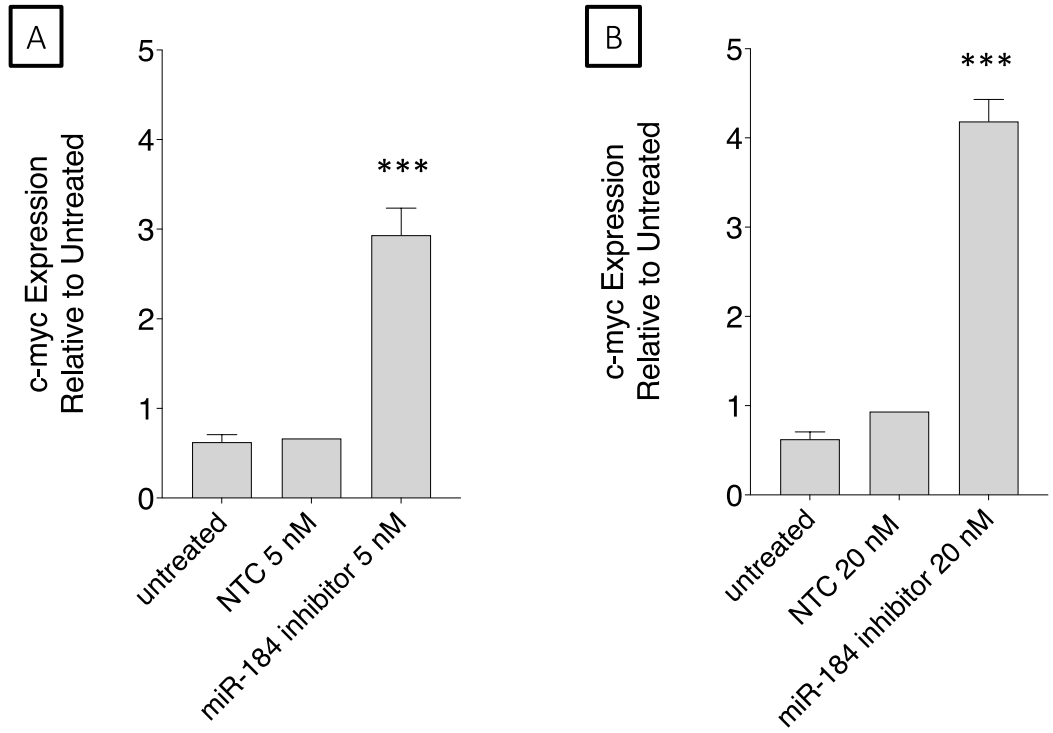

Figure 5.5 Investigation of c-myc expression in Calu-3 following miR-184 inhibitor transfection. Results were normalised to GAPDH and untreated cells used as comparator. One-way ANOVA with Dunnet's post-test was performed (A) A significant increase in c-myc expression was observed for 5 nM miR-184 inhibitor transfection compared to control. (B) Similarly, the 20 nM 184 inhibitor transfection was responsible for a significant increase in c-myc (n=3, mean ± SD; ***p<0.001).

5.4.3 Investigation of TNFAIP-2 expression

The expression of TNFAIP-2 mRNA after miR-184 mimic (delivered via CS HCl NPs) or inhibitor (transfected via INTERFERin®) in Calu-3 cells was investigated (**Figure** 5.6 and **Figure** 5.7).

The expression of TNFAIP-2 increased of 6-fold following the 5 nM miR-184-loaded CS HCl NPs treatment as shown in **Figure** 5.6. In contrast, increasing miR-184-loaded NPs treatment to 20 nM had no effect on the expression of the same target mRNA.

The transfection of 5 nM miR-184 inhibitor led to a 2-fold increase TNFAIP-2 mRNA expression following miR-184 inhibition. The increase was statistically significant compared to both the controls (untreated cells and NTC treatment). On the other hand, the treatment with miR-184 inhibitor 20 nM did not cause any variation in TNFAIP-2 mRNA expression (**Figure** 5.7).

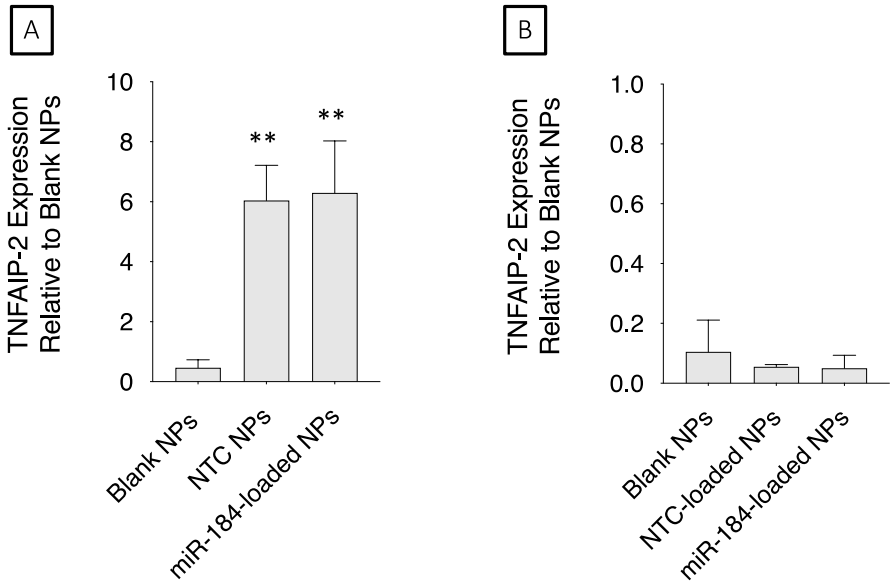

Figure 5.6 TNFAIP-2 expression investigation in Calu-3 cells following treatment with miR-184-loaded CS HCl NPs. Results were normalised to GAPDH and Blank NPs used as comparator. One-way ANOVA with Dunnet's post-test was performed. (A) A significant increase of TNFAIP2 mRNA expression was observed for Calu-3 treatment with 5 nM NTC-loaded or miR-184-loaded CS HCl NPs. (B) The treatment with 20 nM miR-184-loaded CS HCl NPs had no effect on TNFAIP-2 mRNA expression. (n=3, mean ± SD; ** p<0.01).

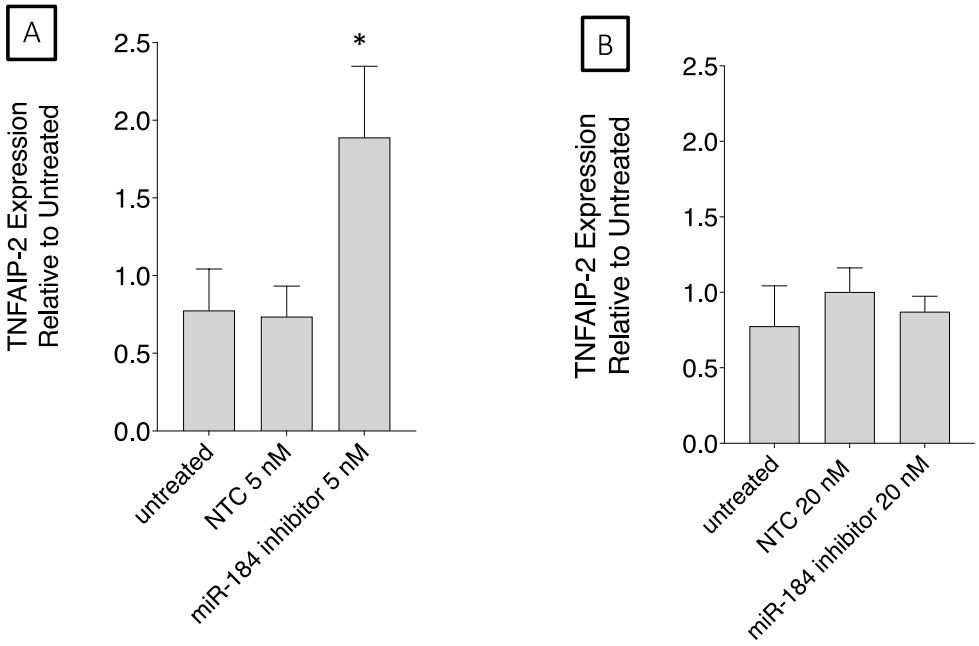

Figure 5.7 Investigation of TNFAIP-2 expression in Calu-3 cells following miR-184 inhibitor transfection. Results were normalised to GAPDH and untreated cells used as comparator. One-way ANOVA with Dunnet's post-test was performed. (A) A significant increase in TNFAIP-2 expression for Calu-3 transfection with 5 nM miR-184 inhibitor was observed. (B) The treatment with 20 nM miR-184 inhibitor did not cause any variation in TNFAIP-2 expression. (n=3, mean ± SD; * p<0.05).

5.4.4 Investigation of AKT-2 expression

An increase in AKT-2 expression of almost 2-fold was registered for the miR-184 mimic-loaded CS HCl NPs 5 nM treatment compared to Blank NPs. Similarly, a rise in AKT-2 expression was reported for the 20 nM treatment. The increase was 5-fold higher compared to NTC-loaded NPs and it was as well statistically significant compared to it (**Figure** 5.8).

The investigation of AKT-2 mRNA expression following miR-184 inhibitor transfection had little effect on AKT-2 expression (**Figure** 5.9). However, the treatment with miR-184 inhibitor 20 nM caused a 0.5-fold decrease in the mRNA expression but, was not statistically significant compared to control.

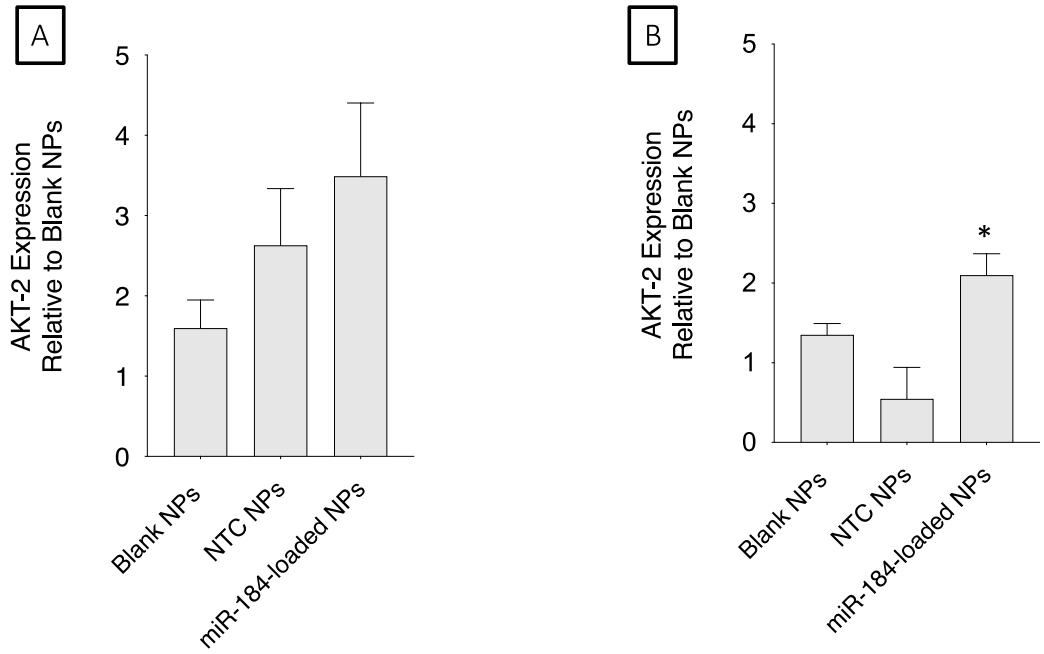

Figure 5.8 Investigation of AKT-2 expression in Calu-3 cells following treatment with miR-184-loaded CS HCl NPs. Results were normalised to GAPDH and Blank NPs used as comparator. One-way ANOVA with Dunnet's post-test was performed (A) A rise of AKT-2 mRNA expression, that was not significant compared to Blank or NTC-loaded NPs, was observed for Calu-3 treatment with 5 nM miR-184-loaded CS HCl NPs. (B) The treatment with 20 nM miR-184-loaded CS HCl NPs increased AKT-2 mRNA expression significantly compared to NTC-loaded NPs, but not to Blank NPs (n=3, mean ± SD; * p<0.05).

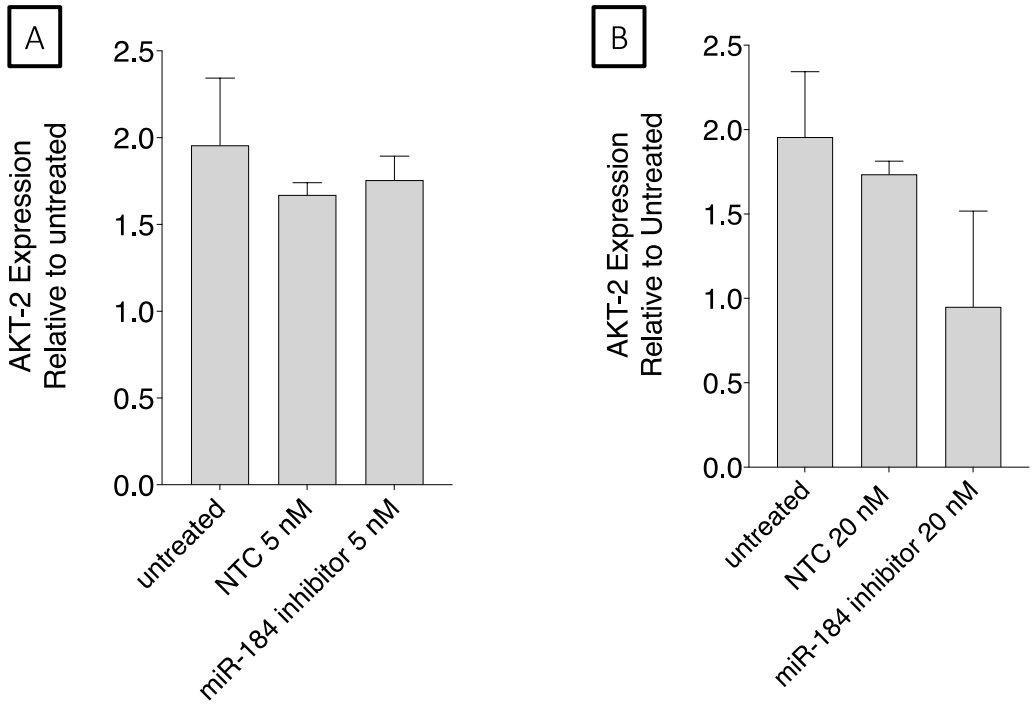

Figure 5.9 Investigation of AKT-2 expression in Calu-3 following miR-184 inhibitor treatment. Results were normalised to GAPDH and untreated cells used as comparator. One-way ANOVA with Dunnet's post-test was performed (A) Calu-3 treatment with 5 nM (A) or 20 nM inhibitor(B) did not impact significantly AKT-2 mRNA expression. Nevertheless, a 1-fold decrease in AKT-2 expression was reported for the treatment with 20 nM miR-184 inhibitor (B) (n=3, mean ± SD).

5.5 Discussion

5.5.1 Investigation of BCL-2 expression

The B-cell lymphoma 2 (BCL-2) family of protein can be divided into three classes: (a) proteins that inhibit apoptosis such as BCL-2 and BCL-XL; (b) proteins that promote apoptosis such as BAX and BAK via initiating the cascade of events culminating in caspase-9 activation and ultimately apoptosis (Youle & Strasser, 2008) (c) proteins such as BAD and BIK, that promote apoptosis via binding protein of group (a) and inhibiting them.

The specific role of the BCL-2 protein (belonging to group a) consists in binding (and inhibiting) the pro-apoptotic proteins of group (b) such as BAX and BAK. For this reason, a decrease in BCL-2 expression results in increased activation of BAX and BAK, thus promoting cell death via apoptosis.

BCL-2 was demonstrated to be a direct target of miR-184 in several types of malignancies. Its upregulation was correlated with increased proliferation of breast cancer (Wang, 2021), oral squamous cell carcinoma (Fang et al., 2017), pancreatic ductal adenocarcinoma (Li et al.,

2020), colon cancer (Wang et al., 2018) and NSCLC (Longqiu et al., 2020; Tung et al., 2016). The downregulation of BCL-2 caused by miR-184 upregulation and its involvement in cisplatin resistance in NSCLC was investigated by Tung (Tung et al., 2016). The increase of miR-184 levels in TL-1 cells obtained via miR-184 mimic transfection, led to a decrease in cisplatin IC50 and to an increase in the apoptotic rate of cells. In addition, miR-184 upregulation caused a marked decrease in BCL-2 protein expression. Therefore the group concluded that miR-184 restored cisplatin sensitivity via targeting and inhibiting BCL-2 (Tung et al., 2016).

Moreover, the study of Longqiu on H1299-CDDP, a NSCLC cell line resistant to cisplatin, revealed that increasing miR-184 expression resulted in a reduction in BCL-2 expression and an increase in BAX protein expression (Longqiu et al., 2020).Similarly to Tung, the upregulation of miR-184 determined a decrease in cell viability and an increase in the percentage of apoptotic cells, that was ultimately linked to BCL-2 targeting by miR-184.

In our study, the slight decrease in BCL-2 expression following miR-184 mimic-loaded CS HCl treatment was not significant compared to controls. This was visible both at the mRNA (**Figure** 5.1) and at protein level (**Figure** 5.3). On the other hand, BCL-2 protein expression decreased when Calu-3 were transfected with miR-184 mimic via INTERFERin®. This difference might be attributable to the NPs not releasing the all of oligonucleotide or only part and therefore not providing the cells with a sufficient amount of miR-184 to reduce BCL-2 expression. The effect of miR-184 inhibitor transfection in BCL-2 expression was also investigated, revealing an increase in BCL-2 mRNA expression (assessed via RT-qPCR) following cells treatment with miR-184 inhibitor (**Figure** 5.2). In accordance with the increase in mRNA levels, an increase in BCL-2 protein expression (assessed via Western Blot) in samples corresponding to miR-184 inhibitor treatment was observed, however this was not significant (**Figure** 5.3).

Therefore, our results from chapter 4 showing that miR-184 mimic sensitises cells to cisplatin can be explained via the decrease in BCL-2. The decrease in BCL-2 expression promoted by miR-184 mimic would clarify the increase of the apoptotic rate observed after miR-184 mimic observed in **sections 4.4.3** and **4.5.4**. In contrast, the increase in BCL-2 expression and decrease in apoptotic rate (**sections 4.4.4** and **4.5.4**) observed following miR-184 inhibition confirms the involvement of BCL-2 in promoting cisplatin resistance in Calu-3 cells. Hence, our findings reveal the miR-184 mimic role in promoting cisplatin resistance through targeting BCL are comparable to Tung and Longqiu studies (Longqiu et al., 2020; Tung et al., 2016).

5.5.2 Investigation of c-myc expression

The c-myc gene controls several aspects of cellular growth and metabolism, via targeting genes involved in numerous cellular functions including cyclin A2 (growth factor responses), LDH-A (glycolysis), p21 (DNA damage response), p15 (TGFB pathway) and integrins (cell adhesion) (Zeller et al., 2003).

Moreover, the expression of c-myc was observed to be regulated by miR-184 in clear-renal cell carcinoma (J. Huang et al., 2016b), pancreatic ductal adenocarcinoma (S. Li et al., 2020), nasopharyngeal carcinoma (Zhen et al., 2013) prostate cancer (Xia et al., 2015) and lung cancer (Lin et al., 2015; Liu et al., 2014). In particular, the study carried out by Liu connects miR-184 downregulation to increased proliferation of lung cancer cell lines A549 and TL-1. They demonstrated that the overexpression of miR-184 in A549 cells caused a decrease in c-myc expression and a consequent decrease in cell proliferation. On the other hand, the knock-down of miR-184 expression and the consequent increase in c-myc promoted in cell proliferation (Liu et al., 2014).

A link between miR-184 downregulation and increased c-myc expression in NSCLC was observed by Lin. They demonstrated that miR-184 downregulation was correlated with an increase in the mRNA levels of c-myc. The overexpression of miR-184 in A549 cells after transfection with miR-184 mimic decreased c-myc expression and resulted in a decreased invasion capacity of the cells (Lin et al., 2015).

At present, there are no published records linking cisplatin resistance to miR-184 targeting of c-myc. Nevertheless, c-myc was correlated with the occurrence of cisplatin resistance in NSCLC (Q. Q. Li et al., 2017; Luanpitpong et al., 2017; Zuo et al., 2018). Given that c-myc was proved to be a target of miR-184, and c-myc role in promoting cell proliferation and cisplatin resistance, the expression of c-myc following miR-184 modulation was investigated.

In this study the expression of c-myc mRNA in Calu-3 cells increased following miR-184 loaded CS HCl NPs. The findings are in opposition to the behaviour reported by Lin and Liu (Zhen Liu et al., 2014), which linked c-myc overexpression to increased cell proliferation. Cytotoxicity results from our studied (sections 4.4.1.2 and 4.5.2) revealed instead a decrease in cisplatin resistance and in cell proliferation after miR-184 mimic Ps treatment. However, the increase in c-myc mRNA observed was approximately less than 2-fold for 5 nM and less than 1-fold for 20 nM treatment compared to controls. The subsequent pooling of the data resulted in the increase not being statistically significant. Thus, it can be concluded that the treatment with miR-184 mimic-loaded CS HCl NPs had little effect on c-myc expression.

The results related to miR-184 inhibitor transfection caused a significant increase in c-myc mRNA, which was comparable to the results obtained by Liu and Lin (Lin et al., 2015; Liu et al., 2014). Therefore, the increase in cell viability following cisplatin treatment and miR-184 inhibitor transfection observed in our previous studies (sections 4.4.1.4 and 4.4.4) can be attributed to the increase in c-myc expression.

In conclusion, c-myc upregulation following miR-184 inhibition was observed. Interestingly, miR-184 inhibition was also responsible for enhancing cisplatin resistance (Ch.4). Therefore, our results might provide preliminary indication of the role of miR-184 in conferring cisplatin resistance via targeting c-myc in NSCLC. However, further assessments are needed to confirm this hypothesis.

5.5.3 Investigation of TNFAIP-2 expression

Tumour necrosis factor alpha-induced protein 2 (TNFAIP2) is a primary response gene for tumour necrosis factor alpha (TNFα), that plays multiple roles in cell proliferation (Xie & Wang, 2017), migration (Jia et al., 2016), angiogenesis (Thair et al., 2016) and inflammation (D. Zhao et al., 2018). Its abnormal expression has been linked to the development and progression of several tumours, such as lymphoma (Kondratiev et al., 2011), breast cancer (Jia et al., 2016) and NSCLC (Li et al., 2020).

Furthermore, the abnormal expression of TNFAIP2 expression was linked to miR-184 downregulation in squamous cell carcinoma of head and neck (Zhensheng Liu et al., 2011), gastric cancer (Yu Xu et al., 2013) and glioma (Cheng et al., 2015). In particular, Cheng study on glioma tissues from patients and glioma cell lines demonstrated that TNFAIP2 expression was higher in both tissues and cell lines compared to non-cancerous samples. They also observed that miR-184 expression was lower (Cheng et al., 2015). The transfection of cell lines with miR-184 mimic resulted in decreased TNFAIP2 expression, thus confirming that miR-184 was a direct target of TNFAIP2. Moreover, the over-expression of miR-184 reduced invasiveness and increased percentage of apoptosis rate of glioma cells *in vitro*. The same study revealed that the delivery of miR-184 in glioma murine-model reduced significantly tumour size compared to untreated tumour-bearing mice (Cheng et al., 2015).

TNFAIP2 was found to be the responsible of promoting cisplatin resistance in urothelial cancer cells (Niwa et al., 2019) and in NSCLC (Li et al., 2020).In particular, Li connected TNFAIP2 upregulation in resistant A549 and H23 cells to cisplatin resistance. They observed that

upregulation of TNFAIP2 was responsible for a decrease in Caspase-3 activation (and therefore decrease in the apoptotic rate) and increase in cell migration and invasiveness. On the other hand, the silencing of TNFAIP2 resulted in a decreased cell viability and increased Caspase3 activity.

Given the involvement of TNFAIP2 in tumorigenesis, its link with miR-184 expression and its potential role in cisplatin resistance, the expression of TNFAIP2 was investigated in Calu-3 cells, to provide an additional explanation of miR-184 involvement in reducing cell proliferation and sensitising cells to cisplatin (chapter 4). In regard to miR-184 mimic-loaded CS HCl NPs treatments, the 5 nM treatment increased significantly TNFAIP-2 expression. However, the same increase was observed for the NTC-loaded CS HCl NPs used as a control. Therefore, the increase in TNFAIP2 cannot be directly attributed to miR-184 action, given that an analogous effect was observed for the NTC control. Thus, it can be concluded that miR-184 mimic -loaded NPs had no effect on TNFAIP2 expression.

Interestingly, the transfection with 5 nM miR-184 inhibitor resulted in a 2-fold increase of TNFAIP2 expression compared to controls. This was in accordance with studies linking TNFAIP2 upregulation to increased cell proliferation (Cheng et al., 2015; Zhensheng Liu et al., 2011; Niwa et al., 2019; Yu Xu et al., 2013) and with the observation of Li in cisplatin-resistant A549. Therefore, the increase in cell proliferation and decreased apoptosis observed following miR-184 inhibitor transfection in cisplatin treated cells (sections 4.4.1.4 and 4.4.4) can also be attributed to the increase in TNFAIP2 expression.

Similarly to what was concluded for c-myc, the findings from this study provide proof of principle of the involvement of miR-184 and INTFAIP2 in promoting cisplatin sensitivity of Calu-3 cells. However, further assessments are necessary to confirm that miR-184 enhances cisplatin sensitivity via targeting TNFAIP2.

5.5.4 Investigation of AKT-2 expression

Lastly, the current study investigated the expression of AKT-2 in Calu-3. AKT-2 is a downstream effector of phosphatidylinositol 3-kinase (PI3K) pathway, a pro-survival pathway in cancer. However, the published literature gave no reports of AKT-2 being a direct target of miR-184 in NSCLC. Nevertheless, AKT-2 has been found to be a target of miRNA 124 (Liu et al., 2020), miRNA-497 (Wang et al., 2020) and miR-126 (Huang et al., 2021) in NSCLC.

Similarly, miR-184 has been demonstrated to target AKT-2 mRNA. Foley firstly demonstrated that neuroblastoma samples presenting miR-184 knockdown had also a higher expression of AKT-2 compared to controls. The same behaviour was reported in four neuroblastoma cell lines cells having low levels of miR-184 and simultaneously presenting high levels of AKT-2. Additionally, the study demonstrated that neuroblastoma cell lines transfected with miR-184 mimic witnessed a decreased cell growth compared to non-transfected cells (Foley, Bray, Tivnan, Bryan, Murphy, Buckley, Ryan, O'meara, et al., 2010).

The current study observed that the treatment with miR-184 mimic-loaded NPs or miR-184 inhibitor transfection had no detectable effect on AKT-2 expression. Possible reasons of this behaviour might include miR-184 non targeting AKT-2 in Calu-3 cells, or AKT-2 presenting a non-detectable expression at the experimental condition used (section 5.4.4 and Figure 5.9).

Therefore, additional studies are needed to confirm the AKT-2 is a direct target of miR-184 in Calu-3 cells and subsequently that AKT-2 is responsible for conferring cisplatin sensitivity.

5.6 Conclusion

In conclusion, following literature investigation of potential targets for miR-184, BCL-2, c-myc, TNFAIP-2 and AKT-2 expression in Calu-3 cells following miR-184 modulation was investigated to understand better the mechanisms through which miR-184 sensitised cells to cisplatin (Ch. 4).

Results revealed a significant impact of miR-184 mimic transfection in BCL-2 protein expression and of miR-184 inhibitor in BCL-2 mRNA expression. Moreover, significant increase in c-myc and TNFAIP-2 mRNA following miR-184 inhibitor transfection was observed.

Altogether, those findings can be used as a confirmation of the pro-apoptotic role played by miR-184 in Calu-3 cells via targeting BCL-2. In addition, our results suggest that miR-184 might promote cisplatin activity via targeting c-myc and TNFAIP2.

6 Overview of the Project and Future Works

6.1 Overview of The Project

Lung cancer is the number one cause of cancer-related death worldwide (Ferlay et al., 2021). The primary reasons for its high mortality are the late detection of the malignancy together with the frequent occurrence of resistance towards commonly used chemotherapy agents (Sung et al., 2021). The first-line therapy for lung cancer patients is cisplatin and platinum-based compounds. However, the development of cisplatin resistance limits favourable outcomes in majority of the cases (Howell et al., 2010; Lemjabbar-Alaoui et al., 2015).

Oligonucleotide therapeutics are emerging as novel tools to tackle numerous pathologies, including cancer (Khvorova & Watts, 2017; Poller et al., 2018; Slaby et al., 2017a). Their mechanism of action consists in mimicking or inhibiting specific RNA targets, which have been discovered to play a crucial role in protein expression (Dunham et al., 2012).

The aim of this project was the evaluation of miR-184 in enhancing the sensitivity to cisplatin of NSCLC cells and to develop a nanocarrier to deliver miR-184 mimic to the cells. The aim was achieved through (i) the development of a nanocarrier to deliver oligonucleotides that can be easily manufactured and scalable, (ii) the Investigation of the expression of miR-184 in NSCLC cells and its involvement in cisplatin sensitivity (**Figure** 6.1).

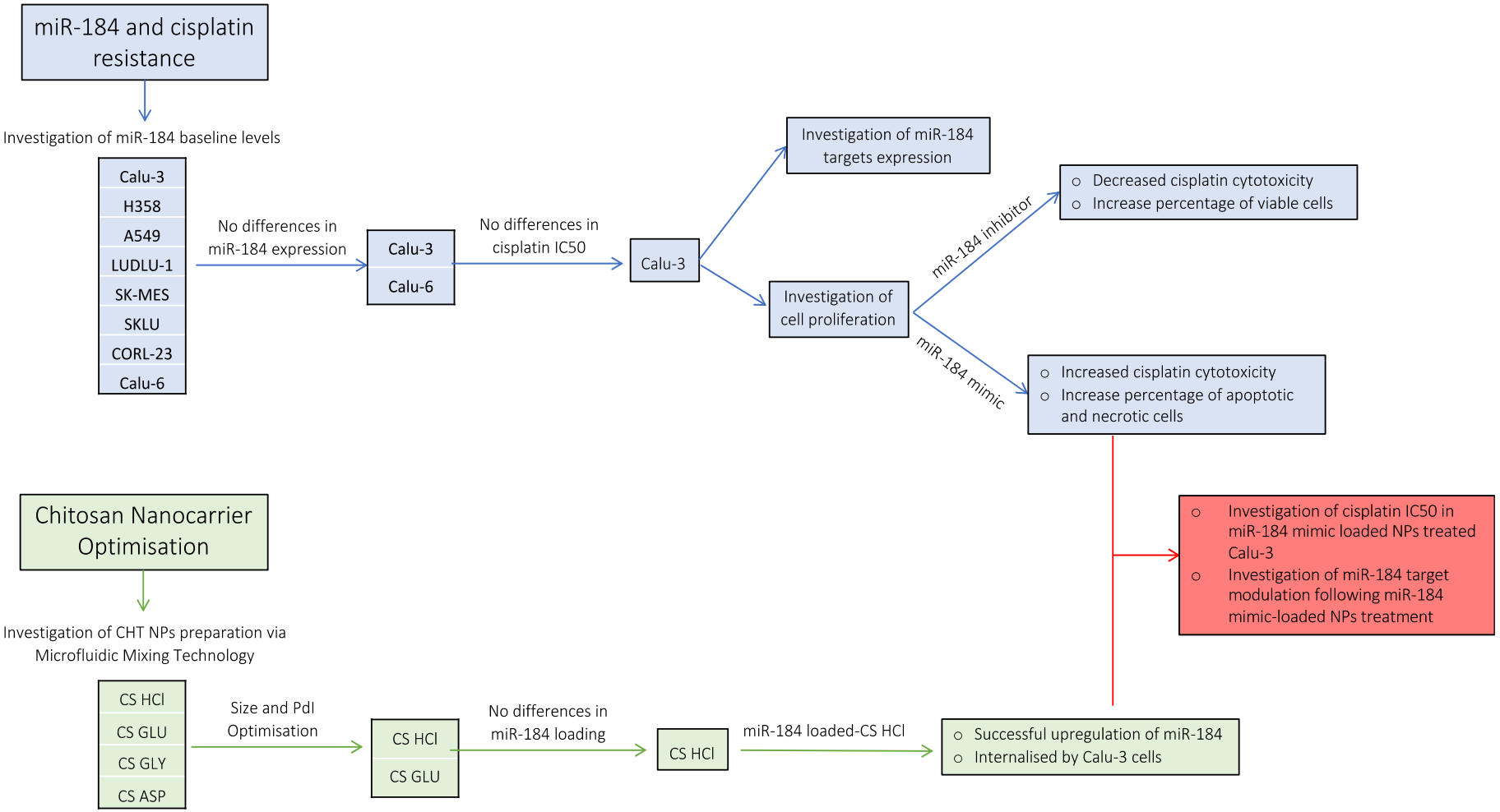

Figure 6.1 Schematic overview of the project.

6.1.1 Evaluation of miR-184 expression and cisplatin sensitivity

Following evaluation of the relevant literature regarding to miRNAs involved in the development of cisplatin resistance in lung cancer, miR-184 was selected. The choice was due to studies revealing that its downregulation was correlated with the occurrence of cisplatin resistant in lung cancer cells (Longqiu et al., 2020; Tung et al., 2016). In addition, miR-184 was also found to be involved in cisplatin resistance in oral squamous cell carcinoma (OSCC) (Fang et al., 2017) and in retinoblastoma (He et al., 2019). These studies revealed that miR-184 expression in cisplatin resistant cells was lower compared to cisplatin sensitive cells. Therefore, the first step involved the evaluation of miR-184 expression in the panel of NSCLC cell lines. Alnefaie previous work on the same cell lines revealed a difference in cisplatin sensitivity among the cell lines (Alnefaie, 2020) (**Table** 6.1). However, the investigation of miR-184 expression in the 8 cell lines revealed no significant differences in miR-184 expression despite their previously assessed sensitivity towards cisplatin (**Table** 6.1 and **Figure** 3.7).

For this reason, among the 8 cell lines initially screened only two were selected. The choice was made depending on the IC50 assessed by Alnefaie: Calu-3 was selected as the most resistant to cisplatin (IC50 7.1 μM) and Calu-6 was chosen as one of the most sensitive (IC50 1.1 μM) (**Table** 6.1). Given that cell lines can considerably change their behaviour if handled in different laboratories following different protocols due to changes in their genetic, epigenetic and phenotypic characteristics (Mi et al., 2019), the IC50 of Calu-3 and Calu-6 was assessed under our laboratory conditions and procedure.

Alamar Blue assay was employed to investigate cisplatin IC50 in Calu-3 and Calu-6. Results revealed similar values of IC50 for the two cell lines: 14.35 ± 1.28 μM for Calu-3 and 17.28 ± 3.74 μM for Calu-6. This is in accordance with the results obtained via the investigation of miR-184 expression that revealed no difference in miR-184 levels in the two cell lines. In fact, as suggested by Tung and Longqiu studies, different sensitivity to cisplatin (and different IC50 values) would result in different levels of miR-184 expression (Longqiu et al., 2020; Tung et al., 2016b). In our study, the expression of miR-184 in Calu-3 and Calu-6 was similar, as were their values of cisplatin IC50. Therefore, given their similar sensitivity towards cisplatin, Calu-3 was selected for further assessments.

Table 6.1 Summary of cell lines initially screened, their cisplatin IC50 values found by previous studies and the miR-184 expression investigated by our work. Results from the miR-184 baseline investigation led to the selection on only two of the cell lines, being Calu-3 (as the most resistant towards cisplatin) and Calu-6 (as the most sensitive).

	IC 50 (µM) (Alnefaie, 2020)	miR-184 expression ΔCt Value ± SD	IC 50 (µM)
Calu-3	7.01	17.35 ± 0.45	14.35 ± 1.28
H358	6.9	16.52 ± 1.03	/
A549	4.92	18.27 ± 1.47	/
LUDLU-1	4.152	16.90 ± 1-57	/
SK-MES	3.079	17.1 ± 1.78	/
SKLU	2.56	16.17 ± 1.45	/
CORL-23	1.61	16.56 ± 1.31	/
Calu-6	1.1	16.08 ± 0.68	17.28 ± 3.74

6.1.2 Investigation of miR-184 role in cisplatin sensitivity

To evaluate the role of miR-184 in enhancing cisplatin sensitivity of Calu-3, the IC50 of cisplatin following miR-184 upregulation or downregulation was investigated. The modulation of miR-184 expression in Calu-3 cells was obtained via transfection of miR-184 mimic (for miR-184 upregulation) or inhibitor (for miR-184 downregulation) using a commercially available liposomal reagent (INTERFERin®).

Our findings revealed that the IC50 of cisplatin changed when miR-184 expression was modified. Cisplatin IC50 decreased from 14.35 ± 1.28 µM (cisplatin alone) to 9.42 ± 1.47 following miR-184 upregulation and increased to 34.78 ± 3.99 and 55.01 ± 4.42 following miR-184 inhibitor transfection (5 nM and 20 nM treatment). Thus, suggesting that miR-184 upregulation sensitises Calu-3 cells to cisplatin and on the other hand, that miR-184 inhibition decreased cisplatin cytotoxicity.

The results were also confirmed via flow cytometry AnnexinV-FITC/PI staining. The experiments were carried out treating miR-184 mimic or inhibitor transfected cells with different concentration of cisplatin. Results showed that miR-184 upregulation brought about an increase in the percentage of apoptotic and necrotic cells, if compared with cisplatin only treatments. On the other hand, miR-184 inhibitor transfected cells registered a significant increase in cell proliferation and a concomitant decrease in the percentage of apoptotic cells in comparison with cisplatin only treatment. These outcomes are in line with published

literature highlighting the ability of cisplatin of promoting cytotoxicity via apoptosis and additionally with the activation of necrosis pathways (Ferrer et al., 2003; Sancho-Martínez et al., 2011; Shibuya et al., 2003). Therefore, the outcomes of this study confirmed that the upregulation of miR-184 sensitises Calu-3 cells to cisplatin.

6.1.3 Investigation of potential miR-184 target expression

To further assess the mechanism through which miR-184 enhanced cisplatin sensitivity in Calu-3 cells, the expression of four known mRNA targets of miR-184 was investigated. They were BCL-2, c-myc (Lin et al., 2015; Zhen Liu et al., 2014), TNFAIP-2 (Cheng et al., 2015; Liu et al., 2011; Xu et al., 2013), AKT-2 (Foley, Bray, Tivnan, Bryan, Murphy, Buckley, Ryan, O'Meara, et al., 2010). These genes are involved in cell metabolism, inflammation and cell cycle control pathways in cancer malignancies (section 5.1).

In line with earlier studies, miR-184 promoted apoptosis via targeting BCL-2, (Longqiu et al., 2020; Tung et al., 2016b). This was concluded given that the expression of miR-184 at the protein level decreased of approximately 10% following miR-184 mimic transfection. In addition, our results revealed a slight decrease of BCL-2 mRNA expression following miR-184 mimic-loaded CS HCL NPs treatment. Even though the pooling of the data resulted in the decrease being non-significant, these initial findings highlighted also the potential of the developed NPs to deliver the mimic into the cells.

Moreover, a further confirmation of our hypothesis that miR-184 promoted apoptosis via targeting BCL-2 was the increased mRNA levels of BCL-2 following miR-184 inhibitor transfection (section 5.4.1 and 5.5.1).

In regard to the evaluation of the expression of the other genes, further investigations are needed to confirm their role in Calu-3 cells.

6.1.4 Chitosan NPs optimisation via microfluidic mixing

The principal issue related to oligonucleotide therapeutics is their challenging delivery, which often limits their translation into clinics (Dorner et al., 2009; Jason et al., 2004b; Juliano, 2016). However, nanotechnology represent a promising tool to overcome the stability and delivery issues, and to allow the intact delivery of the oligonucleotide at the site of action while avoiding side effects (Lee et al., 2019).

Chitosan was selected as a polymer to produce NPs, given its biocompatibility, biodegradability, low cytotoxicity (Abd El-Rehim et al., 2012; Matica et al., 2019). However, the scalability of NPs represents the main burden in the transability of NPs formulation from laboratories to large scale production. Microfluidic mixing was employed in this study as it is a novel methodology employed in NPs preparation that allows elimination of user variability, quicker production and therefore easier scalability of the formulations (Lou et al., 2020; Roces et al., 2019; Roces, Lou, et al., 2020).

Four types of chitosan were employed: three chitosan water-soluble derivatives (CS HCl, CS GLU, CS GLY) and one chitosan derived from fungi (CS ASP). An initial evaluation of the influence on NPs size and PDI by microfluidic parameters was performed via Taguchi DoE, revealing that the primary influence on size was brought about by the ratio of polymer to crosslinker ratio which is a direct reflection of the FRR parameter. Therefore, a further investigation of the influence of FRR on NPs size and PDI was carried out. The results gathered from the optimisation determined the selection of only CS GLU and CS HCl for further studies, as in comparison with the other two polymers they resulted in giving NPs with smaller size, smaller PdI and better reproducibility of the results in accordance with the Taguchi DoE analysis (section 3.4.1, Table 6.2).

6.1.5 Optimisation of Chitosan NPs as Carriers for miR-184 mimic

Given the findings about miR-184 role in enhancing cisplatin sensitivity in Calu-3 cells, the ability of the selected polymers to complex miR-184 mimic was investigated. The preparation of miR-184 mimic-loaded CS HCl and CS GLU NPs, the evaluation of their size (nm), PDI; Zeta Potential (mV) and EE% and the gel retardation assay confirmed that both the chitosan derivatives are suitable carriers for miR-184 mimic.

Furthermore, the outcome from this study highlighted that:

1) miR-184 expression increased following Calu-3 treatment with miR-184 mimic-loaded NPs;
2) The miR-184 mimic-loaded CS HCl NPs were successfully up taken by Calu-3 cells.

Therefore, the optimised CS HCl NPs can successfully be used as a cargo for miR-184 mimic to deliver the drug into Calu-3 cells. Even though the complexation of oligonucleotide within chitosan nanocarriers had already been observed (Denizli et al., 2017; Gaur et al., 2015b; McKiernan et al., 2013), they rely on the traditional method of preparation of chitosan NPs.

Our study reports a novel production of CS HCl NPs carrying miR-184 via microfluidic mixing. Moreover, it is a promising strategy that might open the possibility of loading different oligonucleotide to promote their uptake into a variety of cell lines (**Table** 6.2).

Table 6.2 Summary of optimum CHT NPs size and PDI, and of EE% of the derivatives selected for the investigation of miR-184 loading efficiency. Among the initially employed four CHT derivatives, only CS HCl and CS GLU were selected to evaluate miR-184 mimic loading given their smaller size and PDI, and the better reproducibility of the results in accordance with the analyisis of Taguchi DoE (n=3, mean ± SD).

	Optimum NPs		miR-184 EE (%)		
	Size (nm)	PdI	100:1	50:1	25:1
CS HCl	105.9 ± 11.00	0.29 ± 0.04	92.4 ± 1.49	92.92 ± 0.47	98.76 ± 0.31
CS GLU	142.73 ± 6.60	0.34 ± 0.08	91.83 ± 0.89	98.18 ± 0.50	98.46 ± 0.46
CS GLY	199.20 ± 8.50	0.22 ± 0.01	/	/	/
CS ASP	142.15 ± 5.75	0.52 ± 0.05	/	/	/

6.1.6 Evaluation of miR-184 mimic-loaded NPs activity

Finally, following the assessment of the effect of miR-184 upregulation in promoting cisplatin cytotoxicity, and the demonstration that miR-184 mimic can be internalised by Calu-3 cells via the optimised CS HCl NPs, the IC50 of cisplatin in association with miR-184 mimic-loaded CS HCl NPs was investigated.

However, contrarily to our findings revealing that miR-184 mimic transfection decreased cisplatin IC50, the treatment of Calu-3 with cisplatin and miR-184 mimic-loaded CS HCl increased the IC50. the rise was proportional to the concentration of the treatment and a rise in cisplatin IC50 was observed for controls treatment, being blank CS HCl NPs in association with cisplatin and NTC-loaded CS HCl NPs.

These findings suggested a potential interference of the polymer with the Alamar Blue assay employed to investigate cisplatin cytotoxicity. Therefore, further assessments on the potential interference of chitosan with resazurin were carried out, resulting in the conclusion that the fluorescence readings of the Alamar Blue assay were influenced by the presence of chitosan. Hence, it cannot be concluded that the miR-184 mimic-loaded CS HCl NPs determined a decrease in cisplatin IC50 similar to the drop evidenced following miR-184 transfection via INTERFERin®.

6.2 Future Works

To enhance the findings of this study further and to advance the knowledge in the field, future directions to be taken into consideration.

6.2.1 Further assessment of CS HCl interference with Alamar Blue

In **chapter 4**, the possible interaction of CS HCl with the Alamar Blue assay was highlighted. One potential cause of such interaction is the reduction of resazurin by the NH_3^+ groups on the chitosan molecule (**Figure** 6.2).

All the control treatments suggested the interference of the polymer with the assay readout. to confirm initial results suggesting an increase in IC50 following miR-184 mimic-loaded CS HCl NPs treatment, few controls were carried out: i) Calu-3 transfection with cisplatin and Blank CS HCl NPs, ii) Calu-3 treatment with NTC-loaded CS HCl NPs, iii) Calu-3 treatment with CS HCl only. However, one additional control should be performed to add a further evidence of the interference, which would be the combination of CS HCl and resazurin without Calu-3 cells. If CS HCl reduces resazurin to produce resorufin as hypothesised, the fluorescent reading of CS HCl and resazurin would be higher compared to resazurin only. This control would allow the corroboration of our findings and would enhance the confidence of our theory.

As stressed by Rosslein, performing control studies prior to perform biological assays with nanomaterials is of key importance. This will limit the risk of unreliable and contradictory results that are likely to emerge when testing nanomaterials on cells (Bhattacharya et al., 2011; Krug & Wick, 2011; Rösslein et al., 2015; Som et al., 2013).

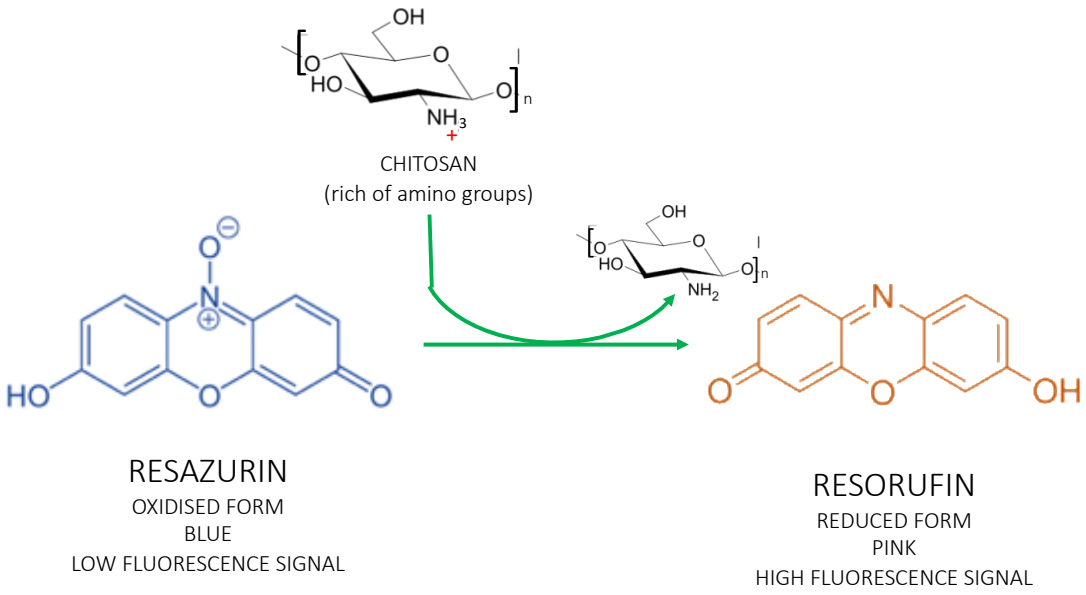

Figure 6.2 Hypothesis of the mechanism of CHT interference with the Alamar Blue assay. Chitosan, as a molecule rich of NH_3^+ groups might be responsible of reducing resazurin (the molecule on which the Alamar Blue assay is based) into its reduced form resorufin.

6.2.2 Evaluate miR-184 mimic-loaded CS HCl NPs + cisplatin cell viability

A future directive includes the IC50 investigation of miR-184 mimic-loaded CS HCl NPs using a different method to monitor cell viability. Thus, will allow a further evaluation of the properties of the carrier develop. However, once confirmed that CS HCl interferes with Alamar Blue assay via resazurin reduction, cytotoxicity assay based on the reduction of tetrazolium salts (such as MTT or MTS) should be avoided. Therefore a valid alternative might be the use of commercially available kits based on protease activity (Posfai et al., 2018) or ATP production (Ni et al., 2017; M. Yang et al., 2017; Zander-Fox et al., 2015).

6.2.3 Investigate the successful Release of miR-184 from CS HCl NPs

Our findings from **chapter 5** regarding the investigation of miR-184 targets revealed little effect of the miR-184 mimic-loaded CS HCl NPs on the expression of the selected targets (BCL-2, c-myc, TNFAIP-2 and AKT-2). On the other hand, there was a considerable variation in BCL-2 expression following miR-184 mimic transfection, together with a significant effect on BCL-2, c-myc and TNFAIP-2 expression following miR-184 inhibitor transfection.

Therefore, it is to be questioned whether the modest effect on target expressions of the miR-184 mimic-loaded CS HCl NPs was due to the NPs non releasing properly the oligonucleotide. This can be due to the nature of the NPs formation, which consists in the establishment of electrostatic interaction between the positively charged chitosan and the negatively charged cross-linker (TPP) and oligonucleotide (miR-184 mimic)(Calvo et al., 1997).

One initial suggestion that miR-184 mimic was released from the CS HCl NPs can be found in the qPCR data (section 3.4.7) demonstrating an increase in miR-184 expression following Calu-3 treatment with miR-184 mimic-loaded CS HCl NPs.

However, given the importance of the drug being release from the carrier to fully exert its action, it would be rather beneficial to conduct the investigation.

6.2.4 Further assessment of miR-184 role in Apoptosis

The action of miR-184 in promoting cisplatin-induced apoptosis was investigated via the AnnexinV-FITC/PI staining assay with a Flow Cytometry device.

However, flow cytometry results are strictly dependent on the gating strategy adopted and on the cell population selected. To ensure reliable results, the gates need to remain the same throughout the independent experiments. On the other hand, cells do not respond always in the same manner to the treatments and may result in having different characteristics that makes the planned gating strategy unsuitable for each individual sample (Ormerod et al., 1993; Zamai et al., 2001). In addition, cytotoxic treatments that diminish considerably the viable cell population render even more complicate the registration of events by the flow cytometry detectors. Cells treated with cytotoxic agents shrink in size and/or reached necrotic stages in which they are lysate completely, and consequently they cannot be detected.

Therefore, the observation that miR-184 mimic increased cytotoxicity of cisplatin through apoptosis and necrosis should be further validated through other methods such as caspase-based assays (Kaufmann et al., 2008;).

6.2.5 Investigation of cell invasion capability

A further investigation of the role of miR-184 in promoting cisplatin sensitivity could be performed via the scratch assay, which allows the measurement of cell migration rate (Liang et al., 2007).

Comparing migration rate of cisplatin only cells and cisplatin together with miR-184 mimic/inhibitor transfected cells would provide a supplementary understanding of the role of miR-184. Moreover, performing the assay with miR-184 mimic-loaded CS HCl NPs would additionally evaluate the suitability of the NPs to deliver the oligonucleotide in Calu-3 cells.

6.2.6 Development of cisplatin-miR-184 mimic loaded NPs

The role of miR-184 in enhancing cisplatin cytotoxicity and its successful delivery via CS HCl NPs, provide the basis for the development of a more complex NPs carrier that will combine miR-184 mimic and cisplatin. Thus, the two drugs would be delivered together with one treatment only.

6.2.7 Inhalation or Nebulisation study

A future directive to bring the miR-184 mimic-loaded CS HCl NPs closer to the clinic might include the development of a carrier for the CS HCl NPs. This would include the formation of a spray-dried powder (whit the use of appropriate excipients, such as sugar and/or amino acids) or the preparation of a NPs saline solution suitable for nebulisation.

Thus, will provide an easier and innovative way to deliver the oligonucleotide therapeutic, which otherwise require hospitalisation in majority of the cases (section 1.2.2)

6.3 Conclusion

Following literature screening of miRNA involved in cisplatin resistance of NSCLC, this PhD thesis focused on deepening the understanding of miR-184 in enhancing cisplatin sensitivity of NSCLC.

The study focused on investigating the expression of miR-184 in a panel of NSCLC cells, that previous studies reported to have different sensitivity towards cisplatin. However, findings from this study observed no statistical differences in miR-184 expression among them. Therefore, the study focused on one cell line, Calu-3. The effect of miR-184 modulation in Calu-3 cells was investigated, showing that the sensitivity of cells towards cisplatin increased following miR-184 mimic transfection. In addition, the effect of miR-184 on apoptosis and necrosis was investigated via AnnexinV-FITC/PI staining. Results gathered suggested that miR-184 mimic also enhanced necrosis and early apoptosis in Calu-3 cells.

The present study aimed at optimising the formulation of CHT NPs with microfluidic mixing technology *no comma*, to develop a carrier for miRNA delivery. Results revealed that microfluidic mixing technology is a promising approach to manufacture CHT NPs and that CS HCl and CS GLU are promising candidates to load miR-184 mimic. Further assessments confirmed that miR-184-loaded CS HCl NPs were successfully delivered into Calu-3 cells.

Therefore, given the ability of miR-184 mimic to increase Calu-3 cells sensitivity towards cisplatin, the possibility of delivering miR-184 into Calu-3 cells via CS HCl NPs was investigated. An increase in cisplatin IC50 was observed following delivery of the oligonucleotide via CS HCl NPs, which initial assessment suggested to be due to the interference of chitosan with the Alamar Blue assay.

Finally, miR-184 targets (BCL-2, c-myc, TNFAIP-2 and AKT-2) expression in Calu-3 cells following miR-184 modulation was also investigated. Even though additional studies should be performed to confirm that miR-184 CS HCl NPs can modulate miR-184 targets expression, initial findings corroborated the outcomes from cytotoxicity studies revealing the involvement of miR-184 in promoting cisplatin-mediated apoptosis.

References

Abd El-Rehim, H. A., El-Sawy, N. M., Hegazy, E. S. A., Soliman, E. S. A., & Elbarbary, A. M. (2012). Improvement of antioxidant activity of chitosan by chemical treatment and ionizing radiation. *International Journal of Biological Macromolecules*, *50*(2), 403–413. https://doi.org/10.1016/J.IJBIOMAC.2011.12.021

Aider, M. (2010). Chitosan application for active bio-based films production and potential in the food industry: Review. *LWT - Food Science and Technology*, *43*(6), 837–842. https://doi.org/10.1016/J.LWT.2010.01.021

Al-Kassas, R., Wen, J., Cheng, A. E. M., Kim, A. M. J., Liu, S. S. M., & Yu, J. (2016). Transdermal delivery of propranolol hydrochloride through chitosan nanoparticles dispersed in mucoadhesive gel. *Carbohydrate Polymers*, *153*, 176–186. https://doi.org/10.1016/J.CARBPOL.2016.06.096

Ali, R., Aouida, M., Sulaiman, A. A., Madhusudan, S., & Ramotar, D. (2022). Can Cisplatin Therapy Be Improved? Pathways That Can Be Targeted. *International Journal of Molecular Sciences*, *23*(13), 7241. https://doi.org/10.3390/IJMS23137241

Alnefaie, G. O. F. (2020). *Epigenetic Sensitisation of Chemotherapeutic Compounds in Non-Small Cell Lung Cancer - The University of Liverpool Repository*. Doctorate Thesis. https://livrepository.liverpool.ac.uk/3093513/

Amin, M. K., & Boateng, J. S. (2019). Comparison and process optimization of PLGA, chitosan and silica nanoparticles for potential oral vaccine delivery. *Therapeutic Delivery*, *10*(8), 493–514. https://doi.org/10.4155/TDE-2019-0038

Andersson, B. (2005). European Science Foundation Policy Briefing 2. *Nanomedicine*.

Arbour, K. C., & Riely, G. J. (2019). Systemic Therapy for Locally Advanced and Metastatic Non-Small Cell Lung Cancer: A Review. *JAMA*, *322*(8), 764–774. https://doi.org/10.1001/JAMA.2019.11058

Arya, M., Shergill, I. S., Williamson, M., Gommersall, L., Arya, N., & Patel, H. R. H. (2005). Basic principles of real-time quantitative PCR. *Expert Review of Molecular Diagnostics*, *5*(2), 209–219. https://doi.org/10.1586/14737159.5.2.209

Bader, A. G. (2012). MiR-34 - a microRNA replacement therapy is headed to the clinic. *Frontiers in Genetics*, *3*(JUL), 120. https://doi.org/10.3389/FGENE.2012.00120/BIBTEX

Bains, A., Cao, Y., Kly, S., Wulff, J. E., & Moffitt, M. G. (2017). Controlling Structure and Function of Polymeric Drug Delivery Nanoparticles Using Microfluidics. *Molecular Pharmaceutics*, *14*(8), 2595–2606. https://doi.org/10.1021/ACS.MOLPHARMACEUT.7B00177

Baldassari, F., Zerbinati, C., Galasso, M., Corrà, F., Minotti, L., Agnoletto, C., Previati, M., Croce, C. M., & Volinia, S. (2018). Screen for MicroRNA and Drug Interactions in Breast Cancer Cell Lines Points to miR-126 as a Modulator of CDK4/6 and PIK3CA Inhibitors. *Frontiers in Genetics*, *9*(MAY). https://doi.org/10.3389/FGENE.2018.00174

Bandi, N., Zbinden, S., Gugger, M., Arnold, M., Kocher, V., Hasan, L., Kappeler, A., Brunner, T., & Vassella, E. (2009). miR-15a and miR-16 are implicated in cell cycle regulation in a Rb-dependent manner and are frequently deleted or down-regulated in non-small cell lung cancer. *Cancer Research*, *69*(13), 5553–5559. https://doi.org/10.1158/0008-5472.CAN-08-4277/654918/P/MIR-15A-AND-MIR-16-ARE-IMPLICATED-IN-CELL-CYCLE

Bartoszewska, S., Kamysz, W., Jakiela, B., Sanak, M., Króliczewski, J., Bebok, Z., Bartoszewski, R., & Collawn, J. F. (2017). miR-200b downregulates CFTR during hypoxia in human lung epithelial cells. *Cellular & Molecular Biology Letters*, *22*(1). https://doi.org/10.1186/S11658-017-0054-0

Beg, M. S., Brenner, A. J., Sachdev, J., Borad, M., Kang, Y. K., Stoudemire, J., Smith, S., Bader, A. G., Kim, S., & Hong, D. S. (2017). Phase I study of MRX34, a liposomal miR-34a mimic, administered twice weekly in patients with advanced solid tumors. *Investigational New Drugs*, *35*(2), 180–188. https://doi.org/10.1007/S10637-016-0407-Y

Bellich, B., D'Agostino, I., Semeraro, S., Gamini, A., & Cesàro, A. (2016). "The Good, the Bad and the Ugly" of Chitosans. *Marine Drugs 2016, Vol. 14, Page 99*, *14*(5), 99. https://doi.org/10.3390/MD14050099

Belliveau, N. M., Huft, J., Lin, P. J., Chen, S., Leung, A. K., Leaver, T. J., Wild, A. W., Lee, J. B., Taylor, R. J., Tam, Y. K., Hansen, C. L., & Cullis, P. R. (2012). Microfluidic Synthesis of Highly Potent Limit-size Lipid Nanoparticles for In Vivo Delivery of siRNA. *Molecular Therapy - Nucleic Acids*, *1*(8), e37. https://doi.org/10.1038/MTNA.2012.28

Benes, V., & Castoldi, M. (2010). Expression profiling of microRNA using real-time quantitative PCR, how to use it and what is available. *Methods*, *50*(4), 244–249. https://doi.org/10.1016/J.YMETH.2010.01.026

Bhattacharya, S., Zhang, Q., Carmichael, P. L., Boekelheide, K., & Andersen, M. E. (2011).

Toxicity Testing in the 21st Century: Defining New Risk Assessment Approaches Based on Perturbation of Intracellular Toxicity Pathways. *PLoS ONE*, *6*(6). https://doi.org/10.1371/JOURNAL.PONE.0020887

Bignotti, E., Calza, S., Tassi, R. A., Zanotti, L., Bandiera, E., Sartori, E., Odicino, F. E., Ravaggi, A., Todeschini, P., & Romani, C. (2016a). Identification of stably expressed reference small non-coding RNAs for microRNA quantification in high-grade serous ovarian carcinoma tissues. *Journal of Cellular and Molecular Medicine*, *20*(12), 2341. https://doi.org/10.1111/JCMM.12927

Bignotti, E., Calza, S., Tassi, R. A., Zanotti, L., Bandiera, E., Sartori, E., Odicino, F. E., Ravaggi, A., Todeschini, P., & Romani, C. (2016b). Identification of stably expressed reference small non-coding RNAs for microRNA quantification in high-grade serous ovarian carcinoma tissues. *Journal of Cellular and Molecular Medicine*, *20*(12), 2341. https://doi.org/10.1111/JCMM.12927

Borchert, G. M., Lanier, W., & Davidson, B. L. (2006). RNA polymerase III transcribes human microRNAs. *Nature Structural & Molecular Biology*, *13*(12), 1097–1101. https://doi.org/10.1038/NSMB1167

Bray, F., Ferlay, J., Soerjomataram, I., Siegel, R. L., Torre, L. A., & Jemal, A. (2018). 394 CA: A Cancer Journal for Clinicians Global Cancer Statistics 2018: GLOBOCAN Estimates of Incidence and Mortality Worldwide for 36 Cancers in 185 Countries. *CA CANCER J CLIN*, *68*, 394–424. https://doi.org/10.3322/caac.21492

Breznan, D., Das, D., MacKinnon-Roy, C., Simard, B., Kumarathasan, P., & Vincent, R. (2015). Non-specific interaction of carbon nanotubes with the resazurin assay reagent: Impact on in vitro assessment of nanoparticle cytotoxicity. *Toxicology in Vitro*, *29*(1), 142–147. https://doi.org/10.1016/J.TIV.2014.09.009

Bueno, C., Villegas, M. L., Bertolotti, S. G., Previtali, C. M., Neumann, M. G., & Encinas, M. V. (2002). The Excited-State Interaction of Resazurin and Resorufin with Aminesin Aqueous Solutions. Photophysics and Photochemical Reaction¶. *Photochemistry and Photobiology*, *76*(4), 385–390. https://doi.org/10.1562/0031-8655(2002)0760385TESIOR2.0.CO2

Büscher, M. (2019). Flow Cytometry Instrumentation - An Overview. *Current Protocols in Cytometry*, *87*(1). https://doi.org/10.1002/CPCY.52

Bustin, S. A., Benes, V., Nolan, T., & Pfaffl, M. W. (2005). Quantitative real-time RT-PCR – a perspective. *Journal of Molecular Endocrinology*, *34*(3), 597–601. https://doi.org/10.1677/JME.1.01755

Cai, X., Hagedorn, C. H., & Cullen, B. R. (2004). Human microRNAs are processed from capped, polyadenylated transcripts that can also function as mRNAs. *RNA (New York, N.Y.)*, *10*(12), 1957–1966. https://doi.org/10.1261/RNA.7135204

Calin, G. A., Dumitru, C. D., Shimizu, M., Bichi, R., Zupo, S., Noch, E., Aldler, H., Rattan, S., Keating, M., Rai, K., Rassenti, L., Kipps, T., Negrini, M., Bullrich, F., & Croce, C. M. (2002a). Frequent deletions and down-regulation of micro- RNA genes miR15 and miR16 at 13q14 in chronic lymphocytic leukemia. *Proceedings of the National Academy of Sciences of the United States of America*, *99*(24), 15524–15529. https://doi.org/10.1073/PNAS.242606799

Calin, G. A., Dumitru, C. D., Shimizu, M., Bichi, R., Zupo, S., Noch, E., Aldler, H., Rattan, S., Keating, M., Rai, K., Rassenti, L., Kipps, T., Negrini, M., Bullrich, F., & Croce, C. M. (2002b). Frequent deletions and down-regulation of micro- RNA genes miR15 and miR16 at 13q14 in chronic lymphocytic leukemia. *Proceedings of the National Academy of Sciences of the United States of America*, *99*(24), 15524–15529. https://doi.org/10.1073/PNAS.242606799

Calvo, P., Remuñán-López, C., Vila-Jato, J. L., & Alonso, M. J. (1997). Novel hydrophilic chitosan-polyethylene oxide nanoparticles as protein carriers. *Journal of Applied Polymer Science*, *63*(1), 125–132. https://doi.org/10.1002/(SICI)1097-4628(19970103)63:1<125::AID-APP13>3.0.CO;2-4

Carbone, D. P., Reck, M., Paz-Ares, L., Creelan, B., Horn, L., Steins, M., Felip, E., van den Heuvel, M. M., Ciuleanu, T.-E., Badin, F., Ready, N., Hiltermann, T. J. N., Nair, S., Juergens, R., Peters, S., Minenza, E., Wrangle, J. M., Rodriguez-Abreu, D., Borghaei, H., … Socinski, M. A. (2017). First-Line Nivolumab in Stage IV or Recurrent Non-Small-Cell Lung Cancer. *The New England Journal of Medicine*, *376*(25), 2415–2426. https://doi.org/10.1056/NEJMOA1613493

Cell Transfection Database - over 4000 publications. (n.d.). Retrieved April 13, 2022, from https://www.polyplus-transfection.com/resources/cell-transfection-database/?type=invitro&cell%5B%5D=1492&biomolecule%5B%5D=1649&reagent%5B%5D=76&fsearch=&subbtn=Search

Cepeda, V., Fuertes, M. A., Castilla, J., Alonso, C., Quevedo, C., & Perez, J. M. (2007). Biochemical mechanisms of cisplatin cytotoxicity. *Anti-Cancer Agents in Medicinal Chemistry*, *7*(1), 3–18. https://doi.org/10.2174/187152007779314044

Chacon-Cortes, D., & Griffiths, L. R. (2014). Methods for extracting genomic DNA from whole blood samples: current perspectives. *Journal of Biorepository Science for Applied Medicine*, *2*, 1–9. https://doi.org/10.2147/BSAM.S46573

Chai, Y., Wang, Y., Li, B., Qi, W., Su, R., & He, Z. (2021). Microfluidic Synthesis of Lignin/Chitosan Nanoparticles for the pH-Responsive Delivery of Anticancer Drugs. *Langmuir*, *37*(23), 7219–7226. https://doi.org/10.1021/ACS.LANGMUIR.1C00778/SUPPL_FILE/LA1C00778_SI_001.PDF

Chapard, C., Meraldi, P., Gleich, T., Bachmann, D., Hohl, D., & Huber, M. (2014). TRAIP is a regulator of the spindle assembly checkpoint. *Journal of Cell Science*, *127*(24), 5149–5156. https://doi.org/10.1242/JCS.152579/259187/AM/THE-TRAF-INTERACTING-PROTEIN-TRAIP-IS-A-REGULATOR

Chaudhary, A. K., Mondal, G., Kumar, V., Kattel, K., & Mahato, R. I. (2017). Chemosensitization and inhibition of pancreatic cancer stem cell proliferation by overexpression of microRNA-205. *Cancer Letters*, *402*, 1–8. https://doi.org/10.1016/J.CANLET.2017.05.007

Chen, L., Gibbons, D. L., Goswami, S., Cortez, M. A., Ahn, Y. H., Byers, L. A., Zhang, X., Yi, X., Dwyer, D., Lin, W., Diao, L., Wang, J., Roybal, J. D., Patel, M., Ungewiss, C., Peng, D., Antonia, S., Mediavilla-Varela, M., Robertson, G., … Qin, F. X. F. (2014). Metastasis is regulated via microRNA-200/ZEB1 axis control of tumour cell PD-L1 expression and intratumoral immunosuppression. *Nature Communications*, *5*. https://doi.org/10.1038/NCOMMS6241

Chen, Shanshan, Li, P., Yang, R., Cheng, R., Zhang, F., Wang, Y., Chen, X., Sun, Q., Zang, W., Du, Y., Zhao, G., & Zhang, G. (2015). microRNA-30b inhibits cell invasion and migration through targeting collagen triple helix repeat containing 1 in non-small cell lung cancer. *Cancer Cell International*, *15*(1), 85. https://doi.org/10.1186/S12935-015-0236-7

Chen, Song, Zhang, H., Shi, X., Wu, H., & Hanagata, N. (2014a). Microfluidic generation of chitosan/CpG oligodeoxynucleotide nanoparticles with enhanced cellular uptake and immunostimulatory properties. *Lab on a Chip*, *14*(11), 1842–1849. https://doi.org/10.1039/C4LC00015C

Chen, Song, Zhang, H., Shi, X., Wu, H., & Hanagata, N. (2014b). Microfluidic generation of chitosan/CpG oligodeoxynucleotide nanoparticles with enhanced cellular uptake and immunostimulatory properties. *Lab on a Chip*, *14*(11), 1842–1849. https://doi.org/10.1039/C4LC00015C

Chen, Wei, Fan, D., Meng, L., Miao, Y., Yang, S., Weng, Y., He, H., & Tang, X. (2012). Enhancing effects of chitosan and chitosan hydrochloride on intestinal absorption of berberine in rats. *Drug Development and Industrial Pharmacy*, *38*(1), 104–110. https://doi.org/10.3109/03639045.2011.592531

Chen, Wenshu, Do, K. C., Saxton, B., Leng, S., Filipczak, P., Tessema, M., Belinsky, S. A., & Lin, Y. (2019). Inhibition of the hexosamine biosynthesis pathway potentiates cisplatin cytotoxicity by decreasing BiP expression in non-small-cell lung cancer cells. *Molecular Carcinogenesis*, *58*(6), 1046–1055. https://doi.org/10.1002/MC.22992

Chen, Y., & Stallings, R. L. (2007). Differential patterns of microRNA expression in neuroblastoma are correlated with prognosis, differentiation, and apoptosis. *Cancer Research*, *67*(3), 976–983. https://doi.org/10.1158/0008-5472.CAN-06-3667

Chendrimada, T. P., Gregory, R. I., Kumaraswamy, E., Norman, J., Cooch, N., Nishikura, K., & Shiekhattar, R. (2005). TRBP recruits the Dicer complex to Ago2 for microRNA processing and gene silencing. *Nature*, *436*(7051), 740–744. https://doi.org/10.1038/NATURE03868

Cheng, Z., Wang, H. Z., Li, X., Wu, Z., Han, Y., Li, Y., Chen, G., Xie, X., Huang, Y., Du, Z., & Zhou, Y. (2015). MicroRNA-184 inhibits cell proliferation and invasion, and specifically targets TNFAIP2 in Glioma. *Journal of Experimental & Clinical Cancer Research : CR*, *34*(1). https://doi.org/10.1186/S13046-015-0142-9

Chiesa, E., Dorati, R., Pisani, S., Conti, B., Bergamini, G., Modena, T., & Genta, I. (2018). The Microfluidic Technique and the Manufacturing of Polysaccharide Nanoparticles. *Pharmaceutics*, *10*(4). https://doi.org/10.3390/PHARMACEUTICS10040267

Chiesa, E., Greco, A., Riva, F., Tosca, E. M., Dorati, R., Pisani, S., Modena, T., Conti, B., & Genta, I. (2019). Staggered Herringbone Microfluid Device for the Manufacturing of Chitosan/TPP Nanoparticles: Systematic Optimization and Preliminary Biological Evaluation. *International Journal of Molecular Sciences*, *20*(24). https://doi.org/10.3390/IJMS20246212

Chiou, G. Y., Cherng, J. Y., Hsu, H. S., Wang, M. L., Tsai, C. M., Lu, K. H., Chien, Y., Hung, S. C., Chen, Y. W., Wong, C. I., Tseng, L. M., Huang, P. I., Yu, C. C., Hsu, W. H., & Chiou, S. H. (2012). Cationic polyurethanes-short branch PEI-mediated delivery of Mir145 inhibited epithelial–mesenchymal transdifferentiation and cancer stem-like properties and in lung adenocarcinoma. *Journal of Controlled Release*, *159*(2), 240–250. https://doi.org/10.1016/J.JCONREL.2012.01.014

Choung, S., Kim, Y. J., Kim, S., Park, H. O., & Choi, Y. C. (2006). Chemical modification of siRNAs to improve serum stability without loss of efficacy. *Biochemical and Biophysical Research Communications*, *342*(3), 919–927. https://doi.org/10.1016/J.BBRC.2006.02.049

cis-Diammineplatinum(II) dichloride Product Number P4394 Store at Room Temperature. (n.d.).

Conner, C. G., Veleva, A. N., Paunov, V. N., Stoyanov, S. D., & Velev, O. D. (2020). Scalable Formation of Concentrated Monodisperse Lignin Nanoparticles by Recirculation-Enhanced Flash Nanoprecipitation. *Particle and Particle Systems Characterization*, *37*(7). https://doi.org/10.1002/PPSC.202000122

Cooper, E. (2008). From Darwin and Metchnikoff to Burnet and beyond. *Contributions to Microbiology*, *15*, 1–11. https://doi.org/10.1159/000135680

Cortez, M. A., Ivan, C., Valdecanas, D., Wang, X., Peltier, H. J., Ye, Y., Araujo, L., Carbone, D. P., Shilo, K., Giri, D. K., Kelnar, K., Martin, D., Komaki, R., Gomez, D. R., Krishnan, S., Calin, G. A., Bader, A. G., & Welsh, J. W. (2015). PDL1 Regulation by p53 via miR-34. *Journal of the National Cancer Institute*, *108*(1). https://doi.org/10.1093/JNCI/DJV303

Coutinho, A. J., Costa Lima, S. A., Afonso, C. M. M., & Reis, S. (2020). Mucoadhesive and pH responsive fucoidan-chitosan nanoparticles for the oral delivery of methotrexate. *International Journal of Biological Macromolecules*, *158*, 180–188. https://doi.org/10.1016/J.IJBIOMAC.2020.04.233

Crona, D. J., Faso, A., Nishijima, T. F., McGraw, K. A., Galsky, M. D., & Milowsky, M. I. (2017). A Systematic Review of Strategies to Prevent Cisplatin-Induced Nephrotoxicity. *The Oncologist*, *22*(5), 609–619. https://doi.org/10.1634/THEONCOLOGIST.2016-0319

Crowley, L. C., Marfell, B. J., Scott, A. P., & Waterhouse, N. J. (2016). Quantitation of Apoptosis and Necrosis by Annexin V Binding, Propidium Iodide Uptake, and Flow Cytometry. *Cold Spring Harbor Protocols*, *2016*(11), 953–957. https://doi.org/10.1101/PDB.PROT087288

Csepregi, R., Lemli, B., Kunsági-Máté, S., Szente, L., Koszegi, T., Németi, B., & Poór, M. (2018). Complex Formation of Resorufin and Resazurin with B-Cyclodextrins: Can Cyclodextrins Interfere with a Resazurin Cell Viability Assay? *Molecules : A Journal of Synthetic Chemistry and Natural Product Chemistry*, *23*(2). https://doi.org/10.3390/MOLECULES23020382

Cummins, L. L., Owens, S. R., Risen, L. M., Lesnik, E. A., Freier, S. M., Mc Gee, D., Cook, C. J., & Cook, P. D. (1995). Characterization of fully 2'-modified oligoribonucleotide hetero- and homoduplex hybridization and nuclease sensitivity. *Nucleic Acids Research*, *23*(11), 2019–2024. https://doi.org/10.1093/NAR/23.11.2019

Dasari, S., & Bernard Tchounwou, P. (2014). Cisplatin in cancer therapy: molecular mechanisms of action. *European Journal of Pharmacology*, *740*, 364. https://doi.org/10.1016/J.EJPHAR.2014.07.025

Dash, M., Chiellini, F., Ottenbrite, R. M., & Chiellini, E. (2011). Chitosan—A versatile semi-synthetic polymer in biomedical applications. *Progress in Polymer Science*, *36*(8), 981–1014. https://doi.org/10.1016/J.PROGPOLYMSCI.2011.02.001

De Jong, W. H., & Borm, P. J. A. (2008). Drug delivery and nanoparticles:applications and hazards. *International Journal of Nanomedicine*, *3*(2), 133–149. https://doi.org/10.2147/IJN.S596

De La Fuente, M., Seijo, B., & Alonso, M. J. (2008). Design of novel polysaccharidic nanostructures for gene delivery. *Nanotechnology*, *19*(7). https://doi.org/10.1088/0957-4484/19/7/075105

de Souza, R. H. F. V., Picola, I. P. D., Shi, Q., Petrônio, M. S., Benderdour, M., Fernandes, J. C., Lima, A. M. F., Martins, G. O., Martinez Junior, A. M., de Oliveira Tiera, V. A., & Tiera, M. J. (2018). Diethylaminoethyl- chitosan as an efficient carrier for siRNA delivery: Improving the condensation process and the nanoparticles properties. *International Journal of Biological Macromolecules*, *119*, 186–197. https://doi.org/10.1016/J.IJBIOMAC.2018.07.072

de Vries, G., Rosas-Plaza, X., van Vugt, M. A. T. M., Gietema, J. A., & de Jong, S. (2020). Testicular cancer: Determinants of cisplatin sensitivity and novel therapeutic opportunities. *Cancer Treatment Reviews*, *88*. https://doi.org/10.1016/J.CTRV.2020.102054

Decker, C. J., & Parker, R. (2012). P-bodies and stress granules: possible roles in the control of translation and mRNA degradation. *Cold Spring Harbor Perspectives in Biology*, *4*(9). https://doi.org/10.1101/CSHPERSPECT.A012286

Deng, X., Cao, M., Zhang, J., Hu, K., Yin, Z., Zhou, Z., Xiao, X., Yang, Y., Sheng, W., Wu, Y., & Zeng, Y. (2014a). Hyaluronic acid-chitosan nanoparticles for co-delivery of MiR-34a and doxorubicin in therapy against triple negative breast cancer. *Biomaterials*, *35*(14), 4333–4344. https://doi.org/10.1016/J.BIOMATERIALS.2014.02.006

Deng, X., Cao, M., Zhang, J., Hu, K., Yin, Z., Zhou, Z., Xiao, X., Yang, Y., Sheng, W., Wu, Y., & Zeng, Y. (2014b). Hyaluronic acid-chitosan nanoparticles for co-delivery of MiR-34a and doxorubicin in therapy against triple negative breast cancer. *Biomaterials*, *35*(14), 4333–4344. https://doi.org/10.1016/J.BIOMATERIALS.2014.02.006

Denizli, M., Aslan, B., Mangala, L. S., Jiang, D., Rodriguez-Aguayo, C., Lopez-Berestein, G., & Sood, A. K. (2017). Chitosan Nanoparticles for miRNA Delivery. *Methods in Molecular Biology (Clifton, N.J.)*, *1632*, 219–230. https://doi.org/10.1007/978-1-4939-7138-1_14

Dhillon, S. (2020). Viltolarsen: First Approval. *Drugs*, *80*(10), 1027–1031. https://doi.org/10.1007/S40265-020-01339-3

Dhuri, K., Bechtold, C., Quijano, E., Pham, H., Gupta, A., Vikram, A., & Bahal, R. (2020). Antisense Oligonucleotides: An Emerging Area in Drug Discovery and Development. *Journal of Clinical Medicine*, *9*(6), 1–24. https://doi.org/10.3390/JCM9062004

Ding, H., Wen, W., Ding, Q., & Zhao, X. (2020). Diagnostic Valuation of Serum miR-184 and miR-191 in Patients With Non-Small-Cell Lung Cancer. *Cancer Control : Journal of the Moffitt Cancer Center*, *27*(1). https://doi.org/10.1177/1073274820964783

Dogra, P., Ramírez, J. R., Butner, J. D., Peláez, M. J., Chung, C., Hooda-Nehra, A., Pasqualini, R., Arap, W., Cristini, V., Calin, G. A., Ozpolat, B., & Wang, Z. (2022). Translational Modeling Identifies Synergy between Nanoparticle-Delivered miRNA-22 and Standard-of-Care Drugs in Triple-Negative Breast Cancer. *Pharmaceutical Research*, *39*(3). https://doi.org/10.1007/S11095-022-03176-3

Dong, C., Liu, X., Wang, H., Li, J., Dai, L., Li, J., & Xu, Z. (2019). Hypoxic non-small-cell lung cancer cell-derived exosomal miR-21 promotes resistance of normoxic cell to cisplatin. *OncoTargets and Therapy*, *12*, 1947. https://doi.org/10.2147/OTT.S186922

Dorner, M., Brandt, S., Tinguely, M., Zucol, F., Bourquin, J. P., Zauner, L., Berger, C., Bernasconi,

M., Speck, R. F., & Nadal, D. (2009). Plasma cell toll-like receptor (TLR) expression differs from that of B cells, and plasma cell TLR triggering enhances immunoglobulin production. *Immunology*, *128*(4), 573. https://doi.org/10.1111/J.1365-2567.2009.03143.X

Duma, N., Santana-Davila, R., & Molina, J. R. (2019). Non–Small Cell Lung Cancer: Epidemiology, Screening, Diagnosis, and Treatment. *Mayo Clinic Proceedings*, *94*(8), 1623–1640. https://doi.org/10.1016/J.MAYOCP.2019.01.013/ATTACHMENT/8AD2FC8B-A320-400D-99C5-46634151C52C/MMC1.MP4

Dunham, I., Kundaje, A., Aldred, S. F., Collins, P. J., Davis, C. A., Doyle, F., Epstein, C. B., Frietze, S., Harrow, J., Kaul, R., Khatun, J., Lajoie, B. R., Landt, S. G., Lee, B. K., Pauli, F., Rosenbloom, K. R., Sabo, P., Safi, A., Sanyal, A., … Lochovsky, L. (2012). An Integrated Encyclopedia of DNA Elements in the Human Genome. *Nature*, *489*(7414), 57. https://doi.org/10.1038/NATURE11247

Eckstein, F. (2014). Phosphorothioates, Essential Components of Therapeutic Oligonucleotides. *Https://Home.Liebertpub.Com/Nat*, *24*(6), 374–387. https://doi.org/10.1089/NAT.2014.0506

Eichhorn, S. W., Guo, H., McGeary, S. E., Rodriguez-Mias, R. A., Shin, C., Baek, D., Hsu, S. hao, Ghoshal, K., Villén, J., & Bartel, D. P. (2014). MRNA Destabilization Is the dominant effect of mammalian microRNAs by the time substantial repression ensues. *Molecular Cell*, *56*(1), 104–115. https://doi.org/10.1016/j.molcel.2014.08.028

Escareño, N., Hassan, N., Kogan, M. J., Juárez, J., Topete, A., & Daneri-Navarro, A. (2021). Microfluidics-assisted conjugation of chitosan-coated polymeric nanoparticles with antibodies: Significance in drug release, uptake, and cytotoxicity in breast cancer cells. *Journal of Colloid and Interface Science*, *591*, 440–450. https://doi.org/10.1016/J.JCIS.2021.02.031

Fang, Z., Zhao, J., Xie, W., Sun, Q., Wang, H., & Qiao, B. (2017). LncRNA UCA1 promotes proliferation and cisplatin resistance of oral squamous cell carcinoma by sunppressing miR-184 expression. *Cancer Medicine*, *6*(12), 2897–2908. https://doi.org/10.1002/CAM4.1253

Fattal, E., & Fay, F. (2021). Nanomedicine-based delivery strategies for nucleic acid gene inhibitors in inflammatory diseases. *Advanced Drug Delivery Reviews*, *175*.

https://doi.org/10.1016/J.ADDR.2021.05.019

Feingold, E. A., Good, P. J., Guyer, M. S., Kamholz, S., Liefer, L., Wetterstrand, K., Collins, F. S., Gingeras, T. R., Kampa, D., Sekinger, E. A., Cheng, J., Hirsch, H., Ghosh, S., Zhu, Z., Patel, S., Piccolboni, A., Yang, A., Tammana, H., Bekiranov, S., … Harvey, S. C. (2004). The ENCODE (ENCyclopedia Of DNA Elements) Project. *Science (New York, N.Y.)*, *306*(5696), 636–640. https://doi.org/10.1126/SCIENCE.1105136

Ferlay, J., Colombet, M., Soerjomataram, I., Parkin, D. M., Piñeros, M., Znaor, A., & Bray, F. (2021). Cancer statistics for the year 2020: An overview. *International Journal of Cancer*, *149*(4), 778–789. https://doi.org/10.1002/IJC.33588

Ferrer, M., Izeboud, T., Ferreira, C. G., Span, S. W., Giaccone, G., & Kruyt, F. A. E. (2003). Cisplatin triggers apoptotic or nonapoptotic cell death in Fanconi anemia lymphoblasts in a concentration-dependent manner. *Experimental Cell Research*, *286*(2), 381–395. https://doi.org/10.1016/S0014-4827(03)00112-5

Finnegan, E. F., & Pasquinelli, A. E. (2013). MicroRNA biogenesis: Regulating the regulators. In *Critical Reviews in Biochemistry and Molecular Biology* (Vol. 48, Issue 1, pp. 51–68). NIH Public Access. https://doi.org/10.3109/10409238.2012.738643

Florea, A. M., & Büsselberg, D. (2011). Cisplatin as an anti-tumor drug: cellular mechanisms of activity, drug resistance and induced side effects. *Cancers*, *3*(1), 1351–1371. https://doi.org/10.3390/CANCERS3011351

Foley, N. H., Bray, I. M., Tivnan, A., Bryan, K., Murphy, D. M., Buckley, P. G., Ryan, J., O'meara, A., O'sullivan, M., & Stallings, R. L. (2010). *MicroRNA-184 inhibits neuroblastoma cell survival through targeting the serine/threonine kinase AKT2*. https://doi.org/10.1186/1476-4598-9-83

Foley, N. H., Bray, I. M., Tivnan, A., Bryan, K., Murphy, D. M., Buckley, P. G., Ryan, J., O'Meara, A., O'Sullivan, M., & Stallings, R. L. (2010). MicroRNA-184 inhibits neuroblastoma cell survival through targeting the serine/threonine kinase AKT2. *Molecular Cancer*, *9*. https://doi.org/10.1186/1476-4598-9-83

Fujita, Y., Yagishita, S., Hagiwara, K., Yoshioka, Y., Kosaka, N., Takeshita, F., Fujiwara, T., Tsuta, K., Nokihara, H., Tamura, T., Asamura, H., Kawaishi, M., Kuwano, K., & Ochiya, T. (2015). The Clinical Relevance of the miR-197/CKS1B/STAT3-mediated PD-L1 Network in Chemoresistant Non-small-cell Lung Cancer. *Molecular Therapy*, *23*(4), 717.

https://doi.org/10.1038/MT.2015.10

Gandhi, L., Rodríguez-Abreu, D., Gadgeel, S., Esteban, E., Felip, E., De Angelis, F., Domine, M., Clingan, P., Hochmair, M. J., Powell, S. F., Cheng, S. Y.-S., Bischoff, H. G., Peled, N., Grossi, F., Jennens, R. R., Reck, M., Hui, R., Garon, E. B., Boyer, M., … Garassino, M. C. (2018). Pembrolizumab plus Chemotherapy in Metastatic Non-Small-Cell Lung Cancer. *The New England Journal of Medicine*, *378*(22), 2078–2092. https://doi.org/10.1056/NEJMOA1801005

Gaur, S., Wen, Y., Song, J. H., Parikh, N. U., Mangala, L. S., Blessing, A. M., Ivan, C., Wu, S. Y., Varkaris, A., Shi, Y., Lopez-Berestein, G., Frigo, D. E., Sood, A. K., & Gallick, G. E. (2015a). Chitosan nanoparticle-mediated delivery of miRNA-34a decreases prostate tumor growth in the bone and its expression induces non-canonical autophagy. *Oncotarget*, *6*(30), 29161–29177. https://doi.org/10.18632/ONCOTARGET.4971

Gaur, S., Wen, Y., Song, J. H., Parikh, N. U., Mangala, L. S., Blessing, A. M., Ivan, C., Wu, S. Y., Varkaris, A., Shi, Y., Lopez-Berestein, G., Frigo, D. E., Sood, A. K., & Gallick, G. E. (2015b). Chitosan nanoparticle-mediated delivery of miRNA-34a decreases prostate tumor growth in the bone and its expression induces non-canonical autophagy. *Oncotarget*, *6*(30), 29161–29177. https://doi.org/10.18632/ONCOTARGET.4971

Geary, R. S., Norris, D., Yu, R., & Bennett, C. F. (2015). Pharmacokinetics, biodistribution and cell uptake of antisense oligonucleotides. *Advanced Drug Delivery Reviews*, *87*, 46–51. https://doi.org/10.1016/J.ADDR.2015.01.008

Ghafouri-Fard, S., Shoorei, H., Branicki, W., & Taheri, M. (2020). Non-coding RNA profile in lung cancer. *Experimental and Molecular Pathology*, *114*, 104411. https://doi.org/10.1016/J.YEXMP.2020.104411

Ghormade, V., Pathan, E. K., & Deshpande, M. V. (2017). Can fungi compete with marine sources for chitosan production? *International Journal of Biological Macromolecules*, *104*, 1415–1421. https://doi.org/10.1016/J.IJBIOMAC.2017.01.112

Givan, A. L. (2001). Principles of flow cytometry: an overview. *Methods in Cell Biology*, *63*(63), 19–50. https://doi.org/10.1016/S0091-679X(01)63006-1

Goldstraw, P., Chansky, K., Crowley, J., Rami-Porta, R., Asamura, H., Eberhardt, W. E. E., Nicholson, A. G., Groome, P., Mitchell, A., Bolejack, V., Ball, D., Beer, D. G., Beyruti, R., Detterbeck, F., Edwards, J., Galateau-Sallé, F., Giroux, D., Gleeson, F., Huang, J., … Yokoi,

K. (2016). The IASLC lung cancer staging project: Proposals for revision of the TNM stage groupings in the forthcoming (eighth) edition of the TNM Classification for lung cancer. *Journal of Thoracic Oncology*, *11*(1), 39–51. https://doi.org/10.1016/j.jtho.2015.09.009

Grainger, D. W., & Castner, D. G. (2008). Nanobiomaterials and Nanoanalysis: Opportunities for Improving the Science to Benefit Biomedical Technologies. *Advanced Materials*, *20*(5), 867–877. https://doi.org/10.1002/ADMA.200701760

Griso, A. B., Acero-Riaguas, L., Castelo, B., Cebrián-Carretero, J. L., & Sastre-Perona, A. (2022). Mechanisms of Cisplatin Resistance in HPV Negative Head and Neck Squamous Cell Carcinomas. *Cells*, *11*(3). https://doi.org/10.3390/CELLS11030561

Guo, Q., Wang, H., Xu, Y., Wang, M., & Tian, Z. (2021). miR-374a-5p inhibits non-small cell lung cancer cell proliferation and migration via targeting NCK1. *Experimental and Therapeutic Medicine*, *22*(3). https://doi.org/10.3892/ETM.2021.10375

Hacking, S. A., & Khademhosseini, A. (2013). Cells and Surfaces in vitro. *Biomaterials Science: An Introduction to Materials: Third Edition*, 408–427. https://doi.org/10.1016/B978-0-08-087780-8.00037-1

Hall, M. D., Telma, K. A., Chang, K. E., Lee, T. D., Madigan, J. P., Lloyd, J. R., Goldlust, I. S., Hoeschele, J. D., & Gottesman, M. M. (2014). Say no to DMSO: dimethylsulfoxide inactivates cisplatin, carboplatin, and other platinum complexes. *Cancer Research*, *74*(14), 3913–3922. https://doi.org/10.1158/0008-5472.CAN-14-0247

Hama, M., Ishima, Y., Chuang, V. T. G., Ando, H., Shimizu, T., & Ishida, T. (2021). Evidence for Delivery of Abraxane via a Denatured-Albumin Transport System. *ACS Applied Materials & Interfaces*, *13*(17), 19736–19744. https://doi.org/10.1021/ACSAMI.1C03065

Han, J., Lee, Y., Yeom, K. H., Kim, Y. K., Jin, H., & Kim, V. N. (2004). The Drosha-DGCR8 complex in primary microRNA processing. *Genes and Development*, *18*(24), 3016–3027. https://doi.org/10.1101/gad.1262504

Hanahan, D., & Weinberg, R. A. (2011). Hallmarks of cancer: the next generation. *Cell*, *144*(5), 646–674. https://doi.org/10.1016/J.CELL.2011.02.013

Havens, M. A., Reich, A. A., Duelli, D. M., & Hastings, M. L. (2012). Biogenesis of mammalian microRNAs by a non-canonical processing pathway. *Nucleic Acids Research*, *40*(10), 4626–4640. https://doi.org/10.1093/nar/gks026

Hayashita, Y., Osada, H., Tatematsu, Y., Yamada, H., Yanagisawa, K., Tomida, S., Yatabe, Y.,

Kawahara, K., Sekido, Y., & Takahashi, T. (2005). A Polycistronic MicroRNA Cluster, miR-17-92, Is Overexpressed in Human Lung Cancers and Enhances Cell Proliferation. *Cancer Research*, *65*(21), 9628–9632. https://doi.org/10.1158/0008-5472.CAN-05-2352

He, T. G., Xiao, Z. Y., Xing, Y. Q., Yang, H. J., Qiu, H., & Chen, J. Bin. (2019). Tumor Suppressor miR-184 Enhances Chemosensitivity by Directly Inhibiting SLC7A5 in Retinoblastoma. *Frontiers in Oncology*, *9*. https://doi.org/10.3389/FONC.2019.01163

Heo, Y. A. (2020). Golodirsen: First Approval. *Drugs*, *80*(3), 329–333. https://doi.org/10.1007/S40265-020-01267-2

Herbst, R. S., Morgensztern, D., & Boshoff, C. (2018). The biology and management of non-small cell lung cancer. In *Nature* (Vol. 553, Issue 7689, pp. 446–454). Nature Publishing Group. https://doi.org/10.1038/nature25183

Hirsch, F. R., Scagliotti, G. V., Mulshine, J. L., Kwon, R., Curran, W. J., Wu, Y. L., & Paz-Ares, L. (2017). Lung cancer: current therapies and new targeted treatments. In *The Lancet* (Vol. 389, Issue 10066, pp. 299–311). Lancet Publishing Group. https://doi.org/10.1016/S0140-6736(16)30958-8

Hong, D. S., Kang, Y. K., Borad, M., Sachdev, J., Ejadi, S., Lim, H. Y., Brenner, A. J., Park, K., Lee, J. L., Kim, T. Y., Shin, S., Becerra, C. R., Falchook, G., Stoudemire, J., Martin, D., Kelnar, K., Peltier, H., Bonato, V., Bader, A. G., … Beg, M. S. (2020a). Phase 1 study of MRX34, a liposomal miR-34a mimic, in patients with advanced solid tumours. *British Journal of Cancer*, *122*(11), 1630–1637. https://doi.org/10.1038/S41416-020-0802-1

Hong, D. S., Kang, Y. K., Borad, M., Sachdev, J., Ejadi, S., Lim, H. Y., Brenner, A. J., Park, K., Lee, J. L., Kim, T. Y., Shin, S., Becerra, C. R., Falchook, G., Stoudemire, J., Martin, D., Kelnar, K., Peltier, H., Bonato, V., Bader, A. G., … Beg, M. S. (2020b). Phase 1 study of MRX34, a liposomal miR-34a mimic, in patients with advanced solid tumours. *British Journal of Cancer*, *122*(11), 1630–1637. https://doi.org/10.1038/S41416-020-0802-1

Hoseinpur, R., Hasani, A., Baradaran, B., Abdolalizadeh, J., Amini, Y., Salehi, R., Samadi Kafil, H., Azizian, K., Memar, M. Y., Gholizadeh, P., & Hasani, A. (2022). Chitosan nanoparticles containing fusion protein (Hspx-PPE44-EsxV) and resiquimod adjuvant (HPERC) as a novel booster vaccine for Mycobacterium tuberculosis. *Journal of Biomaterials Applications*, 088532822210791. https://doi.org/10.1177/08853282221079105

Hou, K., Zhao, J., Wang, H., Li, B., Li, K., Shi, X., Wan, K., Ai, J., Lv, J., Wang, D., Huang, Q., Wang,

H., Cao, Q., Liu, S., & Tang, Z. (2020). Chiral gold nanoparticles enantioselectively rescue memory deficits in a mouse model of Alzheimer's disease. *Nature Communications 2020 11:1*, *11*(1), 1–11. https://doi.org/10.1038/s41467-020-18525-2

Howell, S. B., Safaei, R., Larson, C. A., & Sailor, M. J. (2010). Copper Transporters and the Cellular Pharmacology of the Platinum-Containing Cancer Drugs. *Molecular Pharmacology*, *77*(6), 887. https://doi.org/10.1124/MOL.109.063172

Huang, B., Wu, G., Peng, C., Peng, X., Huang, M., Ding, J., Zhang, H., & Wu, X. (2021). miR-126 regulates the proliferation, migration, invasion, and apoptosis of non-small lung cancer cells via AKT2/HK2 axis. *IUBMB Life*. https://doi.org/10.1002/IUB.2531

Huang, G., Chen, Q., Hu, J., Mao, J., He, Y., Bai, H., & Tang, G. (2021). Chitosan-derived nanoparticles impede signal transduction in T790M lung cancer therapy. *Biomaterials Science*, *9*(22), 7412–7419. https://doi.org/10.1039/D1BM01133B

Huang, J., Kong, W., Zhang, J., Chen, Y. H., Xue, W., Liu, D., & Huang, Y. (2016a). C-Myc modulates glucose metabolism via regulation of miR184/PKM2 pathway in clear-cell renal cell carcinoma. *International Journal of Oncology*, *49*(4), 1569–1575. https://doi.org/10.3892/IJO.2016.3622/HTML

Huang, J., Kong, W., Zhang, J., Chen, Y. H., Xue, W., Liu, D., & Huang, Y. (2016b). C-Myc modulates glucose metabolism via regulation of miR184/PKM2 pathway in clear-cell renal cell carcinoma. *International Journal of Oncology*, *49*(4), 1569–1575. https://doi.org/10.3892/IJO.2016.3622/HTML

Hung, L. D., Irie, H., Goshima, M., & Sakai, S. (2007). Utilization of SECDED for soft error and variation-induced defect tolerance in caches. *Proceedings -Design, Automation and Test in Europe, DATE*, 1134–1139. https://doi.org/10.1109/DATE.2007.364447

Hussain, M. T., Tiboni, M., Perrie, Y., & Casettari, L. (2020). Microfluidic production of protein loaded chimeric stealth liposomes. *International Journal of Pharmaceutics*, *590*, 119955. https://doi.org/10.1016/J.IJPHARM.2020.119955

Hutcherson, S. L., & Lanz, R. (2002). A randomized controlled clinical trial of intravitreous fomivirsen for treatment of newly diagnosed peripheral cytomegalovirus retinitis in patients with aids. *American Journal of Ophthalmology*, *133*(4), 467–474. https://doi.org/10.1016/S0002-9394(02)01327-2

INTERFERin - siRNA / miRNA transfection reagent. (n.d.). Retrieved June 11, 2022, from

https://www.polyplus-transfection.com/products/interferin/

Jaroszeski, M. J., & Radcliff, G. (1999). Fundamentals of flow cytometry. *Molecular Biotechnology*, *11*(1), 37–53. https://doi.org/10.1007/BF02789175

Järver, P., Coursindel, T., Andaloussi, S. El, Godfrey, C., Wood, M. J., & Gait, M. J. (2012). Peptide-mediated cell and in vivo delivery of antisense oligonucleotides and siRNA. *Molecular Therapy - Nucleic Acids*, *1*(6), e27. https://doi.org/10.1038/mtna.2012.18

Jason, T. L. H., Koropatnick, J., & Berg, R. W. (2004a). Toxicology of antisense therapeutics. *Toxicology and Applied Pharmacology*, *201*(1), 66–83. https://doi.org/10.1016/j.taap.2004.04.017

Jason, T. L. H., Koropatnick, J., & Berg, R. W. (2004b). Toxicology of antisense therapeutics. *Toxicology and Applied Pharmacology*, *201*(1), 66–83. https://doi.org/10.1016/J.TAAP.2004.04.017

Jesus, S., Marques, A. P., Duarte, A., Soares, E., Costa, J. P., Colaço, M., Schmutz, M., Som, C., Borchard, G., Wick, P., & Borges, O. (2020). Chitosan Nanoparticles: Shedding Light on Immunotoxicity and Hemocompatibility. *Frontiers in Bioengineering and Biotechnology*, *8*, 100. https://doi.org/10.3389/FBIOE.2020.00100/BIBTEX

Jia, L., Zhou, Z., Liang, H., Wu, J., Shi, P., Li, F., Wang, Z., Wang, C., Chen, W., Zhang, H., Wang, Y., Liu, R., Feng, J., & Chen, C. (2016). KLF5 promotes breast cancer proliferation, migration and invasion in part by upregulating the transcription of TNFAIP2. *Oncogene*, *35*(16), 2040–2051. https://doi.org/10.1038/ONC.2015.263

Jiang, L. P., He, C. Y., & Zhu, Z. T. (2017). Role of microRNA-21 in radiosensitivity in non-small cell lung cancer cells by targeting PDCD4 gene. *Oncotarget*, *8*(14), 23675–23689. https://doi.org/10.18632/oncotarget.15644

Juliano, R. L. (2016). The delivery of therapeutic oligonucleotides. In *Nucleic Acids Research* (Vol. 44, Issue 14, pp. 6518–6548). Oxford University Press. https://doi.org/10.1093/nar/gkw236

Kaban, K., Salva, E., & Akbuga, J. (2016). The effects of chitosan/miR-200c nanoplexes on different stages of cancers in breast cancer cell lines. *European Journal of Pharmaceutical Sciences : Official Journal of the European Federation for Pharmaceutical Sciences*, *95*, 103–110. https://doi.org/10.1016/J.EJPS.2016.05.030

Kaban, K., Salva, E., & Akbuga, J. (2017). In Vitro Dose Studies on Chitosan Nanoplexes for

microRNA Delivery in Breast Cancer Cells. *Nucleic Acid Therapeutics*, *27*(1), 45–55. https://doi.org/10.1089/NAT.2016.0633

Kaban, K., Salva, E., & Akbuga, J. (2019). Modulation of the dual-faced effects of miR-141 with chitosan/miR-141 nanoplexes in breast cancer cells. *The Journal of Gene Medicine*, *21*(9). https://doi.org/10.1002/JGM.3116

Kadlecova, Z., Rajendra, Y., Matasci, M., Baldi, L., Hacker, D. L., Wurm, F. M., & Klok, H. A. (2013). DNA delivery with hyperbranched polylysine: A comparative study with linear and dendritic polylysine. *Journal of Controlled Release*, *169*(3), 276–288. https://doi.org/10.1016/J.JCONREL.2013.01.019

Karger, S., Jiang, G.-N., Lin, L., Tu, H.-B., Wu, L., & Liu, M. (2016). MicroRNA-21 Regulates Non-Small Cell Lung Cancer Cell Invasion and Chemo-Sensitivity through SMAD7. *Cell Physiol Biochem*, *38*, 2152–2162. https://doi.org/10.1159/000445571

Kaufmann, S. H., Lee, S. H., Meng, X. W., Loegering, D. A., Kottke, T. J., Henzing, A. J., Ruchaud, S., Samejima, K., & Earnshaw, W. C. (2008). Apoptosis-associated caspase activation assays. *Methods*, *44*(3), 262–272. https://doi.org/10.1016/J.YMETH.2007.11.005

Khadke, S., Roces, C. B., Donaghey, R., Giacobbo, V., Su, Y., & Perrie, Y. (2020). Scalable solvent-free production of liposomes. *The Journal of Pharmacy and Pharmacology*, *72*(10), 1328–1340. https://doi.org/10.1111/JPHP.13329

Khvorova, A., Reynolds, A., & Jayasena, S. D. (2003). Functional siRNAs and miRNAs exhibit strand bias. *Cell*, *115*(2), 209–216. https://doi.org/10.1016/S0092-8674(03)00801-8

Khvorova, A., & Watts, J. K. (2017a). The chemical evolution of oligonucleotide therapies of clinical utility. *Nature Biotechnology*, *35*(3), 238–248. https://doi.org/10.1038/NBT.3765

Khvorova, A., & Watts, J. K. (2017b). The chemical evolution of oligonucleotide therapies of clinical utility. In *Nature Biotechnology* (Vol. 35, Issue 3, pp. 238–248). Nature Publishing Group. https://doi.org/10.1038/nbt.3765

Kobayashi, H., & Tomari, Y. (2016). RISC assembly: Coordination between small RNAs and Argonaute proteins. In *Biochimica et Biophysica Acta - Gene Regulatory Mechanisms* (Vol. 1859, Issue 1, pp. 71–81). Elsevier. https://doi.org/10.1016/j.bbagrm.2015.08.007

Kondratiev, S., Duraisamy, S., Unitt, C. L., Green, M. R., Pinkus, G. S., Shipp, M. A., Kutok, J. L., Drapkin, R. I., & Rodig, S. J. (2011). Aberrant expression of the dendritic cell marker TNFAIP2 by the malignant cells of Hodgkin lymphoma and primary mediastinal large B

cell lymphoma distinguishes these tumor types from morphologically and phenotypically similar lymphomas. *The American Journal of Surgical Pathology*, *35*(10), 1531. https://doi.org/10.1097/PAS.0B013E31822BD476

Kong, Q., Shu, N., Li, J., & Xu, N. (2018). miR-641 Functions as a Tumor Suppressor by Targeting MDM2 in Human Lung Cancer. *Oncology Research*, *26*(5), 735. https://doi.org/10.3727/096504017X15021536183490

Kotzé, A. F., Lueßen, H. L., De Boer, A. G., Verhoef, J. C., & Junginger, H. E. (1999). Chitosan for enhanced intestinal permeability: Prospects for derivatives soluble in neutral and basic environments. *European Journal of Pharmaceutical Sciences*, *7*(2), 145–151. https://doi.org/10.1016/S0928-0987(98)00016-5

Koukaras, E. N., Papadimitriou, S. A., Bikiaris, D. N., & Froudakis, G. E. (2012). Insight on the formation of chitosan nanoparticles through ionotropic gelation with tripolyphosphate. *Molecular Pharmaceutics*, *9*(10), 2856–2862. https://doi.org/10.1021/MP300162J

Kroemer, G., Galluzzi, L., Kepp, O., & Zitvogel, L. (2013). Immunogenic Cell Death in Cancer Therapy. *Http://Dx.Doi.Org/10.1146/Annurev-Immunol-032712-100008*, *31*, 51–72. https://doi.org/10.1146/ANNUREV-IMMUNOL-032712-100008

Krug, H. F., & Wick, P. (2011). Nanotoxicology: An Interdisciplinary Challenge. *Angewandte Chemie International Edition*, *50*(6), 1260–1278. https://doi.org/10.1002/ANIE.201001037

Kumar, G., Degheidy, H., Casey, B. J., & Goering, P. L. (2015). Flow cytometry evaluation of in vitro cellular necrosis and apoptosis induced by silver nanoparticles. *Food and Chemical Toxicology*, *85*, 45–51. https://doi.org/10.1016/J.FCT.2015.06.012

Kumirska, J., Weinhold, M. X., Thöming, J., & Stepnowski, P. (2011). Biomedical Activity of Chitin/Chitosan Based Materials—Influence of Physicochemical Properties Apart from Molecular Weight and Degree of N-Acetylation. *Polymers 2011, Vol. 3, Pages 1875-1901*, *3*(4), 1875–1901. https://doi.org/10.3390/POLYM3041875

Lagos-Quintana, M., Rauhut, R., Lendeckel, W., & Tuschl, T. (2001). Identification of novel genes coding for small expressed RNAs. *Science (New York, N.Y.)*, *294*(5543), 853–858. https://doi.org/10.1126/SCIENCE.1064921

Lan, W., Li, S., Xu, J., & Luo, G. (2010). One-step synthesis of chitosan-silica hybrid microspheres in a microfluidic device. *Biomedical Microdevices 2010 12:6*, *12*(6), 1087–

1095. https://doi.org/10.1007/S10544-010-9463-9

Lau, N. C., Lim, L. P., Weinstein, E. G., & Bartel, D. P. (2001). An abundant class of tiny RNAs with probable regulatory roles in Caenorhabditis elegans. *Science (New York, N.Y.)*, *294*(5543), 858–862. https://doi.org/10.1126/SCIENCE.1065062

Lee, Feinbaum, R. L., & Ambros, V. (1993). The C. elegans heterochronic gene lin-4 encodes small RNAs with antisense complementarity to lin-14. *Cell*, *75*(5), 843–854. https://doi.org/10.1016/0092-8674(93)90529-Y

Lee, Khan, S. A., & Lim, K. H. (2011). Gelatin nanoparticle preparation by nanoprecipitation. *Journal of Biomaterials Science. Polymer Edition*, *22*(4–6), 753–771. https://doi.org/10.1163/092050610X492093

Lee, S. W. L., Paoletti, C., Campisi, M., Osaki, T., Adriani, G., Kamm, R. D., Mattu, C., & Chiono, V. (2019). MicroRNA delivery through nanoparticles. *Journal of Controlled Release : Official Journal of the Controlled Release Society*, *313*, 80–95. https://doi.org/10.1016/J.JCONREL.2019.10.007

Lemjabbar-Alaoui, H., Hassan, O. U. I., Yang, Y. W., & Buchanan, P. (2015). Lung cancer: Biology and treatment options. *Biochimica et Biophysica Acta*, *1856*(2), 189–210. https://doi.org/10.1016/J.BBCAN.2015.08.002

Li, F., Wang, F., Zhu, C., Wei, Q., Zhang, T., & Zhou, Y. L. (2018). miR-221 suppression through nanoparticle-based miRNA delivery system for hepatocellular carcinoma therapy and its diagnosis as a potential biomarker. *International Journal of Nanomedicine*, *13*, 2295–2307. https://doi.org/10.2147/IJN.S157805

Li, J., Song, Y., Yu, B., & Yu, Y. (2020). TNFAIP2 Promotes Non-Small Cell Lung Cancer Cells and Targeted by miR-145-5p. *Https://Home.Liebertpub.Com/Dna*, *39*(7), 1256–1263. https://doi.org/10.1089/DNA.2020.5415

Li, K., Qiu, Y., Liu, X., & Huang, F. (2022). Biomimetic Nanosystems for the Synergistic Delivery of miR-144/451a for Oral Squamous Cell Carcinoma. *Balkan Medical Journal*. https://doi.org/10.4274/BALKANMEDJ.GALENOS.2022.2021-11-1

Li, L., He, D., Guo, Q., Zhang, Z., Ru, D., Wang, L., Gong, K., Liu, F., Duan, Y., & Li, H. (2022). Exosome-liposome hybrid nanoparticle codelivery of TP and miR497 conspicuously overcomes chemoresistant ovarian cancer. *Journal of Nanobiotechnology*, *20*(1). https://doi.org/10.1186/S12951-022-01264-5

Li, M., Zhang, Y. Y., Shang, J., & Xu, Y. D. (2019). LncRNA SNHG5 promotes cisplatin resistance in gastric cancer via inhibiting cell apoptosis. *European Review for Medical and Pharmacological Sciences*, *23*(10), 4185–4191. https://doi.org/10.26355/EURREV_201905_17921

Li, Q. Q., Xie, Y. K., Wu, Y., Li, L. L., Liu, Y., Miao, X. B., Liu, Q. Z., Yao, K. T., & Xiao, G. H. (2017). Sulforaphane inhibits cancer stem-like cell properties and cisplatin resistance through miR-214-mediated downregulation of c-MYC in non-small cell lung cancer. *Oncotarget*, *8*(7), 12067–12080. https://doi.org/10.18632/ONCOTARGET.14512

Li, S., Li, H., Ge, W., Song, K., Yuan, C., & Yin, R. (2020). Effect of miR-184 on Proliferation and Apoptosis of Pancreatic Ductal Adenocarcinoma and Its Mechanism. *Technology in Cancer Research & Treatment*, *19*. https://doi.org/10.1177/1533033820943237

Li, X., Chen, C., Wang, Z., Liu, J., Sun, W., Shen, K., Lv, Y., Zhu, S., Zhan, P., Lv, T., & Song, Y. (2021). Elevated exosome-derived miRNAs predict osimertinib resistance in non-small cell lung cancer. *Cancer Cell International*, *21*(1). https://doi.org/10.1186/S12935-021-02075-8

Liang, C. C., Park, A. Y., & Guan, J. L. (2007). In vitro scratch assay: a convenient and inexpensive method for analysis of cell migration in vitro. *Nature Protocols 2007 2:2*, *2*(2), 329–333. https://doi.org/10.1038/nprot.2007.30

Lin, T. C., Lin, P. L., Cheng, Y. W., Wu, T. C., Chou, M. C., Chen, C. Y., & Lee, H. (2015). MicroRNA-184 Deregulated by the MicroRNA-21 Promotes Tumor Malignancy and Poor Outcomes in Non-small Cell Lung Cancer via Targeting CDC25A and c-Myc. *Annals of Surgical Oncology*, *22 Suppl 3*, 1532–1539. https://doi.org/10.1245/S10434-015-4595-Z

Ling, H., Fabbri, M., & Calin, G. A. (2013). MicroRNAs and other non-coding RNAs as targets for anticancer drug development. In *Nature Reviews Drug Discovery* (Vol. 12, Issue 11, pp. 847–865). NIH Public Access. https://doi.org/10.1038/nrd4140

Litovchick, L. (2018). Immunoblotting: Transfer of Proteins from Gels to Membranes. *Cold Spring Harbor Protocols*, *2018*(10), 818–824. https://doi.org/10.1101/PDB.PROT098442

Liu, B., Peng, X. C., Zheng, X. L., Wang, J., & Qin, Y. W. (2009). MiR-126 restoration down-regulate VEGF and inhibit the growth of lung cancer cell lines in vitro and in vivo. *Lung Cancer (Amsterdam, Netherlands)*, *66*(2), 169–175. https://doi.org/10.1016/J.LUNGCAN.2009.01.010

Liu, H., Wang, Y., Wang, Y., Wu, D., & Zhang, H. (2021). miR-199a-3p plays an anti-tumorigenic role in lung adenocarcinoma by suppressing anterior gradient 2. *Https://Doi.Org/10.1080/21655979.2021.1967009*, *12*(1), 7859–7871. https://doi.org/10.1080/21655979.2021.1967009

Liu, Li, Fan, J., Ai, G., Liu, J., Luo, N., Li, C., & Cheng, Z. (2019). *Berberine in combination with cisplatin induces necroptosis and apoptosis in ovarian cancer cells*. https://doi.org/10.1186/s40659-019-0243-6

Liu, Lihua, Liu, L., & Lu, S. (2019). lncRNA H19 promotes viability and epithelial-mesenchymal transition of lung adenocarcinoma cells by targeting miR-29b-3p and modifying STAT3. *International Journal of Oncology*, *54*(3), 929. https://doi.org/10.3892/IJO.2019.4695

LIU, M., GAO, J., HUANG, Q., JIN, Y., & WEI, Z. (2016). Downregulating microRNA-144 mediates a metabolic shift in lung cancer cells by regulating GLUT1 expression. *Oncology Letters*, *11*(6), 3772. https://doi.org/10.3892/OL.2016.4468

Liu, T., Zhu, J., Du, W., Ning, W., Zhang, Y., Zeng, Y., Liu, Z., & Huang, J. A. (2020). AKT2 drives cancer progression and is negatively modulated by miR-124 in human lung adenocarcinoma. *Respiratory Research*, *21*(1). https://doi.org/10.1186/S12931-020-01491-0

Liu, Y., Zhang, Z., Li, Q., Zhang, L., Cheng, Y., & Zhong, Z. (2020). Mitochondrial APE1 promotes cisplatin resistance by downregulating ROS in osteosarcoma. *Oncology Reports*, *44*(2), 499–508. https://doi.org/10.3892/OR.2020.7633

Liu, Yu, Z., Yuan, S., Xie, W., Li, C., Hu, Z., Xiang, Y., Wu, N., Wu, L., Bai, L., & Li, Y. (2017). Circulating exosomal microRNAs as prognostic biomarkers for non-small-cell lung cancer. *Oncotarget*, *8*(8), 13048–13058. https://doi.org/10.18632/ONCOTARGET.14369

Liu, Zhen, Mai, C., Yang, H., Zhen, Y., Yu, X., Hua, S., Wu, Q., Jiang, Q., Zhang, Y., Song, X., & Fang, W. (2014). Candidate tumour suppressor CCDC19 regulates miR-184 direct targeting of C-Myc thereby suppressing cell growth in non-small cell lung cancers. *Journal of Cellular and Molecular Medicine*, *18*(8), 1667–1679. https://doi.org/10.1111/JCMM.12317

Liu, Zhensheng, Wei, S., Ma, H., Zhao, M., Myers, J. N., Weber, R. S., Sturgis, E. M., & Wei, Q. (2011). A functional variant at the miR-184 binding site in TNFAIP2 and risk of squamous cell carcinoma of the head and neck. *Carcinogenesis*, *32*(11), 1668.

https://doi.org/10.1093/CARCIN/BGR209

Livak, K. J., & Schmittgen, T. D. (2001). Analysis of Relative Gene Expression Data Using Real-Time Quantitative PCR and the 2−ΔΔCT Method. *Methods*, *25*(4), 402–408. https://doi.org/10.1006/METH.2001.1262

Lokugamage, M. P., Vanover, D., Beyersdorf, J., Hatit, M. Z. C., Rotolo, L., Echeverri, E. S., Peck, H. E., Ni, H., Yoon, J. K., Kim, Y. T., Santangelo, P. J., & Dahlman, J. E. (2021). Optimization of lipid nanoparticles for the delivery of nebulized therapeutic mRNA to the lungs. *Nature Biomedical Engineering 2021 5:9*, *5*(9), 1059–1068. https://doi.org/10.1038/s41551-021-00786-x

Longqiu, W. U., Chi, L. I. U., & Zhang, Z. (2020). Knockdown of lncRNA MIAT inhibits proliferation and cisplatin resistance in non-small cell lung cancer cells by increasing miR-184 expression. *Oncology Letters*, *19*(1), 533–541. https://doi.org/10.3892/OL.2019.11084

Loren, P., Saavedra, N., Saavedra, K., Zambrano, T., Moriel, P., & Salazar, L. A. (2021). Epigenetic Mechanisms Involved in Cisplatin-Induced Nephrotoxicity: An Update. *Pharmaceuticals*, *14*(6). https://doi.org/10.3390/PH14060491

Lou, G., Anderluzzi, G., Schmidt, S. T., Woods, S., Gallorini, S., Brazzoli, M., Giusti, F., Ferlenghi, I., Johnson, R. N., Roberts, C. W., O'Hagan, D. T., Baudner, B. C., & Perrie, Y. (2020). Delivery of self-amplifying mRNA vaccines by cationic lipid nanoparticles: The impact of cationic lipid selection. *Journal of Controlled Release : Official Journal of the Controlled Release Society*, *325*, 370–379. https://doi.org/10.1016/J.JCONREL.2020.06.027

Louw, A. M., Kolar, M. K., Novikova, L. N., Kingham, P. J., Wiberg, M., Kjems, J., & Novikov, L. N. (2016). Chitosan polyplex mediated delivery of miRNA-124 reduces activation of microglial cells in vitro and in rat models of spinal cord injury. *Nanomedicine : Nanotechnology, Biology, and Medicine*, *12*(3), 643–653. https://doi.org/10.1016/J.NANO.2015.10.011

Lu, M., Zhao, X., Xing, H., Liu, H., Lang, L., Yang, T., Xun, Z., Wang, D., & Ding, P. (2019). Cell-free synthesis of connexin 43-integrated exosome-mimetic nanoparticles for siRNA delivery. *Acta Biomaterialia*, *96*, 517–536. https://doi.org/10.1016/J.ACTBIO.2019.07.006

Luanpitpong, S., Angsutararux, P., Samart, P., Chanthra, N., Chanvorachote, P., & Issaragrisil,

S. (2017). Hyper-O-GlcNAcylation induces cisplatin resistance via regulation of p53 and c-Myc in human lung carcinoma. *Scientific Reports*, *7*(1). https://doi.org/10.1038/S41598-017-10886-X

Lucas, D., Scheiermann, C., Chow, A., Kunisaki, Y., Bruns, I., Barrick, C., Tessarollo, L., & Frenette, P. S. (2013). Chemotherapy-induced bone marrow nerve injury impairs hematopoietic regeneration. *Nature Medicine*, *19*(6), 695–703. https://doi.org/10.1038/NM.3155

MacRae, I. J., Zhou, K., & Doudna, J. A. (2007). Structural determinants of RNA recognition and cleavage by Dicer. *Nature Structural & Molecular Biology*, *14*(10), 934–940. https://doi.org/10.1038/NSMB1293

Maghsoudnia, N., Baradaran Eftekhari, R., Naderi Sohi, A., Norouzi, P., Akbari, H., Ghahremani, M. H., Soleimani, M., Amini, M., Samadi, H., & Dorkoosh, F. A. (2020). Mitochondrial delivery of microRNA mimic let-7b to NSCLC cells by PAMAM-based nanoparticles. *Https://Doi.Org/10.1080/1061186X.2020.1774594*, *28*(7–8), 818–830. https://doi.org/10.1080/1061186X.2020.1774594

Majedi, F. S., Hasani-Sadrabadi, M. M., Hojjati Emami, S., Shokrgozar, M. A., Vandersarl, J. J., Dashtimoghadam, E., Bertsch, A., & Renaud, P. (2012). Microfluidic assisted self-assembly of chitosan based nanoparticles as drug delivery agents. *Lab on a Chip*, *13*(2), 204–207. https://doi.org/10.1039/C2LC41045A

Majedi, F. S., Hasani-Sadrabadi, M. M., Hojjati Emami, S., Shokrgozar, M. A., Vandersarl, J. J., Dashtimoghadam, E., Bertsch, A., & Renaud, P. (2013). Microfluidic assisted self-assembly of chitosan based nanoparticles as drug delivery agents. *Lab on a Chip*, *13*(2), 204–207. https://doi.org/10.1039/C2LC41045A

Majedi, F. S., Hasani-Sadrabadi, M. M., Vandersarl, J. J., Mokarram, N., Hojjati-Emami, S., Dashtimoghadam, E., Bonakdar, S., Shokrgozar, M. A., Bertsch, A., & Renaud, P. (2014). On-Chip Fabrication of Paclitaxel-Loaded Chitosan Nanoparticles for Cancer Therapeutics. *Advanced Functional Materials*, *24*(4), 432–441. https://doi.org/10.1002/ADFM.201301628

Makovec, T. (2019). Cisplatin and beyond: molecular mechanisms of action and drug resistance development in cancer chemotherapy. *Radiology and Oncology*, *53*(2), 148–158. https://doi.org/10.2478/RAON-2019-0018

Malik, S., Lim, J., Slack, F. J., Braddock, D. T., & Bahal, R. (2020). Next generation miRNA inhibition using short anti-seed PNAs encapsulated in PLGA nanoparticles. *Journal of Controlled Release : Official Journal of the Controlled Release Society*, *327*, 406–419. https://doi.org/10.1016/J.JCONREL.2020.08.026

Malzkorn, B., Wolter, M., Liesenberg, F., Grzendowski, M., Stühler, K., Meyer, H. E., & Reifenberger, G. (2010). Identification and functional characterization of microRNAs involved in the malignant progression of gliomas. *Brain Pathology (Zurich, Switzerland)*, *20*(3), 539–550. https://doi.org/10.1111/J.1750-3639.2009.00328.X

Mao, F., Zhang, J., Cheng, X., & Xu, Q. (2019). miR-149 inhibits cell proliferation and enhances chemosensitivity by targeting CDC42 and BCL2 in neuroblastoma. *Cancer Cell International*, *19*(1). https://doi.org/10.1186/S12935-019-1082-9

Martin, P. (1995). A New Access to 2'-O-Alkylated Ribonucleosides and Properties of 2'-O-Alkylated Oligoribonucleotides. *Helvetica Chimica Acta*, *78*(2), 486–504. https://doi.org/10.1002/HLCA.19950780219

Masoodi, K. Z., Lone, S. M., & Rasool, R. S. (2021). Agarose gel electrophoresis. *Advanced Methods in Molecular Biology and Biotechnology*, 7–12. https://doi.org/10.1016/B978-0-12-824449-4.00002-5

Matica, M. A., Aachmann, F. L., Tøndervik, A., Sletta, H., & Ostafe, V. (2019). Chitosan as a Wound Dressing Starting Material: Antimicrobial Properties and Mode of Action. *International Journal of Molecular Sciences*, *20*(23). https://doi.org/10.3390/IJMS20235889

McGowan, M. P., Tardif, J. C., Ceska, R., Burgess, L. J., Soran, H., Gouni-Berthold, I., Wagener, G., & Chasan-Taber, S. (2012). Randomized, placebo-controlled trial of mipomersen in patients with severe hypercholesterolemia receiving maximally tolerated lipid-lowering therapy. *PloS One*, *7*(11). https://doi.org/10.1371/JOURNAL.PONE.0049006

McIlwain, D. R., Berger, T., & Mak, T. W. (2013). Caspase functions in cell death and disease. *Cold Spring Harbor Perspectives in Biology*, *5*(4), 1–28. https://doi.org/10.1101/CSHPERSPECT.A008656

McKiernan, P. J., Cunningham, O., Greene, C. M., & Cryan, S. A. (2013). Targeting miRNA-based medicines to cystic fibrosis airway epithelial cells using nanotechnology. *International Journal of Nanomedicine*, *8*, 3907–3915. https://doi.org/10.2147/IJN.S47551

Mello, D. F., Trevisan, R., Rivera, N., Geitner, N. K., Di Giulio, R. T., Wiesner, M. R., Hsu-Kim, H., & Meyer, J. N. (2020). Caveats to the use of MTT, neutral red, Hoechst and Resazurin to measure silver nanoparticle cytotoxicity. *Chemico-Biological Interactions*, *315*, 108868. https://doi.org/10.1016/J.CBI.2019.108868

Mi, Y., Mueller, T., & Kreibich, S. (2019). Multi-omic measurements of heterogeneity in HeLa cells across laboratories. *Nature Biotechnology*. https://doi.org/10.1038/s41587-019-0037-y

Miele, D., Xia, X., Catenacci, L., Sorrenti, M., Rossi, S., Sandri, G., Ferrari, F., Rossi, J. J., & Bonferoni, M. C. (2021). Chitosan Oleate Coated PLGA Nanoparticles as siRNA Drug Delivery System. *Pharmaceutics*, *13*(10). https://doi.org/10.3390/PHARMACEUTICS13101716

Miller, M., & Hanna, N. (2021). Advances in systemic therapy for non-small cell lung cancer. *BMJ*, *375*. https://doi.org/10.1136/BMJ.N2363

Miller, R. P., Tadagavadi, R. K., Ramesh, G., & Reeves, W. B. (2010). Mechanisms of Cisplatin nephrotoxicity. *Toxins*, *2*(11), 2490–2518. https://doi.org/10.3390/TOXINS2112490

Morabito, A. (2018). Second-line treatment for advanced NSCLC without actionable mutations: Is immunotherapy the “panacea” for all patients? In *BMC Medicine* (Vol. 16, Issue 1, p. 24). BioMed Central Ltd. https://doi.org/10.1186/s12916-018-1011-0

Muxika, A., Etxabide, A., Uranga, J., Guerrero, P., & de la Caba, K. (2017). Chitosan as a bioactive polymer: Processing, properties and applications. *International Journal of Biological Macromolecules*, *105*(Pt 2), 1358–1368. https://doi.org/10.1016/J.IJBIOMAC.2017.07.087

Nafee, N., Taetz, S., Schneider, M., Schaefer, U. F., & Lehr, C. M. (2007). Chitosan-coated PLGA nanoparticles for DNA/RNA delivery: effect of the formulation parameters on complexation and transfection of antisense oligonucleotides. *Nanomedicine: Nanotechnology, Biology and Medicine*, *3*(3), 173–183. https://doi.org/10.1016/J.NANO.2007.03.006

Nan, Y., & Zhang, Y. J. (2018). Antisense phosphorodiamidate morpholino oligomers as novel antiviral compounds. *Frontiers in Microbiology*, *9*(APR), 750. https://doi.org/10.3389/FMICB.2018.00750/BIBTEX

Nasti, A., Zaki, N. M., De Leonardis, P., Ungphaiboon, S., Sansongsak, P., Rimoli, M. G., & Tirelli,

N. (2009). Chitosan/TPP and chitosan/TPP-hyaluronic acid nanoparticles: systematic optimisation of the preparative process and preliminary biological evaluation. *Pharmaceutical Research*, *26*(8), 1918–1930. https://doi.org/10.1007/S11095-009-9908-0

Navarro, E., Serrano-Heras, G., Castaño, M. J., & Solera, J. (2015). Real-time PCR detection chemistry. *Clinica Chimica Acta*, *439*, 231–250. https://doi.org/10.1016/J.CCA.2014.10.017

Naylor, E. C., Desani, J. K., & Chung, P. K. (2016). Targeted Therapy and Immunotherapy for Lung Cancer. In *Surgical Oncology Clinics of North America* (Vol. 25, Issue 3, pp. 601–609). W.B. Saunders. https://doi.org/10.1016/j.soc.2016.02.011

Nazir, A., Khenoussi, N., Schacher, L., Hussain, T., Adolphe, D., & Hekmati, A. H. (2015). Using the Taguchi method to investigate the effect of different parameters on mean diameter and variation in PA-6 nanofibres produced by needleless electrospinning. *RSC Advances*, *5*(94), 76892–76897. https://doi.org/10.1039/C5RA13649K

Nguyen, M. A., Wyatt, H., Susser, L., Geoffrion, M., Rasheed, A., Duchez, A. C., Cottee, M. L., Afolayan, E., Farah, E., Kahiel, Z., Cote, M., Gadde, S., & Rayner, K. J. (2019). Delivery of MicroRNAs by Chitosan Nanoparticles to Functionally Alter Macrophage Cholesterol Efflux in Vitro and in Vivo. *ACS Nano*, *13*(6), 6491–6505. https://doi.org/10.1021/ACSNANO.8B09679

Nguyen, M., Wyatt, H., Susser, L., Geoffrion, M., Rasheed, A., Duchez, A.-C., Cottee, M. L., Afolayan, E., Farah, E., Kahiel, Z., Cô Té, Té, M., Gadde, S., & Rayner, K. J. (2019). *Delivery of MicroRNAs by Chitosan Nanoparticles to Functionally Alter Macrophage Cholesterol Efflux in Vitro and in Vivo*. https://doi.org/10.1021/acsnano.8b09679

Ni, Q., Gu, Y., Xie, Y., Yin, Q., Zhang, H., Nie, A., Li, W., Wang, Y., Ning, G., Wang, W., & Wang, Q. (2017). Raptor regulates functional maturation of murine beta cells. *Nature Communications*, *8*, 15755. https://doi.org/10.1038/NCOMMS15755

Nielsen, P. E., Egholm, M., Berg, R. H., & Buchardt, O. (1991). Sequence-Selective Recognition of DNA by Strand Displacement with a Thymine-Substituted Polyamide. *Science*, *254*(5037), 1497–1500. https://doi.org/10.1126/SCIENCE.1962210

Ning, Q., Liu, Y. F., Ye, P. J., Gao, P., Li, Z. P., Tang, S. Y., He, D. X., Tang, S. S., Wei, H., & Yu, C. Y. (2019). Delivery of Liver-Specific miRNA-122 Using a Targeted Macromolecular

Prodrug toward Synergistic Therapy for Hepatocellular Carcinoma. *ACS Applied Materials and Interfaces*, *11*(11), 10578–10588. https://doi.org/10.1021/ACSAMI.9B00634/SUPPL_FILE/AM9B00634_SI_001.PDF

Niwa, N., Tanaka, N., Hongo, H., Miyazaki, Y., Takamatsu, K., Mizuno, R., Kikuchi, E., Mikami, S., Kosaka, T., & Oya, M. (2019). TNFAIP2 expression induces epithelial-to-mesenchymal transition and confers platinum resistance in urothelial cancer cells. *Laboratory Investigation 2019 99:11*, *99*(11), 1702–1713. https://doi.org/10.1038/s41374-019-0285-y

Ormerod, M. G., Sun, X. -M, Snowden, R. T., Davies, R., Fearnhead, H., & Cohen, G. M. (1993). Increased membrane permeability of apoptotic thymocytes: A flow cytometric study. *Cytometry*, *14*(6), 595–602. https://doi.org/10.1002/CYTO.990140603

Osorio, D., Yu, X., Zhong, Y., Li, G., Yu, P., Serpedin, E., Huang, J. Z., & Cai, J. J. (2019). Single-Cell Expression Variability Implies Cell Function. *Cells*, *9*(1). https://doi.org/10.3390/CELLS9010014

Pabla, N., & Dong, Z. (2008). Cisplatin nephrotoxicity: mechanisms and renoprotective strategies. *Kidney International*, *73*(9), 994–1007. https://doi.org/10.1038/SJ.KI.5002786

Pan, L., Wang, H., Jiang, C., Li, W., Chen, Y., & Ying, G. (2019). Multiple MicroRNAs synergistically promote tolerance to epidermal growth factor receptor-targeted drugs in smoked lung cancer therapies. *Journal of Cancer Research and Therapeutics*, *15*(4), 876. https://doi.org/10.4103/JCRT.JCRT_208_18

Pant, A., & Negi, J. S. (2018). Novel controlled ionic gelation strategy for chitosan nanoparticles preparation using TPP-β-CD inclusion complex. *European Journal of Pharmaceutical Sciences : Official Journal of the European Federation for Pharmaceutical Sciences*, *112*, 180–185. https://doi.org/10.1016/J.EJPS.2017.11.020

Parayath, N. N., Hong, B. V., Mackenzie, G. G., & Amiji, M. M. (2021). Hyaluronic acid nanoparticle-encapsulated microRNA-125b repolarizes tumor-associated macrophages in pancreatic cancer. *Https://Doi.Org/10.2217/Nnm-2021-0080*, *16*(25), 2291–2303. https://doi.org/10.2217/NNM-2021-0080

Pardoll, D. M. (2012). The blockade of immune checkpoints in cancer immunotherapy. *Nature Reviews Cancer 2012 12:4*, *12*(4), 252–264. https://doi.org/10.1038/nrc3239

Park, I. K., Yang, J., Jeong, H. J., Bom, H. S., Harada, I., Akaike, T., Kim, S. Il, & Cho, C. S. (2003). Galactosylated chitosan as a synthetic extracellular matrix for hepatocytes attachment. *Biomaterials*, *24*(13), 2331–2337. https://doi.org/10.1016/S0142-9612(03)00108-X

Parodi, A., Quattrocchi, N., Van De Ven, A. L., Chiappini, C., Evangelopoulos, M., Martinez, J. O., Brown, B. S., Khaled, S. Z., Yazdi, I. K., Enzo, M. V., Isenhart, L., Ferrari, M., & Tasciotti, E. (2012). Synthetic nanoparticles functionalized with biomimetic leukocyte membranes possess cell-like functions. *Nature Nanotechnology 2012 8:1*, *8*(1), 61–68. https://doi.org/10.1038/nnano.2012.212

Pasquinelli, A. E., Reinhart, B. J., Slack, F., Martindale, M. Q., Kuroda, M. I., Maller, B., Hayward, D. C., Ball, E. E., Degnan, B., Müller, P., Spring, J., Srinivasan, A., Fishman, M., Finnerty, J., Corbo, J., Levine, M., Leahy, P., Davidson, E., & Ruvkun, G. (2000). Conservation of the sequence and temporal expression of let-7 heterochronic regulatory RNA. *Nature 2000 408:6808*, *408*(6808), 86–89. https://doi.org/10.1038/35040556

Paul, P., Chakraborty, A., Sarkar, D., Langthasa, M., Rahman, M., Bari, M., Singha, R. K. S., Malakar, A. K., & Chakraborty, S. (2018). Interplay between miRNAs and human diseases. *Journal of Cellular Physiology*, *233*(3), 2007–2018. https://doi.org/10.1002/JCP.25854

Pessoa, A. C. S. N., Sipoli, C. C., & De La Torre, L. G. (2017). Effects of diffusion and mixing pattern on microfluidic-assisted synthesis of chitosan/ATP nanoparticles. *Lab on a Chip*, *17*(13), 2281–2293. https://doi.org/10.1039/C7LC00291B

Pezzuto, A., & Carico, E. (2018). Role of HIF-1 in Cancer Progression: Novel Insights. A Review. *Current Molecular Medicine*, *18*(6), 343–351. https://doi.org/10.2174/1566524018666181109121849

Poller, W., Dimmeler, S., Heymans, S., Zeller, T., Haas, J., Karakas, M., Leistner, D. M., Jakob, P., Nakagawa, S., Blankenberg, S., Engelhardt, S., Thum, T., Weber, C., Meder, B., Hajjar, R., & Landmesser, U. (2018). Non-coding RNAs in cardiovascular diseases: Diagnostic and therapeutic perspectives. In *European Heart Journal* (Vol. 39, Issue 29, pp. 2704–2716). Oxford University Press. https://doi.org/10.1093/eurheartj/ehx165

Posfai, D., Sylvester, K., Reddy, A., Ganley, J. G., Wirth, J., Cullen, Q. E., Dave, T., Kato, N., Dave, S. S., & Derbyshire, E. R. (2018). Plasmodium parasite exploits host aquaporin-3 during liver stage malaria infection. *PLoS Pathogens*, *14*(5). https://doi.org/10.1371/JOURNAL.PPAT.1007057

Qi, Z., Cai, S., Cai, J., Chen, L., Yao, Y., Chen, L., & Mao, Y. (2016). miR-491 regulates glioma cells proliferation by targeting TRIM28 in vitro. *BMC Neurology*, *16*(1). https://doi.org/10.1186/S12883-016-0769-Y

Qiu, Y., Liu, Y., Xu, Y., Li, Z., & Chen, J. (2020). Fabrication of antigen-containing nanoparticles using microfluidics with Tesla structure. *Electrophoresis*, *41*(10–11), 902–908. https://doi.org/10.1002/ELPS.201900395

Radwan, S. E.-S., El-Moslemany, R. M., Mehanna, R. A., Thabet, E. H., Abdelfattah, E.-Z. A., & El-Kamel, A. (2022). Chitosan-coated bovine serum albumin nanoparticles for topical tetrandrine delivery in glaucoma: in vitro and in vivo assessment. *Drug Delivery*, *29*(1), 1150–1163. https://doi.org/10.1080/10717544.2022.2058648

Ragelle, H., Riva, R., Vandermeulen, G., Naeye, B., Pourcelle, V., Le Duff, C. S., D'Haese, C., Nysten, B., Braeckmans, K., De Smedt, S. C., Jérôme, C., & Préat, V. (2014). Chitosan nanoparticles for siRNA delivery: Optimizing formulation to increase stability and efficiency. *Journal of Controlled Release*, *176*(1), 54–63. https://doi.org/10.1016/J.JCONREL.2013.12.026

Ragelle, Héloïse, Vanvarenberg, K., Vandermeulen, G., & Préat, V. (2016). Chitosan Nanoparticles for SiRNA Delivery In Vitro. *Methods in Molecular Biology*, *1364*, 143–150. https://doi.org/10.1007/978-1-4939-3112-5_12

Rai, R., Alwani, S., & Badea, I. (2019). Polymeric nanoparticles in gene therapy: New avenues of design and optimization for delivery applications. *Polymers*, *11*(4). https://doi.org/10.3390/polym11040745

Ravar, F., Saadat, E., Gholami, M., Dehghankelishadi, P., Mahdavi, M., Azami, S., & Dorkoosh, F. A. (2016). Hyaluronic acid-coated liposomes for targeted delivery of paclitaxel, in-vitro characterization and in-vivo evaluation. *Journal of Controlled Release*, *229*, 10–22. https://doi.org/10.1016/J.JCONREL.2016.03.012

RealTime-Glo™ Annexin V Apoptosis Assay | Annexin V Staining | Apoptosis Assay. (n.d.). Retrieved July 12, 2022, from https://www.promega.co.uk/products/cell-health-assays/apoptosis-assays/realtime-glo-annexin-v-apoptosis-assay/?catNum=JA1011

Reinhart, B. J., Slack, F. J., Basson, M., Pasquinelll, A. E., Bettlnger, J. C., Rougvle, A. E., Horvitz, H. R., & Ruvkun, G. (2000). The 21-nucleotide let-7 RNA regulates developmental timing in Caenorhabditis elegans. *Nature*, *403*(6772), 901–906.

https://doi.org/10.1038/35002607

Rinaldi, C., & Wood, M. J. A. (2018). Antisense oligonucleotides: the next frontier for treatment of neurological disorders. *Nature Reviews. Neurology*, *14*(1), 9–22. https://doi.org/10.1038/NRNEUROL.2017.148

Rinck, A., Preusse, M., Laggerbauer, B., Lickert, H., Engelhardt, S., & Theis, F. J. (2013). The human transcriptome is enriched for miRNA-binding sites located in cooperativity-permitting distance. *RNA Biology*, *10*(7), 1125–1135. https://doi.org/10.4161/RNA.24955

Ririe, K. M., Rasmussen, R. P., & Wittwer, C. T. (1997). Product Differentiation by Analysis of DNA Melting Curves during the Polymerase Chain Reaction. *Analytical Biochemistry*, *245*(2), 154–160. https://doi.org/10.1006/ABIO.1996.9916

Risnayanti, C., Jang, Y. S., Lee, J., & Ahn, H. J. (2018). PLGA nanoparticles co-delivering MDR1 and BCL2 siRNA for overcoming resistance of paclitaxel and cisplatin in recurrent or advanced ovarian cancer. *Scientific Reports 2018 8:1*, *8*(1), 1–12. https://doi.org/10.1038/s41598-018-25930-7

Roberts, T. C., Langer, R., & Wood, M. J. A. (2020). Advances in oligonucleotide drug delivery. *Nature Reviews Drug Discovery*, *19*(10), 673–694. https://doi.org/10.1038/S41573-020-0075-7

Roces, C. B., Hussain, M. T., Schmidt, S. T., Christensen, D., & Perrie, Y. (2020). Investigating prime-pull vaccination through a combination of parenteral vaccination and intranasal boosting. *Vaccines*, *8*(1). https://doi.org/10.3390/VACCINES8010010

Roces, C. B., Khadke, S., Christensen, D., & Perrie, Y. (2019). Scale-Independent Microfluidic Production of Cationic Liposomal Adjuvants and Development of Enhanced Lymphatic Targeting Strategies. *Molecular Pharmaceutics*, *16*(10), 4372–4386. https://doi.org/10.1021/ACS.MOLPHARMACEUT.9B00730

Roces, C. B., Lou, G., Jain, N., Abraham, S., Thomas, A., Halbert, G. W., & Perrie, Y. (2020). Manufacturing Considerations for the Development of Lipid Nanoparticles Using Microfluidics. *Pharmaceutics*, *12*(11), 1–19. https://doi.org/10.3390/PHARMACEUTICS12111095

Roces, C. B., Port, E. C., Daskalakis, N. N., Watts, J. A., Aylott, J. W., Halbert, G. W., & Perrie, Y. (2020). Rapid scale-up and production of active-loaded PEGylated liposomes.

International Journal of Pharmaceutics, *586*, 119566. https://doi.org/10.1016/J.IJPHARM.2020.119566

Rodriguez-Canales, J., Parra-Cuentas, E., & Wistuba, I. I. (2016). Diagnosis and molecular classification of lung cancer. In *Cancer Treatment and Research* (Vol. 170, pp. 25–46). Kluwer Academic Publishers. https://doi.org/10.1007/978-3-319-40389-2_2

Rojanarata, T., Opanasopit, P., Techaarpornkul, S., Ngawhirunpat, T., & Ruktanonchai, U. (2008). Chitosan-thiamine pyrophosphate as a novel carrier for siRNA delivery. *Pharmaceutical Research*, *25*(12), 2807–2814. https://doi.org/10.1007/S11095-008-9648-6

Rösslein, M., Elliott, J. T., Salit, M., Petersen, E. J., Hirsch, C., Krug, H. F., & Wick, P. (2015). Use of cause-and-effect analysis to design a high-quality nanocytotoxicology assay. *Chemical Research in Toxicology*, *28*(1), 21–30. https://doi.org/10.1021/TX500327Y/SUPPL_FILE/TX500327Y_SI_001.PDF

Rupaimoole, R., & Slack, F. J. (2017). MicroRNA therapeutics: towards a new era for the management of cancer and other diseases. *Nature Reviews. Drug Discovery*, *16*(3), 203–221. https://doi.org/10.1038/NRD.2016.246

Sadat Majedi, F., Hasani-Sadrabadi, M. M., Hojjati Emami, S., Taghipoor, M., Dashtimoghadam, E., Bertsch, A., Moaddel, H., & Renaud, P. (2012). Microfluidic synthesis of chitosan-based nanoparticles for fuel cell applications. *Chemical Communications (Cambridge, England)*, *48*(62), 7744–7746. https://doi.org/10.1039/C2CC33253A

Sancho-Martínez, S. M., Piedrafita, F. J., Cannata-Andía, J. B., López-Novoa, J. M., & López-Hernández, F. J. (2011). Necrotic Concentrations of Cisplatin Activate the Apoptotic Machinery but Inhibit Effector Caspases and Interfere with the Execution of Apoptosis. *Toxicological Sciences*, *122*(1), 73–85. https://doi.org/10.1093/TOXSCI/KFR098

Santos-Carballal, B., Aaldering, L. J., Ritzefeld, M., Pereira, S., Sewald, N., Moerschbacher, B. M., Götte, M., & Goycoolea, F. M. (2015). Physicochemical and biological characterization of chitosan-microRNA nanocomplexes for gene delivery to MCF-7 breast cancer cells. *Scientific Reports 2015 5:1*, *5*(1), 1–15. https://doi.org/10.1038/srep13567

Seifert, W., Kühnisch, J., Maritzen, T., Lommatzsch, S., Hennies, H. C., Bachmann, S., Horn, D.,

& Haucke, V. (2015). Cohen syndrome-associated protein COH1 physically and functionally interacts with the small GTPase RAB6 at the Golgi complex and directs neurite outgrowth. *The Journal of Biological Chemistry*, *290*(6), 3349–3358. https://doi.org/10.1074/JBC.M114.608174

Semenza, G. L. (2003). Targeting HIF-1 for cancer therapy. *Nature Reviews. Cancer*, *3*(10), 721–732. https://doi.org/10.1038/NRC1187

Seok, H., Ham, J., Jang, E. S., & Chi, S. W. (2016). MicroRNA Target Recognition: Insights from Transcriptome-Wide Non-Canonical Interactions. *Molecules and Cells*, *39*(5), 375–381. https://doi.org/10.14348/MOLCELLS.2016.0013

Sezer, A., Kilickap, S., Gümüş, M., Bondarenko, I., Özgüroğlu, M., Gogishvili, M., Turk, H. M., Cicin, I., Bentsion, D., Gladkov, O., Clingan, P., Sriuranpong, V., Rizvi, N., Gao, B., Li, S., Lee, S., McGuire, K., Chen, C. I., Makharadze, T., … Rietschel, P. (2021). Cemiplimab monotherapy for first-line treatment of advanced non-small-cell lung cancer with PD-L1 of at least 50%: a multicentre, open-label, global, phase 3, randomised, controlled trial. *Lancet (London, England)*, *397*(10274), 592–604. https://doi.org/10.1016/S0140-6736(21)00228-2

Shamaeizadeh, N., Varshosaz, J., Mirian, M., & Aliomrani, M. (2022). Glutathione targeted tragacanthic acid-chitosan as a non-viral vector for brain delivery of miRNA-219a-5P: An in vitro/in vivo study. *International Journal of Biological Macromolecules*, *200*, 543–556. https://doi.org/10.1016/J.IJBIOMAC.2022.01.100

Shamsi, M., & Zahedi, P. (2017). On-Chip Preparation of Streptokinase Entrapped in Chitosan Nanoparticles Used in Thrombolytic Therapy Potentially. *Journal of Pharmaceutical Sciences*, *106*(12), 3623–3630. https://doi.org/10.1016/J.XPHS.2017.08.001

Shamsi, M., Zahedi, P., Ghourchian, H., & Minaeian, S. (2017). Microfluidic-aided fabrication of nanoparticles blend based on chitosan for a transdermal multidrug delivery application. *International Journal of Biological Macromolecules*, *99*, 433–442. https://doi.org/10.1016/J.IJBIOMAC.2017.03.013

Sharma, K., Somavarapu, S., Colombani, A., Govind, N., & Taylor, K. M. G. (2013). Nebulised siRNA encapsulated crosslinked chitosan nanoparticles for pulmonary delivery. *International Journal of Pharmaceutics*, *455*(1–2), 241–247. https://doi.org/10.1016/J.IJPHARM.2013.07.024

Shen, D. W., Pouliot, L. M., Hall, M. D., & Gottesman, M. M. (2012). Cisplatin resistance: a cellular self-defense mechanism resulting from multiple epigenetic and genetic changes. *Pharmacological Reviews*, *64*(3), 706–721. https://doi.org/10.1124/PR.111.005637

Shibuya, H., Kato, Y., Saito, M., Isobe, T., Tsuboi, R., Koga, M., Toyota, H., & Mizuguchi, J. (2003). Induction of apoptosis and/or necrosis following exposure to antitumour agents in a melanoma cell line, probably through modulation of Bcl-2 family proteins. *Melanoma Research*, *13*(5), 457–464. https://doi.org/10.1097/00008390-200310000-00004

Siddik, Z. H. (2003). Cisplatin: mode of cytotoxic action and molecular basis of resistance. *Oncogene 2003 22:47*, *22*(47), 7265–7279. https://doi.org/10.1038/sj.onc.1206933

Slaby, O., Laga, R., & Sedlacek, O. (2017a). Therapeutic targeting of non-coding RNAs in Cancer. In *Biochemical Journal* (Vol. 474, Issue 24, pp. 4219–4251). Portland Press Ltd. https://doi.org/10.1042/BCJ20170079

Slaby, O., Laga, R., & Sedlacek, O. (2017b). Therapeutic targeting of non-coding RNAs in Cancer. In *Biochemical Journal* (Vol. 474, Issue 24, pp. 4219–4251). Portland Press Ltd. https://doi.org/10.1042/BCJ20170079

Snijder, B., & Pelkmans, L. (2011). Origins of regulated cell-to-cell variability. *Nature Reviews Molecular Cell Biology 2011 12:2*, *12*(2), 119–125. https://doi.org/10.1038/nrm3044

Som, C., Nowack, B., Krug, H. F., & Wick, P. (2013). Toward the development of decision supporting tools that can be used for safe production and use of nanomaterials. *Accounts of Chemical Research*, *46*(3), 863–872. https://doi.org/10.1021/AR3000458/ASSET/IMAGES/MEDIUM/AR-2012-000458_0005.GIF

Sperveslage, J., Hoffmeister, M., Henopp, T., Klöppel, G., & Sipos, B. (2014). Establishment of robust controls for the normalization of miRNA expression in neuroendocrine tumors of the ileum and pancreas. *Endocrine*, *46*(2), 226–230. https://doi.org/10.1007/S12020-014-0202-5/FIGURES/1

Stavis, S. M., Fagan, J. A., Stopa, M., & Liddle, J. A. (2018). Nanoparticle Manufacturing-Heterogeneity through Processes to Products. *ACS Applied Nano Materials*, *1*(9), 4358–4385. https://doi.org/10.1021/ACSANM.8B01239/SUPPL_FILE/AN8B01239_SI_001.PDF

Stroock, A. D., Dertinger, S. K. W., Ajdari, A., Mezić, I., Stone, H. A., & Whitesides, G. M. (2002).

Chaotic mixer for microchannels. *Science*, *295*(5555), 647–651. https://doi.org/10.1126/SCIENCE.1066238/ASSET/D19F07E3-2F46-45C0-B700-FD95192A2FB9/ASSETS/GRAPHIC/SE0320138004.JPEG

Suardi, R. B., Ysrafil, Y., Sesotyosari, S. L., Martien, R., Wardana, T., Astuti, I., & Haryana, S. M. (2020). The Effects of Combination of Mimic miR-155-5p and Antagonist miR-324-5p Encapsulated Chitosan in Ovarian Cancer SKOV3. *Asian Pacific Journal of Cancer Prevention : APJCP*, *21*(9), 2603–2608. https://doi.org/10.31557/APJCP.2020.21.9.2603

Sun, P., Huang, W., Jin, M., Wang, Q., Fan, B., Kang, L., & Gao, Z. (2016). Chitosan-based nanoparticles for survivin targeted siRNA delivery in breast tumor therapy and preventing its metastasis. *International Journal of Nanomedicine*, *11*, 4931. https://doi.org/10.2147/IJN.S105427

Sun, Y., Zhao, Y., Zhao, X., Lee, R. J., Teng, L., & Zhou, C. (2017). Enhancing the therapeutic delivery of oligonucleotides by chemical modification and nanoparticle encapsulation. *Molecules*, *22*(10). https://doi.org/10.3390/molecules22101724

Sung, Ferlay, J., Siegel, R. L., Laversanne, M., Soerjomataram, I., Jemal, A., & Bray, F. (2021). Global Cancer Statistics 2020: GLOBOCAN Estimates of Incidence and Mortality Worldwide for 36 Cancers in 185 Countries. *CA: A Cancer Journal for Clinicians*, *71*(3), 209–249. https://doi.org/10.3322/CAAC.21660

Syed, Y. Y. (2016). Eteplirsen: First Global Approval. *Drugs 2016 76:17*, *76*(17), 1699–1704. https://doi.org/10.1007/S40265-016-0657-1

Szczepanowicz, K., Bzowska, M., Kruk, T., Karabasz, A., Bereta, J., & Warszynski, P. (2016). Pegylated polyelectrolyte nanoparticles containing paclitaxel as a promising candidate for drug carriers for passive targeting. *Colloids and Surfaces B: Biointerfaces*, *143*, 463–471. https://doi.org/10.1016/J.COLSURFB.2016.03.064

Ta, Q., Ting, J., Harwood, S., Browning, N., Simm, A., Ross, K., Olier, I., & Al-Kassas, R. (2021). Chitosan nanoparticles for enhancing drugs and cosmetic components penetration through the skin. *European Journal of Pharmaceutical Sciences*, *160*, 105765. https://doi.org/10.1016/J.EJPS.2021.105765

Taetz, S., Nafee, N., Beisner, J., Piotrowska, K., Baldes, C., Mürdter, T. E., Huwer, H., Schneider, M., Schaefer, U. F., Klotz, U., & Lehr, C. M. (2009). The influence of chitosan content in cationic chitosan/PLGA nanoparticles on the delivery efficiency of antisense 2′-O-

methyl-RNA directed against telomerase in lung cancer cells. *European Journal of Pharmaceutics and Biopharmaceutics*, *72*(2), 358–369. https://doi.org/10.1016/J.EJPB.2008.07.011

Takamizawa, J., Konishi, H., Yanagisawa, K., Tomida, S., Osada, H., Endoh, H., Harano, T., Yatabe, Y., Nagino, M., Nimura, Y., Mitsudomi, T., & Takahashi, T. (2004). Reduced expression of the let-7 microRNAs in human lung cancers in association with shortened postoperative survival. *Cancer Research*, *64*(11), 3753–3756. https://doi.org/10.1158/0008-5472.CAN-04-0637

Tan, S. C., & Yiap, B. C. (2009). DNA, RNA, and Protein Extraction: The Past and The Present. *Journal of Biomedicine and Biotechnology*, *2009*. https://doi.org/10.1155/2009/574398

Taylor, S. C., & Posch, A. (2014). The Design of a Quantitative Western Blot Experiment. *BioMed Research International*, *2014*. https://doi.org/10.1155/2014/361590

Techaarpornkul, S., Wongkupasert, S., Opanasopit, P., Apirakaramwong, A., Nunthanid, J., & Ruktanonchai, U. (2010). Chitosan-Mediated siRNA Delivery In Vitro: Effect of Polymer Molecular Weight, Concentration and Salt Forms. *AAPS PharmSciTech*, *11*(1), 64. https://doi.org/10.1208/S12249-009-9355-6

Thair, S. A., Topchiy, E., Boyd, J. H., Cirstea, M., Wang, C., Nakada, T. A., Fjell, C. D., Wurfel, M., Russell, J. A., & Walley, K. R. (2016). TNF AIP2 Inhibits Early TNFa-Induced NF-κB Signaling and Decreases Survival in Septic Shock Patients. *Journal of Innate Immunity*, *8*(1), 57. https://doi.org/10.1159/000437330

Tian, J., Hu, L., Li, X., Geng, J., Dai, M., & Bai, X. (2016). MicroRNA-130b promotes lung cancer progression via PPARγ/VEGF-A/BCL-2-mediated suppression of apoptosis. *Journal of Experimental & Clinical Cancer Research : CR*, *35*(1). https://doi.org/10.1186/S13046-016-0382-3

Torbensen, K., Baroud, C. N., Ristori, S., & Abou-Hassan, A. (2021). Tip Streaming of a Lipid-Stabilized Double Emulsion Generated in a Microfluidic Channel. *Langmuir : The ACS Journal of Surfaces and Colloids*, *37*(24), 7442–7448. https://doi.org/10.1021/ACS.LANGMUIR.1C00827

Travis, W. D., Brambilla, E., Nicholson, A. G., Yatabe, Y., Austin, J. H. M., Beasley, M. B., Chirieac, L. R., Dacic, S., Duhig, E., Flieder, D. B., Geisinger, K., Hirsch, F. R., Ishikawa, Y., Kerr, K. M., Noguchi, M., Pelosi, G., Powell, C. A., Tsao, M. S., & Wistuba, I. (2015). The 2015

World Health Organization Classification of Lung Tumors: Impact of Genetic, Clinical and Radiologic Advances since the 2004 Classification. In *Journal of Thoracic Oncology* (Vol. 10, Issue 9, pp. 1243–1260). Elsevier Inc. https://doi.org/10.1097/JTO.0000000000000630

Trivedi, M., Singh, A., Talekar, M., Pawar, G., Shah, P., & Amiji, M. (2017). MicroRNA-34a Encapsulated in Hyaluronic Acid Nanoparticles Induces Epigenetic Changes with Altered Mitochondrial Bioenergetics and Apoptosis in Non-Small-Cell Lung Cancer Cells. *Scientific Reports 2017 7:1*, *7*(1), 1–17. https://doi.org/10.1038/s41598-017-02816-8

Tsao, A. S., Scagliotti, G. V., Bunn, P. A., Carbone, D. P., Warren, G. W., Bai, C., De Koning, H. J., Uraujh Yousaf-Khan, A., McWilliams, A., Tsao, M. S., Adusumilli, P. S., Rami-Porta, R., Asamura, H., Van Schil, P. E., Darling, G. E., Ramalingam, S. S., Gomez, D. R., Rosenzweig, K. E., Zimmermann, S., … Pass, H. I. (2016). Scientific advances in lung cancer 2015. In *Journal of Thoracic Oncology* (Vol. 11, Issue 5, pp. 613–638). Lippincott Williams and Wilkins. https://doi.org/10.1016/j.jtho.2016.03.012

Tu, L., Wang, M., Zhao, W. Y., Zhang, Z. Z., Tang, D. F., Zhang, Y. Q., Cao, H., & Zhang, Z. G. (2017). miRNA-218-loaded carboxymethyl chitosan - Tocopherol nanoparticle to suppress the proliferation of gastrointestinal stromal tumor growth. *Materials Science & Engineering. C, Materials for Biological Applications*, *72*, 177–184. https://doi.org/10.1016/J.MSEC.2016.10.052

Tung, M. C., Lin, P. L., Cheng, Y. W., Wu, D. W., Yeh, S. Der, Chen, C. Y., & Lee, H. (2016a). Reduction of microRNA-184 by E6 oncoprotein confers cisplatin resistance in lung cancer via increasing Bcl-2. *Oncotarget*, *7*(22), 32362–32374. https://doi.org/10.18632/ONCOTARGET.8708

Tung, M. C., Lin, P. L., Cheng, Y. W., Wu, D. W., Yeh, S. Der, Chen, C. Y., & Lee, H. (2016b). Reduction of microRNA-184 by E6 oncoprotein confers cisplatin resistance in lung cancer via increasing Bcl-2. *Oncotarget*, *7*(22), 32362–32374. https://doi.org/10.18632/ONCOTARGET.8708

Tzeyung, A. S., Md, S., Bhattamisra, S. K., Madheswaran, T., Alhakamy, N. A., Aldawsari, H. M., & Radhakrishnan, A. K. (2019). Fabrication, Optimization, and Evaluation of Rotigotine-Loaded Chitosan Nanoparticles for Nose-To-Brain Delivery. *Pharmaceutics*, *11*(1). https://doi.org/10.3390/PHARMACEUTICS11010026

Vadla, G. P., Daghat, B., Patterson, N., Ahmad, V., Perez, G., Garcia, A., Manjunath, Y., Kaifi, J.

T., Li, G., & Chabu, C. Y. (2022). *Combining plasma extracellular vesicle Let-7b-5p, miR-184 and circulating miR-22-3p levels for NSCLC diagnosis and drug resistance prediction*. https://doi.org/10.1038/s41598-022-10598-x

Van Engeland, M., Nieland, L. J. W., Ramaekers, F. C. S., Schutte, B., & Reutelingsperger, C. P. M. (1998). Annexin V-affinity assay: a review on an apoptosis detection system based on phosphatidylserine exposure. *Cytometry*, *31*(1), 1–9. https://doi.org/10.1002/(sici)1097-0320(19980101)31:1<1::aid-cyto1>3.0.co;2-r

van Zandwijk, N., Pavlakis, N., Kao, S. C., Linton, A., Boyer, M. J., Clarke, S., Huynh, Y., Chrzanowska, A., Fulham, M. J., Bailey, D. L., Cooper, W. A., Kritharides, L., Ridley, L., Pattison, S. T., MacDiarmid, J., Brahmbhatt, H., & Reid, G. (2017). Safety and activity of microRNA-loaded minicells in patients with recurrent malignant pleural mesothelioma: a first-in-man, phase 1, open-label, dose-escalation study. *The Lancet Oncology*, *18*(10), 1386–1396. https://doi.org/10.1016/S1470-2045(17)30621-6

Vandesompele, J., De Preter, K., Pattyn, F., Poppe, B., Van Roy, N., De Paepe, A., & Speleman, F. (2002). Accurate normalization of real-time quantitative RT-PCR data by geometric averaging of multiple internal control genes. *Genome Biology*, *3*(7), 1–12. https://doi.org/10.1186/GB-2002-3-7-RESEARCH0034/COMMENTS

Vauthier, C., & Bouchemal, K. (2009). Methods for the preparation and manufacture of polymeric nanoparticles. *Pharmaceutical Research*, *26*(5), 1025–1058. https://doi.org/10.1007/S11095-008-9800-3

Vishwamitra, D., Li, Y., Wilson, D., Manshouri, R., Curry, C. V., Shi, B., Tang, X. M., Sheehan, A. M., Wistuba, I. I., Shi, P., & Amin, H. M. (2012). MicroRNA 96 is a post-transcriptional suppressor of anaplastic lymphoma kinase expression. *The American Journal of Pathology*, *180*(5), 1772–1780. https://doi.org/10.1016/J.AJPATH.2012.01.008

Von Harpe, A., Petersen, H., Li, Y., & Kissel, T. (2000). Characterization of commercially available and synthesized polyethylenimines for gene delivery. *Journal of Controlled Release*, *69*(2), 309–322. https://doi.org/10.1016/S0168-3659(00)00317-5

Vu, H. T. H., Streck, S., Hook, S. M., & McDowell, A. (2019). Utilization of Microfluidics for the Preparation of Polymeric Nanoparticles for the Antioxidant Rutin: A Comparison with Bulk Production. *Pharmaceutical Nanotechnology*, *7*(6), 469–483. https://doi.org/10.2174/2211738507666191019141049

Wallberg, F., Tenev, T., & Meier, P. (2016). Analysis of Apoptosis and Necroptosis by Fluorescence-Activated Cell Sorting. *Cold Spring Harbor Protocols*, *2016*(4), 347–352. https://doi.org/10.1101/PDB.PROT087387

Wang, Jinjun. (2021). Tripterine and miR-184 show synergy to suppress breast cancer progression. *Biochemical and Biophysical Research Communications*, *561*, 19–25. https://doi.org/10.1016/J.BBRC.2021.04.108

Wang, Juan, Chen, H., Liao, Y., Chen, N., Liu, T., Zhang, H., & Zhang, H. (2015). Expression and clinical evidence of miR-494 and PTEN in non-small cell lung cancer. *Tumour Biology : The Journal of the International Society for Oncodevelopmental Biology and Medicine*, *36*(9), 6965–6972. https://doi.org/10.1007/S13277-015-3416-0

Wang, L., Ji, X. B., Wang, L. H., Qiu, J. G., Zhou, F. M., Liu, W. J., Wan, D. Di, Lin, M. C. mi, Liu, L. Z., Zhang, J. Y., & Jiang, B. H. (2020). Regulation of MicroRNA-497-Targeting AKT2 Influences Tumor Growth and Chemoresistance to Cisplatin in Lung Cancer. *Frontiers in Cell and Developmental Biology*, *8*. https://doi.org/10.3389/FCELL.2020.00840/FULL

Wang, T., Larcher, L. M., Ma, L., & Veedu, R. N. (2018). Systematic Screening of Commonly Used Commercial Transfection Reagents towards Efficient Transfection of Single-Stranded Oligonucleotides. *Molecules (Basel, Switzerland)*, *23*(10). https://doi.org/10.3390/MOLECULES23102564

Wang, W., & He, B. (2020). MiR-760 inhibits the progression of non-small cell lung cancer through blocking ROS1/Ras/Raf/MEK/ERK pathway. *Bioscience Reports*. https://doi.org/10.1042/BSR20182483

Wang, Y., Wen, B., Yu, H., Ding, D., Zhang, J. J., Zhang, Y., Zhao, L., & Zhang, W. (2018). Berberine Hydrochloride-Loaded Chitosan Nanoparticles Effectively Targets and Suppresses Human Nasopharyngeal Carcinoma. *Journal of Biomedical Nanotechnology*, *14*(8), 1486–1495. https://doi.org/10.1166/JBN.2018.2596

Wang, Z., Wu, G., Wei, M., Liu, Q., Zhou, J., Qin, T., Feng, X., Liu, H., Feng, Z., & Zhao, Y. (2016). Improving the osteogenesis of human bone marrow mesenchymal stem cell sheets by microRNA-21-loaded chitosan/hyaluronic acid nanoparticles via reverse transfection. *International Journal of Nanomedicine*, *11*, 2091–2105. https://doi.org/10.2147/IJN.S104851

Wei, L., Wang, G., Yang, C., Zhang, Y., Chen, Y., Zhong, C., & Li, Q. (2021). MicroRNA-550a-3-

5p controls the brain metastasis of lung cancer by directly targeting YAP1. *Cancer Cell International*, *21*(1), 491. https://doi.org/10.1186/S12935-021-02197-Z

Whitesides, G. M. (2006). The origins and the future of microfluidics. *Nature 2006 442:7101*, *442*(7101), 368–373. https://doi.org/10.1038/nature05058

Wightman, B., Ha, I., & Ruvkun, G. (1993). Posttranscriptional regulation of the heterochronic gene lin-14 by lin-4 mediates temporal pattern formation in C. elegans. *Cell*, *75*(5), 855–862. https://doi.org/10.1016/0092-8674(93)90530-4

Winter, J., Jung, S., Keller, S., Gregory, R. I., & Diederichs, S. (2009). Many roads to maturity: MicroRNA biogenesis pathways and their regulation. In *Nature Cell Biology* (Vol. 11, Issue 3, pp. 228–234). https://doi.org/10.1038/ncb0309-228

Wong, T. S., Liu, X. B., Wong, B. Y. H., Ng, R. W. M., Yuen, A. P. W., & Wei, W. I. (2008). Mature miR-184 as Potential Oncogenic microRNA of Squamous Cell Carcinoma of Tongue. *Clinical Cancer Research : An Official Journal of the American Association for Cancer Research*, *14*(9), 2588–2592. https://doi.org/10.1158/1078-0432.CCR-07-0666

Wu, G. G., Li, W. H., He, W. G., Jiang, N., Zhang, G. X., Chen, W., Yang, H. F., Liu, Q. L., Huang, Y. N., Zhang, L., Zhang, T., & Zeng, X. C. (2014). Mir-184 Post-Transcriptionally Regulates SOX7 Expression and Promotes Cell Proliferation in Human Hepatocellular Carcinoma. *PLOS ONE*, *9*(2), e88796. https://doi.org/10.1371/JOURNAL.PONE.0088796

Wu, Guangsheng, Feng, C., Hui, G., Wang, Z., Tan, J., Luo, L., Xue, P., Wang, Q., & Chen, X. (2016). Improving the osteogenesis of rat mesenchymal stem cells by chitosan-based-microRNA nanoparticles. *Carbohydrate Polymers*, *138*, 49–58. https://doi.org/10.1016/J.CARBPOL.2015.11.044

Wu, Guannan, Liu, J., Wu, Z., Wu, X., & Yao, X. (2017). MicroRNA-184 inhibits cell proliferation and metastasis in human colorectal cancer by directly targeting IGF-1R. *Oncology Letters*, *14*(3), 3215. https://doi.org/10.3892/OL.2017.6499

Wu, H., Mu, X., Liu, L., Wu, H., Hu, X., Chen, L., Liu, J., Mu, Y., Yuan, F., Liu, W., & Zhao, Y. (2020). Bone marrow mesenchymal stem cells-derived exosomal microRNA-193a reduces cisplatin resistance of non-small cell lung cancer cells via targeting LRRC1. *Cell Death & Disease*, *11*(9). https://doi.org/10.1038/S41419-020-02962-4

Wu, Q. X., Xu, X., Xie, Q., Tong, W. Y., & Chen, Y. (2016). Evaluation of chitosan hydrochloride-alginate as enteric micro-probiotic-carrier with dual protective barriers. *International*

Journal of Biological Macromolecules, *93*(Pt A), 665–671. https://doi.org/10.1016/J.IJBIOMAC.2016.09.034

Xia, B., Tian, C., Guo, S., Zhang, L., Zhao, D., Qu, F., Zhao, W., Wang, Y., Wu, X., Da, W., Wei, S., & Zhang, Y. (2015). c-Myc plays part in drug resistance mediated by bone marrow stromal cells in acute myeloid leukemia. *Leukemia Research*, *39*(1), 92–99. https://doi.org/10.1016/J.LEUKRES.2014.11.004

Xiang, X., Guo, C., Tang, C., Cai, J., & Dong, Z. (2019). Epigenetic Regulation in Kidney Toxicity: Insights From Cisplatin Nephrotoxicity. *Seminars in Nephrology*, *39*(2), 152–158. https://doi.org/10.1016/J.SEMNEPHROL.2018.12.005

Xiao, B., Ma, P., Ma, L., Chen, Q., Si, X., Walter, L., & Merlin, D. (2017). Effects of tripolyphosphate on cellular uptake and RNA interference efficiency of chitosan-based nanoparticles in Raw 264.7 macrophages. *Journal of Colloid and Interface Science*, *490*, 520. https://doi.org/10.1016/J.JCIS.2016.11.088

Xiao, L., Lan, X., Shi, X., Zhao, K., Wang, D., Wang, X., Li, F., Huang, H., & Liu, J. (2017). Cytoplasmic RAP1 mediates cisplatin resistance of non-small cell lung cancer. *Cell Death & Disease*, *8*(5), e2803. https://doi.org/10.1038/CDDIS.2017.210

Xie, Y., & Wang, B. (2017). Downregulation of TNFAIP2 suppresses proliferation and metastasis in esophageal squamous cell carcinoma through activation of the Wnt/β-catenin signaling pathway. *Oncology Reports*, *37*(5), 2920–2928. https://doi.org/10.3892/OR.2017.5557

Xing, J., Jia, J., Cong, X., Liu, Z., & Li, Q. (2020). N-Isopropylacrylamide-modified polyethylenimine-mediated miR-29a delivery to inhibit the proliferation and migration of lung cancer cells. *Undefined*, *198*. https://doi.org/10.1016/J.COLSURFB.2020.111463

Xu, L., Huang, Y., Chen, D., He, J., Zhu, W., Zhang, Y., & Liu, X. (2014). Downregulation of miR-21 increases cisplatin sensitivity of non-small-cell lung cancer. *Cancer Genetics*, *207*(5), 214–220. https://doi.org/10.1016/J.CANCERGEN.2014.04.003

Xu, Yanfang, Ma, H. bin, Fang, Y. lu, Zhang, Z. rong, Shao, J., Hong, M., Huang, C. jun, Liu, J., & Chen, R. qing. (2017). Cisplatin-induced necroptosis in TNFα dependent and independent pathways. *Cellular Signalling*, *31*, 112–123. https://doi.org/10.1016/J.CELLSIG.2017.01.004

Xu, Yanfang, Ma, H., Shao, J., Wu, J., Zhou, L., Zhang, Z., Wang, Y., Huang, Z., Ren, J., Liu, S.,

Chen, X., & Han, J. (2015). A Role for Tubular Necroptosis in Cisplatin-Induced AKI. *Journal of the American Society of Nephrology : JASN*, *26*(11), 2647. https://doi.org/10.1681/ASN.2014080741

Xu, Yu, Ma, H., Yu, H., Liu, Z., Wang, L. E., Tan, D., Muddasani, R., Lu, V., Ajani, J. A., Wang, Y., & Wei, Q. (2013). The miR-184 Binding-Site rs8126 T>C Polymorphism in TNFAIP2 Is Associated with Risk of Gastric Cancer. *PLoS ONE*, *8*(5). https://doi.org/10.1371/JOURNAL.PONE.0064973

Xue, X., Liu, Y., Wang, Y., Meng, M., Wang, K., Zang, X., Zhao, S., Sun, X., Cui, L., Pan, L., & Liu, S. (2016). MiR-21 and MiR-155 promote non-small cell lung cancer progression by downregulating SOCS1, SOCS6, and PTEN. *Oncotarget*, *7*(51), 84508. https://doi.org/10.18632/ONCOTARGET.13022

Yamamoto, H., Ishihara, K., Takeda, Y., Koizumi, W., & Ichikawa, T. (2013). Changes in the mucus barrier during cisplatin-induced intestinal mucositis in rats. *BioMed Research International*, *2013*. https://doi.org/10.1155/2013/276186

Yang, D., Gao, K., Bai, Y., Lei, L., Jia, T., Yang, K., & Xue, C. (2021). Microfluidic synthesis of chitosan-coated magnetic alginate microparticles for controlled and sustained drug delivery. *International Journal of Biological Macromolecules*, *182*, 639–647. https://doi.org/10.1016/J.IJBIOMAC.2021.04.057

Yang, M., Tao, J., Chai, M., Wu, H., Wang, J., Li, G., He, C., Xie, L., Ji, P., Dai, Y., Yang, L., & Liu, G. (2017). Melatonin Improves the Quality of Inferior Bovine Oocytes and Promoted Their Subsequent IVF Embryo Development: Mechanisms and Results. *Molecules (Basel, Switzerland)*, *22*(12). https://doi.org/10.3390/MOLECULES22122059

Yang, S., Phillips, M. D., Betel, D., Mu, P., Ventura, A., Siepel, A. C., Chen, K. C., & Lai, E. C. (2011). Widespread regulatory activity of vertebrate microRNA* species. *RNA*, *17*(2), 312–326. https://doi.org/10.1261/rna.2537911

Yang, X. yan, Li, Y. xia, Li, M., Zhang, L., Feng, L. xia, & Zhang, N. (2013). Hyaluronic acid-coated nanostructured lipid carriers for targeting paclitaxel to cancer. *Cancer Letters*, *334*(2), 338–345. https://doi.org/10.1016/J.CANLET.2012.07.002

Ye, Z., Fang, B., Pan, J., Zhang, N., Huang, J., Xie, C., Lou, T., & Cao, Z. (2017). miR-138 suppresses the proliferation, metastasis and autophagy of non-small cell lung cancer by targeting Sirt1. *Oncology Reports*, *37*(6), 3244. https://doi.org/10.3892/OR.2017.5619

Yetisgin, A. A., Cetinel, S., Zuvin, M., Kosar, A., & Kutlu, O. (2020). Therapeutic Nanoparticles and Their Targeted Delivery Applications. *Molecules (Basel, Switzerland)*, *25*(9). https://doi.org/10.3390/MOLECULES25092193

Yin, H., Kanasty, R. L., Eltoukhy, A. A., Vegas, A. J., Dorkin, J. R., & Anderson, D. G. (2014). Non-viral vectors for gene-based therapy. *Nature Reviews Genetics 2014 15:8*, *15*(8), 541–555. https://doi.org/10.1038/nrg3763

Youle, R. J., & Strasser, A. (2008). The BCL-2 protein family: opposing activities that mediate cell death. *Nature Reviews Molecular Cell Biology 2008 9:1*, *9*(1), 47–59. https://doi.org/10.1038/nrm2308

Younes, I., Rinaudo, M., Harding, D., & Sashiwa, H. (2015). Chitin and Chitosan Preparation from Marine Sources. Structure, Properties and Applications. *Marine Drugs 2015, Vol. 13, Pages 1133-1174*, *13*(3), 1133–1174. https://doi.org/10.3390/MD13031133

Ysrafil, Y., Astuti, I., Anwar, S. L., Martien, R., Sumadi, F. A. N., Wardhana, T., & Haryana, S. M. (2020). MicroRNA-155-5p Diminishes in Vitro Ovarian Cancer Cell Viability by Targeting HIF1α Expression. *Advanced Pharmaceutical Bulletin*, *10*(4), 630–637. https://doi.org/10.34172/APB.2020.076

Yu, C. Y., Li, N. M., Yang, S., Ning, Q., Huang, C., Huang, W., He, Z. N., He, D. X., Tan, X. W., & Sun, L. C. (2015). Fabrication of galactosylated chitosan–5-fluorouracil acetic acid based nanoparticles for controlled drug delivery. *Journal of Applied Polymer Science*, *132*(40), 42625. https://doi.org/10.1002/APP.42625

Zamai, L., Canonico, B., Luchetti, F., Ferri, P., Melloni, E., Guidotti, L., Cappellini, A., Cutroneo, G., Vitale, M., & Papa, S. (2001). *Supravital Exposure to Propidium Iodide Identifies Apoptosis on Adherent Cells*.

Zander-Fox, D. L., Fullston, T., McPherson, N. O., Sandeman, L., Kang, W. X., Good, S. B., Spillane, M., & Lane, M. (2015). Reduction of Mitochondrial Function by FCCP During Mouse Cleavage Stage Embryo Culture Reduces Birth Weight and Impairs the Metabolic Health of Offspring. *Biology of Reproduction*, *92*(5). https://doi.org/10.1095/BIOLREPROD.114.123489

Zeller, K. I., Jegga, A. G., Aronow, B. J., O'Donnell, K. A., & Dang, C. V. (2003). An integrated database of genes responsive to the Myc oncogenic transcription factor: identification of direct genomic targets. *Genome Biology*, *4*(10), 1–10. https://doi.org/10.1186/GB-

2003-4-10-R69/FIGURES/4

Zeng, A., Wei, Z., Yan, W., Yin, J., Huang, X., Zhou, X., Li, R., Shen, F., Wu, W., Wang, X., & You, Y. (2018). Exosomal transfer of miR-151a enhances chemosensitivity to temozolomide in drug-resistant glioblastoma. *Cancer Letters*, *436*, 10–21. https://doi.org/10.1016/J.CANLET.2018.08.004

Zeng, Y., & Cullen, B. R. (2004). Structural requirements for pre-microRNA binding and nuclear export by Exportin 5. *Nucleic Acids Research*, *32*(16), 4776–4785. https://doi.org/10.1093/NAR/GKH824

Zhang, J. guang, Wang, J. jun, Zhao, F., Liu, Q., Jiang, K., & Yang, G. hai. (2010). MicroRNA-21 (miR-21) represses tumor suppressor PTEN and promotes growth and invasion in non-small cell lung cancer (NSCLC). *Clinica Chimica Acta; International Journal of Clinical Chemistry*, *411*(11–12), 846–852. https://doi.org/10.1016/J.CCA.2010.02.074

Zhang, L., & Yu, S. (2018). Role of miR-520b in non-small cell lung cancer. *Experimental and Therapeutic Medicine*, *16*(5), 3987. https://doi.org/10.3892/ETM.2018.6732

Zhang, R., Liu, C., Niu, Y., Jing, Y., Zhang, H., Wang, J., Yang, J., Zen, K., Zhang, J., Zhang, C. Y., & Li, D. (2017). MicroRNA-128-3p regulates mitomycin C-induced DNA damage response in lung cancer cells through repressing SPTAN1. *Oncotarget*, *8*(35), 58098. https://doi.org/10.18632/ONCOTARGET.12300

Zhang, X., Wang, H., Zhang, S., Song, J., Zhang, Y., Wei, X., & Feng, Z. (2012). MiR-134 functions as a regulator of cell proliferation, apoptosis, and migration involving lung septation. *In Vitro Cellular and Developmental Biology - Animal*, *48*(2), 131–136. https://doi.org/10.1007/S11626-012-9482-3/FIGURES/4

Zhao, D., Deng, S. C., Ma, Y., Hao, Y. H., & Jia, Z. H. (2018). miR-221 alleviates the inflammatory response and cell apoptosis of neuronal cell through targeting TNFAIP2 in spinal cord ischemia-reperfusion. *Neuroreport*, *29*(8), 655–660. https://doi.org/10.1097/WNR.0000000000001013

Zhao, J., Tan, W., Zhang, L., Liu, J., Shangguan, M., Chen, J., Zhao, B., Peng, Y., Cui, M., & Zhao, S. (2021). FGFR3 phosphorylates EGFR to promote cisplatin-resistance in ovarian cancer. *Biochemical Pharmacology*, *190*. https://doi.org/10.1016/J.BCP.2021.114536

Zhao, W., Zhao, J. J., Zhang, L., Xu, Q. F., Zhao, Y. M., Shi, X. Y., & Xu, A. G. (2015). Serum miR-21 level: a potential diagnostic and prognostic biomarker for non-small cell lung cancer.

International Journal of Clinical and Experimental Medicine, *8*(9), 14759. /pmc/articles/PMC4658847/

Zhen, Y., Liu, Z., Yang, H., Yu, X., Wu, Q., Hua, S., Long, X., Jiang, Q., Song, Y., Cheng, C., Wang, H., Zhao, M., Fu, Q., Lyu, X., Chen, Y., Fan, Y., Liu, Y., Li, X., & Fang, W. (2013a). Tumor suppressor PDCD4 modulates miR-184-mediated direct suppression of C-MYC and BCL2 blocking cell growth and survival in nasopharyngeal carcinoma. *Cell Death & Disease*, *4*(10). https://doi.org/10.1038/CDDIS.2013.376

Zhen, Y., Liu, Z., Yang, H., Yu, X., Wu, Q., Hua, S., Long, X., Jiang, Q., Song, Y., Cheng, C., Wang, H., Zhao, M., Fu, Q., Lyu, X., Chen, Y., Fan, Y., Liu, Y., Li, X., & Fang, W. (2013b). Tumor suppressor PDCD4 modulates miR-184-mediated direct suppression of C-MYC and BCL2 blocking cell growth and survival in nasopharyngeal carcinoma. *Cell Death & Disease*, *4*(10), e872. https://doi.org/10.1038/CDDIS.2013.376

Zhen, Y., Liu, Z., Yang, H., Yu, X., Wu, Q., Hua, S., Long, X., Jiang, Q., Song, Y., Cheng, C., Wang, H., Zhao, M., Fu, Q., Lyu, X., Chen, Y., Fan, Y., Liu, Y., Li, X., & Fang, W. (2013c). Tumor suppressor PDCD4 modulates miR-184-mediated direct suppression of C-MYC and BCL2 blocking cell growth and survival in nasopharyngeal carcinoma. *Cell Death & Disease 2013 4:10*, *4*(10), e872–e872. https://doi.org/10.1038/cddis.2013.376

Zhou, R., Zhou, X., Yin, Z., Guo, J., Hu, T., Jiang, S., Liu, L., Dong, X., Zhang, S., & Wu, G. (2015). Tumor invasion and metastasis regulated by microRNA-184 and microRNA-574-5p in small-cell lung cancer. *Oncotarget*, *6*(42), 44609–44622. https://doi.org/10.18632/oncotarget.6338

Zhu, B., Cao, X., Zhang, W., Pan, G., Yi, Q., Zhong, W., & Yan, D. (2019). MicroRNA-31-5p enhances the Warburg effect via targeting FIH. *FASEB Journal : Official Publication of the Federation of American Societies for Experimental Biology*, *33*(1), 545–556. https://doi.org/10.1096/FJ.201800803R

Zhu, H. Z., Fang, C. J., Guo, Y., Zhang, Q., Huang, L. M., Qiu, D., Chen, G. P., Pang, X. F., Hu, J. J., Sun, J. G., & Chen, Z. T. (2020). Detection of miR-155-5p and imaging lung cancer for early diagnosis: in vitro and in vivo study. *Journal of Cancer Research and Clinical Oncology*, *146*(8), 1941. https://doi.org/10.1007/S00432-020-03246-2

Zuo, Y., Yang, D., Yu, Y., Xiang, M., Li, H., Yang, J., Li, J., Jiang, D., Zhou, H., Xu, Z., & Yu, Z. (2018). Niclosamide enhances the cytotoxic effect of cisplatin in cisplatin-resistant human lung cancer cells via suppression of lung resistance-related protein and c-myc. *Molecular*

The 20th of March 2017 my dad was diagnosed with lung cancer. To be specific, with a IV stage ADC NSCLC phenotype.

In May 2018 he started a cisplatin-based treatment that, as explained in this thesis, soon became ineffective due to the development of resistance. In early July 2018 a treatment with Paclitaxel was initiated, which had little effect. In August 2019 the last approach with PDL-1 inhibitor led to a favourable, yet very short response (he died the 3rd of February 2018).

Therefore, the statistics described in chapter 1 of this thesis are not only numbers reported in online databases.